AN ABSTRACT OF THE DISSERTATION OF

Lisa Truong for the degree of Doctor of Philosophy in Toxicology present on August 24, 2012.
Title: Developing Rapid *In vivo* Assays to Investigate Structure Response Relationships.

Abstract approved:

_____

Robert L. Tanguay

Incorporation of nanoparticles (NPs) into consumer products is on the rise and human exposure to NPs is unavoidable. Currently, there is insufficient data to assess the safety of nanoparticles. I conducted a series of five studies using the zebrafish model to determine which NP components (i.e., core material or surface functionalization) contribute to biological responses and how ionic strength influences these results. The first study employed a systematic, rapid embryonic zebrafish assay to identify specific responses to precisely engineered lead sulfide (PbS-NPs) and gold nanoparticles (AuNPs) functionalized with different surface ligands. Lead sulfide nanoparticles functionalized with either 3-mercaptopropanesulfane (MT) or sodium 2,3-dimercaptopropanesulfonate (DT) ligands with nearly identical core sizes caused differential responses at the same concentration. I determined that the different responses were because MT-functionalized NPs released more soluble lead ions than DT-functionalized NPs due to different decomposition and oxidation rates. The second study investigated the different biological responses of three NPs identified during toxicity screening of a gold

nanoparticle library. AuNPs functionalized with 2-mercaptoethanesulfonic acid (MES), N,N,N-trimethylammoniumethanethiol (TMAT), or 2-(2-(2-mercaptoethoxy)ethoxy)ethanol (MEEE), induced differential biological responses in embryonic zebrafish at the same concentration. Exposure to MES-AuNPs induced sublethal effects, while TMAT-AuNPs were embryo-lethal and MEEE-AuNPs were benign. Gold tissue concentration was confirmed to be similar in exposed embryos using inductively coupled-mass spectrometry. Microarrays were used to gain insight to the causes of the different responses. This approach identified that MES- and TMAT-AuNPs perturbed inflammatory and immune responses. These differential biological responses may be due to misregulated transport mechanisms causing numerous downstream defects unique to each surface functional group's property. In the next study, I tested the long-term consequences of developmental exposure to TMAT-, MES, and MEEE-AuNPs, and showed that MES- and TMAT-AuNPs affected larval behavior that persisted into adulthood. During the course of these investigations, I found that high ion concentration in exposure solutions results in NP agglomeration, presenting a problem for NP testing in the zebrafish model. For the fourth study, I focused on solving this by determining that zebrafish can be raised in nearly ion-free media without adverse consequences. When 3-MPA-AuNPs were dispersed in this new low ionic media, I observed adverse responses in the embryonic zebrafish toxicity assay, but not when the NPs were suspended in high ionic media. Thus, I demonstrated that the media greatly influences both agglomeration rates and

biological responses, but most importantly, that the zebrafish is insensitive to external ions. The fifth study focused on the adverse response observed when embryonic zebrafish were exposed to 3-MPA-AuNPs. Exposed larvae failed to respond to a touch in the caudal fin at 120 hours post fertilization (hpf). Addition of a neuromuscular stimulus, nicotine, revealed the exposed embryos were not paralyzed, but experienced a reduction in axonal projections. A global genomic analysis (RNA-seq) using embryos exposed to 3-MPA-AuNP and MEEE-AuNPs (non-toxic control) from 6 to 120 hpf suggested that neurophysiological and signal transduction processes were perturbed. Functional analysis of the data led to the hypothesis that the most elevated gene, early growth response 1 (EGR-1), impacts axonogenesis in the caudal fin, interfering with glutaminergic synapses and preventing the connection of sensory neurons and touch perception. Although MEEE-AuNPs did not cause morphological defects, the RNA-seq analysis identified that these NPs perturbed immune and inflammatory system processes. Collectively, these results suggest that surface functional groups drive the differential responses to nanomaterials. The five studies summarized here confirm that a systems toxicological approach using the zebrafish model enables the rapid identification of structure-activity relationships, which will facilitate the design of safer nano-containing products.

# Developing Rapid *In vivo* Assays to Investigate Structure Response Relationships

by
Lisa Truong

A DISSERTATION

submitted to

Oregon State University

in partial fulfillment of
the requirements for the
degree of

Doctor of Philosophy

Presented August 24, 2012
Commencement June 2013

Doctor of Philosophy dissertation of Lisa Truong presented on August 24, 2012.

APPROVED:

---

Major Professor, representing Toxicology

---

Head of the Department of Environmental and Molecular Toxicology

---

Dean of the Graduate School

I understand that my dissertation will become part of the permanent collection of Oregon State University libraries. My signature below authorizes release of my dissertation to any reader upon request.

---

Lisa Truong, Author

# ACKNOWLEDGEMENTS

I would like to thank a lot of people who have helped, guided and inspired me throughout my graduate studies. Firstly, I have to express my deepest gratitude to Dr. Robert Tanguay, who not only provided me the opportunity to join his lab, but for guiding and supporting me every step of the way. Without him, I would not be who I am today. He has truly been my inspiration and has been nothing but encouraging and providing me lots of opportunities such as going to China, attending numerous conferences, being rewarded a prestigious NRSA fellowship and guide/manage/and mentor lots of students independently. I will never forget our adventures in China ranging from the high speed magnetic train to the Pearl Tower to the overnight train ride down to the shopping adventures.

I wanted to thank Dr. Andrew Blaustein who has supported me from the beginning of it all. Without Andy, I would not have applied or attend graduate school, and be going down this path today. His guidance and support is greatly appreciated and will be remembered forever.

Eric Johnson has to be thanked for helping make my transition from being on campus to Sinnhuber Aquatic Research Laboratory (SARL) seamless. Carrie Buchner for her hospitality of sharing her office with me and to Greg Gonnerman for making me feel at home at SARL. Also, Kelly Lindgren for encouraging my type A personality. I want to also thank Carrie Barton for providing invaluable support for my experiments and our great lunch dates.

Dr. Sumitra Sengupta taught me a lot of techniques and provided me with a lot of support through my graduate career. I want to thank Jane Ladu for putting up with my organization, and ordering extravaganzas. Kate Saili deserves special thanks for being a great friend and colleague throughout our graduate studies. She has helped me with experiments and with writing, but most of all, being my conference room buddy. I will always have that great memory of SOT 2011 with us both watching “I didn’t know I was pregnant” and our bond of having sons 6 days apart. I would like to express my thanks to Dr. Kerri Stanley Yip who has always been there and provided me with guidance every step of my graduate studies. Dr. Michael Simonich has been a great source of knowledge, friendship and career guidance. I would like to thank the other members of the Tanguay Lab as well for their support and expertise: Dr. Sean Bugel, Dr. Siba Das, Joe Fisher, Jill Franzosa, Britton Goodale, Derik Haggard, Dr. Kitae Kim, Andrea Knecht, David Mandrell, Dr. Galen Miller, Nadia Stegman, and Leah Wehmas. A special appreciation goes to the students I have mentored and the high throughput screening team (Mitra Geier, Sara Fassio, Mark Halvorson, Cory Vehafric, Lindsey Chalker, Leiyin Su, Jessie Castro, Dana Dunning, Kim Hayward, Kevin Nhan, Daniel Cowan, and Jacob Simson). Chapell Miller has made the screening team memorable and made sure things were “pretty as a panda” while I was gone.

My sincere thanks to everyone in the Department of Environmental and Molecular Toxicology for all their support. and also to National Institute of Environmental Health and Sciences for the Ruth Kirschstein National

Research Service Award that provided funding for my last 3 years of my graduate studies. I want to thank my committee members for serving in my graduate committee: Dr. Stacey Harper, Dr. Alan Bakalinsky, Dr. Chih-hung Chang, Dr. Siva Kolluri, and Dr. Gary Delander.

Most importantly, I wanted to thank my husband, Hao, for his support, encouragement, and love and my son, Tristin for being a happy baby every day of his life and my family, Lynda & John for their support, and my parents for their support and sacrifices they made to allow me to reach my goals.

# CONTRIBUTION OF AUTHORS

This dissertation is a collective effort of many collaborators from different universities and members of the Tanguay laboratory.

- In Chapter 2, Ian Moody synthesized the lead sulfide nanoparticles used for this study. Dylan Stankus performed the dynamic light scattering experiments.
- In Chapter 3, Dr. Susan Tilton performed the microarray analysis, Dr. Tatiana Zaikova synthesized the nanoparticles used in this study, and Dr. Erik Richman characterized the nanoparticles.
- In Chapter 4, Katerine Saili provided technical support for the morphological assessment of the adult zebrafish. Dr. John Miller synthesized the nanoparticles used for this study. Dr. Tatiana Zaikova synthesized the gold nanoparticles and performed the stability studies. Dr. Erik Richman performed transmission emission microscopy on the gold nanoparticle to determine size distribution.
- In Chapter 5, Dr. Tatiana Zaikova synthesized the gold nanoparticles and performed the stability studies. Dr. Erik Richman performed transmission emission microscopy on the gold nanoparticle to determine size distribution.
- In Chapter 6, Dr. Tatiana Zaikova synthesized the gold nanoparticles and performed the stability studies.

# TABLE OF CONTENTS

Page


CHAPTER 1 - INTRODUCTION ..... 1

Nanotechnology ..... 2

Complexity of nanotoxicology ..... 4

Toxic effects of nanomaterials ..... 7

Nanomaterial exposure ..... 9

Screening paradigm and test method requirements ..... 11

Application of embryonic zebrafish ..... 12

Going forward - leveraging good data to design “safer” nanoparticles ..... 14

References ..... 16

CHAPTER 2 - DIFFERENTIAL STABILITY OF LEAD SULFIDE NANOPARTICLES INFLUENCES BIOLOGICAL RESPONSES IN EMBRYONIC ZEBRAFISH ..... 21

Abstract ..... 22

Introduction ..... 24

Materials and Methods ..... 29

Results ..... 36

Discussion ..... 42

Conclusions ..... 48

References ..... 50

Acknowledgements ..... 53

# TABLE OF CONTENTS (CONTINUED)

CHAPTER 3 - SURFACE FUNCTIONALITIES OF GOLD NANOPARTICLES IMPACT EMBRYONIC GENE EXPRESSION RESPONSES ... 59

Abstract ... 60

Introduction ... 61

Materials and Methods ... 64

Results ... 71

Discussion ... 78

References ... 84

Acknowledgements ... 88

CHAPTER 4 - PERSISTENT ADULT ZEBRAFISH BEHAVIORAL DEFICITS RESULTS FROM ACUTE EMBRYONIC EXPOSURE TO GOLD NANOPARTICLES ... 96

Abstract ... 97

Introduction ... 98

Materials and Methods ... 100

Results ... 106

Discussion ... 110

Conclusion ... 113

References ... 115

Acknowledgements ... 117

TABLE OF CONTENTS (CONTINUED)

CHAPTER 5 - MEDIA IONIC STRENGTH IMPACTS EMBRYONIC RESPONSES TO ENGINEERED NANOPARTICLE EXPOSURE ..... 122

Abstract ..... 123

Introduction ..... 124

Materials and Methods ..... 128

Results ..... 132

Discussion ..... 137

References ..... 141

Acknowledgements ..... 144

CHAPTER 6 – RNA-SEQ REVEALS EMBRYONIC EXPOSURE TO GOLD NANOPARTICLES RESULTS IN SURFACE-DEPENDENT CHANGES IN GENE EXPRESSION ..... 150

Abstract ..... 151

Introduction ..... 153

Results ..... 155

Discussion ..... 163

Materials and Methods ..... 169

References ..... 176

Acknowledgements ..... 180

CHAPTER 7 - CONCLUSIONS ..... 201

# TABLE OF CONTENTS (CONTINUED)

APPENDICES ..... 204

Appendix A. Evaluation of embryotoxicity using the zebrafish model ..... 205

Appendix B. Automated zebrafish chorion removal and single embryo placement: optimizing throughput of zebrafish developmental toxicity screen ..... 225

# LIST OF FIGURES


Figure — Page

Figure 2- 1. Physical properties of PbS-MT and PbS-DT nanoparticles..... 54

Figure 2- 2. Mortality and malformation curves for embryos exposed to PbS-MT, PbS-DT, Pb(NO3)2, and MT and DT ligands..... 55

Figure 2- 3. Representative images of exposed zebrafish embryos..... 56

Figure 2- 4. Concentration of lead (Pb) in fresh and aged PbS-MT and PbS-DT solutions..... 57

Figure 2- 5. Tissue concentration of lead in embryos exposed to PbS-MT, PbS-DT and $Pb(NO_3)_2$. ..... 58

Figure 3- 1. Differential biological responses induced by AuNPs. ..... 89

Figure 3- 2. Venn diagram of misregulated transcripts after exposure to MES- and TMAT-AuNPs at (a) 24 hpf and (b) 48 hpf (c) hierarchical clustering and (d) functional enrichment of statistically significant genes ($p<0.05$) elevalted or repressed by MES- and TMAT-AuNPs. ..... 90

Figure 3- 3. Direct comparison of genes differentially expressed by TMAT- v. MES- AuNPs. ..... 91

Figure 3S- 1. Characterization data on MES-, TMAT – and MEEE-AuNPs.... 94

Figure 4- 1. Transient AuNP exposure results in abnormal behavior at 120 hpf..... 118

Figure 4- 2. AuNPs effect on development into adulthood. ..... 119

Figure 4- 3. Total distanced traveled and velocity following a stimulus. ..... 120

Figure 5- 1. Characterization of 1.2 nm 3-MPA-AuNPs..... 145

Figure 5- 2. 1.2 nm 3-MPA-AuNPs in embryo media. ..... 146

Figure 5- 3. Embryonic zebrafish exposed to various percentage of EM. .. 147

Figure 5- 4. Toxicity of 1.2 nm 3-MPA-AuNP in various percentage of EM.148

# LIST OF FIGURES (CONTINUED)


Figure 6- 1. The development and behavior of embryos exposed to gold nanoparticle. ..... 181

Figure 6- 2. Whole mount immunohistochemistry on control and exposed embryos. ..... 182

Figure 6- 3. 3-MPA-AuNPs RNA-seq (a) gene expression profile (b) volcano plot of statistically significant genes and (c) top 10 significant biological process networks identified by metacore. ..... 183

Figure 6- 4. MEEE-AuNPs RNA-seq (a) gene expression profile (b) volcano plot of statistically significant genes and (c) top 10 significant biological process networks identified by metacore. ..... 184

Figure 6- 5. Functional Group Comparison. ..... 185

# LIST OF TABLES


| Table | | Page |
|---|---|---|
| Table 3- 1. | Validation of statistically significant genes identified by the microarray using qRT-PCR | 92 |
| Table 3- 2. | Functional enrichment of biological processes at (a) 24 and (b) 48 hpf. | 93 |
| Table 4- 1. | Mean growth, survival and condition factor indices (± SEM) of adult zebrafish exposed to embryo media, MES- or TMAT- AuNP. | 121 |
| Table 6- 1. | RNA-seq results summary. | 186 |
| Table 6- 2. | Confirmation of statistically significant genes determined by RNA-seq using qRT-PCR. | 187 |
| Table 6S- 1. | Common 5 genes | 189 |
| Table 6S- 2. | List of Statistically significant genes in (a) CON v 3-MPA-AuNPs and (b) CON v MEEE-AuNPs. | 190 |

# LIST OF APPENDIX FIGURES


Figure — Page

Figure A- 1. Six hours post fertilization embryos. ..... 223

Figure A- 2. Visual assessment of zebrafish morphology. ..... 224

Figure B- 1. A modified shaker platform-based instrument for the automation of chorion removal from zebrafish embryos at 4 hours post fertilization……243

Figure B- 2. A custom robotic station for the automated transfer of dechorionated zebrafish embryos from the dish in which chorion removal occurred to a 96-well plate……244

Figure B- 3. Mortal damage typically observed in 1 – 2% of 5-hpf zebrafish embryos immediately after the automated dechorionation process…….. 245

Figure B- 4. Process summary and timeline for automated chorion removal and embryo allocation to plate wells…… 246

# LIST OF APPENDIX TABLES


| Table | | Page |
|---|---|---|
| Table B- 1. | Results of automated chorion removal at 4-hpf, observed at 24- and 120-hpf. | 247 |
| Table B- 2. | Robotic pick & place performance on 6-hpf dechorionated zebrafish embryos compared to manual plate loading. | 248 |

# CHAPTER 1 - INTRODUCTION

There are tens of thousands of chemicals and nanomaterials (NMs) being manufactured but, outside of pharmaceuticals, the marketing and widespread use of these chemicals requires minimal assessments of their potential hazard to human health. People are knowingly and inadvertently exposed to these compounds, and potential hazards are often not known until adverse health effects occur. To know the hazards associated with exposure to a new chemical or a nanomaterial and to prevent costly mistakes requires good toxicological data up front. This is especially important in the case of nanomaterials which often consist of a metal core or other elements of the periodic table (e.g. carbon, oxides, silica) that can be surface functionalized with a vast array of different chemistries. Nanoparticle dispersal in solution, core metal ion release and surface functionalization can individually and in concert affect the nanomaterial toxicity (Harper et al. 2011, Truong et al. 2011, Truong et al. 2011, Truong et al. 2012). Thus, the need for systematic assessments is compounded with the need to understand the mechanisms underlying the biological responses to nanomaterials. Without knowing toxicity mechanisms, it will be difficult to proactively avoid the generation of toxic products.

To move the field forward, a systematic approach using a relevant model must be used to facilitate direct translation of the results to protect human health. In this dissertation, I developed and used a high throughput *in*

vivo screening assay to identify biologically active nanomaterials and conducted transcriptome analysis to begin to identify the early transcriptional responses that precede toxicity (Waters et al. 2009, Truong, et al. 2012). Collectively, applying this approach to the field of nanotechnology has helped the field of nanotoxicology move closer to identifying structure response (SRs) relationships in order to establish design principles for safer nanomaterials design.

## Nanotechnology

Nanotechnology is the development of structure, devices and systems that have novel functional properties with size ranging between 1 and 100 nm (Jiang et al. 2008). This field is rapidly growing with a range of applications in electronics, healthcare, cosmetics, and technologies (Forrest 2001, Lecoanet et al. 2004, Lecoanet and Wiesner 2004, Sun et al. 2005). By manipulating matter at the atomic level, nanoparticles can be precisely engineered to exhibit desired physicochemical properties (Xu et al. 2005). These unique properties can be exploited to improve targeted drug delivery, diagnostics systems, therapeutics, and biocompatibility leading to advances in the biomedical sciences (e.g. prosthetics, regenerative medicine, etc) (Caruthers et al. 2007, Gaumet et al. 2008, Gil and Parak 2008, Biazar et al. 2009). Physicochemical properties unique to nanoparticles are their small size, chemical composition, surface structure, solubility, shape and aggregation (Nel et al. 2006).

The attractiveness of nanoparticle chemistry as a revolutionary technology platform for consumer and industrial product development resides in the ability to synthesize particles with a nearly infinite array of novel physicochemical properties. This characteristic is also reason for concern from a toxicological prospective. A large variety of novel chemistries would suggest the potential to affect a large number of biological targets. With essentially no existing knowledge on how nanomaterials interact with biological systems, the comprehensive toxicology that must, sooner or later, accompany the explosion of nanotechnology is still poignantly lagging. Simple facets alone of nanomaterials suggest the need for comprehensive toxicology.

The properties of nanostructured materials that make them unique and attractive may be the cause of concern for unforeseen health and environmental hazards. The fear of harm is currently slowing down the development of nanotechnology, which can be addressed with sound, independent, and authoritative information on what the risks are and how to avoid them. Currently, there is not a complete understanding of how the size, shape, composition and aggregation of nanomaterials influence biocompatibility. Without this knowledge, it is unclear whether the exposure of humans, animals, insects and plants to nanomaterials could produce harmful biological responses (Zhang et al. 2011, Yu et al. 2012). For risk to be accurately assessed, there is a need for basic toxicological information, including characterizing how specific properties of nanoparticles govern

biological responses. Given the variety of new nanoparticles, this task requires systematic, collaborative scientific investigations. Voluntary testing adopted while the industry is still young might help to avoid introduction of dangerous nanoparticles into the marketplace and environment such as occurred with chemicals in previous decades (i.e., chloroflurocarobons, commercial use of DDT, asbestos, or lead in gasoline and paint products).

## Complexity of nanotoxicology

### Dosimetry and agglomeration

Nanotoxicology is especially complex, precisely because non-traditional physicochemical parameters must be considered in dose estimation. In general, particles and specifically nanoparticles (1- 100 nm), diffuse, settle and agglomerate in medium as a function of density of the medium, viscosity, particle size, shape, charge and density. The dose is a function of the rate of transport. When considering the dose of NPs, the traditional toxicological method of using equal mass concentration (μg/mL) is not appropriate (Teeguarden et al. 2007) because for dissimilar materials, at the same equal mass concentration, the corresponding particle number or surface area concentration doses may differ by orders of magnitude. In addition to using inaccurate dosimetry in the field, particle size and density are often overlooked (Chithrani et al. 2006, Moss and Wong 2006). When diffusion and gravitational rates are considered, significant differences between the exposure dose and

“concentration” doses are evident (Teeguarden, et al. 2007). Without these special considerations (dosimetry, agglomeration, core decomposition, ion release, particle size and surface area), the science is vulnerable to misinterpretation of responses and uptake data for NPs. To address these considerations, it will require material; scientists to use precision engineering, and thoroughly characterize the batches over time, and then relay this critical information to the toxicologist to ensure the appropriate assays are used and the results will advance the field of nanotechnology.

**Decomposition and ion release**

Breakdown of the nanomaterials and the release of toxic constituents are known to occur (Kittler et al. 2010, Domingos et al. 2011, Truong, et al. 2011). NMs can contain toxic metals and compounds that are readily ionized and released when the nanomaterial structurally decays, or from impure nanomaterial preparations. Differentiating the toxicity of intact nanoparticles from their separate constituents can be difficult and it is nearly impossible to determine what state the nanoparticle is in once internalized in biological systems.

The decomposition of metal cores results in ion release. For silver nanoparticles (AgNPs), the release of silver ions (Ag+) increases the toxicity (Powers et al. 2010, Bilberg et al. 2012). Powers et al demonstrated that the AgNP effects are distinct from Ag+ alone, and was dependent on other factors

such as size and coatings (Powers, et al. 2010). Truong et al identified that the differential toxicity observed between two lead based nanoparticles was due to the insufficient encapsulation of the metal core by the surface ligands, resulting in release of lead ions over time (Truong, et al. 2011). Cadmium sulfide quantum dots (CdS-QDs) toxicity is influenced by their coating, however, when not stable, is caused by released metal ions (King-Heiden et al. 2009). The inability to distinctly isolate what is an ion release effect vs. a nanoparticle, adds to the complexity of nanotoxicology and interpreting the results of the field.

**Particle size and surface area**

For instance, smaller particles results in an increase in particle surface area. It allows more chemical molecules to attach to this surface, which would enhance its reactivity and result in an increase in its toxic effects (Linkov et al. 2008, Suh et al. 2009). In addition to crossing cell membranes, they reach the blood, and various organs because of their size, nanoparticles have a bigger surface to volume ratio than larger particles (Ai et al. 2011). This permits just a single particle to display and potentially deliver unseen numbers of potential ligands to intended as well as unintended targets. The smaller particles can cause more pathological and destructive power on the lungs due to their larger surface area, and greater tendency to conjugate (Linkov, et al. 2008, Suh, et al. 2009). The physicochemical and structural property differences of

nanomaterials at the low end of the size range may explain a number of observed toxicological effects such as cytotoxicity (Pan et al. 2007), and inflammatory responses (Waters, et al. 2009, Park et al. 2010).

## Toxic effects of nanomaterials

The toxicity of nanomaterials can be divided into two categories: biological and environmental.

### Biological toxicity

A common approach to understand nanotoxicology is to study structure response relationships of nanomaterials by focusing on elucidating the relationships between the physical and chemical properties of nanomaterials that cause toxic biological responses. Nanoparticles can target the respiratory tract via inhalation, but the gastrointestinal tract and other organs and tissues are likely affected and must be considered (Oberdörster 2010). NPs could get into the gastrointestinal tract indirectly via mucociliary movement, directly by oral intake of water, food, cosmetics, drugs and drug delivery systems at the nanoscale (Oberdörster et al. 2005).

Nanoparticle interactions with biological systems can give rise to numerous toxic effects such as allergies, fibrosis, organ deposition and failure, inflammation, cytotoxicity, reactive oxygen species (ROS) generation, and DNA damage (Maynard et al. 2006, Nel, et al. 2006, Waters, et al. 2009).

Potential mechanistic explanations for the adverse responses are oxidative stress caused by redox activity and ROS (Meng et al. 2007), the dissolution or shedding of toxic ions (Wong et al. 2010, Bilberg, et al. 2012), fibrosis of the lungs (Mangum et al. 2006), inflammasome activation by materials with long-aspect ratio (the length longer than the width) (Meng et al. 2011), and photoactivation, which influences the bioactivity of the NP (Bar-Ilan et al. 2012). This short list of potential mechanisms is based on a very limited toxicological scope to date. Much more comprehensive studies are needed to begin addressing the incredible array of physicochemical properties of nanoparticles and correlating them with whole organism and grounding them in genomic responses.

**Environmental toxicity**

As the applications of nanotechnology rapidly increase, we will likely begin to detect nanoparticle products in the environment virtually anywhere we look. Not only is it critical to understand the properties of the nanoparticles in its initial state, but how these properties will change when exposed to environmental conditions. The type of solution and surface functionalization greatly affects the charge, stability, and agglomeration state, which in turn impacts transport in various matrices (Darlington et al. 2009). Particle size also well correlated with transportability, along with charge of the NPs in solid

matrix. The three factors that greatly influence the nanoparticle mobility in soil is size, charge and agglomeration rate (Darlington, et al. 2009).

A key part of safely manufacturing, using and disposing of nanomaterials is conducting ecological hazard assessment to understand their environmental impacts. It is critical to understand the potential dangers of releasing nanomaterials into the environment. This can start with simply characterizing the solubility and degradability of NPs in soils and water and the chemical and microbial processes that control transport and removal of NPs in water and wastewater.

## Nanomaterial exposure

In general, we can categorize nanomaterial exposure to three groups: 1) occupational exposure, 2) consumer exposure, and 3) environmental exposure. With many new nano-containing products commercialized, concerns about human and environmental exposures are rising. Certain workplace conditions generate NPs that can reach higher exposure concentrations than typically found at ambient levels (Oberdörster, et al. 2005). Occupational exposure of those involved in the manufacture and research and development of nanomaterials is not monitored and adequate protection is yet undefined. The first carbon nanotube measurements in the workplace found very low concentrations; however, it represented a very high particle number concentration (Maynard et al. 2004). Inhalation maybe the

major route of exposure for NPs, but ingestion and dermal exposure needs consideration, especially for manufacture, use and disposal of engineered nanomaterials.

Nanomaterial based products include personal care items such as cosmetics and sunscreens where performance benefits have been realized. However, the incorporation of nanoparticles in commercialized products adds an undefined exposure with undefined hazard potential to uninformed consumers. The norm is still for consumers to assume that items one can buy at the supermarket must be inherently safe to use. No requirement exists for the reporting of NP in consumer product formulations and thus it is already difficult at best to assess the quantities and types of NPs to which consumers may be exposed. Recent studies showed that both zinc and titanium oxides (ZnO, and TiO2, respectively) occur in major sunscreen brands (Newman et al. 2009). Some studies are contradictory regarding NP safety. One study demonstrated that ZnO-NPs, and TiO2-NP formulations used in sunscreens were active photocatalysts and generated free radicals under illumination causing the sunscreen formulation to degrade (Picatonotto et al. 2001). Another found that the NP concentrations used in cosmetic products were non-toxic and conferred skin protection. The weight of toxicological evidence would suggest that not all TiO2- and ZnO-NPs are identical, but the UV protection and durability afforded by NP based sunscreens outweighs human safety concerns about NP exposure from use of these formulations (Schilling

et al. 2010). To understand the toxicological impact TiO2 and ZnO-NPs, structure response relationships must be identified. But many other NP core types and sophisticated surface chemistries are already in industrial and consumer use and, for these, the hazard potential is completely unknown. The use of nano-containing products will inevitably create an opportunity for a wider exposure of the entire ecosystem to nanomaterials through the water and soil. The concentrations of these engineered substances in the environment are directly proportional to their use in society as evidenced by chemical products.

## Screening paradigm and test method requirements

It is now clear that rapid, relevant, and efficient testing methods must be developed to assess emerging nanoparticles. The investigation of nanoparticle interactions with biological systems should be conducted at multiple levels of biological organization (i.e., molecular, cellular, and organismal levels). There are many models that could be used to assess nano-biological interactions, but due to the rapidly increasing number of manufactured nanoparticles, the ideal model must also offer high throughput capabilities. For example, in vitro techniques (cell based systems) are preferred for cost- and time- efficiency, direct translation to whole organisms or humans is difficult. But challenges to in vitro studies include contradictory effects from nano-biological interactions depending on the cell type, organ system, or developmental stage of the cells

being used (Nakamura and Isobe 2003, Bosi et al. 2004, Sayes et al. 2005, Isakovic et al. 2006, Teodoro et al. 2011). *In vivo* models (typically rodents) are more comprehensive, and perhaps predictive, but the animal and labor related cost, and the high-test material demands lend rodent-based studies incompatible for high throughput data collection. Rapid, applicable toxicity screens are necessary to assess the backlog of untested nanoparticles and to begin defining the basic NP characteristics that drive biological responses.

## Application of embryonic zebrafish

As a widely accepted model for mechanistic-based toxicological studies, the embryonic zebrafish offers a rapid, high throughput platform to assess the nanomaterial and biological system interactions (Furgeson and Fako 2009, George et al. 2011). The zebrafish and human genomes are highly homologous. Furthermore, zebrafish share many cellular, anatomical, and physiological characteristics with all vertebrates, including humans (Barbazuk et al. 2000). The embryos are small, develop externally, and are optically clear which allows for non-invasive evaluations. Additionally, a single female zebrafish can produce hundreds of eggs in one spawn (Lessman 2011), which allows for statistical power, and rapid assessments. The small nanomaterial quantities needed to fully evaluate the toxicity of engineered nanomaterials is also a major advantage for high throughput assessments. For example, less than one mg is required to fully evaluate the toxicity of a novel nanomaterial,

and this includes assessments across a wide range of concentrations in many replicate animals. Finally, early developmental life stages are inherently more susceptible to stressors as this is the most dynamic period in an organism's lifespan. The full repertoire of gene products is expressed during embryogenesis because these products are required to successfully accomplish cellular and organ system development (Richardson and Keuck 2002). Thus, if there is a unique biological target for a given nanomaterial that must be “hit” to produce a toxicological response, the probability of identifying this interaction is enhanced during the early developmental stage because all targets are expressed.

To fully exploit the embryonic zebrafish model for nanoparticle testing, I developed a tiered *in vivo* approach to define structural properties that lead to adverse biological consequences. Tier 1: Rapid 96-well plate screening experiments are conducted to assess the toxicity of a wide range of structurally well-characterized nanomaterials. Nanomaterials found to elicit significant adverse effects proceed to Tier 2 testing. Tier 2: Potential cellular targets and modes of action are defined *in vivo* using a suite of transgenic fluorescent reporter zebrafish lines and indicators of cellular oxidative state. Nanomaterials are then grouped according to structural indices and effects. Representative nanomaterials from each group are selected for Tier 3 testing. Tier 3: Global gene expression profiles are used to define the genomic

responses to nanomaterials. Data from these studies are used to define structure response relationships.

A key component necessary for defining a structure response relationship is to begin with well characterized nanoparticles. There are currently many methods to create nanoparticles (Moody et al. 2008, Harper, et al. 2011, Klemm et al. 2011), but there exists no standard guiding the collection or characterization data (i.e., purity, concentration, ligand size, core size, particle size, etc). Without knowing the basic structural and purity information, it is not possible to define the structure variable. Therefore, insufficiently purified or characterized materials are of no value for structure relationship studies.

## Going forward - leveraging good data to design “safer” nanoparticles

Addressing potential risks of nanoparticles should be a priority concern not only for regulatory agencies, but also for the researchers and companies producing the particles. Collaborations between scientific investigators and manufacturers will preemptively minimize negative consequences and allow for development of the most environmentally benign nanochemistries and manufacturing methods. Greener nanotechnology is a practice pioneered at the University of Oregon to include replacing or minimizing usage of hazardous chemicals (Harper et al. 2008). Greener nanoscience also seeks to alter nanoparticles to render them nontoxic (e.g., via new reaction

mechanisms, controlling physical properties, or surface functionalization) (Harper, et al. 2008).

The embryonic zebrafish is the ideal vertebrate model for testing the exponentially increasing number of nanoparticles in development and already in the marketplace. However, the data obtained in this model, or any model will be of little value unless a widely available and easily searchable repository of experimental data and conclusions is available. Data obtained from other in vitro or *in vivo* models is encouraged as a greater wealth of structure response studies, characterized in a diversity of models, will only facilitate better nanoparticle chemistry. A database of SRs that is readily available to manufacturers would be an invaluable resource where R&D budget constraints may not allow for extensive in-house safety testing of promising nanochemistries. A comprehensive knowledge database of SRs in high throughput models, including the embryonic zebrafish, will enable tuning of nanoparticles to maximize performance and safety before they reach commercial production.

## References

Ai J, Biazar E, Jafarpour M, Montazeri M, Majdi A, Aminifard S, Zafari M, Akbari HR, Rad HG. 2011. Nanotoxicology and nanoparticle safety in biomedical designs International Journal of Nanomedicine 6: 1117-1127.

Bar-Ilan O, Louis KM, Yang SP, Pedersen JA, Hamers RJ, Peterson RE, Heideman W. 2012. Titanium dioxide nanoparticles produce phototoxicity in the developing zebrafish. Nanotoxicology 0: 1-10.

Barbazuk WB, Korf I, Kadavi C, Heyen J, Tate S, Wun E, Bedell JA, McPherson JD, Johnson SL. 2000. The syntenic relationship of the zebrafish and human genomes. Genome Res 10: 1351-8.

Biazar E, Beitollahi A, Rezayat SM, Forati T, Asefnejad A, Rahimi M, Zeinali R, Ardeshir M, Hatamjafari F, Sahebalzamani A, et al. 2009. Effect of the mechanical activation on size reduction of crystalline acetaminophen drug particles. International Journal of Nanomedicine 4: 283-287.

Bilberg K, Hovgaard MB, Besenbacher F, Baatrup E. 2012. In Vivo Toxicity of Silver Nanoparticles and Silver Ions in Zebrafish (Danio rerio). Journal of Toxicology 2012.

Bosi S, Feruglio L, Da Ros T, Spalluto G, Gregoretti B, Terdoslavich M, Decorti G, Passamonti S, Moro S, Prato M. 2004. Hemolytic Effects of Water-Soluble Fullerene Derivatives. Journal of Medicinal Chemistry 47: 6711-6715.

Caruthers SD, Wickline SA, Lanza GM. 2007. Nanotechnological applications in medicine. Current Opinion in Biotechnology 18: 26-30.

Chithrani BD, Ghazani AA, Chan WCW. 2006. Determining the Size and Shape Dependence of Gold Nanoparticle Uptake into Mammalian Cells. Nano Letters 6: 662-668.

Darlington TK, Neigh AM, Spencer MT, Nguyen OT, Oldenburg SJ. 2009. Nanoparticle characteristics affecting environmental fate and transport through soil. Environmental toxicology and chemistry / SETAC 28: 1191-9.

Domingos RF, Simon DF, Hauser C, Wilkinson KJ. 2011. Bioaccumulation and Effects of CdTe/CdS Quantum Dots on Chlamydomonas reinhardtii – Nanoparticles or the Free Ions? Environmental Science & Technology 45: 7664-7669.

Forrest DR. 2001. Molecular Nanotechnology. IEEE: 11-20.

Furgeson D, Fako V. 2009. Zebrafish as a correlative and predictive model for assessing biomaterial nanotoxicity. Advanced Drug Delivery Reviews 61: 478-486.

Gaumet M, Vargas A, Gurny R, Delie F. 2008. Nanoparticles for drug delivery: The need for precision in reporting particle size parameters. European Journal of Pharmaceutics and Biopharmaceutics 69: 1-9.

George S, Xia T, Rallo R, Zhao Y, Ji Z, Lin S, Wang X, Zhang H, France B, Schoenfeld D, et al. 2011. Use of a High-Throughput Screening Approach Coupled with In Vivo Zebrafish Embryo Screening To Develop Hazard Ranking for Engineered Nanomaterials. ACS Nano 5: 1805-1817.

Gil PR, Parak WJ. 2008. Composite Nanoparticles Take Aim at Cancer. ACS Nano 2: 2200-2205.

Harper SL, Carriere JL, Miller JM, Hutchison JE, Maddux BLS, Tanguay RL. 2011. Systematic Evaluation of Nanomaterial Toxicity: Utility of Standardized Materials and Rapid Assays. ACS Nano 5: 4688-7697.

Harper SL, Dahl JA, Maddux BLS, Tanguay RL, Hutchison JE. 2008. Proactively designing nanomaterials to enhance performance and minimise hazard. International Journal of Nanotechnology 5: 124-142.

Isakovic A, Markovic Z, Todorovic-Markovic B, Nikolic N, Vranjes-Djuric S, Mirkovic M, Dramicanin M, Harhaji L, Raicevic N, Nikolic Z, et al. 2006. Distinct Cytotoxic Mechanisms of Pristine versus Hydroxylated Fullerene. Toxicological Sciences 91: 173-183.

Jiang W, KimBetty YS, Rutka JT, ChanWarren CW. 2008. Nanoparticle-mediated cellular response is size-dependent. Nat Nano 3: 145-150.

King-Heiden TC, Wiecinski PN, Mangham AN, Metz KM, Nesbit D, Pedersen JA, Hamers RJ, Heideman W, Peterson RE. 2009. Quantum Dot Nanotoxicity Assessment Using the Zebrafish Embryo. Environmental Science & Technology 43: 1605-1611.

Kittler S, Greulich C, Diendorf J, Koìˆller M, Epple M. 2010. Toxicity of Silver Nanoparticles Increases during Storage Because of Slow Dissolution under Release of Silver Ions. Chemistry of Materials 22: 4548-4554.

Klemm D, Kramer F, Moritz S, Lindström T, Ankerfors M, Gray D, Dorris A. 2011. Nanocelluloses: A New Family of Nature-Based Materials. Angewandte Chemie International Edition 50: 5438-5466.

Lecoanet HF, Bottero JY, Wiesner MR. 2004. Laboratory assessment of the mobility of nanomaterials in porous media. Environ Sci Technol 38: 5164-9.

Lecoanet HF, Wiesner MR. 2004. Velocity effects on fullerene and oxide nanoparticle deposition in porous media. Environ Sci Technol 38: 4377-82.

Lessman CA. 2011. The developing zebrafish (Danio rerio): A vertebrate model for high-throughput screening of chemical libraries. Birth Defects Research Part C: Embryo Today: Reviews 93: 268-280.

Linkov I, Satterstrom FK, Corey LM. 2008. Nanotoxicology and nanomedicine: making hard decisions. Nanomedicine: Nanotechnology, Biology and Medicine 4: 167-171.

Mangum J, Turpin E, Antao-Menezes A, Cesta M, Bermudez E, Bonner J. 2006. Single-Walled Carbon Nanotube (SWCNT)-induced interstitial fibrosis in the lungs of rats is associated with increased levels of PDGF mRNA and the formation of unique intercellular carbon structures that bridge alveolar macrophages In Situ. Particle and Fibre Toxicology 3: 15.

Maynard AD, Aitken RJ, Butz T, Colvin V, Donaldson K, Oberdorster G, Philbert MA, Ryan J, Seaton A, Stone V, et al. 2006. Safe handling of nanotechnology. Nature 444: 267-269.

Maynard AD, Baron PA, Foley M, Shvedova AA, Kisin ER, Castranova V. 2004. Exposure to Carbon Nanotube Material: Aerosol Release During the Handling of Unrefined Single-Walled Carbon Nanotube Material. Journal of Toxicology and Environmental Health, Part A 67: 87-107.

Meng H, Chen Z, Xing GM, Yuan H, Chen CY, Zhao F, Zhang CC, Zhao YL. 2007. Ultrahigh reactivity provokes nanotoxicity: Explanation of oral toxicity of nano-copper particles. Toxicology Letters 175: 102-110.

Meng H, Yang S, Li Z, Xia T, Chen J, Ji Z, Zhang H, Wang X, Lin S, Huang C, et al. 2011. Aspect Ratio Determines the Quantity of Mesoporous Silica Nanoparticle Uptake by a Small GTPase-Dependent Macropinocytosis Mechanism. ACS Nano 5: 4434-4447.

Moody IS, Stonas AR, Lonergan MC. 2008. PbS Nanocrystals Functionalized with a Short-Chain, Ionic, Dithiol Ligand. Journal of Physical Chemistry C 112: 19383-19389.

Moss OR, Wong VA. 2006. When Nanoparticles Get in the Way: Impact of Projected Area on In Vivo and In Vitro Macrophage Function. Inhalation Toxicology 18: 711-716.

Nakamura E, Isobe H. 2003. Functionalized Fullerenes in Water. The First 10 Years of Their Chemistry, Biology, and Nanoscience. Accounts of Chemical Research 36: 807-815.

Nel A, Xia T, MÃ¤dler L, Li N. 2006. Toxic Potential of Materials at the Nanolevel. Science 311: 622-627.

Newman MD, Stotland M, Ellis JI. 2009. The safety of nanosized particles in titanium dioxide- and zinc oxide-based sunscreens. Journal of the American Academy of Dermatology 61: 685-692.

Oberdörster G. 2010. Safety assessment for nanotechnology and nanomedicine: concepts of nanotoxicology. Journal of Internal Medicine 267: 89-105.

Oberdörster G, Oberdörster E, Oberdörster J. 2005. Nanotoxicology: An Emerging Discipline Evolving from Studies of Ultrafine Particles. Environ Health Perspect 113.

Pan Y, Neuss S, Leifert A, Fischler M, Wen F, Simon U, Schmid G, Brandau W, Jahnen-Dechent W. 2007. Size-Dependent Cytotoxicity of Gold Nanoparticles. Small 3: 1941-1949.

Park EJ, Bae E, Yi J, Kim Y, Choi K, Lee SH, Yoon J, Lee BC, Park K. 2010. Repeated-dose toxicity and inflammatory responses in mice by oral administration of silver nanoparticles. Environmental Toxicology and Pharmacology 30: 162-168.

Picatonotto T, Vione D, Carlotti ME, Gallarate M. 2001. Photocatalytic Activity of Inorganic Sunscreens. Journal of Dispersion Science and Technology 22: 381-386.

Powers CM, Badireddy AR, Ryde IT, Seidler FJ, Slotkin TA. 2010. Silver Nanoparticles Compromise Neurodevelopment in PC12 Cells: Critical Contributions of Silver Ion, Particle Size, Coating and Composition. Environ Health Perspect.

Richardson MK, Keuck G. 2002. Haeckel's ABC of evolution and development. Biological Reviews 77: 495-528.

Sayes CM, Gobin AM, Ausman KD, Mendez J, West JL, Colvin VL. 2005. Nano-C60 cytotoxicity is due to lipid peroxidation. Biomaterials 26: 7587-7595.

Schilling K, Bradford B, Castelli D, Dufour E, Nash JF, Pape W, Schulte S, Tooley I, van den Bosch J, Schellauf F. 2010. Human safety review of "nano" titanium dioxide and zinc oxide. Photochemical & Photobiological Sciences 9: 495-509.

Suh WH, Suslick KS, Stucky GD, Suh Y-H. 2009. Nanotechnology, nanotoxicology, and neuroscience. Progress in Neurobiology 87: 133-170.

Sun Q, Wang Q, Jena P, Kawazoe Y. 2005. Clustering of Ti on a C60 surface and its effect on hydrogen storage. J Am Chem Soc 127: 14582-3.

Teeguarden JG, Hinderliter PM, Orr G, Thrall BD, Pounds JG. 2007. Particokinetics In Vitro: Dosimetry Considerations for In Vitro

Nanoparticle Toxicity Assessments. Toxicological Sciences 95: 300-312.

Teodoro JS, Simões AM, Duarte FV, Rolo AP, Murdoch RC, Hussain SM, Palmeira CM. 2011. Assessment of the toxicity of silver nanoparticles in vitro: A mitochondrial perspective. Toxicology in Vitro 25: 664-670.

Truong L, Moody I, Stankus D, Nason J, Lonergan M, Tanguay R. 2011. Differential stability of lead sulfide nanoparticles influences biological responses in embryonic zebrafish. Archives of Toxicology 85: 787-798.

Truong L, Tilton SC, Zaikova T, Richman E, Waters KM, Hutchison JE, Tanguay RL. 2012. Surface functionalities of gold nanoparticles impact embryonic gene expression responses. Nanotoxicology 0: 1-10.

Truong L, Zaikova T, Richman EK, Hutchison JE, Tanguay RL. 2011. Media ionic strength impacts embryonic responses to engineered nanoparticle exposure. Nanotoxicology 0: 1-9.

Waters KM, Masiello LM, Zangar RC, Karin NJ, Quesenberry RD, Bandyopadhyay S, Teeguarden JG, Pounds JG, Thrall BD. 2009. Macrophage Responses to Silica Nanoparticles are Highly Conserved Across Particle Sizes. Toxicological Sciences 107: 553-569.

Wong SWY, Leung PTY, Djurisic AB, Leung KMY. 2010. Toxicities of nano zinc oxide to five marine organisms: influences of aggregate size and ion solubility. Analytical and Bioanalytical Chemistry 396: 609-618.

Xu ZH, Gu WW, Huang J, Sui H, Zhou ZH, Yang YX, Yan Z, Li YP. 2005. In vitro and in vivo evaluation of actively targetable nanoparticles for paclitaxel delivery. International Journal of Pharmaceutics 288: 361-368.

Yu T, Greish K, McGill LD, Ray A, Ghandehari H. 2012. Influence of Geometry, Porosity, and Surface Characteristics of Silica Nanoparticles on Acute Toxicity: Their Vasculature Effect and Tolerance Threshold. ACS Nano 6: 2289-2301.

Zhang H, Xia T, Meng H, Xue M, George S, Ji Z, Wang X, Liu R, Wang M, France B, et al. 2011. Differential Expression of Syndecan-1 Mediates Cationic Nanoparticle Toxicity in Undifferentiated versus Differentiated Normal Human Bronchial Epithelial Cells. ACS Nano 5: 2756-2769.

# CHAPTER 2 - DIFFERENTIAL STABILITY OF LEAD SULFIDE NANOPARTICLES INFLUENCES BIOLOGICAL RESPONSES IN EMBRYONIC ZEBRAFISH

Lisa Truong,[1,2] Ian S Moody,[3] Dylan P Stankus,[2,4] , Jeffrey A Nason,[2,4] Mark C Lonergan,[2.3] and Robert L Tanguay[1,2,*]

[1] *Department of Environmental and Molecular Toxicology, Oregon State University, Corvallis, OR 97331*
[2]Safer Nanomaterials and Nanomanufacturing Initiative, Oregon Nanoscience and Microtechnologies Institute, Corvallis,
[3]*Department of Chemistry and the Materials Science Institute, University of Oregon, Eugene, Oregon 97403*
[4]*School of Chemical, Biological and Environmental Engineering, Oregon State University, Corvallis, OR 97331*

## Abstract

As the number of nanoparticle-based products increase in the marketplace, there will be increased potential for human exposures to these engineered materials throughout the product life cycle. We currently lack sufficient data to understand or predict the inherent nanomaterial characteristics that drive nanomaterial-biological interactions and responses. In this study, we utilized the embryonic zebrafish *(Danio rerio)* model to investigate the importance of nanoparticle (NP) surface functionalization, in particular as it pertains to nanoparticle stability, on *in vivo* biological responses. This is a comparative study where two lead sulfide nanoparticles (PbS-NPs) with nearly identical core sizes, but functionalized with either sodium 3-mercaptopropanesulfonate (MT), or sodium 2,3-dimercaptopropanesulfonate (DT) ligand were used. Developmental exposures and assessments revealed differential biological responses to these engineered nanoparticles. Exposures beginning at 6 hours post fertilization (hpf) to MT-functionalized nanoparticles (PbS-MT) led to 100% mortality by 120 hpf while exposure to DT-functionalized nanoparticles (PbS-DT) produced less than a 5% incident in mortality at the same concentration. Exposure to the MT and DT ligands themselves did not produce adverse developmental effects when not coupled to the NP core. Following exposure, we confirmed that the embryos took up both PbS-MT and PbS-DT material using Inductively Coupled Plasma – Mass Spectrometry (ICP-MS). The stability of the nanoparticles in the aqueous solution was also characterized.

The nanoparticles decompose and precipitate upon exposure to air. Soluble lead ions were observed following nanoparticle precipitation and in greater concentration for the PbS-MT sample compared to the PbS-DT sample. These studies demonstrate that *in vivo* assessments can be effectively used to characterize the role of NP surface functionalization in predicting biological responses.

## Introduction

Nanoparticles (NPs) are becoming ubiquitous as they are incorporated into an increasing number of commercial products. Exploiting their unique material properties, nanoparticle-based applications will undoubtedly revolutionize many features of our lives. Nanotechnology is used in a broad spectrum of applications, encompassing cosmetics, biomedical supplies, fluorescent bioimaging, and electronics (Minchin and Martin 2010; Usenko et al. 2007; Bharali et al. 2009; Newman et al. 2009).

Despite the rapid growth of the nanotechnology industry, research into interactions of nanoparticles with environmental and biological systems has not kept pace with material development. Currently, the interplay between nanoscale materials and biological systems is poorly understood, and hazards have not been fully evaluated. Without toxicological data regarding the biocompatibility of nanoparticles, it is impossible to identify risk associated with nanoparticle exposure. An efficient testing method, if proven predictive, would help fill these critical data gaps.

Various biological models have been proposed for toxicological assessments including *in vitro* and *in vivo* methodologies. *In vitro* studies, such as cell culture, are rapid, efficient, and low-cost. However, results from these studies are often difficult to translate to the whole organism. Utilizing *in vivo* models may offer a more immediately relevant platform for translational studies (Teraoka et al. 2003; den Hertog 2005; Hall et al. 2007). The widely

accepted rodent model is both cost and labor intensive; it requires extensive animal care facilities and significant quantities of test materials for the toxicity assessments. A powerful alternative is the zebrafish model (Parng 2005), which is now widely accepted for mechanistic-based toxicological studies (Haendel et al. 2004; Hill et al. 2005; Ton et al. 2006; Usenko et al. 2007; Furgeson et al. 2009).

Zebrafish have a high degree of homology to the human genome and share many cellular, anatomical, and physiological characteristics with other vertebrates (Barbazuk et al. 2000). Their small size, rapid development, and short life cycle make zebrafish an ideal rapid assessment model, which is needed to provide solid and crucial toxicological data (Dodd et al. 2000; Rubinstein 2003; and Yang et al. 2003). Female zebrafish are capable of producing hundreds of embryos a day, thereby providing statistical power to the analysis. Embryos develop externally and are transparent for the first few days of their development, allowing for non-invasive assessments (Kimmel et al. 1995). The small quantity needed to fully evaluate biological responses to a novel engineered nanoparticle (typically, less than 1 mg) is also a major advantage for “green by design” synthesis strategies. With other models, material requirements are orders of magnitude greater. This combination of rapid assessments, unlimited embryos, and minimal material needs, makes the zebrafish model ideal for investigation of nanomaterial-biological interactions.

Lead sulfide nanoparticles (PbS-NPs) have been increasingly developed and studied due to their unique electrical and optical properties. Like other semiconductor nanoparticles, they exhibit quantum confinement below a certain size threshold – the so-called, *quantum size effect* – that allows their optical and electrical properties to be precisely tuned with size. Lead sulfide, in particular, has shown promise as a material that is optically active in the near infrared (NIR) region of the electromagnetic spectrum. Sensitivity to this spectral window is critical for a variety of photonic applications, including single- and multi-junction solar cells (Koleilat et al. 2008 and McDonald et al. 2005), NIR photodetectors for telecommunications (Konstantatos et al. 2006), and NIR light-emitting diodes (LEDs) (Konstantatos et al. 2005). Additionally, solubilized PbS-NPs have been studied as fluorescent biomarkers that can take advantage of the transparent tissue window at 700-1000nm for *in vivo* cellular imaging (Hyun et al. 2007, Hinds et al. 2007, and Lim et al. 2003).

Despite increased interest in PbS-NPs as industrial materials, very little is known about their biological or environmental interactions. Compounds containing lead can induce a wide variety of adverse human effects (ATSDR 2007), such as genotoxicity (Zelikoff 1988), oxidative stress (Sharma 2010), and neurological effects (De Gennardo 1978). It is known that lead can affect multiple systems in the body, most notably the nervous system. Cardiovascular, immune, and reproductive systems as well as bones, teeth,

and kidneys are also sensitive targets (White et al 2007). Lead sulfide (PbS) – *galena* – is an extensively mined ore, which is negligibly soluble in aqueous systems, making bioavailability in solutions limited. PbS can undergo decomposition processes, and reduced particle size is known to increase decomposition rates (Liu et al. 2009), which influences the amount of ionic lead available. To complicate the understanding of nanoparticle-biological interaction, nearly all colloidal nanoparticle preparation has organic stabilizing molecules, ligands, that bind to the surface of the core, passivate surface states, retard particle growth and agglomeration, and imbue the nanoparticles with solubility.

Toxicological studies on other nanoparticle systems have identified key structural features important to understanding nanomaterial-biological interactions (Kirchner et al. 2005; Kotov et al. 2009). One such feature, chemical composition of the nanoparticle core, has been identified as a good predictor of toxicity. Nanoparticles composed of known toxic metals for example cadmium (Samia et al. 2003; Kirchner et al. 2005) and silver (Wise et al. 2009)) – are generally more toxic than those composed of inert materials such as gold (Furgeson et al. 2009). Core size is also an important feature, with smaller particles of the same core material, generally more toxic than larger ones (Meng et al. 2007; Guo et al. 2008). Smaller particles are thought to interact more strongly with biological systems, either through enhanced cellular uptake, or through faster decomposition due to greater surface area-

to-volume ratios compared to larger particles. In addition to the composition of the nanoparticle core, ligand shells can affect nanoparticle toxicity (Hoshino et al. 2004).

This wide array of variables can make correlation of structure-activity relationships difficult. The aim of this study was to isolate one of these variables – ligand head group as a key factor in nanoparticle stability, while keeping all other factors (core material, core size, and ligand tail group) constant. At the same time, we hoped to open investigation into the little understood toxicity of the technologically-relevant nanomaterial – PbS. Specifically, in this study, two types of water soluble PbS-NPs were tested in the embryonic zebrafish system. Both PbS-NP had similar core size (~3nm), and were functionalized with either a sodium 3-mercaptopropanesulfonate (MT) ligand, or its bidentate analogue – sodium 2,3-dimercaptopropanesulfonate (DT). These two ligands are structurally analogous; both ligands have the same carbon backbone and sulfonate tail group, and differ only in the head group – mono- vs. di- thiol, respectively. Prior studies on these nanoparticles revealed that the two ligands offered differential protection against oxidative decomposition, with MT-functionalized particles being less stable to precipitation (Moody et al. 2008). This feature made MT- and DT-capped nanoparticles a compelling set in which to study the effects of particle stability on nanoparticle toxicity, while keeping other structural features unchanged. Utilizing the zebrafish model to screen for

developmental toxicity revealed that the different surface functionalizations of the nanoparticles produced different biological responses.

## Materials and Methods

### Nanoparticles

***Materials:*** Lead (II) oxide (PbO); oleic acid (OLA, 90% technical grade); 1-octadecene (ODE, 90% technical grade); bis-(trimethylsilyl)sulfide; 3-mercaptopropanesulfonic acid, sodium salt (MT, 90%); and, 2,3-dimercaptopropanesulfonic acid, sodium salt, monohydrate (DT, 95%) were all purchased from Aldrich. Deuterium oxide was obtained from Cambridge Isotope Laboratories, Inc. Acetonitrile and toluene were distilled under nitrogen from $P_2O_5$ and Na/benzophenone, respectively, before use. Nanopure water and other solvents were deoxygenated either by sparging with nitrogen or freeze-pump-thaw degassing.

***Synthesis of Lead Sulfide Nanoparticles (PbS-NPs):*** Moody et al (2008) have previously reported this procedure. Briefly, PbO was dissolved in OLA and heated under vacuum to remove water and form lead oleate. To form PbS-NPs, a solution of bis-(trimethylsilyl) sulfide in ODE was quickly injected into the stirring mixture of lead oleate at 130$^{o}$C under nitrogen. After cooling, the crude nanoparticle solution was purified by a series of precipitation-centrifugation-resuspension steps, using distilled toluene and methanol as the

solvent and non-solvent, respectively. Oleic-acid capped PbS-NPs were then exchanged with either MT or DT ligands in a biphasic solution of toluene and water. Biphasic mixtures were manually shaken for one hour and then centrifuged. The organic layer, along with any remaining organic-soluble NPs, were removed from the aqueous layer and discarded. Thiol-functionalized NPs in the aqueous layer were washed with toluene to remove any remaining free OLA. To purify the nanoparticles, another series of precipitation-centrifugation-resuspension steps was performed using nanopure water and acetonitrile, as the solvent and non-solvent, respectively. A typical exchange procedure used equal volumes of a 25 mg/mL solution of PbS-OLA in toluene and either a 180 mM solution of MT or 78 mM solution of DT in water.

At all steps in the synthesis and exchange, standard air-free techniques were employed. Samples and reagents were stored under nitrogen in Schlenk flasks or centrifuge tubes with septa caps, and transferred via gas-tight syringes.

***Physical Characterization of Nanoparticles:***

- **Near-Infrared (NIR) Absorption Spectroscopy-** Absorption spectra were measured on a Perkin-Elmer Lambda 19 UV/VIS/NIR Spectrophotometer. To reduce solvent absorption in the spectral window of interest, deuterium oxide was used in place of water for this measurement. Nanoparticle solutions were diluted to a

concentration regime (~1 mg/mL) where a linear dependence of absorbance on concentration was observed.

- **Transmission Electron Microscopy (TEM) –** Samples of PbS-MT and PbS-DT were prepared using amine-functionalized “Smart Grids” obtained from Dune Sciences, Inc. To prepare, a "Smart-Grid" was floated atop a drop of dilute nanoparticle solution. After 10 seconds, the grid was dipped in deionized water to remove excess sample, then blotted dry from beneath with a Kimwipe. Images were taken using an FEI Titan 80-300 S/TEM microscope operating at 300 keV at 56k magnification and a pixel resolution of 2.58 pixels/nm.

  Size analysis was performed using ImageJ software. Image contrast was enhanced to the minimum level necessary for automated particle counting, and all images were processed identically. To improve contrast, a Gaussian blur function and bandpass filter were applied. Segmenting was achieved using the “MultiThresholder” plug-in, utilizing the “Intermodes” method. Prior to automated counting, size and circularity constraints were used to remove large agglomerates from the count. The results of the automated particle analysis were checked against the original image. Particle diameter was taken to be the average of the major and minor axes of the ellipse fit.

- **Lead Analysis by Inductively Coupled Plasma – Optical Emission Spectrometry (ICP-OES) –**Three aliquots (50 µL each) for both fresh PbS-MT and PbS-DT (nominally, 3 mg/mL) were analyzed. Aliquots were digested with 196 µL of ultra pure nitric acid ($HNO_3$) (VWR: 87003-226) for 12 hours prior to analysis. The remaining nanoparticle solutions were then left to precipitate (age) under ambient conditions for five days. When precipitated, the nanoparticles from both solutions collected as insoluble agglomerates, leaving fractions of solubilized lead in the clear supernatant. For each aged sample, the supernatant was drawn off and centrifuged at 13,000 rpm for 10 minutes to remove any remaining nanoparticles. The centrifuged supernatant (50 µL) was then digested in the same manner as for the fresh nanoparticle solution aliquots (three replicates). Prior to sampling, each sample was diluted to 10 mL with Milli-Q water. Samples were vortexed and placed into autosampler racks prior to being analyzed. The ICP-OES was calibrated using a lead standard in 0.5% $HNO_3$ at seven concentrations (0.25, 0.5, 5, 10, 20, 35 and 50 ppm). The calibration curve created by the standard solutions had an $R^2$ value of 0.996. Measured concentrations of lead in the undiluted nanoparticle solutions were back-calculated from the lead content determined by ICP-OES in the aliquots, and the dilution factor. The percentage of

recovered lead was calculated from the ratio of the measured concentration to the theoretical concentration. The theoretical concentration is based on several assumptions: the nanoparticles are spherical, the Pb to S ratio in the core is 1:1, and the surface Pb atom to ligand ratio is 1:1. Given these assumptions, the calculated theoretical concentrations of lead in the fresh solutions were 2189 ppm for PbS-MT and 2129 ppm for PbS-DT.

- **Dynamic Light Scattering (DLS) –** Equal concentrations (40 ppm) of PbS-MT and PbS-DT were prepared by diluting aqueous nanoparticle stock solutions (20 mg/mL in deionized water) with fish water (FW). Immediately after dilution, solutions underwent a single pass through a 0.2µm filter to remove dust that could influence the scattering experiments. Hydrodynamic radii were taken as the average of three samples, and measured using a Brookhaven 90 Plus Particle Size Analyzer.

**Zebrafish**

***Exposure Protocol:*** Embryonic zebrafish were obtained from a Tropical 5D strain of zebrafish (*Danio rerio*) reared in the Sinnhuber Aquatic Research Laboratory (SARL) at Oregon State University. Adults were kept at standard laboratory conditions of 28°C on a 14h light/10h dark photoperiod in fish water (FW) consisting of reverse osmosis water supplemented with a commercially available salt (Instant Ocean®) to create a salinity of 600 microsiemen and

sodium bicarbonate was added as needed to adjust the pH to 7.4. Zebrafish were group spawned and embryos were collected and staged as described by Kimmel et al (1995). To increase bioavailability, the chorion, an acellular envelope surrounding the embryo, was removed enzymatically with pronase at 4 hours post fertilization (hpf). Briefly, embryos were placed in 25 mL of FW with 50 µL of 50 mg/mL pronase (Fluka #81748) for 4-5 minutes; the water was decanted and replenished with fresh FW for a total of 10 minutes. Embryos were allowed to rest for at least 30 minutes prior to the initiation of nanoparticle exposure. After the rest period, dechorionated embryos were transferred to individual wells of a 96-well plate with 100 µL of prepared nanoparticle solution. Control animals were exposed to FW only. Non-exposed animals (embryos raised in FW with the chorion intact) were also retained to monitor inherent embryo quality. Embryos were exposed to a FW control and six concentrations of nanoparticles (n=24, three replicates), with the highest concentration being 320 µg/mL (ppm) and the remainder from sequential two-fold dilutions down to 10 ppm. The static nanoparticle exposure continued under standard laboratory conditions in sealed plates until 120 hours post fertilization (hpf). Each individual embryo was scored for mortality and morphological malformations at 120 hpf. Only surviving embryos were accounted for when assessing for malformation. Fifteen morphological malformations were evaluated: yolk sac edema, bent body axis, eye, snout, jaw, otolith pericardial edema, brain, somite, caudal fin, pectoral fin,

circulation, pigmentation, trunk length, and swim bladder. Representative images were captured of malformed embryos using an Infinity 3 CCD camera. The percent mortality and total malformations were calculated and graphed as a mean of three replicates with standard error bars.

***Determination of Nanoparticle Uptake by ICP-MS:*** Embryos were exposed beginning at six hpf to PbS nanoparticle solutions of 10, 20, 40, 80, 160, and 320 µg/mL, and the embryos were sampled at 12 hpf to quantify their overall lead tissue concentrations. For each exposure group, three embryos were removed with plastic pipette tips and washed with 40 µL of Milli-Q water three times in a 35mm plastic petri dish. The pooled embryos were placed into individual 14mL round bottom plastic tubes and stored at -20ºC until time to sample. Twelve hours prior to sampling, the embryos were digested using 98 µL nitric acid; 1 ppb of internal standard (Indium, Rhenium and Bismuth) was added; and, the samples were brought to a total volume of 5mL with Milli-Q water. Samples were vortexed for 10 seconds prior to being placed into the autosampler racks. The ICP-MS was calibrated using a lead standard in 0.5% $HNO_3$ at five concentrations (0.01, 0.1, 1, 5, 10 ppb) with 1 ppb internal standards. The calibration curve created by the standard solutions had an $R^2$ value of 0.992. The mass of lead contained in each embryo was calculated from the measured lead concentration of the aliquots and the dilution factor.

***Statistics*:** All analyses were compiled using SigmaStat/Plot 11 (SPSS Inc, Chicago, IL). Dose response significance was determined using one-way ANOVA ($p<0.05$) and Dunnetts post hoc tests. All exposure groups consisted of 24 individually exposed embryos (N=24), three replicates unless otherwise noted with 80% confidence of significant difference.

## Results

### PbS Nanoparticles Synthesized through Ligand Exchange from a Common Core

Sodium 3-mercaptopropanesulfonate (MT), or sodium 2,3-dimercaptopropanesulfonate (DT) capped lead sulfide nanoparticles were synthesized (**Figure 1a**) and purified in an identical manner, using a biphasic exchange from oleic acid-capped lead sulfide nanoparticles (see Materials and Methods). Furthermore, each toxicological trial was performed using PbS-MT and PbS-DT nanoparticles prepared from the same parent batch of oleic-acid-capped nanoparticles. This was done to minimize the possibility that differences in biological response arose from different synthesis preparations. In addition, post-synthesis characterization of the nanoparticle cores was also conducted. Transmission electron microscopy (TEM) was used to image and calculate average nanoparticle sizes. Size analysis performed on TEM micrographs of representative samples of PbS-MT (**Figures 1c**) and PbS-DT (**Figure 1d**) revealed similar average particle diameters (3.0 and 3.5 nm,

respectively). Corresponding near-infrared (NIR) absorption spectroscopy experiments (**Figure 1b**) showed close spectral overlap between the two materials, with exciton peaks observed at 1188 (PbS-MT) and 1202 nm (PbS-DT). Both TEM and NIR absorption measurements were done on freshly-made particles and indicate initial properties. Precipitation of the nanoparticles over the course of the zebrafish exposures made post-exposure characterization infeasible.

## PbS-MT, PbS-DT and Lead Nitrate Elicit Differential Biological Responses

Embryos were exposed to suspensions of lead sulfide nanoparticles capped with either the monothiol sodium 3-mercaptopropanesulfonate (PbS-MT) or the dithiol sodium 2,3- dimercaptopropanesulfonate (PbS-DT) over a two-fold concentration (10 - 320 µg/mL) range to determine if the nanoparticles elicited embryo mortality or induced developmental malformations. Exposure to PbS-MT induced mortality in 100% of the animals at 160 µg/mL **(Figure 2a)**. At concentrations as low as 20 µg/mL, PbS-MT induced 20% mortality in the embryos, the remaining 80% survivors had an average of five malformations **(Figure 2b).** The multiple malformations observed upon PbS-MT exposure are visually represented in **Figure 3b** and include bent body axis, jaw, brain, and snout. At 40 and 80 µg/mL, the incidence of mortality was statistically significant ($p<0.001$) and increased to 75% and 92%, respectively. All surviving embryos exposed to PbS-MT

displayed multiple malformations, with an average of 4.5 at 40 µg/mL (**Figure 2b, 3b**). Embryos exposed to PbS-DT nanoparticles, however, did not display statistically significant mortality at the same concentrations tested for PbS-MT (**Figure 2a,b; 3c**). PbS-DT exposed embryos had a consistent number of malformations (between 1.5 - 2.3) at concentrations between 10 and 320 µg/mL, which is similar to that observed at higher concentrations (>80 µg/mL) for the ionic lead control sample, lead nitrate ($Pb(NO_3)_2$). The lead nitrate control was intended to model the extreme situation where the NPs entirely decomposed into water soluble lead salts, which is admittedly unlikely given the insolubility of PbS ($K_{sp}$ of $2.5 \times 10^{-27}$). Lead nitrate is soluble in pure water, but the presence of carbonate and other anions in the FW used for the experiments leads to some precipitation. Further, the addition of $Pb(NO_3)_2$ also results in acidification of the FW to as low as 5.2 at the highest concentrations. It is noted that PbS-MT and Pb-DT are soluble in FW at the concentrations used in this study, and their addition does not affect the pH. The various equilibria involving lead ion in FW means that the listed concentrations for $Pb(NO_3)_2$ do not necessarily represent the concentration of freely soluble lead. Nevertheless, $Pb(NO_3)_2$ remains a good control because the same equilibria affecting its bioavailability also operate on any ionic lead leached from the nanoparticles. The onset of mortality in $Pb(NO_3)_2$ exposures occurred at a greater concentration than that observed for PbS-MT exposures. Embryos exposed to 10 – 40 µg/mL of lead nitrate had 0.25 or fewer malformations, but

the average number of malformations rose to 2.3 at 160 µg/mL. Lead nitrate induced a statistically significant increase in bent body axis in the embryo (**Figure 3d**) at 160 µg/mL. Near 320 µg/mL, 100% mortality was observed for both $Pb(NO_3)_2$ and PbS-MT. At this concentration, no significant mortality was observed for PbS-DT exposures.

## Monothiol and Dithiol Ligands Did Not Induce Biological Responses

To determine if the ligands themselves were responsible for the adverse biological response, embryonic zebrafish were exposed to MT and DT ligands independent of the nanoparticles. Both ligands were tested at the same concentrations used for the nanoparticle exposures. These concentrations were greater than the ligand concentrations in the corresponding nanoparticle solutions, since the ligands make up only a fraction of the nanoparticle-ligand complex. As seen in **Figures 2c, and d**, there was no statistically significant increase in malformation or mortality observed in embryos exposed to the ligands.

## PbS-MT Nanoparticles Decomposed More Readily Than PbS-DT

PbS-MT and PbS-DT nanoparticles are known to precipitate from aqueous solution upon exposure to air, however, the effects of salinity from exposure to FW were hitherto unexplored. To test the relative stabilities of PbS-MT and PbS-DT nanoparticles in FW, dynamic light scattering (DLS)

measurements were performed. Although zebrafish exposures were made using unfiltered nanoparticle solutions, DLS measurements required pre-filtering to remove dust that could affect the scattering experiments. Hydrodynamic radii were measured at times 0, 24, 48, and 120hr. Both samples showed evidence of agglomeration with hydrodynamic radii greater than the average nanoparticle diameter. However, PbS-MT exhibited greater particle size and destabilized more quickly than the PbS-DT samples. PbS-DT samples maintained a consistent particle size of ~80 nm at 0, 24, and 48hr, but had completely precipitated by 120hr. Conversely, PbS-MT samples had average hydrodynamic radii of 140 nm at 0 hr and 340 nm at 24hr, and had completely precipitated by 48hr.

It was hypothesized that degradation of the nanoparticle cores could follow precipitation and give rise to ionic lead decomposition products. To quantify the concentration of ionic lead after five-day exposure to air (aged), nanoparticle solutions were monitored using an Inductively Coupled Plasma – Optical Emission Spectrometer (ICP-OES). Aged solutions were first centrifuged to remove insoluble species (i.e. precipitated nanoparticles), and the resulting supernatant digested with nitric acid. The lead content in the supernatants of the aged nanoparticle solutions was 87 +/- 0.4 ppm (4% recovery rate) for PbS-MT, and 1.075 +/- 0.002 ppm (0.02% recovery rate) for PbS-DT, a statistically significant difference. It is important to note that the 87 ppm lead content measured for the aged PbS-MT sample is not due to the

original nanoparticles; fresh solutions of PbS-MT nanoparticles at this concentration are clearly colored due to absorption from the nanoparticle core, whereas the supernatant was colorless. Precaution was taken to ensure that differences in lead concentration seen in the supernatants of the aged solutions was not simply due to different starting concentrations of nanoparticles in the fresh solutions. As a control, aliquots of the fresh nanoparticle solutions were digested with nitric acid, and the total lead content measured in an analogous manner using ICP-OES. Analysis of the fresh nanoparticle solutions revealed a similar amount of lead present for the two materials (**Figure 4**). PbS-MT had 1927 +/- 7 ppm of lead while PbS-DT had 2270 +/- 10 ppm (**Figure 4a**), corresponding to approximately 90% and 110% recovered lead for PbS-MT and PbS-DT, respectively (**Figure 4b**). This study demonstrates that the nanoparticles were decomposing over time, releasing ionic lead into solution.

**Lead Quantified in PbS-MT, PbS-DT and Lead Nitrate Exposed Embryos**

Inductively Coupled Plasmas – Mass Spectrometry (ICP-MS) was used to quantify the amount of lead in or tightly associated to the embryo. These measurements were done to determine if the differential biological response to the PbS could be explained by differences in particle uptake. Embryos were exposed to concentrations (0 - 320 µg/mL) of either PbS-MT, PbS-DT, or $Pb(NO_3)_2$ and samples were collected at 12 hpf. At this developmental time

point, there was no strict dose-dependent increase in lead uptake at low concentration; however, there was a significant increase in lead concentration following 160 µg/mL lead exposure for PbS-MT. A dose-dependent increase in the tissue concentration of lead was observed in the PbS-DT and $Pb(NO_3)_2$ exposed embryos **(Figure 5)**. PbS-DT exposed embryos had the highest lead level for all concentrations up until 160 µg/mL, where PbS-MT embryos had significantly more lead tissue burden.

## Discussion

In this *in vivo* study, we find that the biological response following exposure to lead sulfide nanoparticles (PbS-NPs) is influenced greatly by surface functionalization. Two major effects can be gleaned from the exposure trials. First, DT-functionalized PbS nanoparticles (PbS-DT) elicit fewer responses than MT-functionalized PbS nanoparticles (PbS-MT). Exposure to PbS-MT induces 100% mortality at 160 µg/mL in zebrafish embryos at 120 hpf and also a variety of sublethal malformations. Conversely, embryos exposed to PbS-DT elicit little to no mortality and fewer sublethal adverse responses. Second, PbS-MT exposure causes significantly more, and PbS-DT significantly less, mortality than the ionic lead source, lead nitrate ($Pb(NO_3)_2$). PbS-MT and $Pb(NO_3)_2$ exposed embryos were morphologically similar at concentrations near the onset of mortality. The simplest explanation for these results is a correlation between toxicity and nanoparticle stability.

Destabilization of the nanoparticles occurs over the course of the exposure. The two ligands offer differential resistance to this destabilization, leading to differential biological responses in the embryos.

Nanoparticle stability can greatly influence exposure of the core surface. Thiolate ligands at the metal chalcogenide nanoparticle-ligand interface are susceptible to oxidative decomposition (Aldana et al. 2001, Moody et al. 2008). This instability can lead to ligand desorption, resulting in particle agglomeration, greater exposure of the nanoparticle core, and decomposition of the core with the possible generation of soluble ionic lead species.

To our knowledge, no prior toxicity studies have been conducted on PbS-NPs; however, lessons can be learned from studies on other material sets. In general, nanoparticles have been observed to cause cytotoxicity (Lewinski et al. 2008), oxidative stress (Long et al. 2006), and immune responses (Dobrovolskaia and McNeil 2007), either through biochemical interactions with the nanoparticles themselves or from their toxic decomposition products. The ligand shell can influence toxicity by affecting nanoparticle uptake and distribution in biological systems (Goldsmith and Leary 2009) or as an integral part of the entire nanoparticle-ligand assembly. The accessibility of the nanoparticle core has also been implicated as a potentially important factor. Nanoparticles that have a denser coverage of surface ligands, or are encapsulated by an inert material (Zhang et al. 2006),

are generally less toxic than those particles that offer greater access to the core.

Prior comparisons between PbS-MT and PbS-DT nanoparticles have shown that both materials are susceptible to oxidative decomposition in aqueous solution (Moody et al. 2008). Specifically, the thiol head groups of both MT and DT ligands oxidize to form disulfides, which bind poorly to the nanoparticle surface. The MT ligands oxidize relatively quickly, resulting in rapid ligand desorption and nanoparticle precipitation. Oxidation of the DT ligands proceeds more slowly, and in a manner, which leaves the ligands partially attached to the nanoparticle surface. Although these studies were not conducted in fish water, they suggest that differential decomposition could play a role in the observed biological effects.

In this study, differential stability resulting from different surface functionalization is implicated as the major contributor to the differential biological response to the nanoparticles. DLS measurements performed on nanoparticles in fish water showed that although solution salinity affects agglomeration, PbS-DT nanoparticles are more stable than PbS-MT nanoparticles, just as in prior studies using nanoparticle solutions in deionized water. Core size was not a significant variable in the differential response. Direct comparisons of PbS-MT and PbS-DT nanoparticles were conducted using nanoparticles prepared from the same OLA-capped precursor, and exhibited similar core-related properties. Effects from the ligands themselves

were also ruled out as significant factors, as they induce no to low incidence of mortality and morbidity. It is certainly possible that the differential response of the nanoparticles is due to differences in the biological interactions of the entire intact nanoparticle structure. We look to oxidative stability as the likely differentiator, however, because it is the most notable difference in the physicochemical properties of the nanoparticles. The differential oxidative stability is due to the ligand head group (monothiol vs. dithiol).

The mechanism for how the different decomposition rates of PbS-MT and PbS-DT result in differential nanoparticle-biological interactions remains unclear. Two likely causes for the toxicity are interactions with either 1) presumably ionic lead decomposition products or 2) the exposed nanoparticle cores. The primary reason the interaction cannot be distinguished is the challenge of quantifying dose. Two studies shed light on the dose of either nanoparticles or its decomposition products received by the embryos. The first is the ICP-OES measurements performed on aged nanoparticle solutions. Soluble lead products are observed during the oxidative decomposition and precipitation of the nanoparticles, with a much greater concentration of ionic lead observed for PbS-MT relative to PbS-DT. Analysis of the fresh PbS-MT and PbS-DT solutions began with similar concentrations of nanoparticles. However, analysis of the aged solutions show that the two ligands are not equal in their protection of the nanoparticle surface; as they decompose and precipitate, MT-capped nanoparticles leach ~ 80 times more ionic lead into

solution than DT-capped nanoparticles. As the PbS-NP solutions age, ligands are oxidized and desorb from the nanoparticle surface, resulting in nanoparticle precipitation. During this process, lead can leach from exposed sites on the nanoparticle cores. The concentration of soluble lead decomposition products observed in the aging studies was below the onset of toxicity at 160 μg/mL for $Pb(NO_3)_2$, even given the much higher concentration (3000 μg/mL) of nanoparticles used for the ICP-OES studies than for the toxicity studies. What is important, however, is not simply the concentration of soluble lead in the fish water but the actual dose received by the embryos. This dose is dependent on the distribution of nanoparticles, which suggests that the PbS-NPs are associating with the embryos in the exposure media and resulting in localized soluble lead decomposition products.

Tissue uptake studies were performed in an attempt to better define the dose. In these studies, exposed embryos were washed and then analyzed for lead content using ICP-MS. One limitation of this technique is that no distinction can be made between lead tightly bound to, or within the embryo. Visual inspections of the embryos after exposure revealed signs of adsorbed nanoparticles. It is hypothesized that at higher concentrations, nanoparticle solutions are more susceptible to agglomeration, and that these agglomerates may adhere preferentially to the embryos. This effect would substantially increase the local concentration of lead around the embryos, leading to increased uptake relative to a uniform solution distribution. Note that the

uptake studies were performed at early exposure times. At these early times, only the PbS-MT induced substantial mortality at 320 μg/mL. Near the onset of this mortality (160 μg/mL), the PbS-MT nanoparticles exhibited a sharp increase in uptake to levels higher than those observed for either the PbS-DT or $Pb(NO_3)_2$ exposures.

The uptake and decomposition studies do not definitively distinguish between direct nanoparticle toxicity and nanoparticle decomposition product toxicity. The differential toxicity of the PbS-MT vs. PbS-DT nanoparticles can be explained by greater exposure of the nanoparticle core in the former during decomposition. This mechanism also provides a simple explanation for the greater toxicity of the PbS-MT nanoparticles relative to $Pb(NO_3)_2$. Alternatively, nanoparticle decomposition products could be responsible for the increased toxicity of PbS-MT relative to PbS-DT consistent with the greater amount of lead observed to leach from aged solutions of the PbS-MT. The enhanced toxicity of PbS-MT relative to $Pb(NO_3)_2$ is explained by the agglomeration of nanoparticles on or in the embryos, which acts to increase the local lead concentration. Such a local increase is consistent with the substantial lead uptake observed near the onset of toxicity (160 μg/mL) in the 12 hpf uptake studies.

Further studies will be needed to differentiate between the biological interactions with either the nanoparticle cores and/or soluble decomposition products. Regardless, these studies illustrate the substantial changes in

nanoparticle toxicity that can be induced by a relative minor change in ligand composition. With the knowledge that manipulating physicochemical properties of nanoparticles results in differential biological responses, a systematic methodical use of the rapidly developing embryonic zebrafish model will aid in elucidating the key design principles to develop minimal to non-toxic nanoparticles.

Additionally, these studies using the PbS-NPs highlight the important role nanoparticle decomposition plays in toxicity. The possibility of ionic lead leaching from the nanoparticles also suggests that more studies should be conducted to understand the poorly-known mechanisms of lead toxicity. Physicochemical characterization of NPs in their synthesis media is important, but as demonstrated in these studies, it is critical to conduct characterization of the NPs in exposure media in parallel to toxicity assessments to gain a better understanding of aggregation state and other physicochemical properties. As the field of nanotechnology expands and matures, greater understanding of the nanomaterial-biological interface will be imperative.

## Conclusions

The data presented demonstrates the usefulness of the embryonic zebrafish model as a platform to rapidly assess the nanomaterial-biological interaction of nanoparticles. With this set of nanoparticles, different biological responses between PbS-MT and PbS-DT nanoparticles was attributed to

differences in their rates of decomposition. This study illustrates the importance of using well-characterized nanoparticles both from the start, as well as over time. It also opens discussion on the hitherto unexplored biological interactions of lead sulfide nanoparticles. Use of the embryonic zebrafish to conduct nanomaterial-biological interaction assessments will increase the speed at which key physicochemical properties will be identified and used to implement a design rule to produce safer nanomaterials.

## References

Aldana J, Wang YA, Peng XG. 2001. Photochemical instability of CdSe nanocrystals coated by hydrophilic thiols. Journal of the American Chemical Society 123: 8844-8850.

ATSDR (2007). Toxicological profile for lead. U. S. P. H. Service and U. S. D. o. H. a. H. Services. Atlanta, GA.

Barbazuk WB, Korf I, Kadavi C, Heyen J, Tate S, Wun E, Bedell JA, McPherson JD, Johnson SL. 2000. The syntenic relationship of the zebrafish and human genomes. Genome Res 10: 1351-8.

Bharali DJ, Khalil M, Gurbuz M, Simone TM, Mousa SA. 2009. Nanoparticles and cancer therapy: A concise review with emphasis on dendrimers. International Journal of Nanomedicine 4: 1-7.

De Gennardo LD. 1978. The effects of lead nitrate on the central nervous system of the chick embryo I. Observations of light and electron microscopy. Growth 42: 141-55.

Dobrovolskaia MA, McNeil SE. 2007. Immunological properties of engineered nanomaterials. Nature Nanotechnology 2: 469-478.

Dodd A, Curtis PM, Williams LC, Love DR. 2000. Zebrafish: bridging the gap between development and disease. Hum Mol Genet 9: 2443-9.

Furgeson D, Bar-llan O, Albrecht R, Fako V. 2009. Toxicity Assessments of Multisized Gold and Silver Nanoparticles in Zebrafish Embryos. Small 5: 1-14.

Goldsmith M-M, Leary J. 2009. Nanobiosystems. WIREs Nanomed Nanobiotechnology 1: 553-567.

Guo L, Bussche AV, Buechner M, Yan AH, Kane AB, Hurt RH. 2008. Adsorption of essential micronutrients by carbon nanotubes and the implications for nanotoxicity testing. Small 4: 721-727.

Haendel MA, Tilton F, Bailey GS, Tanguay RL. 2004. Developmental toxicity of the dithiocarbamate pesticide sodium metam in zebrafish. Toxicological Science 81: 390-400.

Hall JB, Dobrovolskaia MA, Patri AK, McNeil SE. 2007. Characterization of nanoparticles for therapeutics. Nanomedicine (Lond) 2: 789-803.

Hill AJ, Teraoka H, Heideman W, Peterson RE. 2005. Zebrafish as a model vertebrate for investigating chemical toxicity. Toxicological Sciences 86: 6-19.

Hinds S, Myrskog SH, Levina L, Koleilat GI, Yang J, Kelley SO, Sargent EH. 2007. NIR-Emitting Colloidal Quantum Dots Having 26% Luminescence Quantum Yield in Buffer Solution. Journal of the American Chemical Society 129: 7218-7219.

Hoshino A, Fujioka K, Oku T, Suga M, Sasaki YF, Ohta T, Yasuhara M, Suzuki K, Yamamoto K. 2004. Physicochemical properties and cellular toxicity of nanocrystal quantum dots depend on their surface modification. Nano Letters 4: 2163-2169.

Hyun B, Chen H, Rey DA, Wise FW, Batt CA. 2007. Near-Infrared Fluorescence Imaging with Water-Soluble Lead Salt Quantum Dots. Journal of Physical Chemistry B 111: 5726-5730.

Kimmel CB, Ballard WW, Kimmel SR, Ullmann B, Schilling TF. 1995. Stages of embryonic development of the zebrafish. Dev Dyn 203: 253-310.

Kirchner C, Liedl T, Kudera S, Pellegrino T, Javier AM, Gaub HE, Stolzle S, Fertig N, Parak WJ. 2005. Cytotoxicity of colloidal CdSe and CdSe/ZnS nanoparticles. Nano Letters 5: 331-338.

Koleilat GI, Levina L, Shukla H, Myrskog SH, Hinds S, Pattantyus-Abraham AG, Sargent EH. 2008. Efficient, stable infrared photovoltaics based on solution-cast colloidal quantum dots. ACS Nano 2: 833-40.

Konstantatos G, Howard I, Fischer A, Hoogland S, Clifford J, Klem E, Levina L, Sargent EH. 2006. Ultrasensitive solution-cast quantum dot photodetectors. Nature 442: 180-3.

Konstantatos G, Huang C, Levina L, Lu Z, Sargent EH. 2005. Efficient Infrared Electroluminescent Devices Using Solution-Processed Colloidal Quantum Dots. Advanced Functional Materials 15.

Kotov NA, Winter JO, Clements IP, Jan E, Timko BP, Campidelli S, Pathak S, Mazzatenta A, Lieber CM, Prato M, et al. 2009. Nanomaterials for Neural Interfaces. Advanced Materials 21: 3970-4004.

Lewinski N, Colvin V, Drezek R. 2008. Cytotoxicity of nanoparticles. Small 4: 26-49.

Lim YT, Kim S, Nakayama A, Stott NE, Bawedi MG, Fragioni JV. 2003. Selection of Quantum Dot Wavelengths for Biomedical Assays and Imaging. Molecular Imaging 2: 50-64.

Liu J, Aruguete DM, Murayama M, Hochella MF. 2009. Influence of Size and Aggregation on the Reactivity of an Environmentally and Industrially Relevant Nanomaterial (PbS). Environmental Science & Technology 43: 8178-8183.

Long TC, Saleh N, Tilton RD, Lowry GV, Veronesi B. 2006. Titanium dioxide (P25) produces reactive oxygen species in immortalized brain microglia (BV2): Implications for nanoparticle neurotoxicity. Environmental Science & Technology 40: 4346-4352.

McDonald SA, Konstantatos G, Zhang S, Cyr PW, Klem EJ, Levina L, Sargent EH. 2005. Solution-processed PbS quantum dot infrared photodetectors and photovoltaics. Nat Mater 4: 138-42.

Meng H, Chen Z, Xing GM, Yuan H, Chen CY, Zhao F, Zhang CC, Zhao YL. 2007. Ultrahigh reactivity provokes nanotoxicity: Explanation of oral toxicity of nano-copper particles. Toxicology Letters 175: 102-110.

Minchin RF, Martin DJ. 2010. Nanoparticles for molecular imaging--an overview. Endocrinology 151: 474-81.

Moody IS, Stonas AR, Lonergan MC. 2008. PbS Nanocrystals Functionalized with a Short-Chain, Ionic, Dithiol Ligand. Journal of Physical Chemistry C 112: 19383-19389.

Newman MD, Stotland M, Ellis JI. 2009. The safety of nanosized particles in titanium dioxide- and zinc oxide-based sunscreens. Journal of the American Academy of Dermatology 61: 685-692.

Parng C. 2005. *In vivo* zebrafish assays for toxicity testing. Curr Opin Drug Discov Devel 8: 100-6.

Rubinstein AL. 2003. Zebrafish: from disease modeling to drug discovery. Curr Opin Drug Discov Devel 6: 218-23.

Samia ACS, Chen XB, Burda C. 2003. Semiconductor quantum dots for photodynamic therapy. Journal of the American Chemical Society 125: 15736-15737.

Sharma V, Sharma A, Kansal L. 2010. The effect of oral administration of Allium sativum extracts on lead nitrate induced toxicity in male mice. Food and Chemical Toxicology 48: 928-936.

Teraoka H, Dong W, Hiraga T. 2003. Zebrafish as a novel experimental model for developmental toxicology. Congenit Anom (Kyoto) 43: 123-32.

Ton C, Lin Y, Willet C. 2006. Zebrafish as a model for developmental neurotoxicity testing. Birth Defects Research A Clin Mol Teratol 76: 553-67.

Usenko CY, Harper SL, Tanguay RL. 2007. *In vivo* evaluation of carbon fullerene toxicity using embryonic zebrafish. Carbon N Y 45: 1891-1898.

White LD, Cory-Slechta DA, Gilbert ME, Tiffany-Castiglioni E, Zawia NH, Virgolini M, Rossi-George A, Lasley SM, Qian YC, Basha MR. 2007. New and evolving concepts in the neurotoxicology of lead. Toxicol Appl Pharmacol 225: 1-27.

Wise JS, Goodale B, Wise S, Craig G, Pongan A, Walter R, Thompson W, Ng A, Aboueissa A, Mitani H, et al. 2009. Silver nanospheres are cytotoxic and genotoxic to fish cells. Aquatic Toxicology 97: 34-41.

Yang LX, Ho NY, Alshut R, Legradi J, Weiss C, Reischl M, Mikut R, Liebel U, Muller F, Strahle U. 2009. Zebrafish embryos as models for embryotoxic and teratological effects of chemicals. Reproductive Toxicology 28: 245-253.

## Acknowledgements

We would like to thank Sinnhuber Aquatic Research Laboratory for the embryos and Cari Buchner for her technical assistance. These studies were partially supported by National Institute of Environmental Health Sciences (NIEHS) P3000210, the Air Force Research Laboratory (AFRL) under agreement number FA8650-05-1-5041, Environmental Protection Agency (EPA) RD-833320, and the National Science Foundation (NSF) IGERT Fellowship program under Grant No. DGE-0549503. The views and conclusions contained herein are those of the authors and should not be interpreted as necessarily representing the official policies or endorsements, either expressed or implied, of NIEHS, AFRL, EPA, NSF or the U.S. Government. Further support was provided by the W.M Keck Foundation.

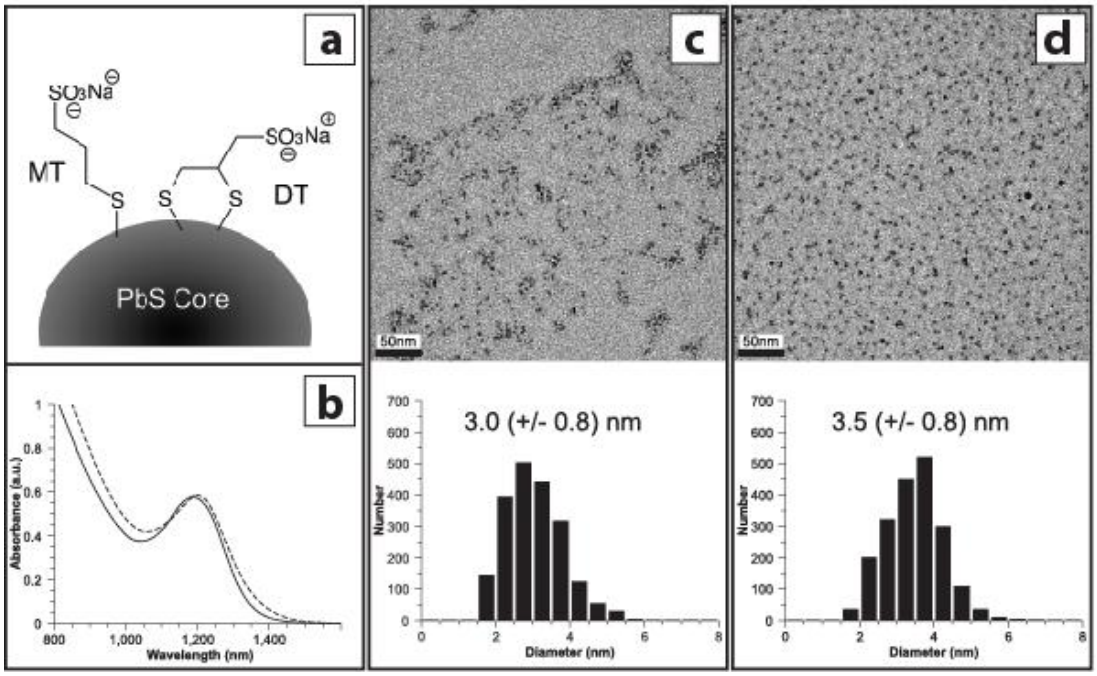


**Figure 2- 1. Physical properties of PbS-MT and PbS-DT nanoparticles.** (a) Schematic of two ligands used in the study – sodium 3-mercaptopropane sulfonate (MT) and sodium 2,3-dimercaptopropane sulfonate (DT). (b) Near-infrared absorption spectra of solutions of PbS-MT(*solid*) and PbS-DT (*dashed*) nanoparticles. Peak position is indicative of average particle size. Plots were scaled to better illustrate spectral overlap. (c and d) TEM images of PbS-MT and PbS-DT, respectively, with corresponding particle size histograms. Scale bars represent 50 nm. Values in histograms show average nanoparticle diameter, with standard deviation in parentheses.

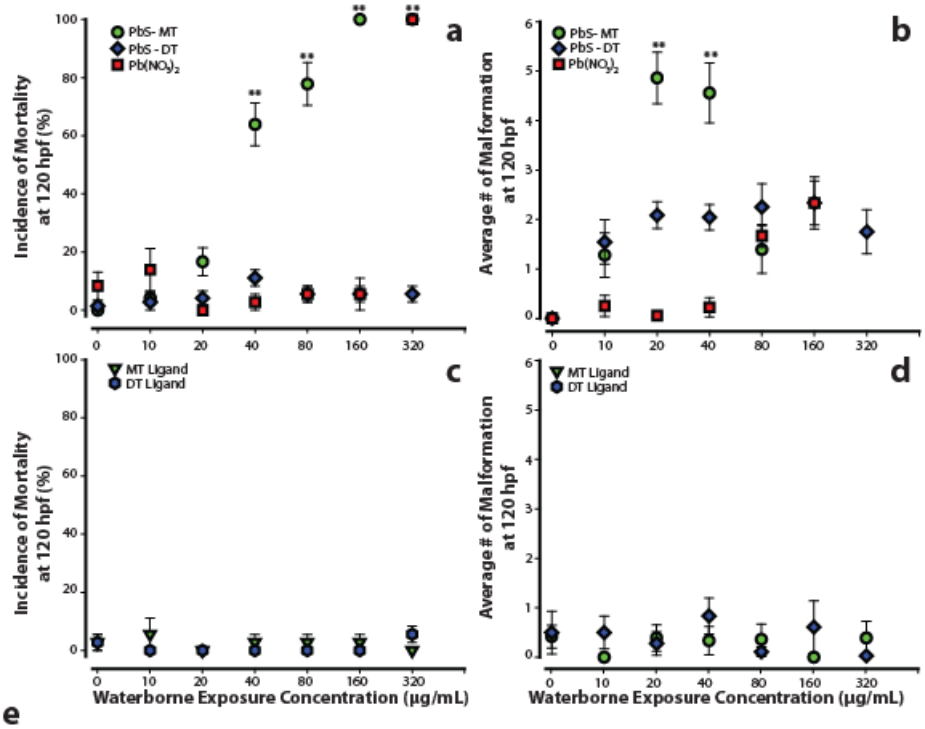


e

| Waterborne Exposure Concentration (µg/mL) | Bent Body Axis (%) | | | Eye Malformation (%) | | | Snout Malformation (%) | | | Jaw Malformation (%) | | |
|---|---|---|---|---|---|---|---|---|---|---|---|---|
| | PbS-MT | PbS-DT | $Pb(NO_3)_2$ | PbS-MT | PbS-DT | $Pb(NO_3)_2$ | PbS-MT | PbS-DT | $Pb(NO_3)_2$ | PbS-MT | PbS-DT | $Pb(NO_3)_2$ |
| 0 | 0 ± 0 | 0 ± 0 | 0 ± 0 | 0 ± 0 | 0 ± 0 | 0 ± 0 | 0 ± 0 | 0 ± 0 | 0 ± 0 | 0 ± 0 | 0 ± 0 | 0 ± 0 |
| 10 | 11.6 ± 3.3 | 72.2 ± 5.5 | 2.8 ± 2.8 | 0 ± 0 | 5.6 ± 2.8 | 2.8 ± 2.8 | 8.6 ± 0.3 | 5.6 ± 2.8 | 2.8 ± 2.8 | 8.6 ± 0.3 | 5.6 ± 2.8 | 2.8 ± 2.8 |
| 20 | 93.3 ± 6.6 | 59.8 ± 7.7 | 2.8 ± 2.8 | 20 ± 6.9 | 23.2 ± 8.1 | 0 ± 0 | 66.7 ± 0 | 5.8 ± 2.9 | 0 ± 0 | 61.1 ± 2.8 | 5.8 ± 2.9 | 0 ± 0 |
| 40 | 88.9 ± 5.6 | 77.8 ± 4.0 | 2.8 ± 2.8 | 88.9 ± 5.6 | 2.8 ± 2.8 | 0 ± 0 | 94.4 ± 5.6 | 2.8 ± 2.8 | 0 ± 0 | 94.4 ± 5.6 | 5.6 ± 2.8 | 4.2± 4.2 |
| 80 | 33.3 ± 0 | 67.2 ± 4.3 | 52.8 ± 3.8 | 33.3 ± 0 | 17.8 ± 4.9 | 6.1 ± 3.0 | 100 ± 0 | 13.3 ± 6.7 | 0 ± 0 | 100 ± 0 | 16.1 ± 3.9 | 0 ± 0 |
| 160 | - | 75 ± 0 | 58.3 ± 4.8 | - | 11.7 ± 2.5 | 11.1 ± 2.8 | - | 2.8 ± 2.8 | 8.3 ± 4.2 | - | 2.8 ± 2.8 | 8.3 ± 4.2 |
| 320 | - | 62.4 ± 8.8 | - | - | 8.6 ± 0.3 | - | - | 2.8 ± 2.8 | - | - | 2.8 ± 2.8 | - |

**Figure 2- 2. Mortality and malformation curves for embryos exposed to PbS-MT, PbS-DT, Pb(NO3)2, and MT and DT ligands.**

Embryos were exposed to PbS-MT, PbS-DT or $Pb(NO_3)_2$ at 6 hpf and were evaluated for malformations and mortality at 120 hpf. Mortality **(a)** was statistically significant for PbS-MT (40 - 320 µg/mL) and $Pb(NO_3)_2$ (only at 320 µg/mL). All surviving embryos exposed to PbS-MT had malformations (average of 5 at 20 µg/mL) **(b)**. $Pb(NO_3)_2$ exposed embryos had little to no malformations (<0.25) up until 40 µg/mL, where a steady increase of malformations was observed at 80 and 160 µg/mL. PbS-DT exposed embryos caused a consistent number of malformations (~2) at all concentrations. A summary of the statistically significant malformations observed in PbS-MT, PbS-DT and $Pb(NO_3)_2$ exposed embryos is visualized in a table **(e)**, where shaded boxes indicate statistical significance (Fishers Exact, $p<0.05$). MT and DT ligands did not induce mortality **(c)** or malformations **(d)** in exposed embryos. Data presented with ** designate statistically significant values (Fishers Exact, **$p<0.001$). Three replicates, n=24.

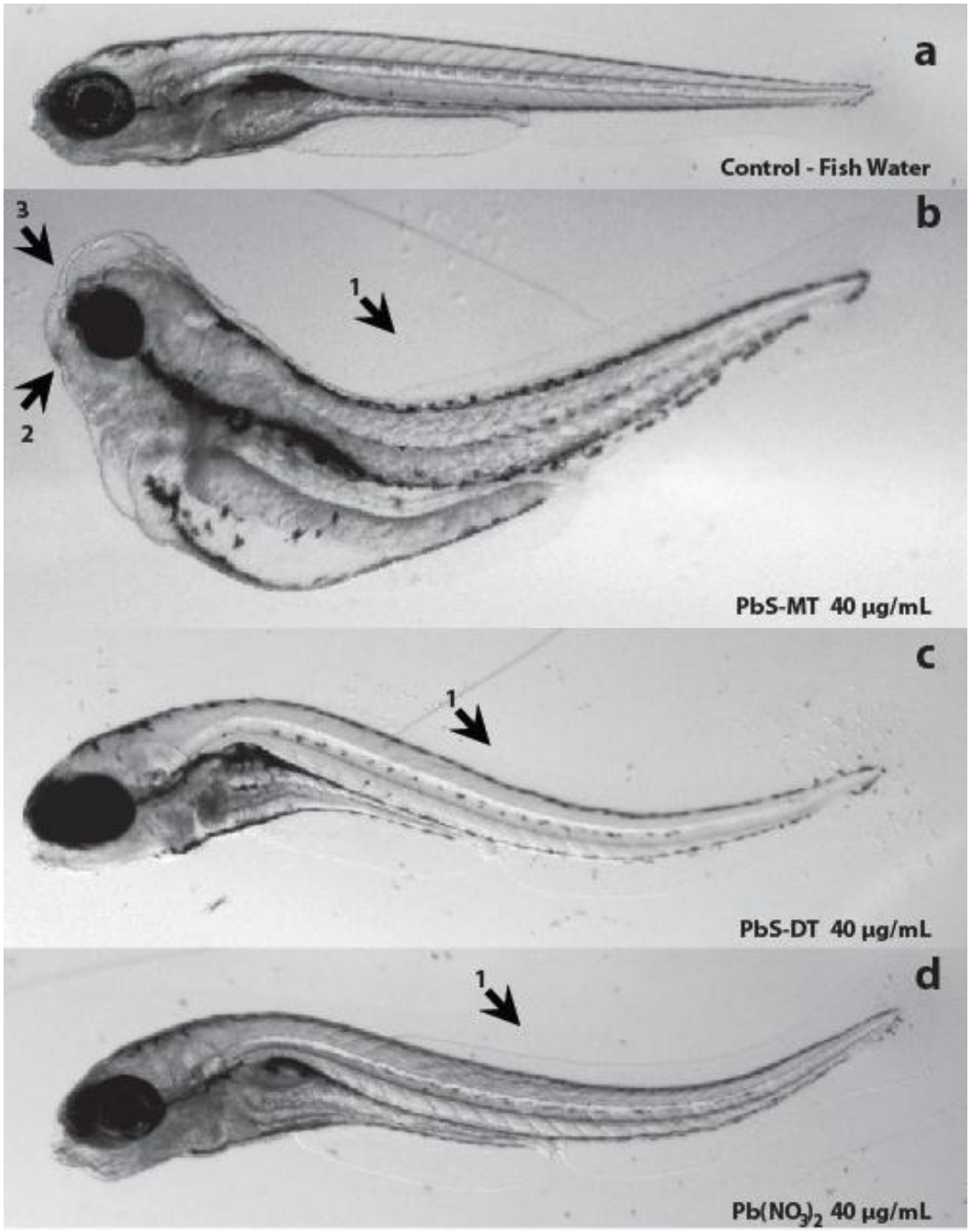


**Figure 2- 3. Representative images of exposed zebrafish embryos.** Embryonic zebrafish exposed to PbS-MT nanoparticles **(b)** and $Pb(NO_3)_2$ **(d)** induced a statistically significant increase in bent body axis (1), jaw (2) and snout (3) malformation compared to control **(a)**. PbS-DT **(c)** elicited a statistically significant increase in bent body axis, and jaw malformation, but not snout abnormalities. All images were taken at 120 hpf, and except for the control embryo, represent exposures at a concentration of 40 µg/mL.

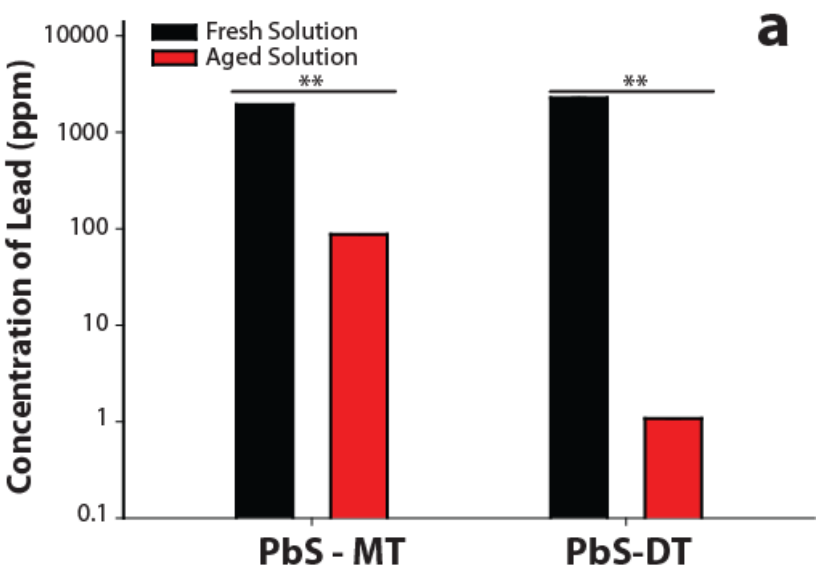


b

| | PbS-MT | PbS-DT |
|---|---|---|
| Theoretical Concentration of Pb (ppm) | 2189 | 2129 |
| Measured Concentration of Fresh Solution (ppm) | 1927 ± 7 | 2270 ± 10 |
| Pb Recovered (%) | 90% | 110% |
| | | |
| Measured Concentration of Aged Solution (ppm) | 87 ± 0.4 | 1.075 ± 0.002 |
| Pb Recovered (%) | 4% | 0.02% |

**Figure 2- 4. Concentration of lead (Pb) in fresh and aged PbS-MT and PbS-DT solutions.**

Nanoparticle solutions that were initially opened (fresh) and left to oxidize for 5 days (aged) were digested with nitric acid, and Pb concentration was measured 18 hours later **(a)** with ICP - Optical Emission Spectrometer (OES). Expected Pb percent recovery concentrations were calculated for both nanoparticles for fresh and aged solutions **(b)**. Data presented with ** designate statistically significant values (Student t-Test, **$p<0.001$).

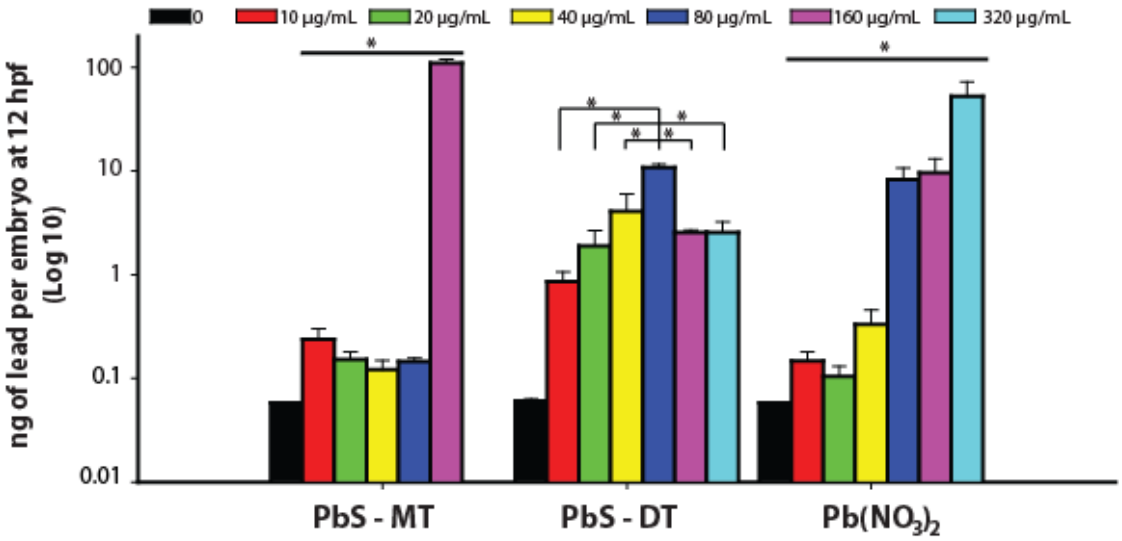


**Figure 2- 5. Tissue concentration of lead in embryos exposed to PbS-MT, PbS-DT and $Pb(NO_3)_2$.**

Embryos were exposed to 10 - 320 µg/mL solutions of PbS-MT, DT, and $Pb(NO_3)_2$ at 6 hpf and sampled at 12 hpf. Embryos exposed to PbS-MT at 320 µg/mL did not survive to the time of sampling. Both $Pb(NO_3)_2$ and PbS-DT tissue concentration followed a dose dependent manner, except PbS-DT only followed this trend until 80 µg/mL. Data presented with * designate statistically significant values (Kruskal-Wallis ANOVA - Tukey Test, $p<0.05$).

# CHAPTER 3 - SURFACE FUNCTIONALITIES OF GOLD NANOPARTICLES IMPACT EMBRYONIC GENE EXPRESSION RESPONSES

Lisa Truong [1,2], Susan C. Tilton[3], Tatiana Zaikova [2,4], Erik Richman [2,4], Katrina M. Waters[3], James E. Hutchison[2,4] and Robert L. Tanguay[1,2]

[1] Department of Environmental and Molecular Toxicology, The Sinnhuber Aquatic Research Laboratory and the Environmental Health Sciences Center at Oregon State University, Corvallis, OR;
[2] The Safer Nanomaterials and Nanomanufacturing Initiative, Oregon Nanoscience and Microtechnologies Institute
[3] Computational Biology and Bioinformatics Group, Pacific Northwest National Laboratory, Richland, Washington 99352, USA
[4] Department of Chemistry and the Materials Science Institute, University of Oregon, Eugene, Oregon 97403, USA

## Abstract

Incorporation of gold nanoparticles (AuNPs) into consumer products is increasing; however, there is a gap in available toxicological data to determine the safety of AuNPs. In this study, we utilized the embryonic zebrafish to investigate how surface functionalization and charge influences molecular responses. Precisely engineered gold nanoparticles with 1.5 nm cores were synthesized and functionalized with three ligands: 2-mercaptoethanesulfonic acid (MES), N,N,N-trimethylammoniumethanethiol (TMAT), or 2-(2-(2-mercaptoethoxy)ethoxy)ethanol (MEEE). Developmental assessments revealed differential biological responses when embryos were exposed to the functionalized AuNPs, at the same concentration. Using Inductively Coupled Plasma – Mass Spectrometry (ICP-MS), AuNP uptake was confirmed in exposed embryos. Following exposure to MES- and TMAT- AuNPs from 6-24 or 6-48 hours post fertilization, pathways involved in inflammation and immune response were perturbed. Additionally, transport mechanisms were misregulated after exposure to TMAT and MES-AuNPs, demonstrating surface functionalization influences many molecular pathways.

## Introduction

Despite the rapid growth of the nanotechnology industry, research assessing the interaction of nanoparticles and biological systems has not kept pace. At present, the mechanisms of how nanoparticles induce biological responses are poorly understood. It will be impossible to identify risk associated with nanoparticle exposure without evaluating nanoparticle interaction with biological systems. The use of an efficient and relevant toxicological model with a systematic approach to assess the nanoparticles can help fill these knowledge gaps.

Gold nanoparticles (AuNPs) have shown great potential to revolutionalize therapeutics as delivery vectors (Kim et al. 2009, Kim et al. 2009) and as ultra sensitive probes for detecting proteins (Nam et al. 2003). A suite of gold nanoparticles (AuNPs) that are well-characterized and precisely engineered is ideal to systematically isolate the effects of individual physicochemical features, or a combination of multiple properties, on biological responses. AuNPs can be synthesized with precise control over size, shape, purity, surface charge and functionalization, enabling the independent evaluation of each aspect (Shipway et al. 2000, Kim et al. 2005, Dahl et al. 2007). They are characterized using transmission electron microscopy (TEM) to determine shape and size; ultraviolet-visible absorption spectroscopy (UV-Vis) to assess core size and agglomeration state and nuclear magnetic resonance (1H NMR) to confirm that the ligands are attached to the gold core and the samples are free of or other molecular

impurities. In addition, AuNPs dose can be quantified within complex biological systems by using either Instrumental Neutron Activation Analysis (INAA) or Inductively Coupled Plasma – Mass Spectrometry (ICP-MS). It is, therefore, critical to understand all aspects of how AuNPs interact with biological systems.

There have been many proposed biological models to screen for nanomaterial bioactivity, such as cell culture and rodent models. Cell culture-based approaches are rapid, cost effective, and amendable to high-throughput analysis, but lack the complexity of whole animal systems, making it difficult to extrapolate to human safety (Teraoka et al. 2003, den Hertog 2005). Rodent models are the gold standard for safety prediction (Paigen 2003), but are labor and cost intensive, and require hundreds of milligrams or larger quantities of test material, which is impractical for evaluating numerous types of precisely engineered nanoparticles. A useful toxicological model must enable rapid assessment of the backlog of untested nanoparticles and facilitate definition of the basic nanoparticle characteristics that drive the biological response.

An emerging model to investigate how nanoparticle physicochemical properties influence biological responses is the embryonic zebrafish (Usenko et al. 2007, Truong et al. 2010, Harper et al. 2011, Truong et al. 2011, Truong et al. In Press). Zebrafish have a high degree of homology to the human genome (~80%) (Barbazuk et al. 2000) and share many cellular, anatomical and physiological characteristics with other vertebrates. The embryos are

optically clear, small in size, and have a short life cycle (Dodd et al. 2000, Rubinstein 2003, Yang et al. 2009). Embryos develop externally (Kimmel et al. 1995), thereby allowing for non-invasive assessments of the embryo over time. One of the clear advantages of using the embryonic zebrafish to assess nanomaterial-biological interactions is that much less material is required compared to rodent-based studies.

The aim of this study was to isolate one feature – surface functionalization - while keeping all the other factors (core size, composition, and shape) constant. We hoped to gain insight into understanding the toxicity of these medically relevant nanoparticles. In a previous study, three types of water soluble AuNPs were evaluated in the embryonic zebrafish (Harper, et al. 2011). The AuNPs had similar core size (~1.5 nm) and were functionalized with different ligands either N,N,N-trimethylammoniumethanethiol (TMAT), 2-mercaptoethanesulfonic acid (MES) or 2-(2-(2-mercaptoethoxy)ethoxy)ethanol (MEEE). Differential biological responses were observed for each nanoparticle type. TMAT-AuNPs were lethal to embryos, MES-AuNPs induced sublethal malformations, and MEEE-AuNPs did not induce any *in vivo* biological response. The focus of this study was to evaluate how these nanoparticle physicochemical properties induce differential biological response at a molecular level by evaluating tissue concentration and gene expression profiling.

## Materials and Methods

**Materials:** Hydrogen tetrachloroaurate (HAuCl4• H2O) was purchased from Strem (Newburyport, MA) and was used as received. Dichloromethane was distilled over phosphorous pentoxide prior to use. Chloroform was filtered through a plug of basic alumina prior to use to remove acid impurities. 2-[2-(2-mercaptoethoxy)ethoxy]ethanol (Woehrle et al. 2004) and thiocholine (N,N,N-trimethylaminoethanethiol iodide) (Warner and Hutchison 2003) were synthesized according to known procedures. All other compounds were purchased from Sigma-Aldrich Chemical Co. (St. Louis, MO) and used as received.

**Procedure for preparation of MES-, TMAT- and MEEE-AuNPs:** Water soluble 1.5 nm particles were synthesized using known procedures (Woehrle et al. 2005).

**Physicochemical characterization of nanoparticles:** Proton Nuclear Magnetic Resonance (NMR) spectra were collected at 25°C on a Varian Unity Inova 300 MHz spectrometer in D2O. UV-visible (UV-Vis) spectra were obtained on a Hewlett-Packard 8453 diode array instrument with using 1-cm quartz cuvettes. Transmission electron microscopy (TEM) images were collected at 300kV with an FEI Titan using a Cs aberration corrector. Nanoparticle samples were prepared on amine functionalized SMART grids by

soaking each in a dilute nanoparticle solution (0.2 mg/mL) and then in nanopure water for 2 minutes each. The grid was air dried. Zeta potentials were measured on samples diluted in reverse osmosis (RO) water (~ 2.5 – 9 ppm) using the ZetaPALs system (Brookhaven Instruments, Redditch, Worcestershire, UK). Each sample was diluted, vortexed and read on the machine within 5 minutes. The zeta potential for 1.5 nm MES-, TMAT- and MEEE-AuNPs in fish water were -13.3, 8.71, 2.91, respectively.

**Zebrafish maintenance and exposure protocols:** Tropical 5D zebrafish (Danio rerio) were reared in the Sinnhuber Aquatic Research Laboratory (SARL) at Oregon State University (OSU). Adults were kept at standard laboratory conditions of 28°C on a 14 h light/10 h dark photoperiod in fish water (FW) consisting of reverse osmosis water supplemented with a commercially available salt solution (0.6% Instant Ocean®). Embryos were collected and staged (Kimmel, et al. 1995) from group-spawned zebrafish. The chorion was enzymatically removed with pronase to increase bioavailability at 4 hours post fertilization (hpf) using protocols previously published (Truong, et al. 2011). Dechorionated embryos were left to rest for at least 30 minutes prior to the initiation of nanoparticle exposure. Embryos were transferred to individual wells of a 96-well plate with 100 µl of prepared nanoparticle solution. A subset of embryos with intact chorions was kept to monitor inherent clutch

quality. Exposure plates were sealed to prevent evaporation and wrapped with aluminum foil to guard against potential photo-oxidation of the nanoparticles.

**Nanoparticle Exposure:** Embryos were exposed to seven concentrations and an embryo media (EM) control (n=12, three replicates) with the highest concentration at 250 µg/mL (ppm), and five-fold dilutions down to 0.016 ppm. The static nanoparticle exposure continued under standard laboratory conditions in covered, sealed plates until 120 hpf. At 120 hpf, individual embryos were scored for mortality, then euthanized prior to evaluation of morphological malformations. For malformation statistics, only embryos that survived were considered. Fifteen morphological malformations were evaluated. The percent mortality and total malformations were calculated and graphed as a mean of three replicates. Embryo media consisted of 15 mM NaCl, 0.5 mM KCl, 1 mM MgSO4, 0.15 mM KH2PO4, 0.05 mM Na2HPO4, and 0.7 mM NaHCO3 (Westerfield 2000).

**Nanoparticle Uptake by ICP-MS**: Six hpf embryos were statically exposed to embryo media, 2, 10, 50, 250 ppm of each AuNP solution and sampled at 24 and 48 hpf to quantify overall gold tissue concentration. Briefly, for each exposure group, three embryos were washed thoroughly with milli-Q water and then placed individually into 14 mL round bottom plastic tubes and stored at -20ºC until time to sample. Twelve hours prior to sampling, the embryos

were digested using nitric acid, a final concentration of 1 ppb of internal standards (Indium, Rhenium and Bismuth) were added, and the samples were brought to a total volume of 5 mL with milli-Q water. Samples were vortexed, then placed into the autosampler racks. A five-point calibration curve (0.01, 0.1, 1, 5, 10 ppb) was created using a purchased gold standard and had a R2 value of 0.996. The number of gold particles per embryo was back-calculated using the assumption that a 1.5 nm AuNP core consists of 101 gold atoms.

**NimbleGen Zebrafish Expression Array:** Zebrafish expression arrays were printed by Roche NimbleGen (Madison, WI), based on Ensembl Zv7 build. MES- and TMAT-AuNPs gene expression was completed on the 385K format that had 37,157 genes, with 12 probes per target (60mer).

**Gene Expression Exposure and RNA Collection:** Six hpf dechorinated embryos were exposed to 1.5 nm MES- and TMAT-AuNPs at 50 and 10 ppm, respectively, and to vehicle control (fish water) as described in the above exposure protocol. Embryos were pooled into three replicates of forty embryos, euthanized using MS-222, and washed with milli-Q water. Once thoroughly washed, embryos were transferred to sterile 1.7 mL microcentrifuge tubes where excess water was removed from samples and 400 µL of TriReagent (Sigma Aldrich St. Louis, MO) was added to extract RNA. Samples were homogenized using a plastic pestle and battery operated

mortar. After homogenization, 600 µL of TriReagent was added and the samples were stored at -80ºC until processing. Twenty four and 48 hpf samples were collected for 1.5 nm MES- and TMAT-AuNPs. Once all samples were collected, homogenates were thawed on ice and centrifuged at 12,000 g at 4ºC. The supernatant was removed and transferred to a new microcentrifuge tube, where 200 µL of chloroform was added. The samples were centrifuged and the clear aqueous layer was extracted and transferred to a new microcentrifuge tube. Five hundred µL of isopropanol was added to each microcentrifuge tube. The samples were once again centrifuged, then all liquid was removed, and the RNA pellet was washed several times with 75% ethanol: RNase Free H2O. The RNA pellets were air dried and then resuspended in 12 µL with RNase Free water. A small aliquot (1 µL) was removed and diluted in 3 µL of RNase Free water. The remaining RNA was stored at -80 ºC. The aliquot was used to verify quality and quantity using a NanoDrop 1000 spectrophotometer (Thermo Scientific, Wilmington, DE) and an Agilent BioAnalyzer 2100 (Palo Alto, CA) at the Center for Genome Research and Biocomputing (CGRB) at OSU.

**Nimblegen Microarray Processing:** Ten µg of total RNA was reverse transcribed using SuperScript III and oligo (dT) primer (Invitrogen, Carlsbad, CA), and double stranded cDNA was synthesized and purified using Qiagen Minelute PCR Purification spin column. Double strand cDNA were labeled with

Cy5 dNTP, and then the samples were hybridized to 385K zebrafish gene expression arrays (Roche Nimblegen, Madison, WI) and scanned using the Axon GenePix 4200A Pro scanner (Molecular Devices, Sunnyvale, CA) with a green laser (532nm) and a hardware setting of 450 pmt, laser power of 100, and a pixel size of 5. Histogram analysis was performed to assure that the normalized counts lie between 1e-4 and 1e-5 at the signal intensity of saturation (65,000).

**Data and Pathway Analysis:** Raw data were extracted, background subtracted and quantile normalized (Bolstad et al. 2003) using NimbleScan v2.5 software. Gene calls were generated using the Robust Multichip Average (RMA) algorithm (Irizarry et al. 2003, Irizarry et al. 2003). Statistical analysis was performed by one-way ANOVA for unequal variance or by unpaired t-test with Tukey's posthoc test ($p<0.05$) and 5% FDR in GeneSpring GX. Unsupervised hierarchical clustering was performed using Euclidean distance metric and centroid linkage clustering to group gene expression patterns by similarity. The clustering algorithms, heat map visualizations and centroid calculations were performed in Multi-Experiment Viewer, MEV, (Saeed et al. 2003) software. Functional enrichment statistics and network analysis were determined using DAVID (http://david.abcc.ncifcrf.gov/home.jsp) (Dennis et al. 2003, Lempicki et al. 2007) and Metacore (GeneGo, St. Joseph, MI) to identify the most significant biological processes affected by nanoparticle treatment.

The DAVID functional annotation tool utilizes the Fisher Exact test to measure gene enrichment in biological process. Gene Ontology (GO) category terms for significant genes were compared to a background list, which included all genes on the zebrafish Nimblegen platform. Functional annotation clustering with high stringency was used to group similar annotations together into non-redundant functional groups. The statistical scores in MetaCore were calculated using a hypergeometric distribution, where the p value represents the probability of a particular mapping arising by chance for experimental data compared to the background. Networks were built in MetaCore for experimental data utilizing the direct interactions algorithm.

**Gene Validation:** RNA was isolated from embryos exposed to 50 µg/mL MES-AuNPs and 10 µg/mL TMAT- AuNPs, as described above. cDNA was synthesized from 1 µg of RNA in a 20 µL reaction following the SuperScript III First Strand Synthesis Kit Protocol (Invitrogen, Carlsbad, CA). After cDNA was synthesized, samples were diluted to 1:10 prior to storage. Six genes (PTRH1, HOXC9A, BTR29, PDE11A, KIF4A, and RPH3AL) were selected to represent both elevated and repressed transcripts from the microarray. Quantitative real time –PCR (qRT-PCR) was used to validate these genes. Briefly, a melt curve was generated for each primer set (Supplemental Table 1) at six temperatures (55, 57, 58, 59, 60, and 61) to find an optimal temperature that worked for most primers. Using the Lonza (Basel, Switzerland) Flashgel system, the PCR

products were assessed to ensure the product was the expected size. Each sample included three biological replicates for both the control and treated, along with a no template control (no cDNA) and adult zebrafish cDNA. For each sample, a reference gene was used (beta actin) for normalization. CT mean values were used and normalized to beta actin, and then corresponding biological replicates were averaged. The average value of treated and controls were transformed to a ratio to determine the fold change magnitude of the treated sample compared to the control.

**Statistics:** All analyses were compiled using SigmaStat/Plot 11 (SPSS Inc, Chicago, IL). Dose response significance was determined using one-way ANOVA ($p<0.05$) and Dunnetts post hoc test. A two-way ANOVA ($p<0.05$) and Dunnetts post hoc test with time and concentration as factors was used to determine tissue concentration significance. Statistically significant genes supporting microarray data was determined using a Student t-Test.

## Results

### Characterization of functionalized 1.5 nm gold nanoparticles

Previously, we developed a precisely engineered gold nanoparticle (AuNPs) library to determine how the individual effects of core size, and surface functionalization impacts biological responses (Harper, et al. 2011). These AuNPs are rigorously purified by diafiltration and are thoroughly

characterized using TEM, 1H-NMR and UV-Vis spectral analysis. Transmission electron microscopy (TEM) was used to determine nanoparticle size and distribution for each formulation. As illustrated in Supplemental Figure 1a, d, g, the functionalized AuNPs were monodispersed and did not agglomerate. Size analysis of the TEM micrographs of MES- **(Supplemental Figure 1a**), TMAT- (**Supplemental Figure 1d**), and MEEE- (**Supplemental Figure 1g**) AuNPs revealed an average size of 1.6 ± 0.5 nm (N=250), D=1.6 ± 0.5 nm (N=199), D=1.3 ± 0.5 nm (N=657), respectively. Further characterization using nuclear magnetic resonance (1H NMR) spectrometry (**Supplemental Figure 1b, e, h**) showed peaks at approximately 4.3 – 4.5, which illustrate the residual proton from the solvent used for NMR, while the other peak around 3.5 corresponds to the protons of the ligand shell. This confirms that the free ligand and other small molecular impurities were successfully removed.

**Stability of 1.5 nm AuNPs in test media (embryo media)**

The characterization of these AuNPs in nanopure water illustrated that they are highly dispersed and were not agglomerated in solution. However, the embryo media (EM) used for these toxicological studies consisted of ions that buffer the pH. Those ions may cause the nanoparticles to agglomerate and precipitate. Thus, prior to conducting toxicity studies, AuNPs were dispersed in embryo media and monitored with UV-Vis spectroscopy at least through the

experimental duration (0 – 120 hpf) to determine whether the particles remained in solution. As **Supplemental Figure 1c, f, and i** illustrate, when MES-, TMAT- and MEEE- AuNPs were suspended in embryo media at 250 µg/mL, the absorbance patterns at 24 hpf, 120 hpf, 14 days, and one month, were similar to when the first measurements were taken (t=0). The surface functionalized 1.5 nm AuNPs were stable in the test media, and any responses observed in the assay would not be attributed to agglomeration.

**Functionalized gold nanoparticles induce differential biological responses**

In a previous study conducted by our lab, MES-, TMAT- and MEEE-AuNPs were assessed for developmental toxicity in the embryonic zebrafish model (Harper, et al. 2011), but without controlling for factors that influence NP stability. Here, we have conducted all experiments with EM, a defined matrix with a known pH (7.4) buffering capacity for at least seven days. MES-, TMAT- or MEEE-AuNPs were dispersed in EM, and embryos were statically exposed to seven concentrations (0 – 250 µg/mL) from 6 - 120 hpf. As illustrated in **Figure 1a**, at 120 hpf, TMAT-AuNPs induced 100% morphological malformations at 10 µg/mL, while MES-AuNPs induced 40% and MEEE-AuNPs did not. At 50 µg/mL, TMAT-AuNPs induced 80% mortality, while MES- and MEEE-AuNPs did not. MES-AuNPs induced statistically significant higher incidence of malformations compared to MEEE-AuNPs at 2 µg/mL.

These results are comparable to our previous study using fish water, confirming that the observed toxicological responses were influenced by NP surface functionalization and not the pH or media composition.

**AuNPs are bioavailable to embryonic zebrafish**

The differential toxicity of the three AuNPs led us to ask whether responses were associated with differential bioavailability. Inductively Coupled Plasma – Mass Spectrometry (ICP-MS) was used to quantify the amount of gold tightly associated with the embryos after exposure (followed by careful washing to remove free particles and digestion in nitric acid) to 2 – 250 µg/mL of either MES-, TMAT- or MEEE- AuNPs. As illustrated in **Figure 1b**, at both 24 and 48 hpf, and at the same concentration, the numbers of gold particles per embryo were similar for all three nanoparticles. The one exception was at 250 µg/mL, exposure to TMAT-AuNPs resulted in no embryos surviving to the sample time point. The number of particles associated with an embryo increased with NP concentration in the water. The quantity of AuNPs associated with an embryo did not significantly change from 24 to 48 hpf for any exposure concentration or type of AuNP. We observed that the control embryos had detectable gold, which can be explained by our use of nitric acid, with its low level (ppb) of elemental gold. The use of nitric acid was unavoidable since it is the preferred acid for the ICP-MS. This finding suggested that (1) the surface functionalizations studied did not differentially

influence uptake into the embryo, (2) the uptake was rapid, and (3) none of the AuNP types accumulated over time.

**Gene expression changes elicited by MES and TMAT at 24 and 48 hpf**

To explore the mechanism of how surface functionalized AuNPs are inducing differential biological responses over time, we conducted global gene expression studies using embryos exposed to 50 µg/mL of 1.5 nm MES- and 10 µg/mL of TMAT-AuNPs from 6 to 24 and 6 to 48 hpf. Due to the lack of biological response in other assays by MEEE-AuNPs, this nanoparticle was not included in these experiments. At 24 hpf, exposure to MES-AuNPs led to the misexpression of more transcripts, than TMAT-AuNPs (24 and 18, respectively). Fourteen misexpressedd transcripts were common between both AuNPs (**Figure 2a**). By 48 hpf, the number of transcripts misexpressed by MES- and TMAT-AuNPs increased to 316 and 58, respectively. The number of transcripts common to both were 184 (**Figure 2b**). The statistically significant genes for all samples (606) were grouped using bi-hierarchical clustering by Multi-Experiment Viewer (MeV) to produce a heat map (**Figure 2c**). The heatmap had a gene expression pattern that was consistent over time. By taking the generally elevated- or repressed transcripts by AuNPs from the heat map, significant biological process networks were identified (**Figure 2d**). As Figure 2d illustrates, the most significant biological process networks relating to the elevated transcripts were inflammation – complement system,

cell adhesion-leucocyte interactions, immune response - phagocytosis and signal transduction- nitric oxide signaling. While the significant pathways for repressed transcripts were signal transduction – WNT and NOTCH signaling, inflammation – IL-12, 15, 18 signaling, cell cycle – G1-S growth factor regulation, muscle contraction, reproduction-gonadotropin regulation, inflammation – histamine signaling, and immune response – IL-5 signaling. There were more elevated transcripts than repressed, however, there were fewer statistically significant biological process networks (only 4). These networks were involved in inflammation and immune response. Biological processes such as immune and inflammatory responses are elevated by both surface functional groups.

From this heat map, we used qRT-PCR to confirm that the changes in gene expression were similar to gain confidence that the networks identified were, in fact, a result of exposure to 1.5 nm MES- or TMAT- AuNPs. We validated 6 misregulated transcripts that were elevated or repressed. As illustrated in **Table 1**, the direction and magnitude of the gene expression changes observed by qRT-PCR corresponded to those of the microarray, thereby confirming the changes caused by MES- and TMAT-AuNPs at 24 or 48 hpf.

**Pathway analysis comparison of MES- and TMAT- AuNPs**

Due to the differential biological responses caused by exposure to MES- and TMAT-AuNPs, we specifically analyzed the gene expression data to identify genes that are differentially expressed between MES- and TMAT-AuNPs. When the surface functional groups on the nanoparticles, TMAT and MES, were directly compared to one another, 512 and 1,737 statistically significant differentially expressed transcripts were identified at 24 and 48 hpf, respectively. To accomplish this analysis, each surface functionality was normalized to their time matched control, and then a Student T-test was performed. As **Figures 3a** and **3b** illustrate, there is a difference in response for each nanoparticle. However, the magnitude of response varied among one another. **Figure 3c** demonstrates that when comparing the gene lists generated for each time point, at 24 hpf there were 486 unique genes, while at 48 hpf there were 1,711. There were 26 common genes between the two time points. This direct comparison of the TMAT- and MES- response provided evidence that as early as 24 hpf, the surface functional groups were already perturbing the embryo in different ways, and these events led to more molecular disruption at 48 hpf. Additionally, the surface functionalities are driving the gene expression changes and are undergoing differential mechanisms to induce these differential biological responses.

The significantly enriched biological processes at 24 hpf were associated with immune system, inflammation, protein folding, proliferation

and G-protein coupled receptor protein signaling (**Table 2a**). Immune response and inflammatory related biological processes were the most prevalent processes, which included three genes (ELF4, RUNX3, and c-Fos) that were elevated by TMAT compared to MES, and eight genes (STAT4, PAK2, PP2A cat [alpha], PP2A catalytic, p70 S6 kinases1, Ubiquitin, NF-AT1 and ATF-2) that were repressed by TMAT vs. MES. The G-protein coupled receptor signaling pathway was also elevated by TMAT-AuNPs, meaning TMAT-AuNPs causes an increase in cellular responses.

At 48 hpf, the significantly enriched biological pathways identified by Metacore were mainly related to G-protein coupled receptor protein signaling pathways, transport, proliferation and responses to protein stimulus (Table 2b). The proliferation pathway was one of the largest biological pathways and include a large number transcripts that were repressed by TMAT vs. MES (PKR, NDPK A, NF2, GRB2, KLF4, and PAX6) compared to those that were elevated (VEGF, CDK2m TGFB-1, and TGFB-3).

## Discussion

In this *in vivo* study, we report that exposure to 1.5 nm gold nanoparticles functionalized with TMAT, MES, and MEEE induced differential biological responses in dechorionated embryonic zebrafish. TMAT functionalized AuNPs induced embryo lethality, while mortality was not observed after exposure to MES- and MEEE-AuNPs. MES functional group

caused sublethal malformations to the embryos. No adverse responses were observed after exposure to MEEE-AuNPs. The differential biological response was not due to a difference in the ability of the embryos to uptake certain AuNPs. Here, we report that the different adverse responses observed can be attributed to the surface functional groups. We found that surface functionality influenced the gene expression profile when the two surface groups (MES and TMAT) was directly compared to one another.

In a previous study (Harper, et al. 2011), we used these same functionalized gold nanoparticles dissolved in fish water, which is made up of reverse osmosis water and Instant Ocean and found that each AuNP induced differential biological response in the zebrafish. However, since the media used for the toxicological study consist of Instant Ocean, which has a proprietary recipe, it makes it near impossible to control or predict how the nanoparticles will behave in repeated studies. Characterization of AuNPs in ion-rich vs. low ion media often yields different agglomeration and precipitation properties. Ions in media are known to cause nanoparticles to agglomerate and to display unpredictable surface area, charge and size characteristics compared to the original synthesized particles (Saleh et al. 2008, Liu et al. 2009). These changes in parameters influence the toxicological outcome (Truong, et al. In Press). Although agglomeration did not occur for MES-, TMAT- and MEEE-AuNPs in ion-rich media, it is critical to evaluate the stability

of the NPs over time to ensure that the biological responses observed are ascribed to a known NP formulation.

There is great interest in efficiently assessing toxic potential of NPs and in understanding the physicochemical properties that elicit the toxic response. The effects of core material size and surface functionalization have been assessed for gold, silver, and titanium NPs (Euliss 2005, Sayes et al. 2006, Pan et al. 2007, Furgeson et al. 2009, Li et al. 2010, Park et al. 2010). Under some circumstances, gold nanoparticles cause cytotoxicity (Pan, et al. 2007), cell death (Homberger and Simon 2010) and immune-responses (Karthikeyan et al. 2010). While NP size is an important determinant of biological response (Pan, et al. 2007, Liu et al. 2010), so are the NP surface functionalization (Toru et al. 2004). In other studies, cationic AuNPs exposed to Japanese medaka fish resulted in mortality in less than 24 hours (Zhu et al. 2010), which is similar to what we observed in our cationic AuNPs (TMAT-AuNPs) (Harper, et al. 2011). Our studies indicate that alteration of a NP physical property changes the biological response.

Understanding the differential toxicities is a challenge. Differential uptake was hypothesized, but this study suggests it is not a factor. We demonstrated that the uptake is not predictive of toxicity, which is consistent with other studies. In a study using Daphnia magna, exposure to 13-17 nm AuNPs did not cause toxicity at low concentrations, even though the nanoparticles accumulated over time in the gut (Lovern et al. 2008). The D.

magna observation supports our finding that a lack of biological response to AuNPs cannot be attributed to low or no uptake. From this study alone, we conclude that at 24 and 48 hpf, regardless of surface functionalization on the AuNPs, gold was detected in exposed embryos and that the uptake level is not directly correlated to any specific physical parameter.

Our gene expression profiling is not the first study to identify misregulation in pathways related to inflammation and immune responses. A study using gold nanoparticles found that when macrophages were exposed to 35nm AuNPs in vitro, some toxicity was observed (Shukla et al. 2005). Silica particles stimulated inflammatory protein and induced macrophage cytotoxicity (Waters et al. 2009). These studies used nanoparticles that varied in size, core material, and surface functionalization to ours, but illustrate that a general immune response can be initiated by varying NP structural attributes.

NP effects on cell cycle control and proliferation are not without precedent. AuNPs with a diameter of 300 nm inhibited VEGF and induced cell proliferation and migration (Karthikeyan, et al. 2010). It is likely that when such pathways are impacted during development there will be deleterious consequences. Transport mechanisms were more elevated by TMAT than MES, including metal ion transport. The ion transport process was also repressed by TMAT. In general, transport channels are always open, but they are highly selective and will only allow specific molecules through (Zilman et al. 2010). Zilman et al (2010) demonstrated that certain particles can be

strongly trapped and have an enhanced presence for transport regardless of the presence of other particles. However, there is a certain range of intermediate trapping strength for the ion transporters that allows the particles to penetrate the channel to a certain degree, and mostly accumulate near the entrance (Zilman, et al. 2010). This clogging causes a change of particle density inside the channel. It could be that TMAT-AuNPs have a high trapping strength for metal ion transporter and are able to get into the cell readily at 24 hpf, resulting in the perturbation of the G-coupled protein receptor signaling pathway, and in the end, various transport mechanisms within the cell. In comparison, it is possible that MES-AuNPs have an intermediate trapping strength, which causes a blockage of the channel, resulting in a disruption of the metabolic processes at 24 and 48 hpf, due to the imbalance of ions inside and outside the cell. This identification of affected pathway candidates has provided a first pass at understanding the molecular mechanism by which MES- and TMAT-AuNPs induce differential biological responses at both the molecular and phenotypical level.

In summary, surface functionalization of gold nanoparticles influences the biological response at the phenotypical and molecular levels. From this study, we have identified that inflammation and immune response is a relatively general response to NPs exposure. Additionally, transport mechanisms were misregulated after exposure to different surface functional group AuNPs. Further studies using different surface functional groups can

help identify pathways that are driving these adverse responses at the mRNA level. Collectively, these results suggest that surface functionalization plays the largest role in producing differential responses. We believe that this and other recent NP toxicity studies demonstrate efficacy of systematic toxicology studies to establish structure-activity relationships between size, surface functionalization and charge, and the biological response.

## References

Barbazuk WB, Korf I, Kadavi C, Heyen J, Tate S, Wun E, Bedell JA, McPherson JD, Johnson SL. 2000. The syntenic relationship of the zebrafish and human genomes. Genome Res 10: 1351-8.

Bolstad BM, Irizarry RA, Ã…strand M, Speed TP. 2003. A comparison of normalization methods for high density oligonucleotide array data based on variance and bias. Bioinformatics 19: 185-193.

Dahl J, Maddux BLS, Hutchison JE. 2007. Green Nanosynthesis. Chemical Reviews.

den Hertog J. 2005. Chemical Genetics: Drug screens in Zebrafish. Biosci Rep 25: 289-97.

Dennis G, Sherman B, Hosack D, Yang J, Gao W, Lane HC, Lempicki R. 2003. DAVID: Database for Annotation, Visualization, and Integrated Discovery. Genome Biology 4: P3.

Dodd A, Curtis PM, Williams LC, Love DR. 2000. Zebrafish: bridging the gap between development and disease. Hum Mol Genet 9: 2443-9.

Euliss LE. 2005. Gold nanoshell bioconjugates used for molecular imaging in living cells. Mrs Bulletin 30: 418-419.

Furgeson D, Bar-llan O, Albrecht R, Fako V. 2009. Toxicity Assessments of Multisized Gold and Silver Nanoparticles in Zebrafish Embryos. Small X: 1-14.

Harper SL, Carriere JL, Miller JM, Hutchison JE, Maddux BLS, Tanguay RL. 2011. Systematic Evaluation of Nanomaterial Toxicity: Utility of Standardized Materials and Rapid Assays. ACS Nano 5: 4688-7697.

Homberger M, Simon U. 2010. On the application potential of gold nanoparticles in nanoelectronics and biomedicine. Philosophical Transactions of the Royal Society A: Mathematical, Physical and Engineering Sciences 368: 1405-1453.

Irizarry RA, Bolstad BM, Collin F, Cope LM, Hobbs B, Speed TP. 2003. Summaries of Affymetrix GeneChip probe level data. Nucleic Acids Research 31: e15.

Irizarry RA, Hobbs B, Collin F, Beazerâ€• Barclay YD, Antonellis KJ, Scherf U, Speed TP. 2003. Exploration, normalization, and summaries of high density oligonucleotide array probe level data. Biostatistics 4: 249-264.

Karthikeyan B, Kalishwaralal K, Sheikpranbabu S, Deepak V, Haribalaganesh R, Gurunathan S. 2010. Gold nanoparticles downregulate VEGF-and IL-1[beta]-induced cell proliferation through Src kinase in retinal pigment epithelial cells. Experimental Eye Research 91: 769-778.

Kim CK, Ghosh P, Rotello VM. 2009. Multimodal drug delivery using gold nanoparticles. Nanoscale 1: 61-67.

Kim CS, Wilder-Smith P, Ahn YC, Liaw LHL, Chen ZP, Kwon YJ. 2009. Enhanced detection of early-stage oral cancer *in vivo* by optical coherence tomography using multimodal delivery of gold nanoparticles. Journal of Biomedical Optics 14.

Kim T, Lee K, Gong M-s, Joo S-W. 2005. Control of Gold Nanoparticle Aggregates by Manipulation of Interparticle Interaction. Langmuir 21: 9524-9528.

Kimmel CB, Ballard WW, Kimmel SR, Ullmann B, Schilling TF. 1995. Stages of embryonic development of the zebrafish. Dev Dyn 203: 253-310.

Lempicki R, Lane C, Huang D, Sherman B, Tan Q, Collins J, Alvord G, Roayaei J, Stephens R, Baseler M. 2007. The DAVID Gene Functional Classification Tool: a novel biological module-centric algorithm to functionally analyze large gene lists. Genome Biology 8: 183.

Li T, Albee B, Alemayehu M, Diaz R, Ingham L, Kamal S, Rodriguez M, Whaley Bishnoi S. 2010. Comparative toxicity study of Ag, Au, and Ag–Au bimetallic nanoparticles on Daphnia magna. Analytical and Bioanalytical Chemistry 398: 689-700.

Liu J, Aruguete DM, Murayama M, Hochella MF. 2009. Influence of Size and Aggregation on the Reactivity of an Environmentally and Industrially Relevant Manomaterial (PbS). Environmental Science & Technology 43: 8178-8183.

Liu W, Wu Y, Wang C, Li H, Wang T, Liao C, Cui L, Zhou Q, Yan B, Jiang G. 2010. Impact of silver nanoparticles on human cells: effect of particle size. Nanotoxicology 4: 319-330.

Lovern SB, Owen HA, Klaper R. 2008. Electron microscopy of gold nanoparticle intake in the gut of Daphnia magna. Nanotoxicology 2: 43-48.

Nam JM, Thaxton CS, Mirkin CA. 2003. Nanoparticle-based bio-bar codes for the ultrasensitive detection of proteins. Science 301: 1884-1886.

Paigen K. 2003. One hundred years of mouse genetics: An intellectual history. I. The classical period (1902-1980). Genetics 163: 1-7.

Pan Y, Neuss S, Leifert A, Fischler M, Wen F, Simon U, Schmid G, Brandau W, Jahnen-Dechent W. 2007. Size-Dependent Cytotoxicity of Gold Nanoparticles. Small 3: 1941-1949.

Park EJ, Bae E, Yi J, Kim Y, Choi K, Lee SH, Yoon J, Lee BC, Park K. 2010. Repeated-dose toxicity and inflammatory responses in mice by

oral administration of silver nanoparticles. Environmental Toxicology and Pharmacology 30: 162-168.

Rubinstein AL. 2003. Zebrafish: from disease modeling to drug discovery. Curr Opin Drug Discov Devel 6: 218-23.

Saeed AI, Sharov V, White J, Li J, Liang W, Bhagabati N, Braisted J, Klapa M, Currier T, Thiagarajan M, et al. 2003. TM4: A free, open-source system for microarray data management and analysis. Biotechniques 34: 374-8.

Saleh N, Kim H-J, Phenrat T, Matyjaszewski K, Tilton RD, Lowry GV. 2008. Ionic Strength and Composition Affect the Mobility of Surface-Modified Fe0 Nanoparticles in Water-Saturated Sand Columns. Environmental Science & Technology 42: 3349-3355.

Sayes CM, Wahi R, Kurian PA, Liu YP, West JL, Ausman KD, Warheit DB, Colvin VL. 2006. Correlating nanoscale titania structure with toxicity: A cytotoxicity and inflammatory response study with human dermal fibroblasts and human lung epithelial cells. Toxicological Sciences 92: 174-185.

Shipway AN, Lahav M, Gabai R, Willner I. 2000. Investigations into the Electrostatically Induced Aggregation of Au Nanoparticlesâ€ Langmuir 16: 8789-8795.

Shukla R, Bansal V, Chaudhary M, Basu A, Bhonde RR, Sastry M. 2005. Biocompatibility of gold nanoparticles and their endocytotic fate inside the cellular compartment: A microscopic overview. Langmuir 21: 10644-10654.

Teraoka H, Dong W, Hiraga T. 2003. Zebrafish as a novel experimental model for developmental toxicology. Congenit Anom (Kyoto) 43: 123-32.

Toru N, Hioko H, Kunio F. 2004. Application of apatite coated titanium dioxide. Photocatal. Ceram. 39: 534-537.

Truong L, Harper SL, Tanguay R 2011. Evaluation of embryotoxicity using the zebrafish model, Humana Press.

Truong L, Moody I, Stankus D, Nason J, Lonergan M, Tanguay R. 2010. Differential stability of lead sulfide nanoparticles influences biological responses in embryonic zebrafish. Archives of Toxicology: 1-12.

Truong L, Zaikova T, Richman E, Hutchison JE, Tanguay RL. In Press. Media ionic strength impacts embryonic responses in engineered nanoparticle exposure. Nanotoxicology.

Usenko CY, Harper SL, Tanguay RL. 2007. *In vivo* evaluation of carbon fullerene toxicity using embryonic zebrafish. Carbon N Y 45: 1891-1898.

Warner MG, Hutchison JE. 2003. Linear assemblies of nanoparticles electrostatically organized on DNA scaffolds. Nature Materials 2: 272-277.

Waters KM, Masiello LM, Zangar RC, Karin NJ, Quesenberry RD, Bandyopadhyay S, Teeguarden JG, Pounds JG, Thrall BD. 2009. Macrophage Responses to Silica Nanoparticles are Highly Conserved Across Particle Sizes. Toxicological Sciences 107: 553-569.

Westerfield M 2000. The Zebrafish Book. Eugene, OR.

Woehrle GH, Brown LO, Hutchison JE. 2005. Thiol-functionalized, 1.5-nm gold nanoparticles through ligand exchange reactions: Scope and mechanism of ligand exchange. Journal of the American Chemical Society 127: 2172-2183.

Woehrle GH, Warner MG, Hutchison JE. 2004. Molecular-level control of feature separation in one-dimensional nanostructure assemblies formed by biomolecular nanolithography. Langmuir 20: 5982-5988.

Yang LX, Ho NY, Alshut R, Legradi J, Weiss C, Reischl M, Mikut R, Liebel U, Muller F, Strahle U. 2009. Zebrafish embryos as models for embryotoxic and teratological effects of chemicals. Reproductive Toxicology 28: 245-253.

Zhu Z-J, Carboni R, Quercio MJ, Yan B, Miranda OR, Anderton DL, Arcaro KF, Rotello VM, Vachet RW. 2010. Surface Properties Dictate Uptake, Distribution, Excretion, and Toxicity of Nanoparticles in Fish. Small 6: 2261-2265.

Zilman A, Di Talia S, Jovanovic-Talisman T, Chait BT, Rout MP, Magnasco MO. 2010. Enhancement of Transport Selectivity through Nano-Channels by Non-Specific Competition. PLoS Comput Biol 6: e1000804.

## Acknowledgements

The authors would like to thank the staff of the Sinnhuber Aquatic Research Laboratory for the embryos, Dr. Michael Simonich for manuscript assistance and John Miller for his assistance in preparation of the materials. These studies were partially supported by National Institute of Environmental Health Sciences (NIEHS), R01ES016896, P30 ES000210, P42 ES016465, F31 ES019445-02, NIEHS Superfund Basic Research Program Grant P42 ES016465 to RLT and KMW, the Air Force Research Laboratory (AFRL) under agreement number FA8650-05-1-5041, and Environmental Protection Agency (EPA) RD-833320. The views and conclusions contained herein are those of the authors and should not be interpreted as necessarily representing the official policies or endorsements, either expressed or implied, of NIEHS, AFRL, EPA, or the U.S. Government. Further support was provided by the W.M Keck Foundation.

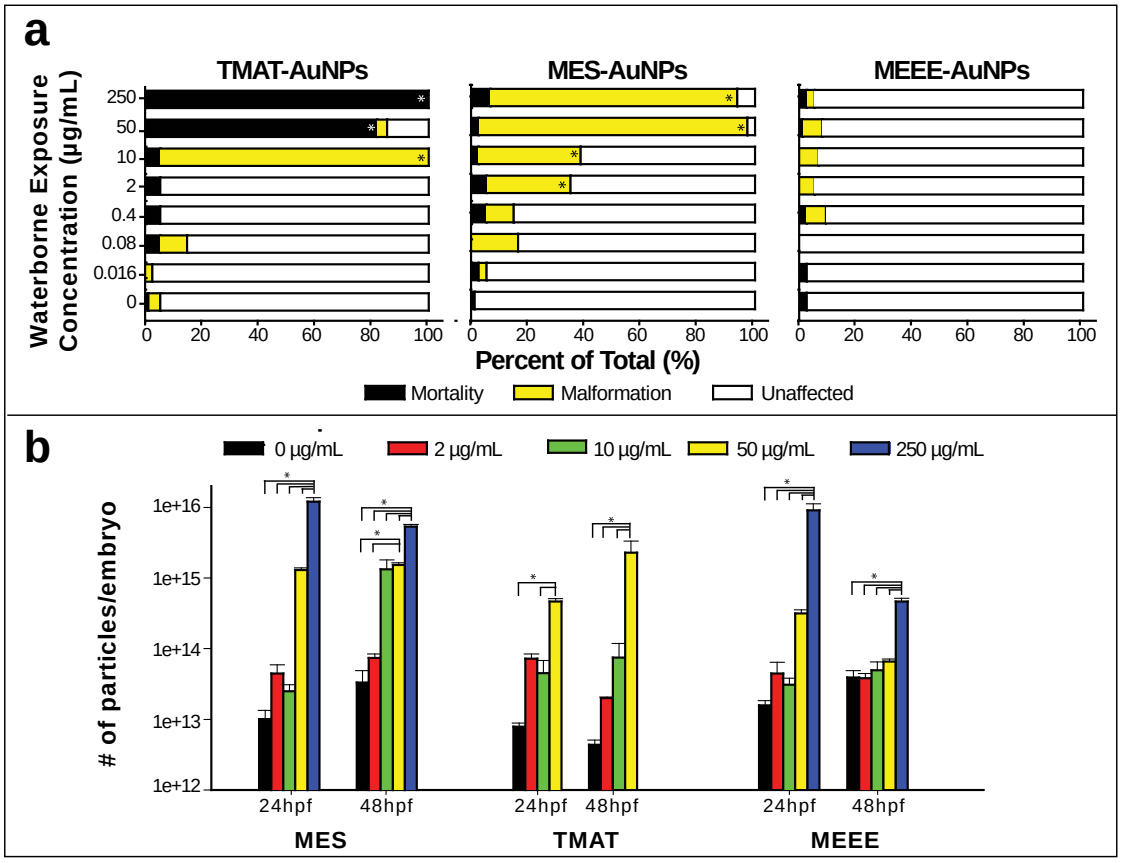


**Figure 3- 1. Differential biological responses induced by AuNPs.**
**(a)** Embryos were dechorionated and exposed from 6 to 120 hpf . 1.5 nm TMAT-AuNPs was embryo lethal, causing mortality in 100% of exposed embryo at 250 µg/mL, while MES-AuNPs induced little mortality, but did induce malformations at concentrations of 2 µg/mL and above. MEEE-AuNPs did not induce any differential biological response. **(b)** Tissue concentration of embryos exposed to 2-250 µg/mL of MES-, TMAT- and MEEE-AuNP from 6 to 24 and 6 to 48 hpf. Error bars are standard error. Data with * denotes statistical significance ($p<0.05$).

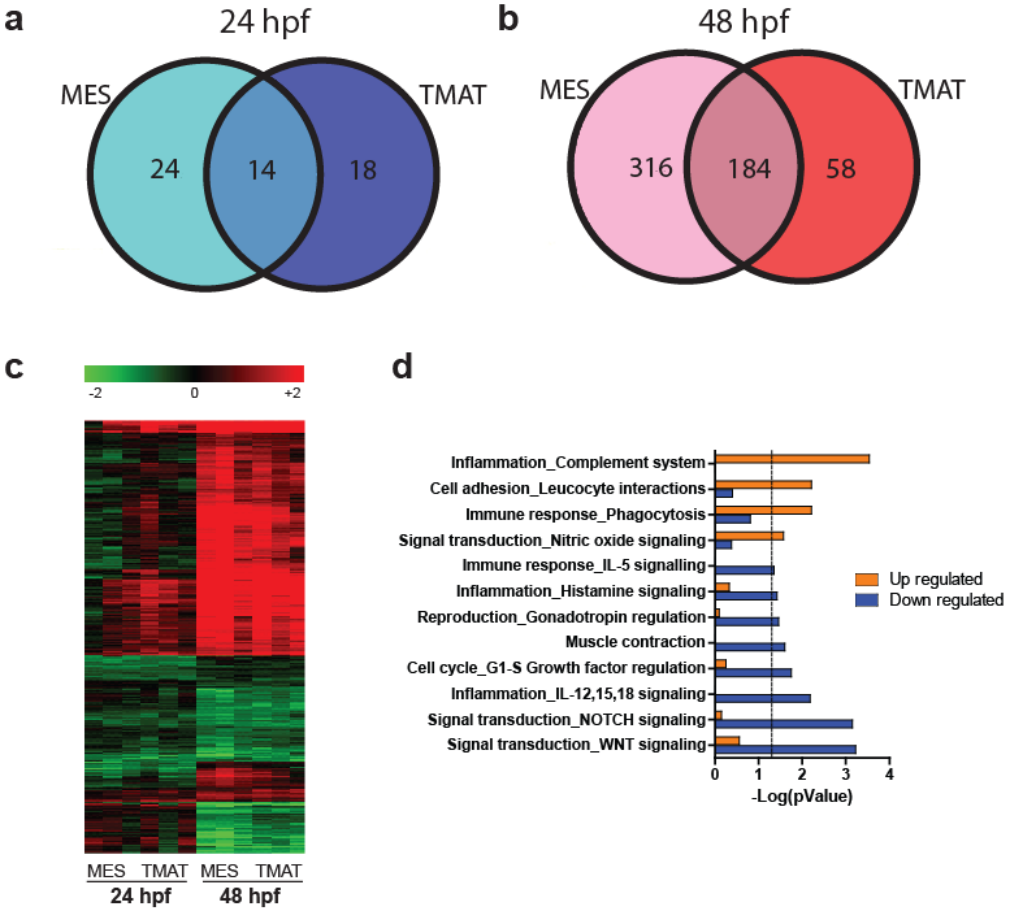


**Figure 3- 2. Venn diagram of misregulated transcripts after exposure to MES- and TMAT-AuNPs at (a) 24 hpf and (b) 48 hpf (c) hierarchical clustering and (d) functional enrichment of statistically significant genes ($p<0.05$) elevalted or repressed by MES- and TMAT-AuNPs.**

Orange bars represent significant Biological Process networks (MetaCore, GeneGo) for elevated transcripts and blue bars for the repressed transcripts compared to the control.

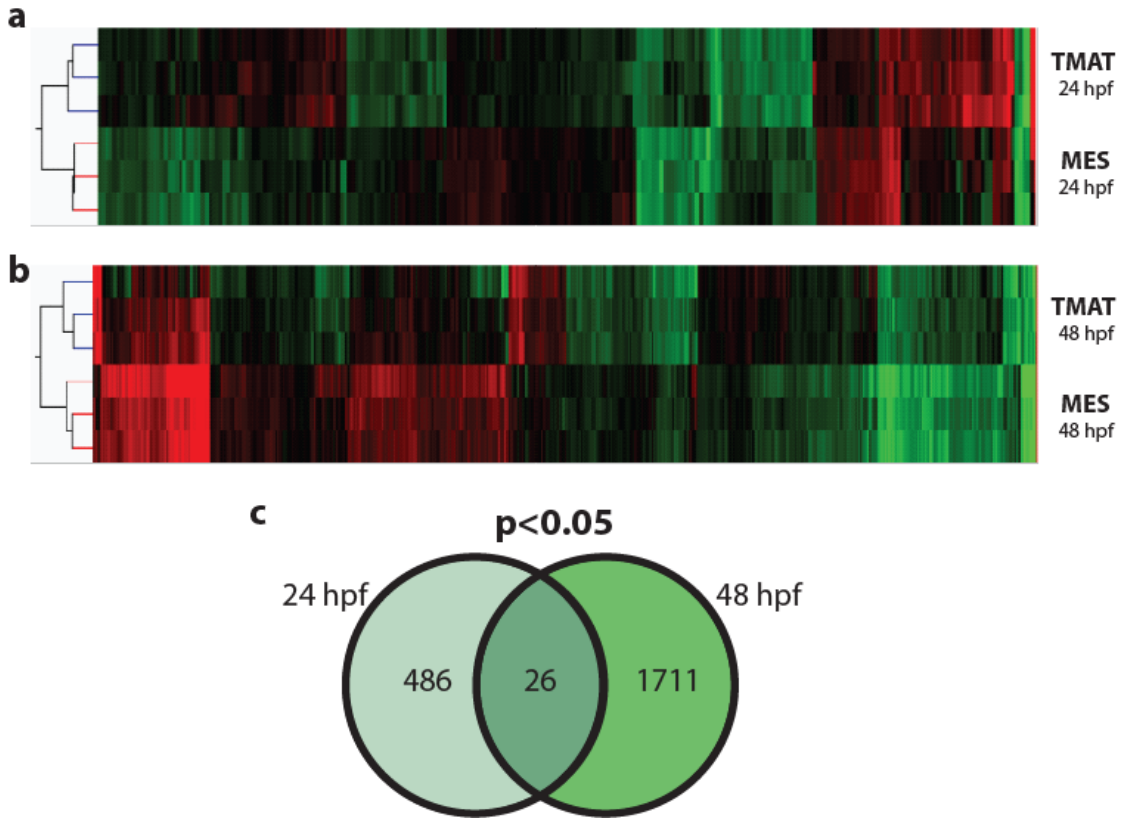


**Figure 3- 3. Direct comparison of genes differentially expressed by TMAT- v. MES- AuNPs.**
Heat map of significantly different genes($p<0.05$) at 24 hpf **(a, 512 genes)** and 48 hpf **(b, 1737 genes)**. A venn diagram comparing the gene lists for each time point at 24 and 48 hpf **(c)**.

**Table 3- 1. Validation of statistically significant genes identified by the microarray using qRT-PCR**

Genes were selected from the statistically significant gene lists generated from the heatmap to determine if the misregulation identified by the microarray was valid. These transcripts were selected to represent both elevated and repressed transcripts. qRT-PCR was used to confirm that the direction of the misregulation is consistent; but not necessarily that the magnitude of the change is not identical. * denotes a gene identified using Ensembl database, and ± from TIGR.

| Gene Symbol | Gene Accession ID | Gene Name | Fold Change of MES | | | |
|---|---|---|---|---|---|---|
| | | | 24 hpf | | 48 hpf | |
| | | | Microarray | qPCR | Microarray | qPCR |
| PTRH1 | NM_001013330 | peptidyl-tRNA hydrolase 1 homolog | 2.01 ↓ | 2.68 ↓ | | |
| HOXC9A | NM_131528 | homeo box C9a | 2.11 ↓ | 1.43 ↓ | | |
| BTR29 | NM_001166134 | bloodthirsty-related gene family, member 29 | 3.02 ↑ | 2.20 ↑ | | |
| PDE11A | NM_201102 | phosphodiesterase 10A | | | 2.71 ↓ | 1.43 ↓ |
| KIF4A | - | - | | | 2.76 ↓ | 1.63 ↓ |
| RPH3AL | - | *B8K0F3_DANRE | | | 2.36 ↑ | 1.55 ↑ |

**Table 3- 2. Functional enrichment of biological processes at (a) 24 and (b) 48 hpf.**

Significantly ($p<0.05$) enriched biological network processes (Metacore, GeneGo) and biological process GO terms for genes differentially expressed at (a) 24 and (b) 48 hpf.

**a**

| Biological Process Network | P Value | Count (%) |
|---|---|---|
| Translation Elongation - Termination | 4.10E-03 | 9/115 (7.8%) |
| Immune Response - TCR signaling | 8.33E-03 | 8/106 (7.6%) |
| Inflammation - IgE signaling | 8.47E-03 | 6/65 (9.2%) |
| Protein Folding - Protein folding nucleus | 1.34E-02 | 4/34 (11.8%) |
| Regulation of cellular metabolic process | 2.18E-02 | 45/135 (33.3%) |
| G-protein coupled receptor protein signaling pathway | 2.25E-02 | 14/97 (14.4%) |
| Immune Response - T helper cell differentiation | 2.34E-02 | 6/81 (7.4%) |
| Protein biosynthesis | 2.35E-02 | 7/172 (4.1%) |
| Protein folding - Folding in normal condition | 3.03E-02 | 6/86 (7%) |
| Proliferation - Lymphocyte proliferation | 3.42E-02 | 8/137 (5.8%) |
| Organ regeneration | 3.68E-02 | 3/135 (2.2%) |
| Protein folding - Response to unfolded proteins | 4.49E-02 | 4/49 (8.2%) |
| Cell Cycle - S phase | 4.80E-02 | 6/96 (6.3%) |

**b**

| Biological Process Network | P Value | Count (%) |
|---|---|---|
| G-protein coupled receptor protein signaling pathway | 7.34E-08 | 59/385 (15.3%) |
| Transport - Synaptic vesicle exocytosis | 6.93E-03 | 15/94 (15.9%) |
| Regulation of vesicle-mediated transport | 1.38E-02 | 8/304 (2.6%) |
| Metal ion transport | 1.77E-02 | 22/304 (7.2%) |
| Proliferation - Negative regulation of cell proliferation | 2.00E-02 | 17/125 (13.6%) |
| Bone remodeling | 2.25E-02 | 4/340 (1.2%) |
| Response to protein stimulus | 2.26E-02 | 8/340 (2.4%) |
| Neurophysiological process - Transmission of nerve impulse | 2.47E-02 | 17/128 (13.3%) |
| Regulation of nucleotide biosynthetic process | 2.84E-02 | 10/385 (2.6%) |
| Regulation of catecholamine secretion | 3.37E-02 | 4/385 (1.0%) |
| Protein folding - Response to unfolded proteins | 3.83E-02 | 8/49 (16.3%) |
| Biogenic amine metabolic process | 4.57E-02 | 8/385 (2.1%) |
| Cellular macromolecular complex assembly | 4.78E-02 | 15/330 (4.5%) |
| Signal Transduction - CREM pathway | 4.96E-02 | 10/70 (14.3%) |

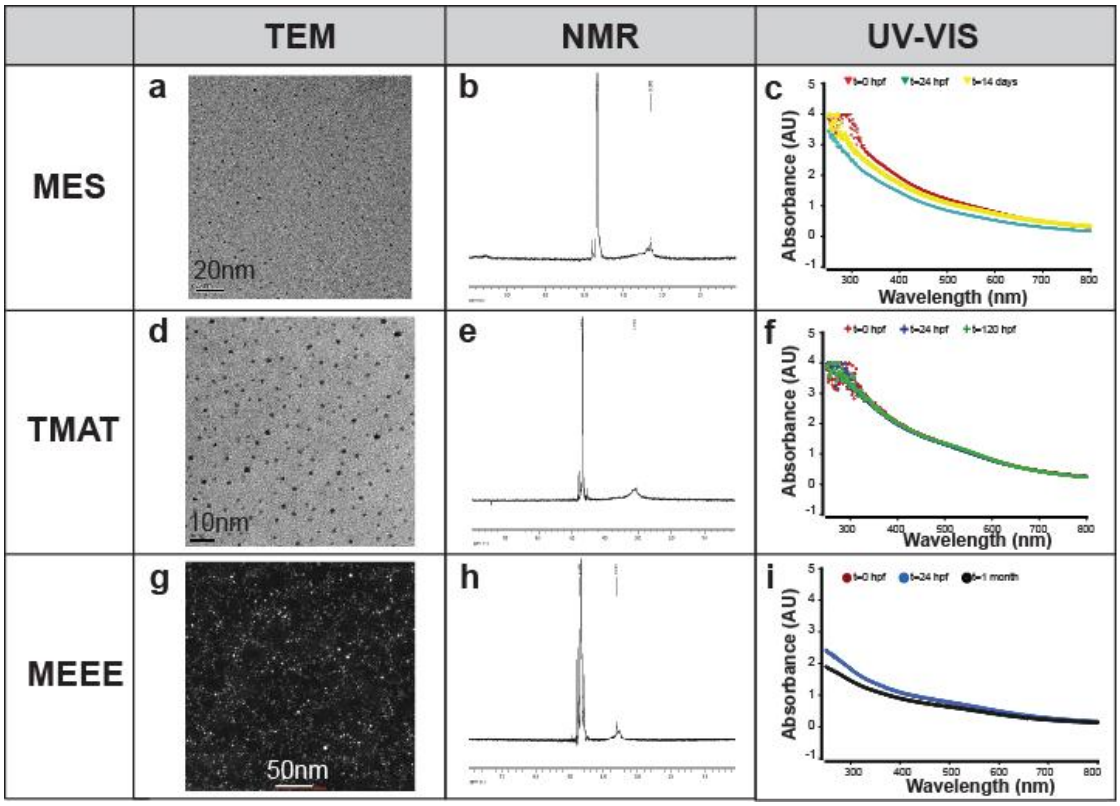


**Figure 3S- 1. Characterization data on MES-, TMAT – and MEEE-AuNPs.** TEM, NMR and UV-VIS characterization of MES- **(a-c),** TMAT-**(d-f),** and MEEE- AuNP **(g-i)**. Scale bars for the TEM images are 20, 10 and 50nm (respectively). UV-VIS spectra show the stability of the nanoparticles in the exposure media: MES-AuNPs remain stable in solution through at least 14 days (yellow); TMAT-AuNPs remain stable in solution up to 114 hours (green); and MEEE-AuNP remain stable in solution up to one month (black). The proton NMR spectra show broadened signals for bound ligand between 3-4 ppm. The lack of intense, narrow signals in this region suggests that there is no free ligand. The peaks at greater than 4.5 ppm are due to residual protons in the deuterated NMR solvent.

**Table 3S- 1. qRT-PCR Primer Sequences.**

| Gene Symbol | Gene Accession ID | UC# | Primer Sequence | Amplicon Size (bp) |
|---|---|---|---|---|
| PTRH1 | NM_001013330 | UC1234/1235 | 5'- TGTGGCAAAAGCAGCCAGCAG-3' (F)<br>5'- ACGTCCCAAAACGTAGCGGTCG-3' (R) | 235 |
| HOXC9A | NM_131528 | UC1254/1255 | 5'- ACATCGCCATGTCGGCTACG-3' (F)<br>5'- TCCGCGCATTCCGGTACCAG-3' (R) | 154 |
| BTR29 | NM_001166134 | UC 1390/1391 | 5'-GCAGCAGAGGAACAGGATTC-3' (F)<br>5'-TGTTTCTGCTCTCCAGCTCA-3' (R) | 193 |
| PDE11A | NM_201102 | UC 1370/1371 | 5'-TTGATGGGATCTGCGCGCCG-3' (F)<br>5'-TGGAGGGGCTCTGCACAGCT-3' (R) | 205 |
| KIF4A | - | UC 1464/1465 | 5'-GCACTTTCATGCGAGGGCGACTAG-3' (F)<br>5'-AATGCAACCCTCACGGGAATGGC-3' (R) | 204 |
| RPH3AL | - | UC 1382/1383 | 5'-GCCATGGGAAACGGCCTGTCA-3' (F)<br>5'-TGCAAAGCCACTGGGTCCGTT-3' (R) | 160 |

# CHAPTER 4 - PERSISTENT ADULT ZEBRAFISH BEHAVIORAL DEFICITS RESULTS FROM ACUTE EMBRYONIC EXPOSURE TO GOLD NANOPARTICLES

Lisa Truong[1,2], Katerine S. Saili[1,2], John M. Miller [2,3], James E. Hutchison[2,3] and Robert L. Tanguay[1,2]

[1] Department of Environmental and Molecular Toxicology, the Sinnhuber Aquatic Research Laboratory and the Environmental Health Sciences Center at Oregon State University, Corvallis, OR, USA;
[2] The Safer Nanomaterials and Nanomanufacturing Initiative, Oregon Nanoscience and Microtechnologies Institute, Eugene, OR, USA;
[3] Department of Chemistry and the Materials Science Institute, University of Oregon, Eugene, Oregon 97403, USA;

## Abstract

As the number of products containing nanomaterials increase, human exposure to nanoparticles (NPs) is unavoidable. Presently, few studies focus on the potential long-term consequences of developmental NP exposure. In this study, zebrafish embryos were acutely exposed to three gold NPs that possess functional groups with differing surface charge. Embryos were exposed to 50 µg/mL of 1.5 nm gold nanoparticles (AuNPs) possessing negatively charged 2-mercaptoethanesulfonic acid (MES) or neutral 2-(2-(2-mercaptoethoxy)ethoxy)ethanol (MEEE) ligands or 10 µg/mL of the AuNPs possessing positively charged trimethylammoniumethanethiol (TMAT). Both MES- and TMAT-AuNP exposed embryos exhibited hypo-locomotor activity, while those exposed to MEEE-AuNPs did not. A subset of embryos that were exposed to 1.5 nm MES- and TMAT-AuNPs during development from 6-120 hours post fertilization were raised to adulthood. Behavioral abnormalities and the number of survivors into adulthood were evaluated at 122 days post fertilization. We found that both treatments induced abnormal startle behavior following a tap stimulus. However, the MES-AuNPs exposed group also exhibited abnormal adult behavior in the light and had a lower survivorship into adulthood. This study demonstrates that acute, developmental exposure to 1.5 nm MES- and TMAT- AuNPs, two NPs differing only in the functional group, affects larval behavior, with behavioral effects persisting into adulthood.

## Introduction

With the number of nanotechnology-enabled products entering the consumer world increasing steadily (Scholars et al. 2011) exposure to nanoparticles (NPs) is inevitable. At present, there are many unknowns about how NPs affect human and environment health. Most studies have focused on understanding how acute nanoparticle exposure affects organ system development or causes mortality using both in vitro and *in vivo* models (Powers et al. 2010; Zhu et al. 2010; Gao et al. 2011). While these studies are critical and provide informative data, there are other areas of potential concern regarding nanoparticles that have yet to be explored, including potential long-term effects following short-term developmental exposure. Because many NPs are designed with metal cores, some of which are known neurotoxicants (e.g., lead), there is particular interest in the long-term effects of NP exposure on the nervous system. While some groups are beginning to address this data gap by either investigating the effects of NPs on brain development following in utero exposure (Gao et al. 2011) or behavior following long-term exposure as adults (Oszlanczi et al. 2011) few groups have coupled these endpoints and tested the behavior of adults following developmental exposure. Additionally, because metal cores are often the focus of toxicity studies, few groups have considered the potential effects of surface functional groups on nervous system development and function, even when the metal NP core is apparently benign (e.g., gold). The paucity of research in these two areas leaves a data gap regarding potential long-term effects of NP exposure on the developing

nervous system. The first objective of this research was to investigate the short- and long-term behavioral effects of developmental NP exposure. The second objective was to investigate whether surface functional groups surrounding a benign metal core (i.e., gold) affect nervous system development and long-term behavior.

We conducted this study using the zebrafish model. The zebrafish is the most appropriate model for this type of study because embryos develop externally, all of their organs have formed within 5 days (Amacher 2001), and the fish mature to adulthood in just 3 months (Brand et al. 2002). Due to their small size and external development, an entire cohort of embryos can be exposed using just ~1 mg of nanoparticles, while the traditional rodent model would require gram quantities. Furthermore, due to their predictable swimming habits, both larval and adult behavior tests using locomotor activity as the endpoint can be quickly and efficiently conducted.

Based on a previous study (Truong et al. Submitted), we elected to use three types of gold nanoparticles with a core diameter of 1.5 nm and functionalized with either 2-mercaptoethanesulfonic acid (MES), trimethylammoniumethanethiol (TMAT) or 2-(2-(2-mercaptoethoxy)ethoxy)ethanol (MEEE). The primary difference between these three NPs is the charge of their surface functional groups. MES has a negative charge, TMAT has a positive charge, and MEEE has a neutral charge. These different surface charges greatly influence biological

responses. Previously, we found that the positively charge surface functional group (TMAT) induced embryo lethality, the negatively charge (MES) induced sublethal toxic effects, while the neutral group (MEEE) caused no adverse biological response (Harper et al. 2011). Our goal was to identify whether acute exposure to MES- and TMAT-AuNPs during development would lead to deleterious effects that persist into adulthood. Specifically, we wanted to detect whether the charged surface functional groups on these gold nanoparticles would impact development of the central nervous system leading to abnormal behavior or survivorship in adulthood.

## Materials and Methods

**Preparation of TMAT-, MES- and MEEE-AuNPs:** 1.5 nm gold particles were synthesized using published procedures (Woehrle et al. 2005). All reagents were purchased from Sigma (St. Louis, MO) or Strem (Newburyport, MA) and used as received. Dichloromethane was distilled over phosphorous pentoxide, and chloroform was filtered through a plug of basic alumnia prior to use. 2-[2-(2-mercaptoethoxy)ethoxy]ethanol (Woehrle et al. 2004) and thiocholine (N,N,N-trimethylaminoethanethiol iodide) (Warner et al. 2003) were synthesized according to known procedures.

**Nanoparticle Characterization and Analytical Procedures:**

Proton NMR spectra, UV-visible spectra and transmission electron microscopy (TEM) images were collected for each nanoparticle to confirm the size, composition and purity of the samples. Varian Unity Inova 300 MHz was used to collect proton NMR spectra in D2O. A Hewlett-Packard 8453 diode array instrument was used to obtain UV-visible spectra in a 1-cm quartz cuvette. TEM images were obtained on an FEI Titan at 300kV using a Cs aberration corrector. Amine functionalized SMART grids (Dune Sciences, Inc) were used for TEM imaging. SMART grids were soaked in the nanoparticle solution and then in nanopure water for 2 minutes each to produce samples for TEM with an even distribution of particles across the grid. Characterization data for the batch of MES-, TMAT- and MEEE-AuNPs used in this study can be found in a study conducted in parallel (Harper et al. 2011).

**Zebrafish:** Adult Tropical 5D strain of zebrafish (*Danio rerio*) were reared at Oregon State University - Sinnhuber Aquatic Research Laboratory (SARL). Fish were kept at standard laboratory conditions of 28°C on a 14h light/10h dark photoperiod in fish water (FW) consisting of reverse osmosis water supplemented with a commercially available salt (Instant Ocean®).

**Exposure Protocol**: Adult zebrafish were group spawned, and their embryos were collected and staged according to Kimmel et al. (Kimmel et al. 1995). At

4 hours post fertilization (hpf), the embryonic chorion was enzymatically removed with pronase to increase bioavailability using protocols previously published (Truong et al. 2011). Dechorionated embryos were rested for 30 minutes prior to nanoparticle exposure. For both the larval behavior assessment and the adult studies, embryos were exposed from 6 to 120 hpf in the individual wells of a 96-well plate with 100 µl of either embryo media (Kimmel et al. 1995), 10 µg/mL of TMAT-AuNPs, 50 µg/mL of MES-AuNPs, or 50 µg/mL of MEEE-AuNPs. The NP exposure concentrations were selected as the most appropriate for behavior testing based on a previous study showing that developmental exposure to these concentrations does not lead to significant morphological defects (e.g., yolk sac edema) which could affect swimming behavior and confound the results of the behavior tests (Truong et al. Submitted). Additionally, TMAT-AuNPs induced 100% embryo lethality at 50 µg/mL, therefore a lower concentration was selected that did not induce mortality or sublethal effects. For the larval behavior assessment, 24 embryos were exposed per treatment (3 replicates); for the adult assessments, 96 embryos were exposed per treatment, but only 50 were selected to be raised into adulthood. Note that embryo media was used as the control for the adult study based on the results of the larval behavior tests, which showed no statistical behavioral difference between embryos exposed to MEEE or embryo media (see Figure 1b). Embryos for the adult study were thoroughly washed at 120hpf then raised under standard conditions until adulthood. A

subset of embryos with intact chorions was kept to monitor inherent clutch quality. Exposure plates were sealed to prevent evaporation and wrapped with aluminum foil to eliminate potential light degradation of the NPs during exposure.

**Larval Behavior Assay**: At 120 hpf, exposed embryos were tested in the original 96-well exposure plate by placing the plate in a Viewpoint ZebraBox (software version 3.0, Viewpoint Life Sciences, Lyon, France) and measuring locomotor activity using the tracking setting during alternating periods of light and dark. This test is a modification of that described by MacPhail et al. [13]. Larvae subjected to this test typically move less during the light periods and more during dark periods (**Figure 1a**) and behavioral differences following developmental exposures can be determined by comparing distances moved during the light or dark periods. Briefly, the test consisted of acclimating embryos in the light for 20 minutes, after which a cycle of 10 minutes in the light, then 10 minutes in the dark, was repeated three times over a course of one hour. Raw data files were processed using a custom perl script to average total distance traveled for each of the three dark periods. Twenty-four embryos were used for each replicate, with a total of three replicates for each of the three AuNPs or embryo media controls. A two way ANOVA-Dunnetts Post Hoc Test using conditions of cycle and treatment was used to compare whether larval locomotor activity differed across each of the three dark cycles.

**Survivorship Measurements**: Ninety-six embryos were exposed from 6 - 120 hpf to embryo media control, TMAT- and MES-AuNPs. At 120 hpf, 50 phenotypically normal larvae were selected from each treatment and washed with fish water prior to being raised to adulthood on a recirculating FW system. The larvae were initially reared at a density of 50 per tank. At 22 days post fertilization (dpf), larvae were split to a density of 25 per tank. On 44 dpf, each treatment group was evenly distributed between two tanks to control for possible density effects. The number of surviving larvae was recorded at 22, 44 and 122 dpf. These evaluation dates correspond to when juvenile zebrafish transition to different sized food (based on the mouth size). A Fisher Exact Test ($p<0.05$) was applied to the raw data (the number of survivors into adulthood). For ease of visualization, percent survivors was graphed rather than number of individuals.

**Adult Behavior Assay**: One day prior to behavioral assessment, five fish (n=5) were randomly selected from each treatment group and placed into individual 2 liter tanks in the behavior testing room. The behavior room was temperature controlled on a 14 h light/10h dark cycle and had a custom built shelf that held 15 tanks at a time, and at each location, had a solenoid that was manually triggered from a remote location to create a brief tap on the outside of the tank. A custom light setup with a sheet diffuser was placed behind the shelf system and controlled remotely using a light switch placed in

a different part of the room. A Sony High Definition camcorder (HDR-SR11) was set up on a tripod 15 feet away from the tank arrays to capture movement of the fish. After capturing the videos, Noldus Ethovision XT version 7 software (Leesburg, VA) was used to quantify total distance moved and velocity. All data obtained were normalized by averaging the total velocity or distance travelled among the five fish per treatment and dividing this value by the average length for the same five fish for each treatment (see section 2.8). A one way ANOVA and Dunnett's post hoc test was used to assess total distance travelled after a light and startle stimulus and the velocity after the light stimulus for each nanoparticle-treated group for the adult behavior assessments. An ANOVA on ranks with Dunn post hoc test was used to assess average velocity after startle assay for control compared to each treatment.

**Light Stimulus:** After moving fish to the behavior testing room, they were left in the dark for 20 minutes to acclimate to their new environment; afterwards, the light stimulus was produced by turning on the lights. The camcorder was used to record the movement of the fish for 10 minutes following the light stimulus, after which the fish were allowed to settle down in the dark.

**Startle Stimulus:** Approximately 60 minutes after the light stimulus test was conducted, the same fish underwent a startle stimulus assay. The

test began when the tap trigger was manually initiated and lasted 10 minutes during which the fish movements were recorded.

**Adult Weight and Length Measurement:** On 117 days post exposure, and after behavioral analysis was complete, all adult zebrafish were humanely euthanized using MS-222. Body mass was measured using a digital scale length was measured from the snout to the end of the caudal fin using digital calipers. Condition factor (K) indices was calculated for each treatment to quantify the condition of the fish [K=weight (g)x 100/ length$^3$ (mm)][14]. An ANOVA on ranks with Dunn post hoc test was used to assess average weight, and condition factor indice for control compared to each treatment. A one way ANOVA and Dunnett's post hoc test was used to average length for control compared to each treatment.

## Results

### Surface functionalization of 1.5nm AuNPs impacts larval behavior

After exposure to the three types of gold nanoparticles, we conducted a 1-hour larval behavior test consisting of recording distance moved during three cycles of alternating 10-minute light and dark periods. After determining that there was no statistical difference between the distances moved during each of the three dark periods (data not shown), total distance traveled in the three dark periods was averaged and distance moved was compared across

treatments (**Figure 1b**). Embryos exposed to MES- and TMAT- AuNPs swam 50% and 33% less distance in the dark compared to the control, respectively, while those exposed to MEEE-AuNPs showed no difference in distance traveled compared to the control. This data suggests that the MES- and TMAT surface functionalizations (i.e., charge) impacted development leading to altered locomotor behavior. Note that since the larval test showed no difference in behavior between MEEE-exposed embryos and those raised in embryo media, the embryo media exposed were used as the control for the adult tests rather than adding an additional NP control (MEEE). As a control, embryo media exposed embryos was used rather than fish water because the embryo media composition is known, while fish water chemistry is unknown due to the use of a commercial product with proprietary ingredients.

**Acute exposure to AuNPs impacts survivorship into adulthood**

Embryos that were exposed to TMAT-AuNPs at 10 µg/mL, MES-AuNPs at 50 µg/mL or an embryo media control from 0 to 5 dpf were raised in fresh water until 122 dpf. By 117 days post exposure (dpe) to the nanoparticles or the control, there was a statistically significant decrease in the percentage of MES-AuNP-exposed survivors, while survivorship of fish that had been exposed to TMAT-AuNPs was not statistically different from the control survival rate . At 117 dpe, both the control and TMAT-AuNPs exposed groups had 80% survivors, while MES-AuNPs had only 50%. **Figure 2** illustrates that

both control and TMAT-AuNP-exposed fish had similar rates of mortality throughout the experiment, while the majority of the death to the MES-AuNP-exposed fish occurred between 17 to 39 dpe. The MES-AuNP treated group's survivorship dropped from 90% at 17 dpe to 60%, 22 days later. Overall, this data shows that acute exposure to 1.5nm MES-AuNPs decreases the number of survivors into adulthood.

**Surviving adults exhibit higher condition factor indices**

To determine if acute exposure to MES- and TMAT-AuNPs affects zebrafish development, we measured the length and weight of all survivors for each of the three groups. The surviving fish in both MES- and TMAT-AuNPs treatment groups were statistically longer than the control (34 ± 0.22 mm) with an average length of 38 ± 0.32 and 36 ± 0.31 mm, respectively. MES-AuNP treated fish weighed more than the control (0.53 +/- 0.03 g vs 0.42 +/- 0.02 g). To account for the different number of survivors per treatment, we calculated a condition factor index (K) to evaluate the quality of the fish. The condition factor index (K= weight x 100 / length$^3$) for the control group was 0.97 +/- 0.049, while both the MES- and TMAT-AuNPs fish had an average K of 1.12 (**Table 1**). These results demonstrate the importance of taking into consideration the different number of survivors per treatment and that exposure to either positively or negatively charged AuNPs during development leads to an increase in both weight and length of adult zebrafish.

**Behavioral abnormality detected in acutely exposed zebrafish**

Zebrafish exposed during development to MES- and TMAT-AuNPs exhibited behavioral abnormalities at 5 dpf. We wanted to evaluate whether these behavioral abnormalities persistent into adulthood. To assess this, we performed two adult assays of locomotor activity. Since the NP-exposed adults were bigger than the controls, and bigger fish may be expected to travel larger distances than smaller fish, all locomotor data was normalized to the average body length. The first assay was to measure the total distance travelled and the average velocity for 10 minutes following a tap on the tank. As **Figure 3a** illustrates, after the startle stimulus, the control fish moved a total distance of 207 cm, while both MES and TMAT-AuNP treated fish travelled a statically significant shorter distance, 35 and 69 cm, respectively. The velocity for the control and TMAT-AuNPs exposed fish were 0.60 and 0.27 cm/s, respectively, while the velocity of MES-AuNP exposed fish was lower than the control (0.22 cm/s). The second assay consisted of measuring the total distance travelled and the average velocity during 10 minutes in the light following a light stimulus (**Figure 3b**). For this assay, the control fish travelled a total distance of 197 cm, while TMAT-AuNP-exposed fish travelled 421 cm). MES-AuNPs exposed fish travelled a statistically significant greater distance (527 cm than the control. The velocity of the fish followed the same trend, where MES-AuNP exposed fish had an average velocity that was greater than the control (1,04 vs 0.65 cm/s, respectively), while both the control and TMAT-AuNP-exposed

fish had an average velocity of 0.79 cm/s. These results demonstrate that acute exposure to both MES- and TMAT-AuNPs cause behavioral abnormalities that persists into adulthood. However, the negatively charged MES-AuNPs have a more severe impact on both larval and adult behavior compared to the effects of the positively charged TMAT-AuNPs.

## Discussion

In this study, we report for the first time that acute exposure to 1.5 nm MES- and TMAT- AuNPs during embryonic development results in larval behavioral abnormalities that persist into adulthood. Additionally, developmental exposure to both NPs resulted in larger adults, and exposure to 1.5 nm MES-AuNPs at 50 µg/mL resulted in reduced adult survivorship. Although there is a lack of significant differences in condition factor index (K), the data suggests that the fish are compositionally similar when adjusted for length and weight. Historically, the condition factor index is considered a good indicator of health in fish; however, it has only been applied to one zebrafish study where the average K was 1, which is similar to our finding in this study (Siccardi et al. 2009). Applying a condition factor index to adult zebrafish studies is appropriate as it illustrates the health of the fish and allows comparison to other studies.

Ours is the first study where embryonic zebrafish were exposed to nanoparticles only during development, then raised in freshwater to adulthood.

Previous studies have tested chemicals using this same method and model (Görge et al. 1990; Gerlai et al. 2006). What we are learning from these studies is that even brief exposure during development can result in potentially maladaptive effects later in life. As others have suggested, embryonic development is the most critical and sensitive life stage (Aparicio et al. 2002; Rubinstein 2003) and if any molecular pathways are perturbed during this period, permanent derailment of development may occur. Effects on development can be minute or cause a cascade of effects that result in either mortality or inhibition of growth and possibly central nervous system damage. While behavior tests are a comprehensive assessment of potential impacts on nervous system development, follow-up studies are required to determine the "window of exposure" and the mode of action underlying the observed effects.

While altered locomotor activity suggests an impact on nervous system development, it does not exclude the possibility that the NP is impacting other target organs such as the eye (i.e., ability to detect light) or neuromuscular system (i.e., ability to swim). By utilizing both a light and tap stimulus tests, we tested the effects of the NPs on both vision and sensory perception. The ability to sense a tap is achieved through the hair cells on the lateral line of teleosts (Crispino 1983). Our results suggest that while MES may impact both vision and sensory perception, TMAT is unlikely to have an impact on vision. The next step in determining whether these NPs impact nervous system, vision, sensory-motor perception, or all three target organ systems, is to begin to look

at the molecular events underlying the observed changes in behavior. The zebrafish is an excellent model for investigating mode of action underlying observed phenotypes mainly due to being genetically tractable. The shared genomic homology between humans and zebrafish (Barbazuk et al. 2000) makes studies using developing zebrafish highly relevant to human health. We can use this model to investigate gene expression changes underlying a given phenotype, and begin to identify which genes or pathways in any organ of interest (e.g., brain, eye, or somites) are being misexpressed following developmental NP exposure.

In a previous study, global gene expression data were collected on embryos exposed to 1.5 nm TMAT- and MES-AuNPs from 6 - 24 and 6 - 48 hpf (Truong et al. Submitted). Analysis of this data using Ingenuity Pathway Analysis software (Ingenuity® Systems, www.ingenuity.com), found that for both exposure time points, nervous system development and function was one of the biological processes most perturbed. Although the gene expression profiling was conducted using samples collected during the most rapid development of the zebrafish central nervous system (suggesting that our results could be merely reflective of normal developmental patterns), pathways related to cellular function and maintenance, and nervous system development and function were significantly impacted compared to their time-matched control. The gene expression data corroborates our hypothesis that exposure to TMAT- and MES-AuNPs during development perturbs

neurophysiological processes by 5 dpf leading to permanent damage to the central nervous system that persists into adulthood. Further analyses will be required to determine the extent to which the central nervous system or other target organs contribute to the observed behavioral phenotypes.

An additional clue to the molecular impact of the tested NPs comes from the NPs, themselves. Our study demonstrates that exposure to gold nanoparticles functionalized with MES or TMAT, induces unexpected behavioral effects that are driven by the surface functionalities.. The behavioral abnormalities detected cannot be generalized to every gold nanoparticle. For example, MEEE-AuNP exposed embryos did not exhibit any behavior defects, but MES- and TMAT-AuNP exposed embryos did. These results suggest that surface coatings, and in this case the charge specifically, either positive or negative, has a significant impact on development. Further studies are currently being conducted by our group to begin to determine how NP surface charge impacts development.

## Conclusion

In summary, evaluation of adult zebrafish after acute exposure to nanoparticles during embryonic development provides critical information for predicting potential long-term effects of specific NPs. From this study, we have learned that exposure to NPs during development can have lasting impacts on the central nervous system. More follow-up studies using different

nanoparticles must be conducted to determine what physicochemical properties are driving these responses. Collectively, all data point to surface functionalization of a nanoparticle being a critical driver to adverse response since the effects observed are isolated to only certain functional groups. Utilizing the zebrafish model for acute NP exposure and long-term development studies provides insight into potential human health implications and allows for follow-up investigation at the molecular level to address the mode of action underlying these undesired effects. Studies using this model will help regulatory agencies establish safety precautions to minimize detrimental effects from nanoparticles and provide data that will aid NP manufacturers in developing safer NPs that are both effective and nontoxic.

## References

Amacher, S.L., 2001. Zebrafish Embryo as a Developmental System. John Wiley & Sons, Ltd.

Aparicio, S., Chapman, J., Stupka, E., Putnam, N., Chia, J.-m., Dehal, P., Christoffels, A., Rash, S., Hoon, S., Smit, A., Gelpke, M.D.S., Roach, J., Oh, T., Ho, I.Y., Wong, M., Detter, C., Verhoef, F., Predki, P., Tay, A., Lucas, S., Richardson, P., Smith, S.F., Clark, M.S., Edwards, Y.J.K., Doggett, N., Zharkikh, A., Tavtigian, S.V., Pruss, D., Barnstead, M., Evans, C., Baden, H., Powell, J., Glusman, G., Rowen, L., Hood, L., Tan, Y.H., Elgar, G., Hawkins, T., Venkatesh, B., Rokhsar, D., Brenner, S., 2002. Whole-Genome Shotgun Assembly and Analysis of the Genome of Fugu rubripes. Science 297, 1301-1310.

Barbazuk, W.B., Korf, I., Kadavi, C., Heyen, J., Tate, S., Wun, E., Bedell, J.A., McPherson, J.D., Johnson, S.L., 2000. The syntenic relationship of the zebrafish and human genomes. Genome Res 10, 1351-1358.

Brand, M., Granato, M., Nusslein-Volhard, C., 2002. Keeping and raising zebrafish. In: Nusslein-Volhard, C.D., R. (Ed.) In Zebrafish: A Practical Approach, Oxford University Press, Oxford, pp. 7-37

Crispino, L., 1983. Modification of responses from specific sensory systems in midbrain by cerebellar stimulation: experiments on a teleost fish. Journal of Neurophysiology 49, 3-15.

Gao, X., Yin, S., Tang, M., Chen, J., Yang, Z., Zhang, W., Chen, L., Yang, B., Li, Z., Zha, Y., Ruan, D., Wang, M., 2011. Effects of Developmental Exposure to TiO(2) Nanoparticles on Synaptic Plasticity in Hippocampal Dentate Gyrus Area: an *In vivo* Study in Anesthetized Rats. Biol Trace Elem Res.

Gerlai, R., Lee, V., Blaser, R., 2006. Effects of acute and chronic ethanol exposure on the behavior of adult zebrafish (Danio rerio). Pharmacology Biochemistry and Behavior 85, 752-761.

Görge, G., Nagel, R., 1990. Toxicity of lindane, atrazine, and deltamethrin to early life stages of zebrafish (Brachydanio rerio). Ecotoxicology and Environmental Safety 20, 246-255.

Harper, S.L., Carriere, J.L., Miller, J.M., Hutchison, J.E., Maddux, B.L.S., Tanguay, R.L., 2011. Systematic Evaluation of Nanomaterial Toxicity: Utility of Standardized Materials and Rapid Assays. ACS Nano 5, 4688-7697.

Jones, R.E., Petrell, R.J., Pauly, D., 1999. Using modified length-weight relationships to assess the condition of fish. Aquacultural Engineering 20, 261-276.

Kimmel, C.B., Ballard, W.W., Kimmel, S.R., Ullmann, B., Schilling, T.F., 1995. Stages of embryonic development of the zebrafish. Dev Dyn 203, 253-310.

MacPhail, R.C., Brooks, J., Hunter, D.L., Padnos, B., Irons, T.D., Padilla, S., 2009. Locomotion in larval zebrafish: Influence of time of day, lighting and ethanol. Neurotoxicology 30, 52-58.

Oszlanczi, G., Papp, A., Szabo, A., Nagymajtenyi, L., Sapi, A., Konya, Z., Paulik, E., Vezer, T., 2011. Nervous system effects in rats on subacute exposure by lead-containing nanoparticles via the airways. Inhal Toxicol 23, 173-181.

Powers, C.M., Badireddy, A.R., Ryde, I.T., Seidler, F.J., Slotkin, T.A., 2010. Silver Nanoparticles Compromise Neurodevelopment in PC12 Cells: Critical Contributions of Silver Ion, Particle Size, Coating and Composition. Environ Health Perspect.

Rubinstein, A.L., 2003. Zebrafish: from disease modeling to drug discovery. Curr Opin Drug Discov Devel 6, 218-223.

Scholars, W.W.I.C.f., PEW, 2011. Project on Emerging Nanotechnologies. In: vol. 2011. Woodrow Wilson International Center for Scholars,

Siccardi, A.J., Garris, H.W., Jones, W.T., Moseley, D.B., D'Abramo, L.R., Watts, S.A., 2009. Growth and Survival of Zebrafish (Danio rerio) Fed Different Commercial and Laboratory Diets. Zebrafish 6, 275-280.

Truong, L., Harper, S.L., Tanguay, R., 2011. Evaluation of embryotoxicity using the zebrafish model. Humana Press.

Truong, L., Tilton, S.C., Zaikova, T., Richman, E., Waters, K.M., Hutchison, J.E., Tanguay, R.L., Submitted. Surface Functionalities of Gold Nanoparticles (AuNPs) Impact Gene Expression in the Developing Zebrafish. Small.

Warner, M.G., Hutchison, J.E., 2003. Linear assemblies of nanoparticles electrostatically organized on DNA scaffolds. Nature Materials 2, 272-277.

Woehrle, G.H., Brown, L.O., Hutchison, J.E., 2005. Thiol-functionalized, 1.5-nm gold nanoparticles through ligand exchange reactions: Scope and mechanism of ligand exchange. Journal of the American Chemical Society 127, 2172-2183.

Woehrle, G.H., Warner, M.G., Hutchison, J.E., 2004. Molecular-level control of feature separation in one-dimensional nanostructure assemblies formed by biomolecular nanolithography. Langmuir 20, 5982-5988.

Zhu, Z.-J., Carboni, R., Quercio, M.J., Yan, B., Miranda, O.R., Anderton, D.L., Arcaro, K.F., Rotello, V.M., Vachet, R.W., 2010. Surface Properties Dictate Uptake, Distribution, Excretion, and Toxicity of Nanoparticles in Fish. Small 6, 2261-2265.

## Acknowledgements

We thank Sinnhuber Aquatic Research Laboratory for the embryos and Dr. Tatiana Zaikova for her assistance in preparation of the materials. These studies were partially supported by National Institute of Environmental Health Sciences (NIEHS), R01ES016896, P3000210, F31 ES019445-02, the Air Force Research Laboratory (AFRL) under agreement number FA8650-05-1-5041, and Environmental Protection Agency (EPA) RD-833320. The views and conclusions contained herein are those of the authors and should not be interpreted as necessarily representing the official policies or endorsements, either expressed or implied, of NIEHS, AFRL, EPA, or the U.S. Government. Further support was provided by the W.M Keck Foundation.

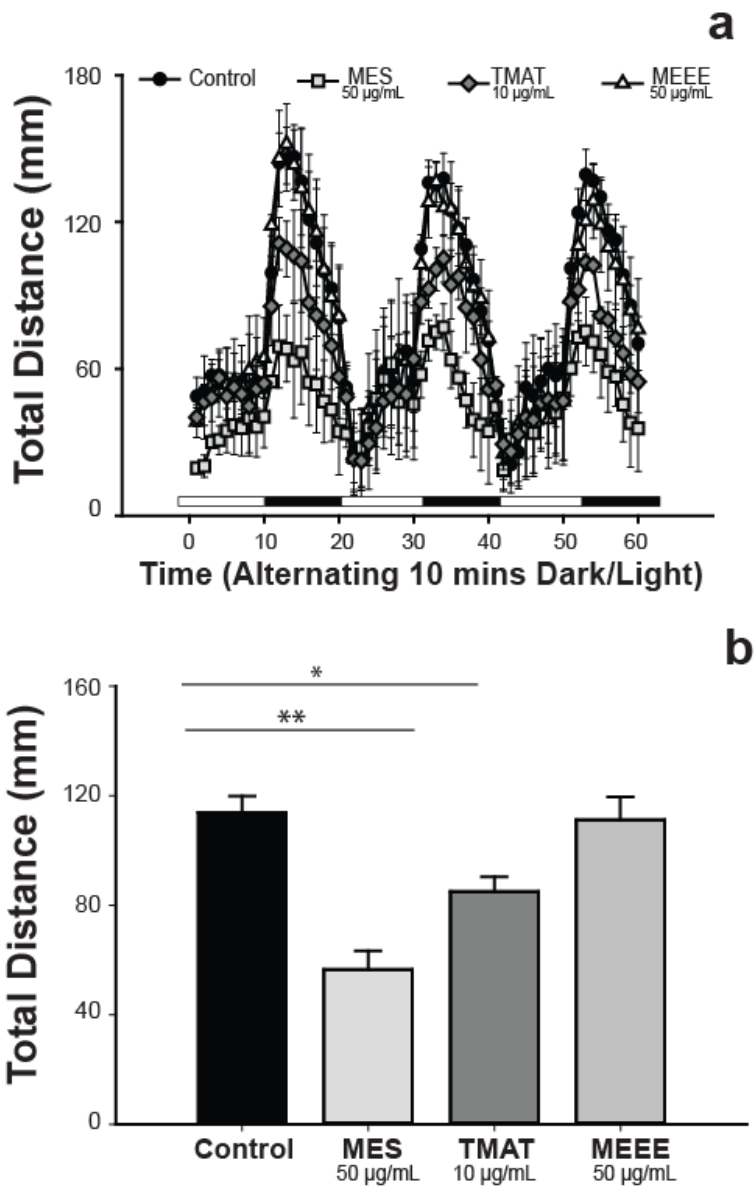


**Figure 4- 1. Transient AuNP exposure results in abnormal behavior at 120 hpf.**

**(a)** Distance moved for embryos exposed to 50 µg/mL of MES- and MEEE-AuNP or 10 µg/mL TMAT-AuNPs. **(b)** Analysis of the total distance traveled during the dark cycle for the sum of three consecutive cycles. Data with * denotes statistical significance determined by one-way ANOVA, Dunnet's post-test. *$p$<0.05, **$p$<0.01. Error bars represent standard error.

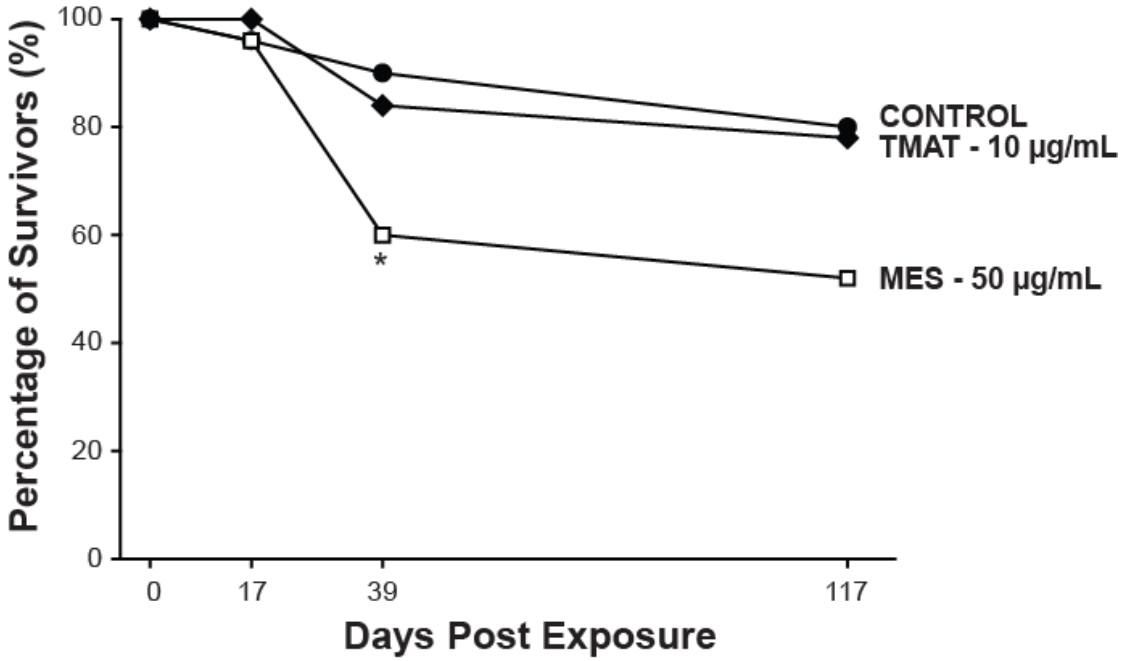


**Figure 4- 2. AuNPs effect on development into adulthood.**
Percent of adult survivorship of embryos exposed to 1.5 nm MES- or TMAT-AuNPs, or embryo media control from 0 to 5 days post fertilization (dpf), and were rinsed prior to being raised in fresh water until 122 dpf. Statistical significance was determined using a Fisher Exact Test. *$p$<0.05.

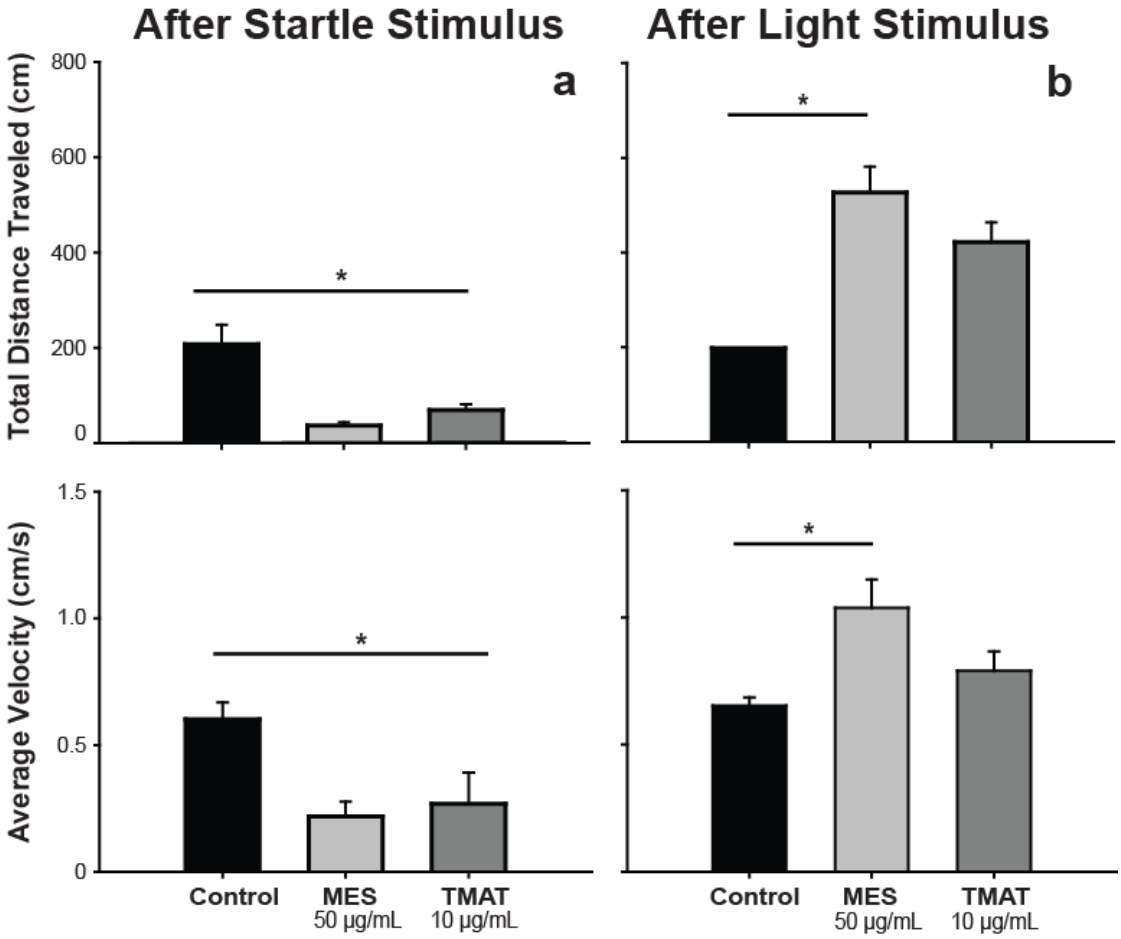


**Figure 4- 3. Total distanced traveled and velocity following a stimulus.** Immediately after a tap on the tank **(a**) or a light stimulus **(b)**, total distance travelled and velocity was recorded for 10 minutes for 5 fish (n=5). To account for size difference in the treated versus control fish, movement data were normalized to fish size using the average morphometric index determined for each treatment group. Statistical significance ($p$<0.05) relative to control was determined using One way ANOVA with a Dunnett's Post Hoc Test. Error bars represent standard error.

**Table 4- 1. Mean growth, survival and condition factor indices (± SEM) of adult zebrafish exposed to embryo media, MES- or TMAT- AuNP.**
Means with different superscript letter designations within columns are statistically significantly different from the embryo media control ($p$<0.05).

| *Exposure* | *Survival (%)* | *Length (mm)* | *Weight (g)* | *Condition factor (K)* |
|---|---|---|---|---|
| Embryo media | 80 | 34.78 (0.22) | 0.50 (0.011) | 0.97 (0.049) |
| MES-AuNPs | 52 | 38.25 (0.32) [a] | 0.63 (0.021) [b] | 1.12 (0.032) |
| TMAT-AuNPs | 78 | 36.27 (0.31) [a] | 0.54 (0.016) | 1.12 (0.022) |

# CHAPTER 5 - MEDIA IONIC STRENGTH IMPACTS EMBRYONIC RESPONSES TO ENGINEERED NANOPARTICLE EXPOSURE

Lisa Truong[1,2],Tatiana Zaikova[2,3],Erik K. Richman[2,3],James E. Hutchison[2,3], and Robert L. Tanguay[1,2,]

[1] Department of Environmental and Molecular Toxicology, the Sinnhuber Aquatic Research Laboratory and the Environmental Health Sciences Center at Oregon State University, Corvallis, OR;

[2]Safer Nanomaterials and Nanomanufacturing Initiative, Oregon Nanoscience and Microtechnologies Institute, Corvallis, OR;

[3]Department of Chemistry, University of Oregon, Eugene, OR

## Abstract

Embryonic zebrafish were used to assess the impact of solution ion concentrations on agglomeration and resulting *in vivo* biological responses of gold nanoparticles (AuNPs). The minimum ion concentration necessary to support embryonic development was determined. Surprisingly, zebrafish exhibit no adverse outcomes when raised in nearly ion free media. During a rapid throughput screening of gold nanoparticles, 1.2 nm 3-mercaptopropionic acid-functionalized gold nanoparticles (1.2 nm 3-MPA-AuNPs) rapidly agglomerate in exposure solutions. When embryos were exposed to 1.2 nm 3-MPA AuNPs dispersed in low ionic media, both morbidity and mortality were induced, but when suspended in high ionic media, there was little to no biological response. We demonstrated that the media ionic strength greatly affects agglomeration rates and biological responses. Most importantly, the insensitivity of the zebrafish embryo to external ions indicates that it is possible, and necessary, to adjust the exposure media conditions to optimize NP dispersion prior to assessment.

## Introduction

The use and incorporation of nanoparticles (NPs) into industrial and consumer products is increasing. At the present, their impact on the environment and human health remains largely unknown. Although many studies have investigated NP effects, the materials used, the experimental assays, the model and platform (*in vivo* or *in vitro*) are highly diverse. These non-systematic approaches make it difficult to interpret the results and understand potential health and environmental implications of NPs. Without toxicological data collected systematically (with similar materials, relevant platforms and assays), it will be challenging to identify potential risks associated with NP exposure. Efficient, relevant, and reliable toxicological models will help acquire this data.

One means of bridging this knowledge gap is by assessing nanoparticle toxicity in complex biological systems. Toxicological assessments can utilize both in vitro and *in vivo* methodologies. While cell culture-based approaches are rapid, cost effective and amendable to high throughput analysis, the utility and predictivity of in vitro data is limited as individual cells in artificial culture environments lack the complexity of whole animal systems. Commonly used *in vivo* systems, such as laboratory rodents (Paigen 2003), are likely more relevant and are extensively used for hazard identification as part of a risk assessment process. However, for the evaluation of numerous nanoparticles, the animal and labor related cost, and the high-test material demands lend rodent-based studies incompatible for high throughput data collection. Rapid,

applicable toxicity screens are necessary to assess the backlog of untested nanoparticles and to begin defining the basic NP characteristics that drive biological responses.

An alternative model to help understand the influence of nanoparticle stability on biological responses is the embryonic zebrafish model (Parng 2005, Bowman and Zon 2010). As a widely accepted model for mechanistic-based toxicological studies, the embryonic zebrafish offers a rapid, high throughput platform to assess chemical and biological system interactions (Rubinstein 2003, Furgeson and Fako 2009, Yang et al. 2009). Female zebrafish produce a few hundred embryos each spawn, which allows for large sample sizes and rapid assessments. Embryos develop externally and are optically clear, allowing for non-invasive evaluations. While other researchers have used zebrafish to assess NPs toxicity (Lee et al. 2007, Bar-Ilan et al. 2009), our group has developed rapid methods using this model to quickly evaluate NP responses in a multi-well plate format in a systematic manner (Usenko et al. 2007, Harper et al. 2008, Truong et al. In Press). Using this *in vivo* platform, the impact of NP exposure on mortality, morbidity, and complex central nervous system function can be rapidly assessed. These assessments are simultaneous and allow for evaluations using a minimal amount of nanomaterials, which further favors rapid throughput data collection.

Most *in vivo* and in vitro screening approaches utilize media that are rich in ionic species. These ions are often critical for viability and cellular

function. It is well established that suspension of nanoparticles in ion-rich aqueous solution often agglomerate resulting in a loss of NPs monodispersion (Murdock et al. 2008). This issue of nanoparticle agglomeration in aqueous conditions extends to effect assessment of NPs in other systems such as cell culture (Jin et al. 2010) and *in vivo* models such as embryonic zebrafish. Agglomeration of nanoparticles is problematical since the resulting surface area, charge, and sizes are drastically different compared to the synthesized particle. Clearly, these parameters influence resulting toxicological outcome.

At present, most researchers assess nanoparticle stability following synthesis in deionized or reverse osmosis (RO) water (Sayes and Warheit 2009), while toxicological studies are often evaluated in ion-rich assay systems. Many groups have tackled the dispersion challenge by coating NPs with various moieties. These include surfactants and compounds such as sodium dodecyl sulfate (SDS), sodium citrate, gum arabic, polyvinylpyrrolidone (PVP), or ligands and polymers (Olenin et al. 2008, Tolaymat et al. 2008). Although these agents are effective in favoring dispersion, they dramatically alter NP surface properties. Coating types on quantum dots are the primary determinant of cytotoxicity and immunotoxicity in HEK cell lines (Ryman-Rasmussen et al. 2007). Alteration to the surface coatings results in significantly varied cytotoxic response to iron oxide nanoparticles (Ying and Hwang 2010). When natural organic matter is added, the surface properties and size characteristics are dramatically altered. For example, Suwannee

River humic acid and fulvic acid, when added to C60 fullerenes, agglomerate size, and morphology significantly changed (Xie et al. 2008). The widespread use of coatings is a major concern as they are used to modify the surface properties of the suspended test material. Since NP surface properties are major drivers of the nanoparticle-biological interface, NP coating for experimental convenience may complicate data interpretation. We propose that the zebrafish offers an alternative method to assessing NP toxicity by overcome some of these limitations. Zebrafish are brackish fish that can tolerate a wide range of ion concentrations (Lawrence 2007, Uliano et al. 2010), but the tolerable range is not well-defined for embryonic development. Embryos can tolerate increased salinity level of 0.196 parts per thousand [ppt] up to 2 ppt (Sawant et al. 2001).

With this information, we instead focused on defining the minimum ion concentration necessary to support normal embryonic zebrafish development. We reasoned that if zebrafish could develop normally in low ionic concentration media, more classes of NPs could be assessed because NP agglomeration could be minimized during the exposure period. In previous studies, we assessed nanoparticle-biological interactions from a library of gold nanoparticles. During that screening, 1.2 nm gold nanoparticles functionalized with 3-mercaptopropionic acid (1.2 nm 3-MPA-AuNPs) rapidly agglomerated and fell out of solution. The goal of the current proof of concept study was to determine the influence of ionic strength on agglomeration and resulting

biological responses. We determined that zebrafish can develop normally up to 120 hours post fertilization (hpf) in the absence of externally added ions and that the ionic concentration of the media greatly influenced the agglomeration rate and biological responses of 1.2 nm 3-MPA-AuNPs. The tolerance of zebrafish embryos to various ionic strength media will have the practical advantage in extending the range of materials that can be more accurately assessed in this powerful *in vivo* model.

## Materials and Methods

### Nanoparticles

**Materials:** Hydrogen tetrachloroaurate (HAuCl4• H2O) was purchased from Strem. Dichloromethane and tetrahydrofuran (THF) were purchased from Mallinckrodt Chemicals. All other compounds were purchased from Sigma-Aldrich Chemical Co. All chemicals were used as received. Nanopure water (18.2 MΩ•cm resistivity) was prepared with a Barnstead Nanopure filtration system and used for all aqueous samples. Polyethersulfone diafiltration membranes Omega TI10K were obtained from Pall Life Sciences. The amine functionalized SMART Grids for TEM imaging were purchased from Dune Sciences.

**Procedure for preparation of 3-mercaptopropionic (MPA) protected gold nanoparticle:** Water soluble, 3-mercaptopropionic stabilized nanoparticles

were prepared through interfacial ligand exchange reaction between 1.5 nm phosphine-stabilized nanoparticles (Au101(PPh)21Cl5) dissolved in dichloromethane/THF mixture with 3-mercaptopropionic acid in water using the literature procedure (Woehrle et al. 2005). Briefly, a solution of 45 mg of 1.5 nm Au101(PPh)21Cl5 in 20 mL of dichloromethane/THF (1:1 mixture) was added to a solution of 23 mg of 3-mercaptopropionic acid in 30 mL of phosphate KH2PO4/K2HPO4 buffer (10mM, pH=8). The biphasic reaction mixture was stirred rapidly at room temperature for 4 hours. The reaction was completed when dark colored nanoparticles transferred from the organic to aqueous phase. The layers were separated, and organic impurities were removed by washing the aqueous layer with dichloromethane. Solvents were removed under reduced pressure at room temperature and crude material was purified from excess ligand by diafiltration using 10 kDa membrane with 50 volumes of nanopure water. After lyophilization, the powdered material was obtained and characterized.

**Analytical procedures:** Proton NMR spectra were collected at 25°C on a Varian Unity Inova 300 MHz instrument in D2O. Chemical shifts are in □ units (ppm) with residual solvent peak (D2O □4.65) as the internal standard. UV-visible (UV-Vis) spectra were obtained on a Hewlett-Packard 8453 diode array instrument with a fixed slit width of 1 nm using 1-cm quartz cuvettes. Transmission electron microscopy (TEM) images were collected at 300kV with

an FEI Titan using a Cs aberration corrector. Nanoparticle samples were prepared on amine functionalized SMART grids by soaking the grid in a dilute nanoparticle solution (0.2 mg/mL) and then in nanopure water for 2 minutes each. The grid was then dried in the air.

**Zebrafish**

Exposure protocol: Adult Tropical 5D strain of zebrafish (Danio rerio) were kept at standard laboratory conditions of 28°C on a 14h light/10h dark photoperiod in fish water (FW) consisting of RO water supplemented with a commercially available salt solution (0.6% Instant Ocean®). Zebrafish were housed and reared at Sinnhuber Aquatic Research Laboratory (SARL) at Oregon State University. Adult zebrafish were group spawned and embryos were collected and staged (Kimmel et al. 1995). To increase bioavailability, at four hours post fertilization (hpf), the chorion, an acellular envelope surrounding the embryo was removed by pronase. Briefly, embryos were placed in 25mL of FW with 50 µL of 41 mg/mL pronase (Sigma Aldrich) and gently agitated for 6.5 minutes; the water was decanted and replenished with fresh FW for 10 minutes. Embryos were rested for 30 minutes prior to transferring into exposure solution. After resting, dechorionated embryos were transferred to individual wells of a 96-well plate with 100 µL of exposure solution (n=16, three replicates). Exposures were static and continued under standard laboratory conditions in sealed plates and kept in the dark until 120

hpf. At 24 hpf, each individual embryo was scored for mortality and developmental progression. By 120 hpf, each embryo was assessed for mortality, and fifteen morphological malformations(Truong et al. 2010). The percent of mortality and total morbidity were calculated and graphed as mean of three replicates with standard error bars.

**Exposure solutions:** 1.2 nm 3-MPA-AuNPs was suspended with varying ionic concentrations of embryo media (EM), these solutions were used to create working solutions with a concentration of 50 µg/mL. A Calipher Zephyr Liquid Handler was used to create five-fold serial dilutions (0 – 50 µg/mL, five concentrations) for each ionic strength medium in 96- well plates. Embryo medium consisted of 15 mM NaCl, 0.5 mM KCl, 1 mM MgSO4, 0.15 mM KH2PO4, 0.05 mM Na2HPO4, and 0.7 mM NaHCO3 (Westerfield 2000). Six ionic strength media were made by diluting 100% EM with RO water [0% (11µS, 0.007 ppt), 0.16% (14µS, 0.01 ppt), 0.8% (34 µS, 0.024 ppt), 4% (113 µS, 0.08 ppt), 20% (480 µS, 0.34 ppt), and 100% (2420 µS, 1.7 ppt) EM]. Since the buffering capacity of the solution would be reduced at the lower ionic strength solutions, the pH of 1.2 nm 3-MPA-AuNPs suspended in the various ionic concentrations was measured and did not vary more than 0.5 units from an average pH of 6.5.

**Behavior assay:** Using Viewpoint LifeScience Zebrabox Quantization System, behavioral responses were evaluated in exposed embryos prior to the toxicity assessment. Prior to evaluation, embryos were acclimated to the light for 20 minutes, after which the lights were turned off (dark period) for 10 minutes, and then on for five minutes (light period). The output data files were processed using a custom perl script to average total movement (pixel changes per second) for the dark period. Sixteen embryos were used per concentration and three replicates were completed.

**Statistics:** All analyses were compiled using SigmaPlot 11 (SPSS Inc, Chicago, IL). One-way ANOVA ($p<0.05$) and Dunnetts post hoc test were used to assess mortality, morbidity and behavioral changes. Each exposure group for each concentration consisted of 16 individual exposed embryos (n=16) and three replicates

## Results

### Characterization of 1.2 nm 3-MPA-AuNPs

Each toxicological assessment was performed using the same parent batch of 1.2 nm 3-MPA-AuNPs. After synthesis, characterization was completed to define the core size and surface functionalization. TEM was used to calculate the average size of the nanoparticles. Size analysis (Figure 1a)

revealed the average particle diameter was 1.2 ± 0.3 nm (N=399). Proton NMR showed broad peak at 2.4–4.2 ppm (Figure 1c) confirming the 3-MPA ligand (Figure 1b) was attached to the gold core and no impurities (which would appear as sharp signals) were detected. Additionally, ultraviolet-visible absorption spectroscopy (UV-Vis) was used to confirm the core size and degree of agglomeration of 1.2 nm 3-MPA-AuNPs in nanopure water (Figure 1d). These methods demonstrate that these AuNPs are free of molecular impurities and are precisely engineered 1.2 nm gold particles functionalized with 3-mercaptopropionic acid ligands.

**Embryo medium causes precipitation of 1.2 nm 3-MPA-AuNPs**

Embryos were exposed to 1.2 nm 3-MPA-AuNPs suspended in 100% embryo medium over a five-fold concentration range (0.08 - 50 µg/mL) to determine if the nanoparticles elicited mortality or if they induced developmental malformations. Upon suspension of the dried 1.2 nm 3-MPA-AuNPs, no precipitation was immediately visible. However, when the embryos were assessed at 24 hpf, nanoparticle precipitants were detected on the bottom of the wells and surrounding the animal. This exposure scenario continued until 120 hpf, when the zebrafish were evaluated. We tracked the agglomeration state of 1.2 nm 3-MPA-AuNPs using UV-VIS and we found that after 18 hours, most of the AuNPs were no longer in solution (Figure 2a). Under these conditions, exposure to 1.2 nm 3-MPA-AuNPs did not increase

mortality or malformations. However, at 50 µg/mL, 100% of the exposed embryos lacked a touch response (data not shown). Although the nanoparticles had agglomerated, they still induced a subtle adverse biological response.

We took the approach to identify a dilution of embryo medium (EM) with a level of ions that could support a stable NP dispersion which should favor an increase in nanoparticle bioavailability throughout an extended exposure period. We evaluated nanoparticle agglomeration at the two highest concentrations (10 and 50 µg/mL) over six percentages of EM (0 - 100%). Absorbance was measured at 18 and 114 hours, which corresponded to the time points the when exposed zebrafish would be evaluated for toxicological responses. As illustrated in Figure 2b, in 0% EM, the 1.2nm 3-MPA-AuNPs did not agglomerate. On the other hand, when 1.2 nm 3-MPA-AuNPs were suspended in 100% EM, only 3 and 0.1% of the particles remained in suspension at 114 hours, at 10 and 50 µg/mL, respectively (Figure 2c). At concentrations between 4 and 100% EM, there was a low percentage of dispersed 1.2 nm 3-MPA-AuNPs. With the decreased ionic concentration, the amount of suspended AuNPs increased. At concentrations between 0 - 0.8% EM, the amount of dispersed AuNPs was typically greater than 90%. This demonstrates that the concentration of ions in the test media indeed plays a major role in the degree of 1.2 nm 3-MPA-AuNPs agglomeration.

**Dechorionated zebrafish embryos can tolerate low ion concentrations**

Although embryonic zebrafish are sensitive to toxicants and well suited for mechanistic-based toxicological studies, the importance of media ionic strength for embryonic development in the absence of the chorion is unknown. To reveal the minimum ionic strength required to support embryonic development, embryos were dechorionated and exposed to six different ion concentration media (five-fold serial dilution: 0, 0.16, 0.8, 4, 20, 100% EM in RO water) at six hpf. The initial assessments at 24 hpf revealed no differences between the groups when scoring for mortality or changes in developmental progression. At 120 hpf, exposed embryos were evaluated for mortality and a full suite of complex morphological endpoints. As Figure 3a illustrates, even at the lower concentrations of EM (0 – 0.8%), the incidence of mortality and malformation at 120 hpf were not statistically different. To determine if varying ion concentration affected central nervous system function, exposed embryos were assessed for motor activity in the dark using ViewPoint LifeScience Zebralab. Larvae in 100% EM had a movement level of five pixels per second in the dark (Figure 3b). At the lower concentrations (0 and 0.16% EM) there was only a modest and not statistically significant decrease in pixels per second (~4). Visually, the embryos exposed to 0% and 100% EM were morphologically indistinguishable (Figure 3c). These studies indicate that dechorionated embryos can tolerate low ionic strength solutions and develop normally to at least 120 hpf.

**1.2 nm 3-MPA-AuNPs developmental toxicity**

To investigate whether the agglomeration of 1.2 nm 3-MPA-AuNPs was masking toxic potential, the AuNPs were prepared at five concentrations (0 – 50 µg/mL) in various ionic strength media. These solutions were then continuously and statically exposed to six hpf dechorionated embryos until 120 hpf. As Figure 4a illustrates, at the higher ionic concentrations (20 - 100% EM), there was little mortality and malformation above background (less than 13%). This correlates well with the stability data showing that less than 20% of the AuNPs was in solution by 120 hpf. For the other ion concentrations (0 - 4% EM), the percent of mortality and malformations increased as the ion concentration decreased. For each ionic concentration, a dose dependent increase in mortality and malformation was observed. At 120 hpf, exposed embryos were assessed for behavioral abnormalities. Data generated from dead or malformed embryos was removed prior to processing. At the higher ion concentrations (4 - 100% EM) there were no statistically significant differences in the motor activity level between the groups, while the lower concentrations (0 – 0.8% EM) motor deficits were significant at the higher nanoparticle concentrations (Figure 4b). Collectively, as the ionic concentration decreased, more 1.2 nm 3-MPA-AuNPs remained in solution and there was a corresponding increase in the percent of mortality, malformation, and behavioral deficits in the exposed embryos.

## Discussion

In this *in vivo* study, we report that dechorionated zebrafish embryos develop normally up to 120 hpf in low ionic strength medium. Furthermore, we report that the response to 1.2 nm 3-MPA-AuNPs exposure is highly dependent on the medial constituents. When suspended in high ionic strength medium, agglomeration occurs within 18 hours and the AuNPs precipitate and elicit little to no adverse biological responses. On the other hand, when suspended in low ionic strength, the AuNPs remain dispersed in solution and induce significant morbidity and mortality.

One potential explanation for the increased sensitivity to 1.2 nm 3-MPA-AuNPs in low ionic strength solutions is that the low salt conditions lead to a general increase in embryonic stress, and the changes in agglomeration state plays little or no role in the differential toxicological response. To directly address this possibility, we exposed embryonic zebrafish to gold nanoparticles with a 1.5 nm core and functionalized either with MES (2-mercaptoethanesulfonic acid) or TMAT (2-mercapto-N, N, N – trimethylethanaminium). Previous studies have demonstrated that these materials induce differential biological responses in zebrafish, but they do not agglomerate over time in standard high ionic strength medium (Harper et al. In press, Truong et al. Submitted). When these particular nanoparticles were suspended in RO water, the biological responses for 1.5nm TMAT-AuNPs (unpublished data) and MES-AuNPs (Supplemental Figure 1) were

indistinguishable from the responses observed when the particles were suspended in high ionic strength medium. This strongly suggests that altering the medium's ionic strength does not lead to a general stress response, and the increase in 1.2 nm 3-MPA-AuNPs toxicity is attributed to changes in the particle properties themselves. The embryo medium used for most embryonic zebrafish toxicity studies typically contains high concentrations of divalent ions, and these ions are known to lead to nanoparticles agglomeration and produce complex particle behaviors (Saleh et al. 2008, Liu et al. 2009). By diluting the EM with RO water, we found that ion concentration of medium influenced agglomeration rate, which is consistent with what was found for cell culture (Jin, et al. 2010) and other mediums (Elimelech and Omelia 1990). When NPs agglomerate, their dissolution is impacted. Agglomeration of silver nanoparticle causes dissolution rate to be reduced, but this is highly dependent on the electrolytes and its concentration in the medium (Li et al. 2010). The number of available particles is drastically different when solutions are monodispersed versus clustering together. When nanoparticles agglomerate, this effectively changes the surface area to volume ratio. Particle surface area is a major player in nanoparticle-induced toxicity. For example, particle surface area was the principle driver in producing differential gene expression changes than was particle mass or number in alveolar macrophages (Waters et al. 2009). Cytotoxicity is also induced by iron oxide in a surface area dependent manner (Ying and Hwang 2010). When NPs

agglomerate, there is a wide distribution of sizes produced. It is currently impossible to understand what fractional agglomerate size is responsible for producing a biological response. In a recent study, cytotoxicity was size-dependent when exposed to 0.8 to 15 nm gold nanoparticles (Pan et al. 2007) and 5, 20 and 50 nm silver nanoparticles (Liu et al. 2010) where the smaller nanoparticles were more toxic than their larger counterpart. Gold and silver nanoparticles regulate membrane receptor internalization in a size-dependent manner (Jiang et al. 2008). These studies suggest that particle size influences the biological response. So effectively, agglomeration of nanoparticle causes a change in concentration, dissolution, surface area, and particle size, which ultimately results in complex differential responses.

We found, for the first time, that dechorionated embryos develop morphologically normal and display normal CNS function up to at least 120 hpf when raised in reverse osmosis (RO) water. These finding will provide new opportunities to exploit embryonic zebrafish to identify the physico-chemical NP properties that are important to produce specific biological responses. With this flexibility, we can now adapt the testing model to conditions ideal for the NPs rather than the other way around. For example, researchers are routinely adding agents to the NP solutions that favor dispersion, but after addition of these agents, the NP surface properties are drastically changed. Although these coating agents help to disperse NPs in aqueous medias, the addition of

capping agents at the very least, complicates the interpretation of toxicological response data with the added variability.

In summary, since embryonic and larval zebrafish can tolerate wide ranges of ionic strength, we recommend an approach where initial NP agglomeration studies are performed under multiple ionic strengths covering the exposure duration. Adjusting the assay to match optimal dispersion conditions will enhance bioavailability and thus increase assay sensitivity. Controlling agglomeration without the addition of arbitrary capping agents will allow assessment of a more broad range of nanoparticles and move us one-step closer to identifying the key physico-chemical NP properties that drive specific biological responses.

## References

Bar-Ilan O, Albrecht RM, Fako VE, Furgeson DY. 2009. Toxicity Assessments of Multisized Gold and Silver Nanoparticles in Zebrafish Embryos. Small 5: 1897-1910.

Bowman TV, Zon LI. 2010. Swimming into the Future of Drug Discovery: *In vivo* Chemical Screens in Zebrafish. ACS Chemical Biology 5: 159-161.

Elimelech M, Omelia CR. 1990. Effect of Electrolyte Type on the Electrophoretic Mobility of Polystyrene Latex Colloids. Colloids and Surfaces 44: 165-178.

Furgeson D, Fako V. 2009. Zebrafish as a correlative and predictive model for assessing biomaterial nanotoxicity. Advanced Drug Delivery Reviews 61: 478-486.

Harper SL, Carriere J, Miller J, Hutchison JE, Maddux BLS, Tanguay RL. In press. Systematic Evaluation of Nanomaterials Toxicity: Utility of Standarized Materials and Rapid Assays.

Harper SL, Dahl JA, Maddux BLS, Tanguay RL, Hutchison JE. 2008. Proactively designing nanomaterials to enhance performance and minimise hazard. International Journal of Nanotechnology 5: 124-142.

Jiang W, Kim BYS, Rutka JT, Chan WCW. 2008. Nanoparticle-mediated cellular response is size-dependent. Nature Nanotechnology 3: 145-150.

Jin X, Li M, Wang J, Marambio-Jones C, Peng F, Huang X, Damoiseaux R, Hoek EMV. 2010. High-Throughput Screening of Silver Nanoparticle Stability and Bacterial Inactivation in Aquatic Media: Influence of Specific Ions. Environmental Science & Technology 44: 7321-7328.

Kimmel CB, Ballard WW, Kimmel SR, Ullmann B, Schilling TF. 1995. Stages of embryonic development of the zebrafish. Dev Dyn 203: 253-310.

Lawrence C. 2007. The husbandry of zebrafish (Danio rerio): A review. Aquaculture 269: 1-20.

Lee KJ, Nallathamby PD, Browning LM, Osgood CJ, Xu XH. 2007. *In vivo* imaging of transport and biocompatibility of single silver nanoparticles in early development of zebrafish embryos. ACS Nano 1: 133-43.

Li X, Lenhart JJ, Walker HW. 2010. Dissolution-Accompanied Aggregation Kinetics of Silver Nanoparticles. Langmuir: null-null.

Liu J, Aruguete DM, Murayama M, Hochella MF. 2009. Influence of Size and Aggregation on the Reactivity of an Environmentally and Industrially Relevant Manomaterial (PbS). Environmental Science & Technology 43: 8178-8183.

Liu W, Wu Y, Wang C, Li H, Wang T, Liao C, Cui L, Zhou Q, Yan B, Jiang G. 2010. Impact of silver nanoparticles on human cells: effect of particle size. Nanotoxicology 4: 319-330.

Murdock RC, Braydich-Stolle L, Schrand AM, Schlager JJ, Hussain SM. 2008. Characterization of nanomaterial dispersion in solution prior to In vitro exposure using dynamic light scattering technique. Toxicological Sciences 101: 239-253.

Olenin AY, Krutyakov YA, Kudrinskii AA, Lisichkin GV. 2008. Formation of surface layers on silver nanoparticles in aqueous and water-organic media. Colloid Journal 70: 71-76.

Paigen K. 2003. One hundred years of mouse genetics: An intellectual history. I. The classical period (1902-1980). Genetics 163: 1-7.

Pan Y, Neuss S, Leifert A, Fischler M, Wen F, Simon U, Schmid G, Brandau W, Jahnen-Dechent W. 2007. Size-Dependent Cytotoxicity of Gold Nanoparticles. Small 3: 1941-1949.

Parng C. 2005. *In vivo* zebrafish assays for toxicity testing. Curr Opin Drug Discov Devel 8: 100-6.

Rubinstein AL. 2003. Zebrafish: from disease modeling to drug discovery. Curr Opin Drug Discov Devel 6: 218-23.

Ryman-Rasmussen JP, Riviere JE, Monteiro-Riviere NA. 2007. Surface coatings determine cytotoxicity and irritation potential of quantum dot nanoparticles in epidermal keratinocytes. Journal of Investigative Dermatology 127: 143-153.

Saleh N, Kim H-J, Phenrat T, Matyjaszewski K, Tilton RD, Lowry GV. 2008. Ionic Strength and Composition Affect the Mobility of Surface-Modified Fe0 Nanoparticles in Water-Saturated Sand Columns. Environmental Science & Technology 42: 3349-3355.

Sawant MS, Zhang S, Li L. 2001. Effect of salinity on development of zebrafish, Brachydanio rerio. Current Science 81: 1347-1350.

Sayes CM, Warheit DB. 2009. Characterization of nanomaterials for toxicity assessment. Wiley Interdisciplinary Reviews: Nanomedicine and Nanobiotechnology 1: 660-670.

Tolaymat TM, El Badawy AM, Genaidy A, Scheckel KG, Luxton TP, Suidan M. 2008. An evidence-based environmental perspective of manufactured silver nanoparticle in syntheses and applications: A systematic review and critical appraisal of peer-reviewed scientific papers. Science of the Total Environment 408: 999-1006.

Truong L, Moody I, Stankus D, Nason J, Lonergan M, Tanguay R. 2010. Differential stability of lead sulfide nanoparticles influences biological responses in embryonic zebrafish. Archives of Toxicology: 1-12.

Truong L, Moody IS, Stankus DP, Nason JA, Lonergan MC, Tanguay RL. In Press. Differential Stability of Lead Sulfide Nanoparticles Influences Biological Responses in Embryonic Zebrafish. Archives of Toxicology.

Truong L, Tilton SC, Zaikova T, Richman E, Waters KM, Hutchison JE, Tanguay RL. Submitted. Surface Functionalities of Gold Nanoparticles (AuNPs) Impact Gene Expression in the Developing Zebrafish. Small.

Uliano E, Cataldi M, Carella F, Migliaccio O, Iaccarino D, Agnisola C. 2010. Effects of acute changes in salinity and temperature on routine metabolism and nitrogen excretion in gambusia (Gambusia affinis) and zebrafish (Danio rerio). Comparative Biochemistry and Physiology - Part A: Molecular & Integrative Physiology 157: 283-290.

Usenko CY, Harper SL, Tanguay RL. 2007. *In vivo* evaluation of carbon fullerene toxicity using embryonic zebrafish. Carbon N Y 45: 1891-1898.

Waters KM, Masiello LM, Zangar RC, Karin NJ, Quesenberry RD, Bandyopadhyay S, Teeguarden JG, Pounds JG, Thrall BD. 2009. Macrophage Responses to Silica Nanoparticles are Highly Conserved Across Particle Sizes. Toxicological Sciences 107: 553-569.

Westerfield M 2000. The Zebrafish Book. Eugene, OR.

Woehrle GH, Brown LO, Hutchison JE. 2005. Thiol-functionalized, 1.5-nm gold nanoparticles through ligand exchange reactions: Scope and mechanism of ligand exchange. Journal of the American Chemical Society 127: 2172-2183.

Xie B, Xu Z, Guo W, Li Q. 2008. Impact of Natural Organic Matter on the Physicochemical Properties of Aqueous C60 Nanoparticles. Environmental Science & Technology 42: 2853-2859.

Yang LX, Ho NY, Alshut R, Legradi J, Weiss C, Reischl M, Mikut R, Liebel U, Muller F, Strahle U. 2009. Zebrafish embryos as models for embryotoxic and teratological effects of chemicals. Reproductive Toxicology 28: 245-253.

Ying E, Hwang H-M. 2010. In vitro evaluation of the cytotoxicity of iron oxide nanoparticles with different coatings and different sizes in A3 human T lymphocytes. Science of the Total Environment 408: 4475-4481.

## Acknowledgements

We the authors thank Sinnhuber Aquatic Research Laboratory for the embryos, Jane La Du for her assistance in preparation of this manuscript and John Miller for helpful discussions regarding nanoparticle preparation. These studies were partially supported by National Institute of Environmental Health Sciences (NIEHS), R01ES016896, P3000210, the Air Force Research Laboratory (AFRL) under agreement number FA8650-05-1-5041, and Environmental Protection Agency (EPA) RD-833320. The views and conclusions contained herein are those of the authors and should not be interpreted as necessarily representing the official policies or endorsements, either expressed or implied, of NIEHS, AFRL, EPA, or the U.S. Government.

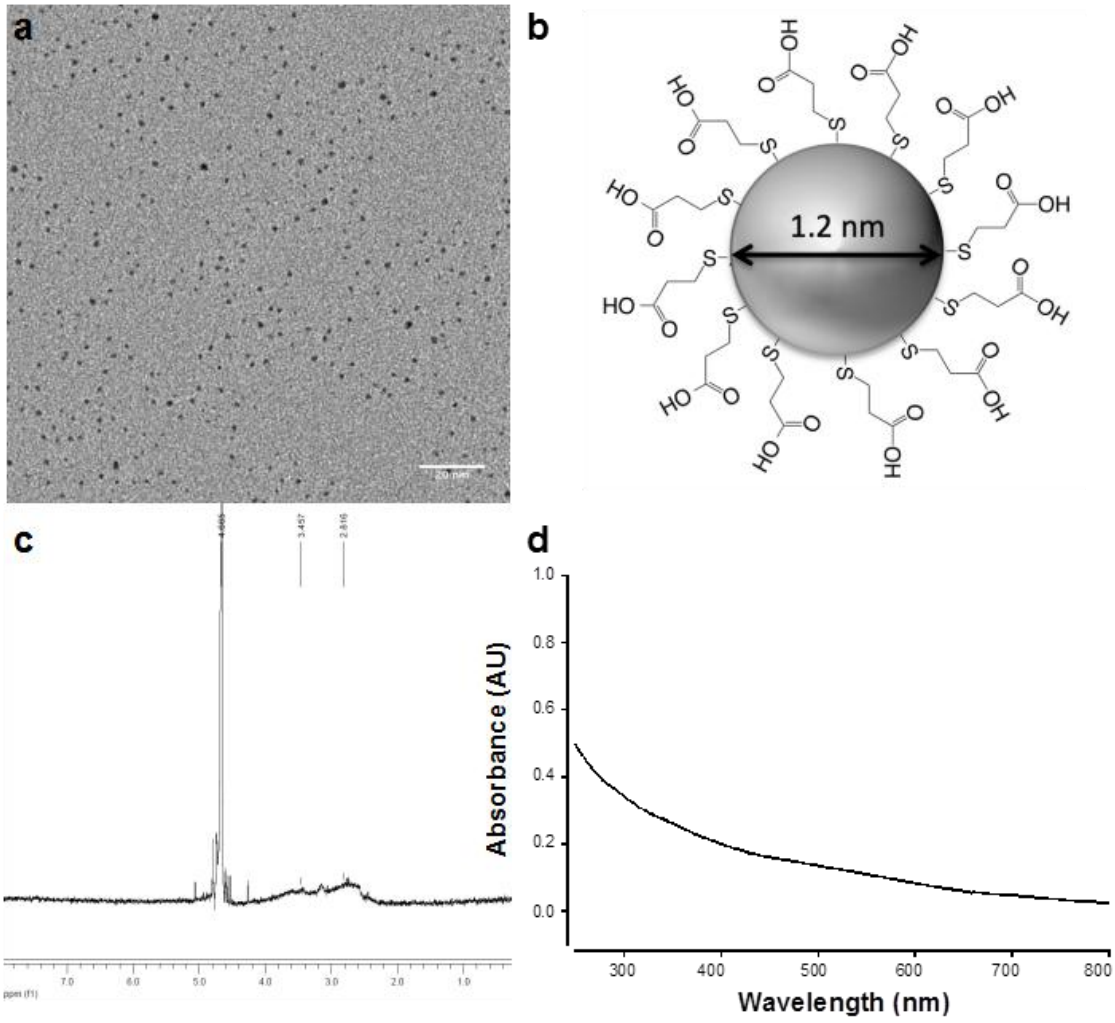


**Figure 5- 1. Characterization of 1.2 nm 3-MPA-AuNPs.**
**(a)** Transmission electron microscopy (TEM) image of 1.2 nm 3-MPA-AuNPs with a scale bar of 20 nm. Analysis of 399 individual particles yields an average particle core size of 1.2 +/- 0.3nm. **(b)** Structure of AuNP with 3-mercaptopropionic acid ligands. **(c)** $^{1}$HNMR analysis demonstrating that the 3-MPA is attached to the surface of the nanoparticle. Impurities, if present would lead to sharp signals at less than 4 ppm chemical shift. The sharp signals at higher than 4 ppm are due to the NMR measurement solvent. **(d)** UV-visible spectrum of 1.2 nm 3-MPA-AuNPs dissolved in nanopure water.

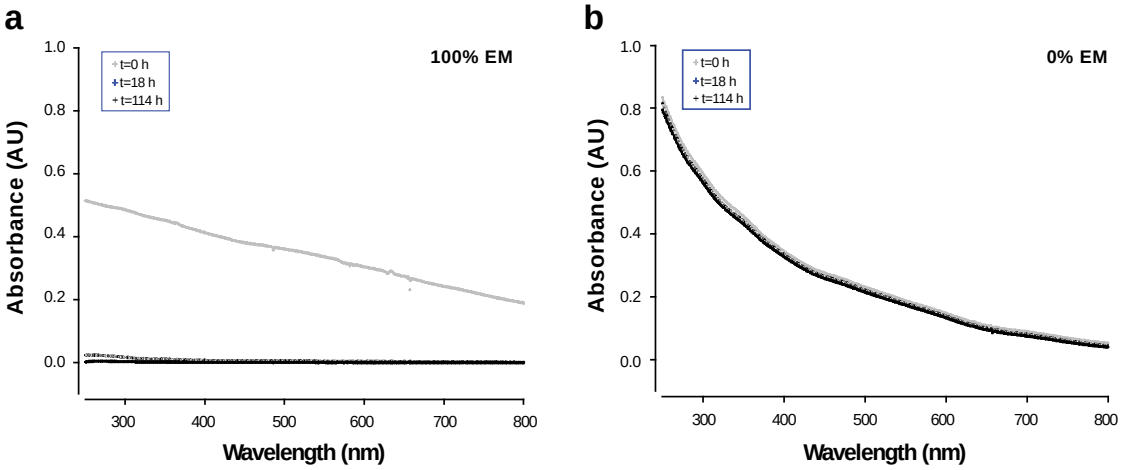


**c**

| Percentage of Embryo Media (%) | 10 (µg/mL) | | 50 (µg/mL) | |
|---|---|---|---|---|
| | 18 hr | 114 hr | 18 hr | 114 hr |
| 100 | 25% | 3% | 1.5% | 0.1% |
| 20 | 62% | 11% | 9% | 0.3% |
| 4 | 78% | 63% | 86% | 79% |
| 0.8 | 77% | 75% | 89% | 90% |
| 0.16 | 87% | 81% | 91% | 94% |
| 0 | 92% | 92% | 97% | 95% |

**Figure 5- 2. 1.2 nm 3-MPA-AuNPs in embryo media.**
Stability of solutions of 1.2 nm 3-MPA-AuNP at 50 µg/mL in **(a)** 100% embryo media (EM) and **(b)** 0% EM at 0, 18 and 114 hrs using UV-Vis. The decrease in absorbance across the spectra to zero in (a) indicates complete loss of nanoparticles from solution, as opposed (b) where essentially no loss of particles is observed. **(c)** Table of nanoparticles that remain in solution at both 10 and 50 µg/mL over time when suspended in varying concentration of embryo media.

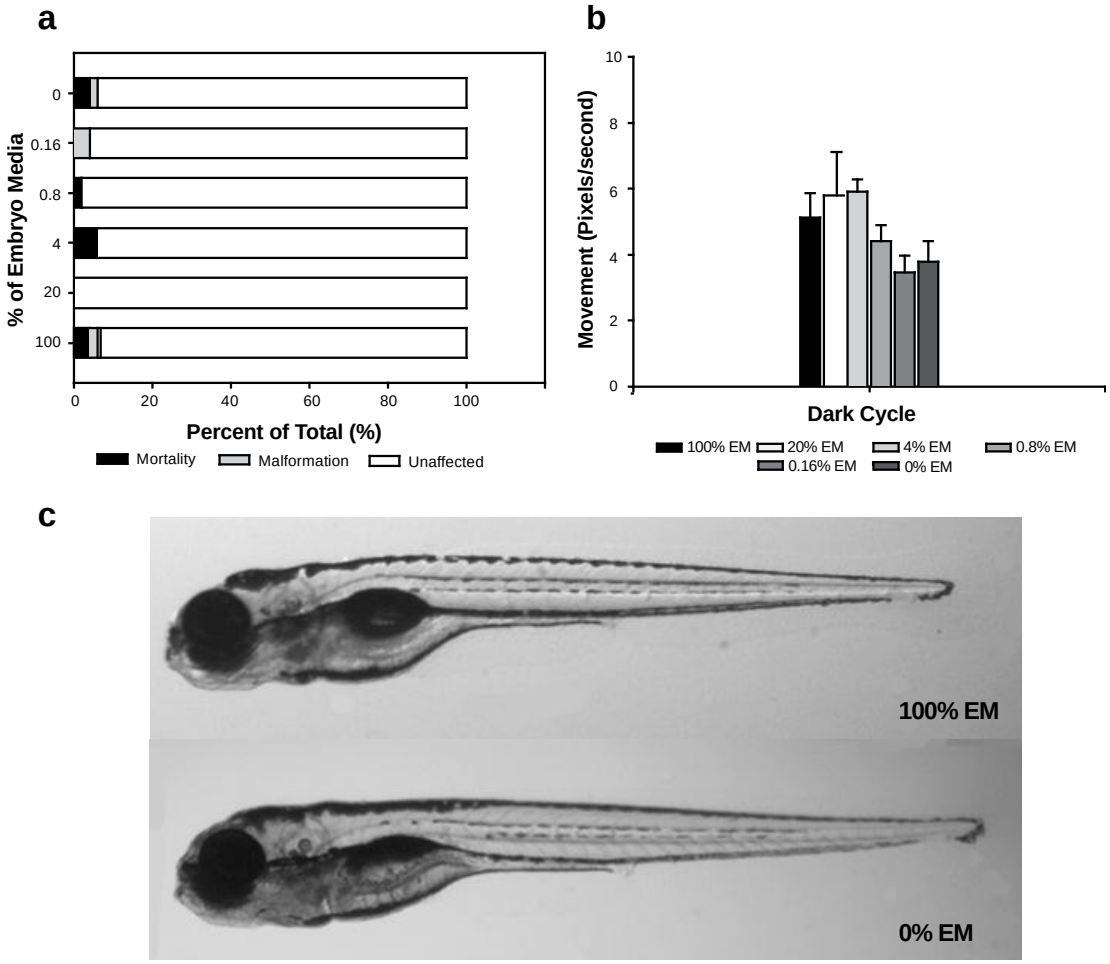


**Figure 5- 3.Embryonic zebrafish exposed to various percentage of EM.** Embryos were dechorionated and exposed to various percentage of embryo media (0, 0.16, 0.8, 4, 20, and 100%) exhibited low mortality and malformation **(a)**. Exposed 120 hours post fertilizations (hpf) embryos did not exhibit a statistically significant change in behavior **(b)**. Images were taken of embryos exposed to 0 and 100% EM at 120 hours post fertilization (hpf) **(c).**

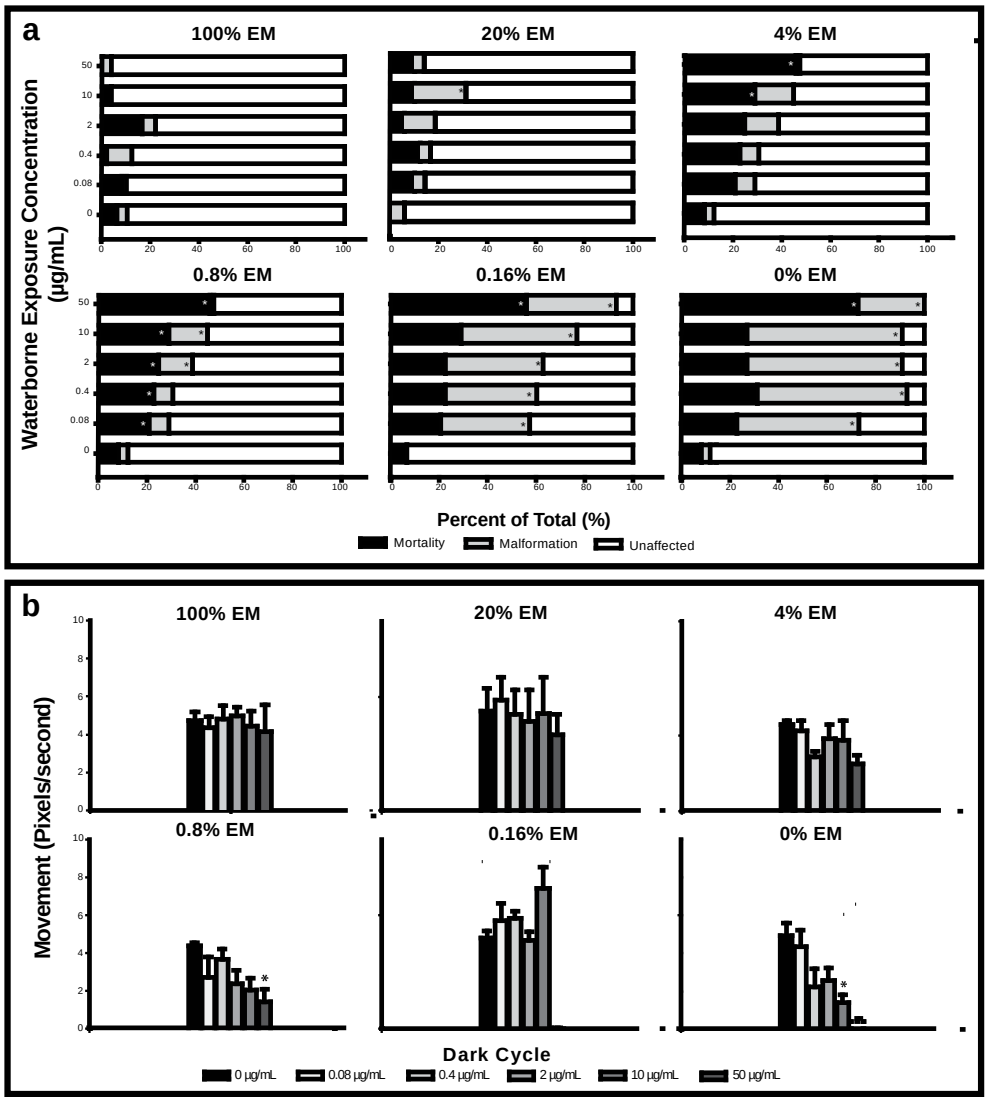


**Figure 5- 4.Toxicity of 1.2 nm 3-MPA-AuNP in various percentage of EM.** Dechorionated embryos were exposed to five concentrations of 1.2 nm 3-MPA-AuNPs and six different solutions with varying ionic concentrations. As the ionic concentration decreased, mortality and malformations increased **(a)**. Surviving embryos at 120 hpf were assessed for behavioral effects. Similarly, the lower concentrations (0-0.8%) caused behavioral changes at higher concentration, while the higher ionic concentrations (4-100%) did not **(b)**. Significance was determined using One Way ANOVA and a Dunnetts Post Hoc Test ($p<0.05$).

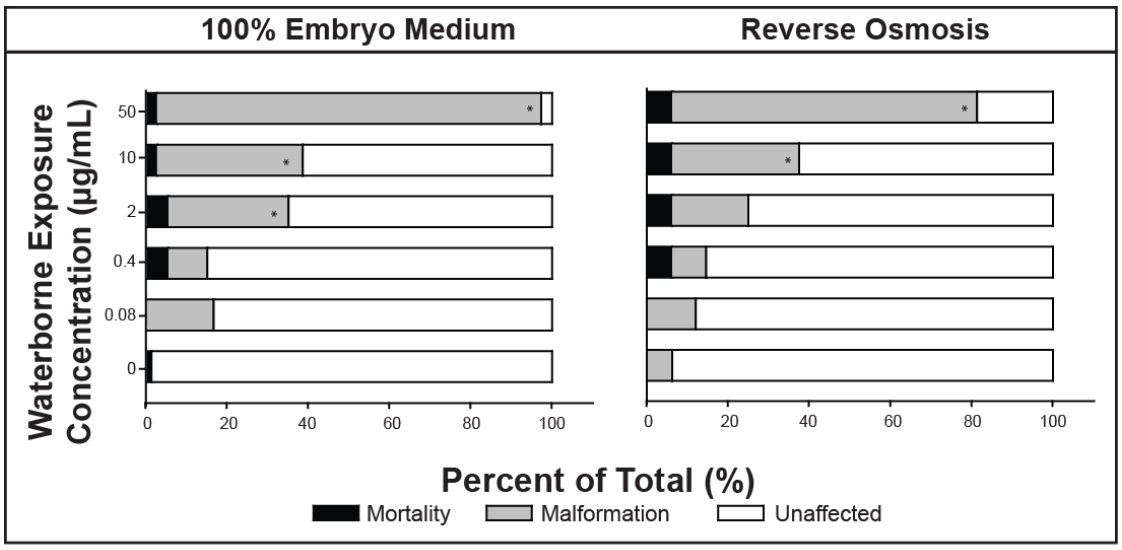


**Figure 5S- 1. 1.5 nm MES-AuNP toxicity in EM and RO.**
Dechorionated embryos were exposed to five concentrations of 1.5 nm MES-AuNPs suspended in 100% embryo medium and reverse osmosis water. The biological responses were indistinguishable between the two media. Data with * was statically significant when using a One Way ANOVA and a Dunnetts Post Hoc Test ($p<0.05$).

# CHAPTER 6 – RNA-SEQ REVEALS EMBRYONIC EXPOSURE TO GOLD NANOPARTICLES RESULTS IN SURFACE-DEPENDENT CHANGES IN GENE EXPRESSION

Lisa Truong[1,2], Tatiana Zaikova [2,3], James E. Hutchison[2,3] and Robert L. Tanguay[1,2]

[1] Department of Environmental and Molecular Toxicology, the Sinnhuber Aquatic Research Laboratory and the Environmental Health Sciences Center at Oregon State University, Corvallis, OR, USA;
[2] The Safer Nanomaterials and Nanomanufacturing Initiative, Oregon Nanoscience and Microtechnologies Institute, Eugene, OR, USA;
[3] Department of Chemistry and the Materials Science Institute, University of Oregon, Eugene, Oregon 97403, USA;

Formatted for Publication in ACSnano

## Abstract

Embryonic zebrafish exposed to 1.2 nm gold nanoparticles (AuNPs) with 3-mercaptopropionic acid (3-MPA) surface group fail to respond to a touch on the caudal fin at 120 hours post fertilization (hpf), while those exposed to 1.3 nm 2-(2-(2-mercaptoethoxy)ethoxy)ethanol (MEEE) respond normally. Addition of a known neuromuscular stimulus, nicotine, revealed the 3-MPA-AuNPs exposed embryos were not paralyzed. Immunohistochemistry labeling axons on Tg(NBT:MAPTGFP)zc3 embryos expressing GFP in primary motor neurons revealed that exposure to 3-MPA-AuNPs did not impact the number of motor neurons, but significantly reduced axonal projections, which may explain the observed inability to sense touch in the caudal fin. To provide insight into the molecular pathways that may mediate the lack of a touch response and the differential gene expression between 3-MPA-AuNP and MEEE-AuNPs, RNA-seq was performed at 48 hpf following 10 µg/mL exposure. We found 64 and 88 genes were differentially expressed by 3-MPA-AuNPs and MEEE-AuNPs, respectively, compared to the control. We identified the most statistically perturbed pathways by 3-MPA-AuNPs were neurophysiological process and signal transduction, with the most misregulated gene being early growth response 1 (egr1). Collectively, these data suggest that exposure to 3-MPA-AuNPs misregulates egr1, which impacts axongenesis in the caudal fin and interferes with glutaminergic synapses preventing the connection of sensory neurons and impede touch

perception. MEEE-AuNPs impacted genes involved in immune and inflammatory systems processes. These findings confirm that surface functionalities of these nanoparticles contribute to the biological response and a systems toxicological approach in a relational and cost-effective model is a highly productive strategy for gaining insight into nanomaterial-biological interactions.

## Introduction

Gold nanoparticles (AuNPs) are utilized in drug delivery, cellular imaging and cancer therapeutics [1]. With the increase in its application, the toxicological data on AuNPs is slowly growing. *In vitro* studies have demonstrated that some AuNPs can induce oxidative stress [2], inflammation [3] and DNA damage [4]. These responses were dependent on the composition, size, and surface chemistry of the AuNPs. In a previous study, we assessed the interactions between nanoparticles and biological systems using a library of gold nanoparticles and the embryonic zebrafish. We found that embryos exposed to 1.2 nm gold nanoparticles functionalized with 3-mercaptopropionic acid [3-MPA] (3-MPA-AuNPs) did not exhibit the characteristic normal swimming response after being touched on the caudal fin [5]. However, exposure to a 1.3 nm gold nanoparticle functionalized with 2-(2-(2-mercaptoethoxy)ethoxy)ethanol [MEEE] (MEEE-AuNPs) had a robust and normal touch response [6]. Since mechanosensory neurons mediate the zebrafish touch response [7], determining the molecular mechanism underlying its absence is a simple assessment of sensory neurons and neuromusculature function.

While there is a growing body of knowledge on the physical effects of NPs on development [6, 8], there is virtually no data available on the genomic responses that precede effects. A valuable approach to investigating the mode of action underlying observed toxic effects is through the global measurements

of gene expression changes. There are multiple methods to conduct transcriptomics to identify gene expression changes after exposure to a chemical or toxicant [6, 9]. The current method of choice is deep sequencing of cDNA fragments (RNA-seq), which is highly sensitive and provides single-base resolution to understand gene expression changes [10]. RNA-seq can be used to quantify and study genome-wide gene expression changes by aligning RNA-seq reads to a reference sequence to identify which genes (features) are expressed in a biological sample at a given point in time. The number of reads per feature is counted and statistics are applied to calculate and infer expression levels [11]. Application of transcriptomics to understand the nanoparticle-biological interaction will help advance the field of nanotechnology by providing data that can be used to understand structure-activity relationships associated with NP toxicity.

The focus of this study was to gain a better understanding of how exposure to 3-MPA-AuNPs, but not MEEE-AuNPs, leads to a larvae with impaired touch response. We conducted RNA-seq using embryos exposed to vehicle control versus 10 µg/mL 3-MPA-AuNPs or 10 µg/mL MEEE-AuNPs from 6 to 48 hpf to understand how exposure to 3-MPA-AuNPs result in an abnormal touch response, impaired locomotor activity, and reduced peripheral axonal projections. We found that developmental 3-MPA-AuNP exposure impacts genes involved in neurophysiological process, apoptosis, signal transduction, and neurogenesis; therefore, we propose that perturbed

neurogenesis pathways, specifically EGR1, mediates the touch response deficiency.

## Results

### Gold nanoparticle characterization and biological response

Two types of gold nanoparticles were precisely engineered with nearly identical attributes, except one was functionalized with 3-mercaptopronic acid (3-MPA) [5]] and the other 2-(2-(2-mercaptoethoxy)ethoxy)ethanol (MEEE) [6]. The average size and size distribution of the AuNPs determined by transmission electron microscopy (TEM) revealed the average particle size for AuNPs functionalized with 3-MPA was 1.2 ± 0.3 nm (N=399) and 1.3 ± 0.5 nm (N=667) for MEEE (**Supplemental Figure 1 a and d**). Characterization using nuclear magnetic resonance ($^1$H-NMR) spectrometry showed a broad peak at 2.4 - 4.5 ppm (**Supplemental Figure 1 b and e**) which confirmed that the ligand was covalently attached and no impurities were detected. We used UV-Vis absorption spectroscopy (Supplemental **Figure 1 c and f**) to confirm the degree of agglomeration. The thorough characterization techniques demonstrate the gold nanoparticles are pure and precisely engineered with 3-MPA and MEEE ligands.

In this study, we assessed the AuNPs's impact on embryonic zebrafish (**Figure 1a**). Exposure to either 3-MPA- or MEEE-AuNPs induced less than 20 percent morphological malformations for all concentrations (0.016 – 50

µg/mL). However, embryos exposed to 3-MPA-AuNPs failed to respond to touch in a dose-dependent manner suggesting that the surface functional group drives the biological response. Embryos exposed to the ligands (MEEE, and 3-MPA) did not exhibit morphological malformations and had normal touch response (data not shown).

**3-MPA-AuNPs exposures impairs locomotor activity**

To determine whether embryos exposed to 3-MPA-AuNPs exhibited an abnormal touch response in the caudal fin because of a neuromuscular deficit, we exploited a known nicotinic acetylcholine (Ach) receptor agonist, nicotine, [12] to stimulate muscular movement at 120 hpf. We found that immediately following exposure to 20 µM nicotine **(Figure 1b)**, larvae from both the control and 3-MPA-AuNP treatments exhibited a burst of swimming activity. For the first 10 seconds, there was a statistical difference in the total activity between the control and the 3-MPA-AuNP treated larvae. In the first 5 seconds, the control larvae swam more than the 3-MPA-AuNP treated. In the next 4 seconds, the 3-MPA-AuNP exposed larvae swam steadily at ~0.4 pixels, while the control larvae decreased to 0.2 pixels at 7 seconds with no further movement afterwards. Despite this difference, the total movement for larvae exposed to control or 3-MPA-AuNPs was not statistically different after the addition of nicotine. Thus, while these data demonstrate that exposure to 3-MPA-AuNPs impacts locomotion, it does not cause paralysis. To more thoroughly investigate the impact of 3-MPA-AuNP on locomotor activity, we

tracked the average speed of the swimming larvae exposed to the control or 3-MPA-AuNPs in a 5 minute light and dark cycle. As **Figure 1c** illustrates, the treated larvae average swim speed was significantly higher in the light, and lower in the dark, compared to the control. In the light, the control larvae speed was less than 1 mm/s, while the treated was ~1.25 mm/s. An inverse trend was observed in the dark, where the average control larvae speed was ~2.0 mm/s, and average speed of the 3-MPA-AuNPs exposed larvae was 1.75 mm/s **(Figure 1d)**. The 3-MPA-AuNP exposed larvae swam a total distance of 105 mm in the dark, while the controls travelled a total of 120 mm in the dark cycle, similar to the total swim distance (115 mm) of MEEE-AuNPs exposed larvae [13]. The swim speed/distance difference between the 3-MPA-AuNPs-exposed larvae and control group further demonstrates that the exposure significantly impacted locomotor activity. In contrast, MEEE-AuNPs exposure did not impact locomotor activity [13], suggesting that the surface functionalization plays a role in the behavioral defects.

**Axonal projection is diminished in the caudal fin following exposure to 3-MPA-AuNPs**

Based on the abnormal touch response and swim behavior data demonstrating impaired locomotor activity, we hypothesized that exposure to 3-MPA-AuNPs impaired neuronal development. To test this, we employed 72

hpf transgenic embryos that express GFP in primary motor neurons (Tg(NBT:MAPTGFP)zc3) to investigate the potential impact on the development of the peripheral nervous system, including innervation of the caudal fin by whole animal immunohistochemistry targeting acetylated alpha tubulin (AAT). This labels most axons and major peripheral processes in developing embryos. Epi-fluorescent images of control **(Figure 2a, c)** and 3-MPA-AuNPs exposed embryos **(Figure 2b, d)** revealed a reduction of axonal projections in the caudal fin fold in the treated embryos.

**Transcriptional profile of control, 3-MPA-AuNPs and MEEE-AuNPs**

For each of 3 replicates per treatment, there was approximately 12 million reads per replicate with a sequence length of 78 base pairs. These reads were mapped using Tophat [14] to ensembl zebrafish assembly 9, which consisted of 17,919 annotated vega genes. Transcripts for each sample were identified using Cufflink [15] and assembled together to create a merged annotation file with 32,480 genes. Each sample was analyzed with FastQC to determine the number of sequences and quality. As **Table 1a** illustrates, the average total sequence length for control, 3-MPA- and MEEE-AuNPs were 11,352,318, 13,536,905, and 13493,012 reads, respectively. Less than 127 genes for each replicate failed to map (0.4%). These values passed quality control and provided confidence for future analysis.

We determined differential gene expression between the two different functionalized gold nanoparticles and the control using the Cuffdiff program [15]. For each set of comparisons (control vs. 3-MPA-AuNPs, or control vs. MEEE-AuNPs), the number of unmapped reads was identified (**Table 1b**). Cuffdiff provided the unmapped reads. Unmapped reads fell in the categories of fail, low data, no test or ok. Genes with a status of "no test" were placed in this category due to insufficient alignments for that gene to test, and those with "low data" were categorized accordingly due to shallow sequencing or excessive complexity of the gene. Only reads with an "OK" status proceeded in the analysis. Approximately 60% of the reads tested belonged to the "OK" category for both comparisons (control vs 3-MPA-AuNPs, and control vs MEEE-AuNPs). We found 64 genes were differentially expressed by 3-MPA-AuNPs and 88 genes by MEEE-AuNPs compared to the control **(Table 1b, Supplemental Table 2)**. Within the 64 statistically significant genes differentially expressed by 3-MPA-AuNP exposure, 57 were elevated, while 7 were repressed. In this comparison, there were ~1% of failed reads, and 60.4% that mapped successfully. MEEE-AuNP exposure resulted in differential expression of 88 genes of which 8 were elevated and 79 were repressed. 0.8% of reads failed to map while 59.4% were successful. Only 5 genes were common between the two treatments (**Supplemental Table 1**).

To confidently ascertain that exposure to 3-MPA- or MEEE-AuNPs caused gene misregulation, we used qRT-PCR to confirm the changes

identified by RNA-seq. We confirmed four misregulated transcripts, two from each comparison that were elevated or repressed. As **Table 2** illustrates, the direction and the magnitude of the gene expression changes observed correspond between qRT-PCR and RNA-seq.

## 3-MPA-AuNPs induced transcriptional activity and impacts on neurophysiological processes

We analyzed the differential gene expression changes between the control and 3-MPA-AuNPs by generating a heatmap using the reads per kilobase of exon per million mapped reads (RPKM) values, which is a measure of transcriptional activity [16]. Genes with RPKM values above 25 are considered to exhibit high levels of transcriptional activity [14b]. As **Figure 3a** illustrates, the control expression pattern comprised ~25% of genes with associated RPKM values >25, while the expression pattern following 3-MPA-AuNPs exposure comprised 40% of genes with RPKM values > 25. To visualize differential expression between 3-MPA-AuNPs and the control, a volcano plot was used to display the 64 statistically significant genes (**Figure 3b**, red), Within the 64 differentially expressed genes, there were 28 and 48 genes with a RPKM greater than 25 in the control and 3-MPA-AuNPs samples, respectively. The gene with the greatest transcriptional activity was BX296557.1 with a baseline RPKM value of 7,916 in the control and 74,377 in 3-MPA-AuNPs.

To understand the pathways that may have been affected by 3-MPA-AuNPs, we utilized commercially available software, Metacore (GeneGo, St. Joseph, MI) to identify the most significant biological processes affected by this nanoparticle. We found that the top 10 statistically significant biological pathways ($p$<0.05) were related to neurophysiological process, apoptosis, signal transduction, inflammation signaling, development, reproduction and immune response **(Figure 5c)**. Neurophysiological processes were the most prevalent with three genes (EGR1, Junbl, PER2).

**MEEE-AuNPs impacts immune and inflammatory response**

We identified that exposure to MEEE-AuNPs leads to differential expression of 88 genes compared to the control. Approximately 26% of the control expression pattern consisted of moderately transcribed genes (RPKM values less than 10), while 53% of the MEEE-AuNPs expression profile consisted of moderately transcribed genes **(Figure 4a)**. For both the control and MEEE-AuNPs samples, over 60% of the genes were highly transcribed with RPKM values greater than 25. A total of 88 genes were significantly misexpressed (**Figure 4b**). Of these 88 differentially expressed genes, the control had 31 genes with a RPKM value higher than 25, while MEEE-AuNPs had 19. The most transcribed gene was zgc:158463 with a RPKM of 258 in the control and 666 in MEEE-AuNPs.

A pathway analysis approach was used for these 88 annotated differentially expressed genes **(Figure 4c)**. We found the top 10 statistically significant biological processes perturbed by MEEE-AuNPs were related to immune response – Th17-derived cytokines, proliferation (positive and negative regulation of cell proliferation), signal transduction, neurophysiological process, and apoptosis. The most statistically significant and prevalent pathway was immune response and inflammation, which comprised four genes: C/EBP, c-Fos, PTGS2, C/EBPbeta.

**Common gold nanoparticle response**

To find common gold nanoparticle gene expression pattern, we took the individual gene lists of control vs 3-MPA-AuNPs and control vs. MEEE-AuNPs gene list and compared those lists to one another **(Figure 5a)**. By doing this, the new list consisted of genes common between the two AuNPs. We found that for 3-MPA-AuNPs, 59 of 64 differentially expressed genes were unique to that gold nanoparticle. For MEEE-AuNPs, 83 of 88 differentially expressed genes were uniquely expressed. There were 5 genes that were common in both comparisons (control vs each gold nanoparticles). These genes were hsp47, fos, BX548011.3, fkbp5, and mmp9. Of these 5 genes, hsp47, BX548011.3 and fkbp5 were differentially expressed in the same direction by both 3-MPA- and MEEE-AuNPs, while the rest were elevated following 3-MPA-AuNPs exposure and repressed following MEEE-AuNPs exposure.

**Gold nanoparticle impacts reproduction, signal transduction and inflammation**

We chose to investigate how surface functionalization of nanoparticles affects biological processes. To accomplish this, the 3-MPA- and MEEE-AuNPs gene lists were compared to the control, and then we directly compared each functional group to identify the top ten statistically significant biological processes **(Figure 5b)**. Figure 5b illustrates that the biological processes that were significantly perturbed by both surface functional groups ($p<0.05$) were reproduction – gonadotropin regulation, signal transduction – leptin signaling, inflammation – IL-6 signaling, and anti-apoptosis. The genes involved in the reproduction – gonadotropin regulation pathway following exposure to MEEE-AuNPs were c-FOS, NUR77, COX-2, and for 3-MPA-AuNPs, the genes misregulated were EGR1 and JunB. EGR1 played a large role in a number of the neuro-related pathways identified by Metacore.

## Discussion

We found that exposure to 3-MPA-AuNPs caused morphological malformations and an abnormal touch response (i.e., failure to respond to a light touch on the caudal fin) [5], while MEEE-AuNPs failed to produce adverse responses [6, 13]. To determine if this response failure was due to a neuromuscular defect, we used nicotine to assess locomotor activity in larvae lacking a touch response. The ability to sense and to move is achieved

through different mechanisms. In this example, 3-MPA-AuNP exposed larvae lack a touch response in the caudal fin region, which can be interpreted two ways. Either the larvae can perceive touch but cannot physically move or they are not able to perceive touch. Therefore, the results of the behavioral experiments involving addition of nicotine to 3-MPA-AuNP exposed larvae demonstrate that because mobility was preserved, the 3-MPA-AuNPs perturbed the sensory portion of the circuit. To our knowledge, this is the first study to use nicotine as a challenge to determine if larvae had motor neuron defects after exposure to a nanoparticle. The larvae exposed to 3-MPA-AuNPs maintain swimming ability, even though locomotor activity was impacted. However, because the 3-MPA-AuNPs exposed larvae responded to nicotine, this test is not appropriate to evaluate whether the larvae can sense the touch. The ability to swim normally indicates that neither the muscle function nor circuits underlying patterned motor output were impacted; suggesting that the sensory side of the touch response circuit is impaired.

Nanoparticle physicochemical properties, specifically surface functionality, greatly influence developmental toxicity [6, 8a]. The nanoparticle core material (lead [8a, 17], silver [18], gold [2, 19], etc) contributes to the toxicity when the core is not sufficiently stabilized. This study confirms that the surface functionalization, in this case, 3-MPA, can impact bioactivity and causes both morphological and behavioral defects. Since every combination of core and surface functional group cannot be tested, a systematic approach to test

precisely designed materials will allow us to determine which components of NPs contribute to in vivo toxicity and establish design principles for safer nanoparticle products.

Embryos exposed to 3-MPA-AuNPs had a lack of a touch response at 120 hpf. Glutamate drives touch response in zebrafish embryos through a rostral loop in the spinal cord [20]. The touch response is dependent on AMPA-type glutamate receptor activation and confined to the most rostral part of the spinal cord. Using whole mount immunohistochemistry and acetylated α-tubulin antibody, we found decreased axongenesis in the caudal fin following 3-MPA-AuNP exposure [21]. Axons grow from head to tail into the tract of the post optic commissure (TPOC) beginning at 18 hpf [22]. In this study, the nanoparticles are present at 6 hpf, which is prior to axongenesis, suggesting the NPs disrupt the axonal growth that initiates at the brain. The immunohistochemistry at 72 hpf shows that the axons extending from the dorsorostral cluster (drc) are not affected, however, the drc axons extend into two directions and pioneer separate tracts; these peripheral extensions were less innervated, shorter and less branched compared to controls. Trowe et al (1996) found that mutation of three genes, oxer, dackel and pinscher, disrupted the mapping of axons along the optic nerve and tract [23]. There are a number of touch-insensitive mutants identified by the 1996 Tubingen large-scale chemical mutagenesis zebrafish screen [24]. For example, the *macho* mutant had the most severe reduction in touch sensitivity compared to the

three other touch-insensitive mutants with reduced voltage-gated sodium current amplitudes in the rohan beard (RB). The severe reduction in touch sensitivity is similar to what is observed in fish exposed to 3-MPA-AuNPs. Upon further characterization of these mutants, the researchers found that most had reduced voltage-gated sodium current amplitudes in the primary mechanosensory RB that are specialized neurons with mechanoreceptors. This suggests that the functional group – 3-MPA – is perturbing the electrophysiology of the RBs and thereby reducing the number of axonal projections.

Using pathway analysis software, we found the neurophysiological processes were perturbed by 3-MPA-AuNPs. A key gene in these pathways is early growth response 1 (EGR-1). This gene was elevated in the RNA-seq. EGR-1 is a highly conserved zinc finger protein that is expressed early and plays an important role in vertebrate development [25]. Its diverse biological functions include cell growth, differentiation and apoptosis. In zebrafish, it is only expressed in specific brain areas at 21 hpf, and expression increases in distinct domains of the central nervous system [26]. To cause an abnormal touch response, 3-MPA-AuNPs must be present from 6 to 48 hpf, which is the same time period EGR-1 is expressed in the forebrain and hindbrain. Pignatelli et al. found that the EGR-1 transcription factor promotes apoptosis of neuronal cells, and this apoptotic activity is mediated by a member of p53 family of proteins [25]. Furthermore, using morpholino oligonucleotides, Hu demonstrated that by

knocking down EGR-1, axonogenesis was reduced in zebrafish [21]. Based on mutant zebrafish exhibiting touch insensitivity, Hortopan et al investigated the role of electrical activity and found that the *mind bomb* mutant zebrafish's brain exhibited spontaneous electrical activity [27]. They conducted a transcriptome analysis using microarray and found that several genes necessary for GABA-mediated signaling were suppressed. These 150 differentially misregulated genes were responsible for the abnormal electrical discharge in the zebrafish. These genes including glutamate decarboxylase, GAD1, a general marker for GABA-mediated synaptic function. It is an enzyme responsible for catalyzing the production of GABA from L-glutamic acid. *Mind bomb* mutants have a drastically reduced level of GAD1. This reduction of GAD1 impacts the level of glutamic acid in the *mind bomb* mutant. The electrophysiological analysis demonstrated that touch response in early embryonic zebrafish arises only after glutamatergic synapses connect sensory neurons. The functional group, mercaptoproponic acid was used to induce seizures and also inhibits GAD [28], which inhibits GABA synthesis. EGR-1 is also inducibility by seizure activity, stimulants, and salient physiological stimuli [29]. We hypothesize that embryos exposed to 3-MPA-AuNPs have reduced glutamate levels potentially affecting levels of GABA and L-glutamic acid and that EGR-1 plays a role in the reduced axonal projections. Based on other research and this study, we suspect that exposure to 3-MPA-AuNPs prior to the onset of axonogenesis causes misregulation of egr-1, which interferes with glutaminergic synpases

and neuroplasticity, thereby preventing the connection of sensory neurons and touch perception.

**Conclusion and Prospects**

In this study, we learned that functional groups can interfere with embryogenesis and this interference causes morphological defects, neurological perturbation and differential gene expression. Specifically, we demonstrated that surface functional groups on two gold nanoparticles caused differential biological responses at the phenotypic and transcriptome level. One functional group – 3-MPA, caused an abnormal touch response, while the other functional group – MEEE – did not. We found that exposure to 3-MPA-AuNPs from 6 to 120 hpf resulted in embryos that were not paralyzed and had unaffected motor neurons. However, at 72 hpf, these embryos had a significant reduction in axonal projection at the caudal fin, which could explain the lack of sensation at that location. Transcriptome analysis of 3-MPA-AuNPs at 48 hpf, identified neurophysicological processes and signal transduction pathways to be significantly misregulated and MEEE-AuNPs perturbed immune and inflammatory systems. Surface functional groups greatly influence the adverse responses and transcriptome profile. These data support the usage of the zebrafish model with a systems transcriptome approach to help develop safer design principles.

## Materials and Methods

**Nanoparticle Materials:** Hydrogen tetrachloroaurate ($HAuCl_4 \bullet H_2O$), was purchased from Sterm. Dichloromethane, tetrahydrofuran (THF), and all other compounds were purchased from Mallinckrodt Chemicals and Sigma-Aldrich Chemical Co, respectively. All chemicals were used as received. Barnstead Nanopure filtration system was used to prepare nanopure water (18.2 MΩ•cm resistivity). Dune Science amine functionalized SMART Grids were used for TEM imaging. Polyethersulfone diafiltration membranes Omega $^{TI}$10K were purchased from Pall Life Sciences.

**Nanoparticle Synthesis of 3-MPA- and MEEE-AuNPs:** This procedure has been reported previously by Truong et al (2011) [6]. Briefly, 1.3 nm phosphine-stabilized nanoparticles ($Au_{101}(PPh)_{21}Cl_5$) were dissolved in dichloromethane/THF mixture with 3-mercaptopropionic acid or MEEE- according to published literature procedure [30]. A solution of 45 mg of 1.3 nm $Au_{101}(PPh)_{21}Cl_5$ in 20 mL of dichloromethane/THF (1:1 mixture) was added to a solution of 23 mg of 3-mercaptopropionic acid in 30 mL of phosphate $KH_2PO_4/K_2HPO_4$ buffer (10mM, pH=8).The mixture was stirred rapidly for 4 hours at room temperature. Dark colored nanoparticles were transferred from the organic to aqueous phase, creating distinct layers that were later separated and the organic impurities were removed by washing the aqueous layer with dichloromethane. The crude material was purified from excess

ligand by diafiltration using 10kDA membrane with 50 volumes of nanopure water.

**AuNPs Characterization:** Transmission electron microscopy (TEM) and UV-Visible (UV-Vis) and proton NMR spectra were used to characterize the 3-MPA- and MEEE-AuNPs. A Varian Unity Inova 300 MHZ instrument was used to collect proton NMR spectra at 25°C in deuterium ($D_2O$). UV-spectra were obtained on a Hewlett-Packard 8453 diode array instrument using 1-cm quartz cuvettes. TEM images were collected using a FEI Titian microscope with Cs aberration corrector. Amine functionalized SMART grids were soaked in a diluted nanoparticle solution (0.2 mg/mL) and then in nanopure water for 2 minutes each. The grids were then air dried prior to imaging.

**Zebrafish Exposure:** Adult Tropical 5D strain zebrafish (*Danio rerio)* were reared and housed in standard laboratory conditions [31] at Oregon State University Sinnhuber Aquatic Research Laboratory (SARL) in Corvallis, Oregon. Embryos were produced by group spawns of adult zebrafish and staged according to Kimmel et al [32]. The chorion, an acellular envelope, was enzymatically removed at 4 hours post fertilization (hpf) according to published protocols to increase bioavailability [33]. Dechorionated embryos were transferred to individual wells of a 96 well plate with 100 µL of control (reverse osmosis water) or exposure solution.

**Zebrafish Behavior Assays:** Dechorionated 5D embryos were exposed in individual wells of a 96 well plate filled with either reverse osmosis water (RO) water or exposure solution of 10 µg/mL of 3-MPA-AuNPs suspended in RO water from 6 to 120 hpf. These exposures were static and kept in the dark. At 120 hpf, we evaluated behavioral responses using Viewpoint LifeScience Zebrabox (Montreal, Canada).

**A) Locomotor behavior (light/dark):** To assess the embryos ability to respond to a light stimulus, embryos were acclimated to the light for 5 minutes (light period), followed by a 5 minute dark period, followed by a second 5 minute light period. Forty-eight embryos were used per treatment, and three replicates were completed for the average speed in the light/ dark stimulus.

**B) Sensory response**: To evaluate whether the embryos exhibited normal motor response, we used the quantization algorithm in the Zebrabox. Under video recording, 20 µL of 100 mM nicotine (Sigma product number: N3876) was added using two multichannel pipettes to both the control and the 3-MPA-AuNPs treated. The activity level was recorded for 17 seconds in the light. Eight embryos per treatment and three biological replicates were used in the nicotine spike experiment.

**Behavior Data Processing & Statistics:** The Zebrabox output files were processed using a custom perl (http://www.perl.org/) script to summarize the

total movement (pixel changes per second) of the larvae in the dark and immediately after the addition of nicotine. To evaluate for statistical difference in the light/dark behavior assay, the average distance sum was compared between control vs 3-MPA-AuNPs using an unpaired T-Test. The total pixel changes over the 17 seconds were summed per treatment to determine whether the locomotor activity was affected. An ANOVA with repeated measures was used for every second to evaluate for differences in the response to the nicotine stimulus.

**Immunohistochemistry:** Adult Tg(*NBT*:MAPT-GFP)zc3 were spawned, and the embryos were dechorionated at 4 hpf. Embryos were exposed to either a vehicle control (RO water) or 10 µg/mL of 3-MPA-AuNPs from 6 to 72 hpf. At 72 hpf, embryos were collected and fixed overnight in 4ºC using 4% paraformaldehyde in phosphate buffered saline (PBS). Details on the immunohistochemistry protocol used were previously published [34]. Monoclonal antibody, acetylated alpha tubulin was used at a dilution of 1:2000. A fluorescent secondary antibody Alexa 555 (Molecular Probes, Eugene, OR) was used at 1:1000 dilution to reveal the primary antibody labeling. Representative images of the caudal fin were taken within one week on a Zeiss Axiovert 200M motorized inverted microscope (Zeiss, Thornwood, NY). The Z stack feature on Axiovision software was set to create 16 micron-thick slices, a total of 11 slices of the caudal fin. Images were taken at a 10x magnification.

**Ilumina Direct RNA Sequencing - Sample Preparation:** 5D embryos were dechorionated and exposed to RO water, 1.3 nm MEEE-AuNPs and 1.2 nm 3-MPA-AuNPs from 6 to 48 hpf. Exposed embryos were pooled into three replicates of 25 embryos, euthanized using MS-222 and washed with Milli-Q water. Excess water was removed from each replicate and 1 scoop of 0.5 mm zirconium oxide beads (Next Advance, Product #ZrOB05) and 500 µL of RNAzol (Molecular Research Center, Product #190) was added, and placed into a Bullet blender (Next Advance, Averill Park, NY) for 3 minutes at a speed of 8. Afterwards, samples were left in room temperature for 5 minutes prior to storage in -80ºC. RNA was isolated using standard protocol published previously [6]. The supernatant was removed, and the RNA pellet was washed four times with 500 µL of 75% ethanol. Between each ethanol wash, the samples were centrifuged for 3 minutes at 8,000 rcf. To suspend the RNA pellet, all ethanol was removed, and almost immediately (to avoid over drying the pellet), 12 µL of RNase- and DNase- free water was added to each sample and vortexed for 2-5 minutes at room temperature. The remaining samples were stored in the -80ºC until all quality assessments were conducted. The quantity and quality of the total RNA isolated was measured using a Nanodrop-1000 Spectrophotometer and an Agilent Bioanalyzer (Center for Gene Research and Biocomputing, CGRB, Oregon State University, OR). All RNA samples passed concentration, and quality requirements (A260/A280≥1.8, and A260/A230≥1.8).

**Illumina Processing:** Three µg of total RNA for 12 samples (three replicates of each treatment) were diluted to a final concentration of 200 ng/µL and submitted for library preparation at the Genomics Core of Lerner Research Institute (Cleveland, Ohio). The core generated standard bar-coded mRNA-seq libraries. Three lanes of a flow cell were used in an Illumina Genome Analyzer IIx. Each lane contained one replicate of each treatment (RO water, 1.3 nm MEEE- and 1.2 nm 3-MPA-AuNPs) and was sequenced using single-ended reads at a length of 78 base pairs. Bar-coded results for each lane were separated and then sequence.txt output files were generated. FastQC (Babraham Bioinformatics) was used to assess the quality of the sequencing experiments.

**RNA-seq Data Analysis:** To check the quality of the sequencing experiments, FastQC (Babraham Bioinformatics, http://www.bioinformatics.babraham.ac.uk/projects/fastqc/) was run for each sample. Each sequence.txt output file was mapped to the zebrafish Ensembl reference genome 9 using Tophat v1.3.3 with Bowtie 2 [14] to align short RNA-seq reads. A custom zebrafish bowtie index was created for aligning the sequencing reads. Tophat default settings were used with the additional setting changes: a minimum intron length of 50, max intron set as 10000, and inner distance between mate set as 165. The resulting aligned reads from Tophat were further processed using Cufflinks v1.1.0 [15] with a max intron length of 10,000, $p<0.05$, an FDR of 0.05, and upper quantile normalization

was used. Cufflinks was used to assemble the aligned reads into transcripts with a reference genome and to express these transcripts in *Fragments per Kilobase of exon per Million fragments mapped* (FPKM). The FPKM is an expression of relative abundance of the transcript. To determine differential expression of genes and isoforms between control, 3-MPA- and MEEE-AuNPs, Cuffdiff analysis was performed. The resulting cufflink assemblies were merged to create a final, merged annotation file. This merged annotation file was used in Cuffdiff to identify differential expression between treatments. The biological replicates were pooled for these analyses comparing the control to each of the nanoparticle treatments using the merged annotation file and *Danio rerio* Zv9 version 61 genome. CummeRbund v1.1.3 [16] was used to visualize results from Cufflinks.

## References


1. Boisselier, E.; Astruc, D., Gold nanoparticles in nanomedicine: preparations, imaging, diagnostics, therapies and toxicity. *Chemical Society Reviews* 2009, *38* (6), 1759-1782.
2. Pan, Y.; Leifert, A.; Ruau, D.; Neuss, S.; Bornemann, J.; Schmid, G.; Brandau, W.; Simon, U.; Jahnen-Dechent, W., Gold Nanoparticles of Diameter 1.4 nm Trigger Necrosis by Oxidative Stress and Mitochondrial Damage. *Small* 2009, *5* (18), 2067-2076.
3. Albanese, A.; Sykes, E. A.; Chan, W. C. W., Rough around the Edges: The Inflammatory Response of Microglial Cells to Spiky Nanoparticles. *ACS Nano* 2010, *4* (5), 2490-2493.
4. Kang, B.; Mackey, M. A.; El-Sayed, M. A., Nuclear Targeting of Gold Nanoparticles in Cancer Cells Induces DNA Damage, Causing Cytokinesis Arrest and Apoptosis. *J. Am. Chem. Soc.* 2010, *132* (5), 1517-1519.
5. Truong, L.; Zaikova, T.; Richman, E. K.; Hutchison, J. E.; Tanguay, R. L., Media ionic strength impacts embryonic responses to engineered nanoparticle exposure. *Nanotoxicology* 2011, *0* (0), 1-9.
6. Truong, L.; Tilton, S. C.; Zaikova, T.; Richman, E.; Waters, K. M.; Hutchison, J. E.; Tanguay, R. L., Surface functionalities of gold nanoparticles impact embryonic gene expression responses. *Nanotoxicology* 2012, *0* (0), 1-10.
7. Carmean, V.; Ribera, A. B., Genetic Analysis of the Touch Response in Zebrafish (Danio rerio). *International Journal of Comparative Psychology* 2010, *23* (1), 91-102.
8. (a) Truong, L.; Moody, I.; Stankus, D.; Nason, J.; Lonergan, M.; Tanguay, R., Differential stability of lead sulfide nanoparticles influences biological responses in embryonic zebrafish. *Archives of Toxicology* 2011, *85* (7), 787-798; (b) Usenko, C. Y.; Harper, S. L.; Tanguay, R. L., In vivo evaluation of carbon fullerene toxicity using embryonic zebrafish. *Carbon N Y* 2007, *45* (9), 1891-1898.
9. Mathew, L. K.; S., S.; Kawakami, A.; Andreasen, E. A.; Lohr, C. V.; Loynes, C. A.; Renshaw, S. A.; Peterson, R. T.; Tanguay, R. L., Unraveling tissue regeneation pathways using chemical genetics. *Journal of Biological Chemical* 2007.
10. Wang, Z.; Gerstein, M.; Snyder, M., RNA-Seq: a revolutionary tool for transcriptomics. *Nat Rev Genet* 2009, *10* (1), 57-63.

11. Cumbie, J. S.; Kimbrel, J. A.; Di, Y.; Schafer, D. W.; Wilhelm, L. J.; Fox, S. E.; Sullivan, C. M.; Curzon, A. D.; Carrington, J. C.; Mockler, T. C.; Chang, J. H., GENE-Counter: A Computational Pipeline for the Analysis of RNA-Seq Data for Gene Expression Differences. *PLoS One* 2011, *6* (10), e25279.

12. Svoboda, K. R.; Vijayaraghavan, S.; Tanguay, R. L., Nicotinic receptors mediate changes in spinal motoneuron development and axonal pathfinding in embryonic zebrafish exposed to nicotine. *J Neurosci* 2002, *22* (24), 10731-41.

13. Truong, L.; Saili, K. S.; Miller, J. M.; Hutchison, J. E.; Tanguay, R. L., Persistent adult zebrafish behavioral deficits results from acute embryonic exposure to gold nanoparticles. *Comparative biochemistry and physiology. Toxicology & pharmacology : CBP* 2012, *155* (2), 269-74.

14. (a) Langmead, B.; Trapnell, C.; Pop, M.; Salzberg, S., Ultrafast and memory-efficient alignment of short DNA sequences to the human genome. *Genome Biology* 2009, *10* (3), R25; (b) Trapnell, C.; Pachter, L.; Salzberg, S. L., TopHat: discovering splice junctions with RNA-Seq. *Bioinformatics* 2009, *25* (9), 1105-1111.

15. (a) Roberts, A.; Pimentel, H.; Trapnell, C.; Pachter, L., Identification of novel transcripts in annotated genomes using RNA-Seq. *Bioinformatics* 2011; (b) Roberts, A.; Trapnell, C.; Donaghey, J.; Rinn, J.; Pachter, L., Improving RNA-Seq expression estimates by correcting for fragment bias. *Genome Biology* 2011, *12* (3), R22; (c) Trapnell, C.; Williams, B. A.; Pertea, G.; Mortazavi, A.; Kwan, G.; van Baren, M. J.; Salzberg, S. L.; Wold, B. J.; Pachter, L., Transcript assembly and quantification by RNA-Seq reveals unannotated transcripts and isoform switching during cell differentiation. *Nat Biotech* 2010, *28* (5), 511-515.

16. Trapnell, C.; Roberts, A.; Goff, L.; Pertea, G.; Kim, D.; Kelley, D. R.; Pimentel, H.; Salzberg, S. L.; Rinn, J. L.; Pachter, L., Differential gene and transcript expression analysis of RNA-seq experiments with TopHat and Cufflinks. *Nat. Protocols* 2012, *7* (3), 562-578.

17. Liu, J.; Hurt, R. H., Ion Release Kinetics and Particle Persistence in Aqueous Nano-Silver Colloids. *Environmental Science & Technology* 2010, *44* (6), 2169-2175.

18. (a) Asharani, P. V.; Wu, Y. L.; Gong, Z. Y.; Valiyaveettil, S., Toxicity of silver nanoparticles in zebrafish models. *Nanotechnology* 2008, *19* (25); (b) Kittler, S.; Greulich, C.; Diendorf, J.; KoÌˆller, M.; Epple, M., Toxicity of Silver Nanoparticles Increases during Storage Because of Slow Dissolution under Release of Silver Ions. *Chemistry of Materials* 2010, *22* (16), 4548-4554; (c) Chio, C.-P.; Chen, W.-Y.; Chou, W.-C.; Hsieh,

N.-H.; Ling, M.-P.; Liao, C.-M., Assessing the potential risks to zebrafish posed by environmentally relevant copper and silver nanoparticles. *Sci. Total Environ.* 2012, *420* (0), 111-118.

19. Pan, Y.; Neuss, S.; Leifert, A.; Fischler, M.; Wen, F.; Simon, U.; Schmid, G.; Brandau, W.; Jahnen-Dechent, W., Size-Dependent Cytotoxicity of Gold Nanoparticles. *Small* 2007, *3* (11), 1941-1949.

20. Pietri, T.; Manalo, E.; Ryan, J.; Saint-Amant, L.; Washbourne, P., Glutamate Drives the Touch Response Through a Rostral Loop in the Spinal Cord of Zebrafish Embryos. *Dev. Neurobiol.* 2009, *69* (12), 780-795.

21. Hu, C.-Y.; Yang, C.-H.; Chen, W.-Y.; Chen, Y.-H.; Huang, C.-J.; Tsai, H.-J., The change in the early retinal development of zebrafish after Egr1 gene knockdown. *Invest. Ophthalmol. Vis. Sci.* 2004, *45* (5), 687-.

22. Hjorth, J.; Key, B., Development of axon pathways in the zebrafish central nervous system. *Int. J. Dev. Biol* 2002, *46*, 609-619.

23. Trowe, T.; Klostermann, S.; Baier, H.; Granato, M.; Crawford, A. D.; Grunewald, B.; Hoffmann, H.; Karlstrom, R. O.; Meyer, S. U.; Muller, B.; Richter, S.; Nusslein-Volhard, C.; Bonhoeffer, F., Mutations disrupting the ordering and topographic mapping of axons in the retinotectal projection of the zebrafish, Danio rerio. *Development* 1996, *123* (1), 439-450.

24. (a) Granato, M.; van Eeden, F. J.; Schach, U.; Trowe, T.; Brand, M.; Furutani-Seiki, M.; Haffter, P.; Hammerschmidt, M.; Heisenberg, C. P.; Jiang, Y. J.; Kane, D. A.; Kelsh, R. N.; Mullins, M. C.; Odenthal, J.; Nusslein-Volhard, C., Genes controlling and mediating locomotion behavior of the zebrafish embryo and larva. *Development* 1996, *123* (1), 399-413; (b) Haffter, P.; Granato, M.; Brand, M.; Mullins, M. C.; Hammerschmidt, M.; Kane, D. A.; Odenthal, J.; van Eeden, F. J.; Jiang, Y. J.; Heisenberg, C. P.; Kelsh, R. N.; Furutani-Seiki, M.; Vogelsang, E.; Beuchle, D.; Schach, U.; Fabian, C.; Nusslein-Volhard, C., The identification of genes with unique and essential functions in the development of the zebrafish, Danio rerio. *Development* 1996, *123* (1), 1-36.

25. Pignatelli, M.; Luna-Medina, R.; Perez-Rendon, A.; Santos, A.; Perez-Castillo, A., The transcription factor early growth response factor-1 (EGR-1) promotes apoptosis of neuroblastoma cells. *Biochem J* 2003, *373*, 739-46.

26. Close, R.; Toro, S.; Martial, J. A.; Muller, M., Expression of the zinc finger Egr1 gene during zebrafish embryonic development. *Mechanisms of Development* 2002, *118* (1–2), 269-272.

27. Hortopan, G. A.; Dinday, M. T.; Baraban, S. C., Spontaneous Seizures and Altered Gene Expression in GABA Signaling Pathways in a mind bomb Mutant Zebrafish. *The Journal of Neuroscience* 2010, *30* (41), 13718-13728.

28. Lamar, C., MERCAPTOPROPIONIC ACID: A CONVULSANT THAT INHIBITS GLUTAMATE DECARBOXYLASE1. *Journal of Neurochemistry* 1970, *17* (2), 165-170.

29. Snyder-Keller, A.; Chandra, R.; Lin, Y.; Mitchell, E. S., Basal EGR-1 (zif268, NGFI-A, Krox-24) expression in developing striatal patches: role of dopamine and glutamate. *Brain Research* 2002, *958* (2), 297-304.

30. Woehrle, G. H.; Brown, L. O.; Hutchison, J. E., Thiol-functionalized, 1.5-nm gold nanoparticles through ligand exchange reactions: Scope and mechanism of ligand exchange. *J. Am. Chem. Soc.* 2005, *127* (7), 2172-2183.

31. Westerfield, M., *The Zebrafish Book*. Eugene, OR, 2000.

32. Kimmel, C. B.; Ballard, W. W.; Kimmel, S. R.; Ullmann, B.; Schilling, T. F., Stages of embryonic development of the zebrafish. *Dev Dyn* 1995, *203* (3), 253-310.

33. Truong, L.; Harper, S. L.; Tanguay, R., *Evaluation of embryotoxicity using the zebrafish model*. 1 ed.; Humana Press: 2011; Vol. 691, p 431.

34. Svoboda, K. R.; Linares, A. E.; Ribera, A. B., Activity regulates programmed cell death of zebrafish Rohon-Beard neurons. *Development* 2001, *128* (18), 3511-3520.

## Acknowledgements

The authors would like to thank the staff of the Sinnhuber Aquatic Research Laboratory for the embryos, Katerine Saili and Leah Wehmas for manuscript assistance, and Christopher Sullivan for his technical assistance in processing RNA-seq data. These studies were partially supported by National Institute of Environmental Health Sciences (NIEHS), R01 ES01696, P30 ES000210, P42 ES016465, and F31 ES019445. The views and conclusions contained herein are those of the authors and should not be interpreted as necessarily representing the official policies or endorsements, either expressed or implied of NIEHS, or the US Government.

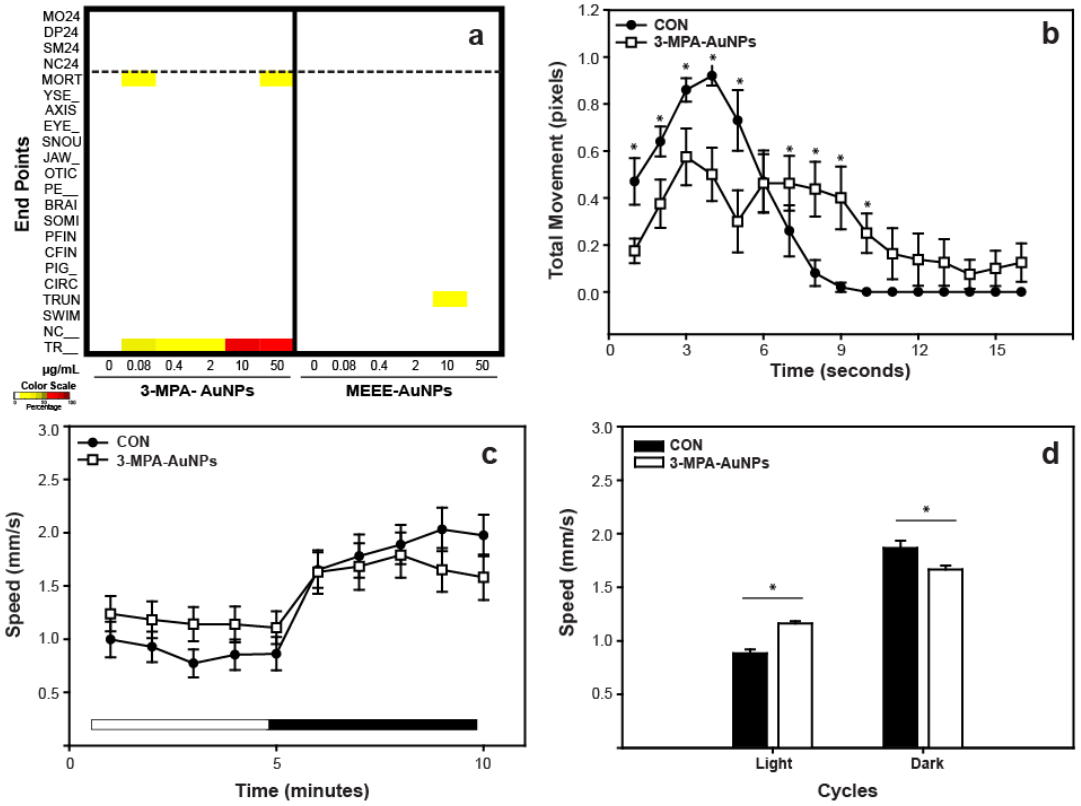


**Figure 6- 1. The development and behavior of embryos exposed to gold nanoparticles.**

**(a)** Heatmap demonstrating that exposure to MEEE functionalized gold nanoparticle does not induce adverse responses, but MPA caused a dose dependent abnormal touch response. Mortality was assessed at both 24 and 120 hpf, while only the surviving embryos at 120 hpf were evaluated for 16 morphological malformations (n=16, two replicates). When 100% mortality was observed, the endpoints were grayed out to illustrate there were no survivors at that concentration. Surface functionalities influenced the toxicity of the cellulose nanocrystals. Endpoint evaluated are defined as follows: MO24 = mortality observed at 24 hpf; DP24 = developmental progression at 24 hpf; SM24 = spontaneous movement at 24 hpf; NC24 = notochord malformation at 24 hpf. Endpoints evaluated at 120 hpf were: MORT = cumulative mortality; YSE = yolk sac edema; AXIS = axis defects; EYE = eye defects; SNOU = snout defect; JAW = jaw defect, OTIC = otic (ear) defect; PE = pericardial edema; BRAI = brain defect; SOMI = somite defect; PFIN and CFIN = pectoral and cadual fin defect; PIG = pigmentation abnormalities; CIRC = circulation defects; TRUN = trunk defect; SWIM = swim bladder abnormalities; NC = notochord defect at 120 hpf and TR = touch response abnormality. **(b)** 3-MPA and control exposed 5 day old larvae were stimulated with a neuromuscular stimulus, nicotine, and swimming activity was measured for 17 seconds afterwards. Statistical significance determined by a one way ANOVA with repeated measures. **(c)** Swimming behavior of control and 3-MPA larvae that were in 5 minute of the light, and 5 minute in the dark. **(d)** The average speed of the control and 3-MPA larvae for the 5 minute light periods. Statistical significance determined by T-test, $p<0.05$.

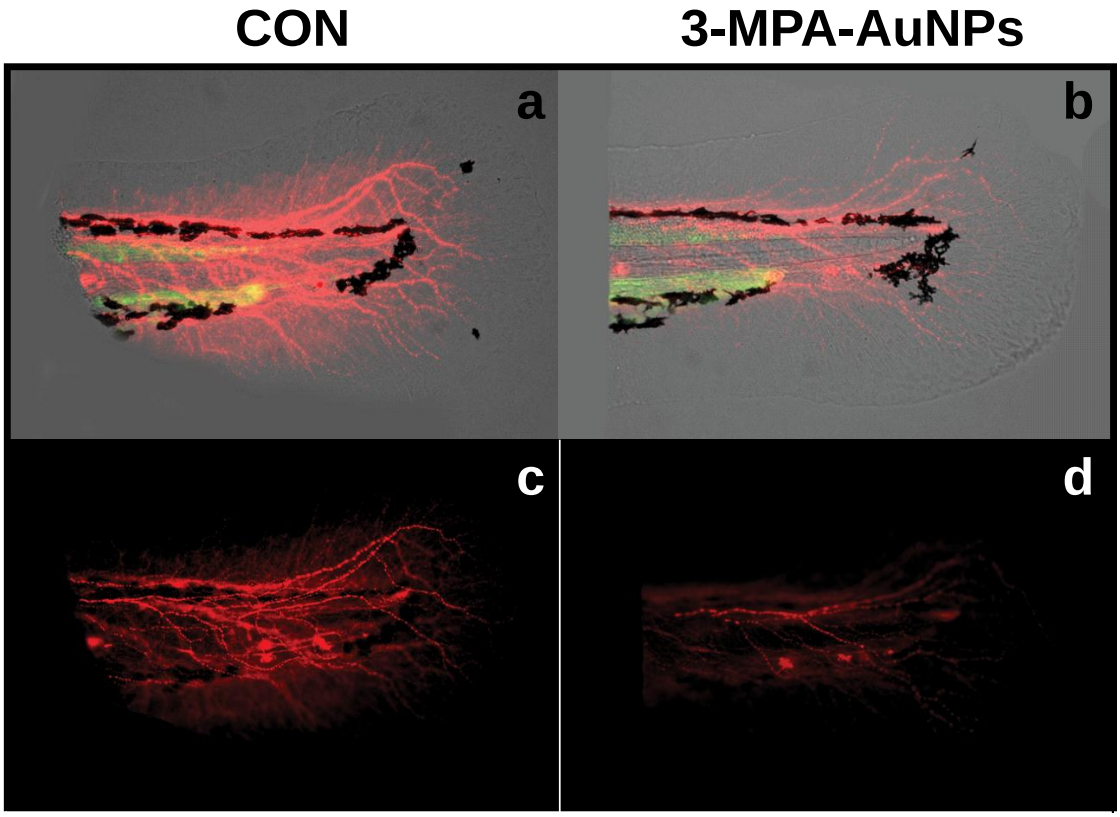


**Figure 6- 2. Whole mount immunohistochemistry on control and exposed embryos.**
Brightfield imaging **(a)** control and **(b)** 3-MPA-AuNP exposed embryos **(c,d)** Axonal projection labeled with acetylated alpha tubulin antibody.

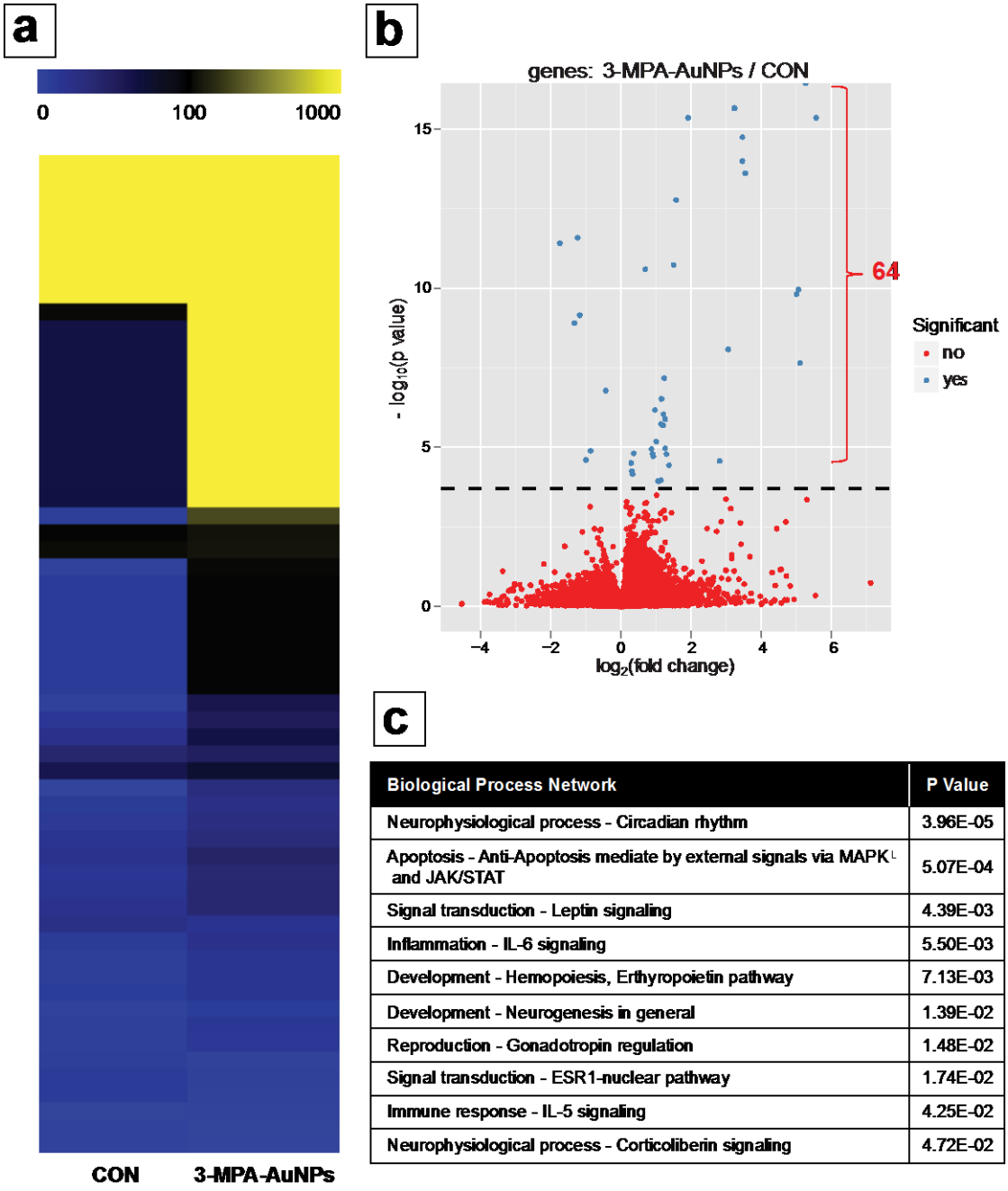


| Biological Process Network | P Value |
|---|---|
| Neurophysiological process - Circadian rhythm | 3.96E-05 |
| Apoptosis - Anti-Apoptosis mediate by external signals via MAPK$^{L}$ and JAK/STAT | 5.07E-04 |
| Signal transduction - Leptin signaling | 4.39E-03 |
| Inflammation - IL-6 signaling | 5.50E-03 |
| Development - Hemopoiesis, Erthyropoietin pathway | 7.13E-03 |
| Development - Neurogenesis in general | 1.39E-02 |
| Reproduction - Gonadotropin regulation | 1.48E-02 |
| Signal transduction - ESR1-nuclear pathway | 1.74E-02 |
| Immune response - IL-5 signaling | 4.25E-02 |
| Neurophysiological process - Corticoliberin signaling | 4.72E-02 |

**Figure 6- 3. 3-MPA-AuNPs RNA-seq (a) gene expression profile (b) volcano plot of statistically significant genes and (c) top 10 significant biological process networks identified by metacore.**

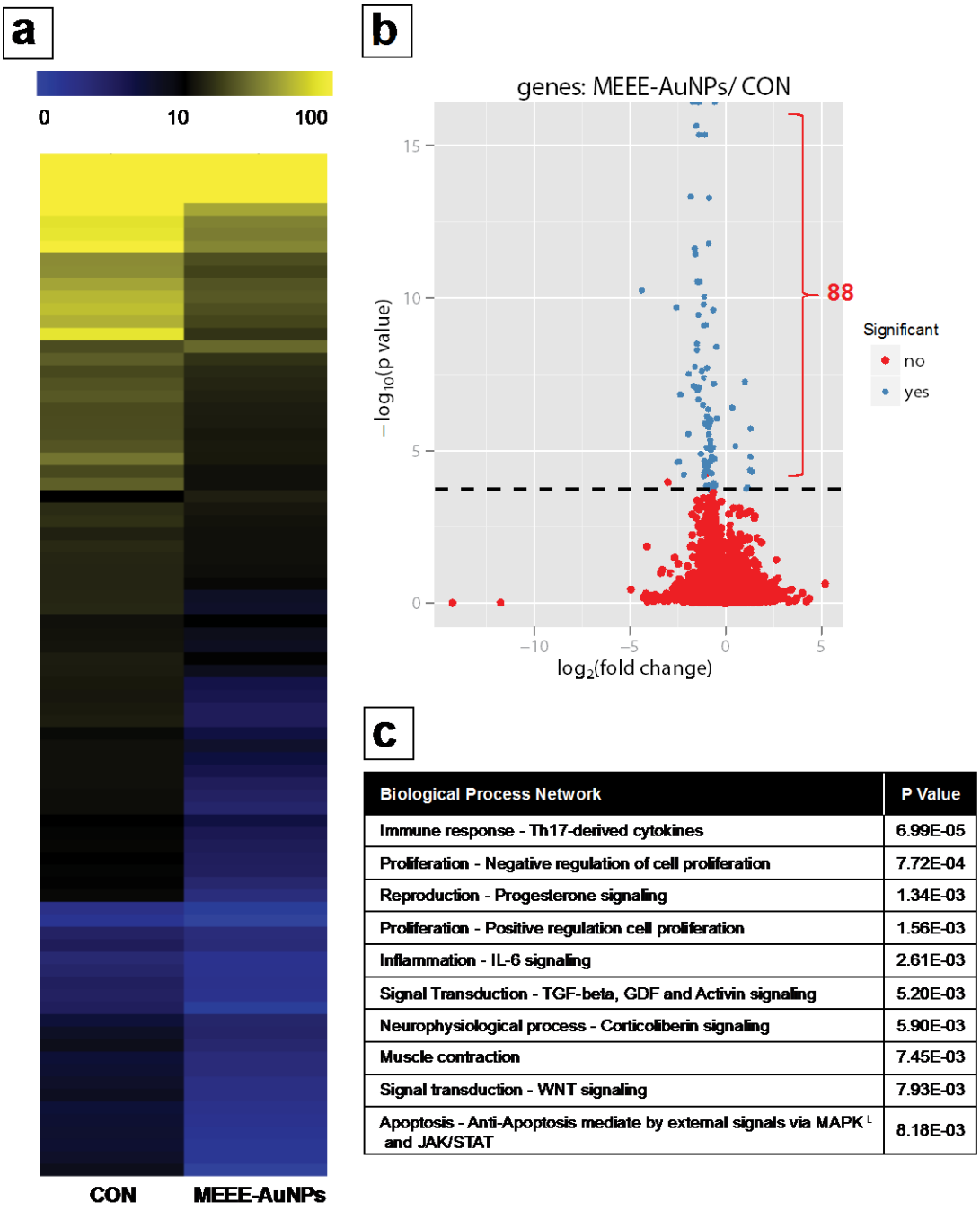


c

| Biological Process Network | P Value |
|---|---|
| Immune response - Th17-derived cytokines | 6.99E-05 |
| Proliferation - Negative regulation of cell proliferation | 7.72E-04 |
| Reproduction - Progesterone signaling | 1.34E-03 |
| Proliferation - Positive regulation cell proliferation | 1.56E-03 |
| Inflammation - IL-6 signaling | 2.61E-03 |
| Signal Transduction - TGF-beta, GDF and Activin signaling | 5.20E-03 |
| Neurophysiological process - Corticoliberin signaling | 5.90E-03 |
| Muscle contraction | 7.45E-03 |
| Signal transduction - WNT signaling | 7.93E-03 |
| Apoptosis - Anti-Apoptosis mediate by external signals via MAPK L and JAK/STAT | 8.18E-03 |

**Figure 6- 4. MEEE-AuNPs RNA-seq (a) gene expression profile (b) volcano plot of statistically significant genes and (c) top 10 significant biological process networks identified by metacore.**

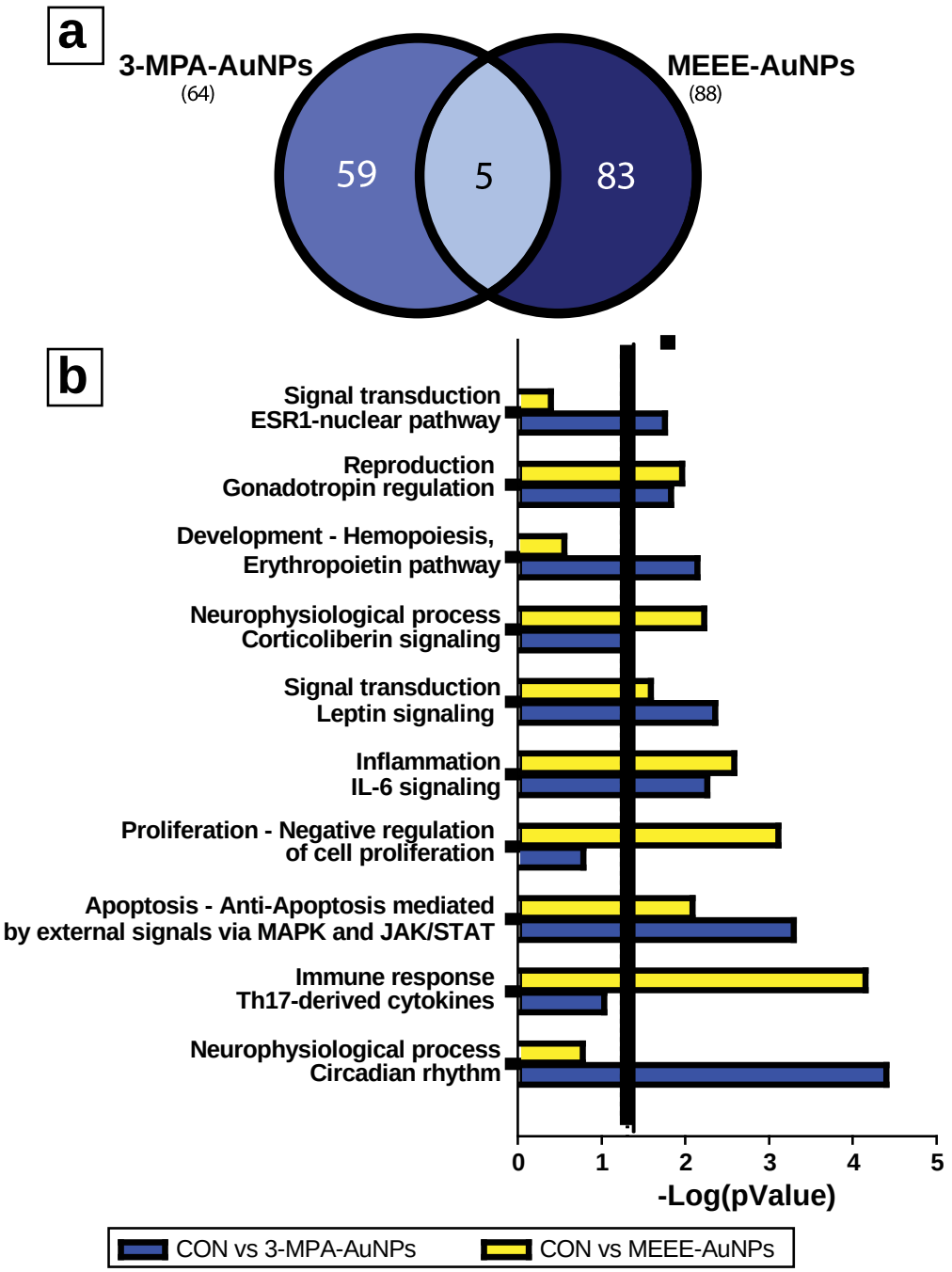


**Figure 6- 5.Functional group comparison.**
**(a)** Venn diagram comparing statistically significant genes between 3-MPA and MEEE. **(b)** Significant pathway comparison between the two surface functional groups. The black line indicates signifies ($p<0.05$).

**Table 6- 1. Data analysis of RNA-seq results.**
**(a)** Total sequence reads for each replicate in the control, 3-MPA-AuNPs, and MEEE-AuNPs. **(b)** Detailed table illustrating the number of significant reads, and the quality of the reads out of 30,509.

(a)

| Samples | Total Sequences | # of failed genes |
|---|---|---|
| **Control** | **11,362,318** | |
| **Rep 1** | 12,099,368 | 125 (0.38%) |
| **Rep 2** | 12,766,649 | 124 (0.38%) |
| **Rep 3** | 9,220,937 | 121 (0.37%) |
| **3-MPA-AuNPs** | **13,536,905** | |
| **Rep 1** | 15,985,052 | 122 (0.37%) |
| **Rep 2** | 9,371,914 | 124 (0.38%) |
| **Rep 3** | 15,253,749 | 127 (0.39%) |
| **MEEE-AuNPs** | **13,493,012** | |
| **Rep 1** | 12,318,958 | 121 (0.37%) |
| **Rep 2** | 15,687,783 | 127 (0.39%) |
| **Rep 3** | 12,471,297 | 124 (0.38%) |

(b)

| | Total # of Statistically Significant Genes | # genes elevated | # genes repressed | Distribution of Reads | | |
|---|---|---|---|---|---|---|
| | | | | # of Failed | # of no test | # of Ok |
| **Control vs 3-MPA-AuNP** | 64 | 57 | 7 | 311/30,509 (1%) | 11,759 (38.5%) | 18,439 (60.4%) |
| **Control vs MEEE-AuNP** | 88 | 9 | 79 | 245 (0.8%) | 12,124 (39.7%) | 18,137 (59.4%) |

5% FDR, Upper Quantile Normalized

**Table 6- 2. Confirmation of statistically significant genes determined by RNA-seq using qRT-PCR.**

Genes were selected from the statistically significant gene lists from control vs 3-MPA-AuNPs, and control vs MEEE-AuNPs to determine if the misregulation identified by RNA-seq was correct. qRT-PCR confirmed that the direction of the misregulation was consistent, but the magnitude was not necessarily identical.

| Gene Symbol | Gene Accession ID | Gene Name | Fold Change at 48 hpf | | | |
|---|---|---|---|---|---|---|
| | | | 3-MPA-AuNPs | | MEEE-AuNPs | |
| | | | RNA-seq | qPCR | RNA-seq | qPCR |
| EGR1 | NM_131248 | early growth response 1 | 1.92↑ | 1.89↑ | - | - |
| JUNBB | NM_212750 | jun B proto-oncogene b | 1.56↑ | 2.14↑ | - | - |
| FOSL1 | NM_0011552 | FOS-like antigen a | - | - | 4.39↑ | 2.03↑ |
| FOSB | NM_001007312 | FBJ murine osteosarcoma viral oncogene homolog B | - | - | 2.57↑ | 2.67↑ |

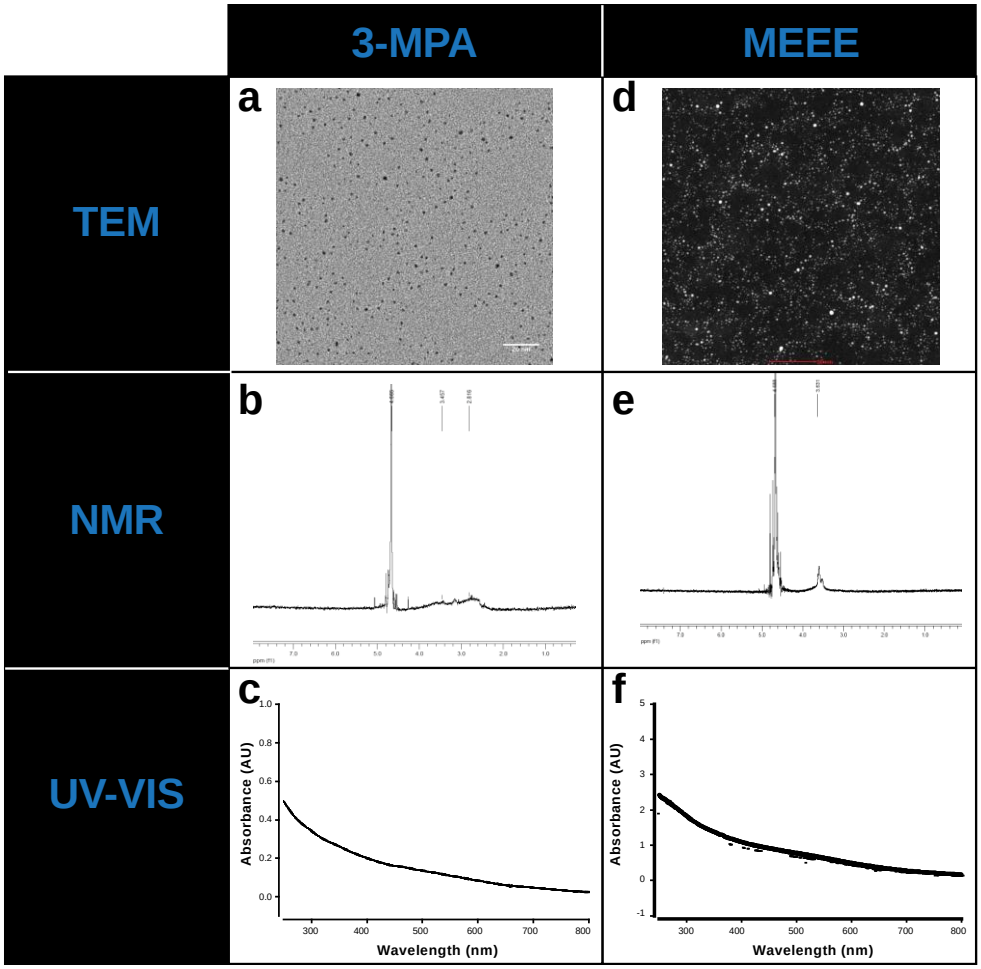


**Figure 6S- 1. Characterization data of 3-MPA and MEEE-AuNPs using (a,d) TEM, (b,e) NMR, and (c,f) UV-Vis absorbance.**

**Table 6S- 1. Common 5 genes**

| Ensembl Gene ID | ZF Gene Symbol | ZF Description | ZF Gene ID | Locus | CON_ RPKM | MPA_ RPKM | log2 (fold_ change) | MEEE_ RPKM | log2 (fold_ change) |
|---|---|---|---|---|---|---|---|---|---|
| ENSDARG00000019949 | hsp47 | heat shock protein 47 | 30449 | 15:28732297-28736597 | 22.37 | 36.091 | 0.69 | 31.44 | 0.50 |
| ENSDARG00000031683 | fos | v-fos FBJ murine osteosarcoma viral oncogene homolog | 394198 | 20:46803307-46805437 | 27.49 | 78.34 | 1.51 | 14.53 | -0.91 |
| | BX548011.3 | | | 4:49787860-49789795 | 46.53 | 388.23 | 3.06 | 112.76 | 1.29 |
| ENSDARG00000028396 | fkbp5 | FK506 binding protein 5 | 368924 | 6:41026921-41046917 | 39.22 | 17.45 | -1.17 | 14.90 | -1.39 |
| ENSDARG00000042816 | mmp9 | matrix metalloproteinase 9 | 406397 | 8:25134454-25148890 | 6.20 | 13.62 | 1.14 | 2.22 | -1.47 |

**Table 6S- 2. List of Statistically significant genes in (a) CON v 3-MPA-AuNPs and (b) CON v MEEE-AuNPs.**

(a) CON vs 3- MPA-AuNPs

| Ensembl Gene ID | ZF Gene Symbol | ZF Description | ZF Gene ID | Locus | CON_ RPKM | MPA_ RPKM | log2 (FC) |
|---|---|---|---|---|---|---|---|
| ENSDARG00000008969 | fgb | fibrinogen, B beta polypeptide | 337315 | 1:9127846-9135580 | 113.21 | 146.46 | 0.37 |
| ENSDARG00000074378 | junb | jun B proto-oncogene | 407086 | 1:52226931-52228476 | 7.28 | 16.81 | 1.21 |
| ENSDARG00000036840 | krt15 | keratin 15 | 406844 | 11:11635466-11764765 | 59.96 | 74.78 | 0.32 |
| ENSDARG00000056322 | ldb3a | LIM-domain binding factor 3a | 794339 | 13:22616976-22690023 | 125.57 | 154.30 | 0.30 |
| ENSDARG00000075121 | hbegfa | heparin-binding EGF-like growth factor a | 797938 | 14:7015234-7018245 | 9.11 | 17.33 | 0.93 |
| ENSDARG00000037421 | egr1 | early growth response 1 | 30498 | 14:22333788-22337652 | 14.24 | 53.84 | 1.92 |
| ENSDARG00000055752 | npas4 | neuronal PAS domain protein 4 | 724016 | 14:31506583-31512448 | 1.18 | 2.59 | 1.13 |
| ENSDARG00000019949 | hsp47 | heat shock protein 47 | 30449 | 15:28732297-28736597 | 22.37 | 36.09 | 0.69 |
| ENSDARG00000090352 | si:dkey-97i18.5 | si:dkey-97i18.5 | | 16:33930174-33932357 | 7.68 | 17.61 | 1.20 |
| ENSDARG00000040432 | klf2b | Kruppel-like factor 2b | 117509 | 19:17847487-17853240 | 7.05 | 12.96 | 0.88 |
| ENSDARG00000004539 | ptgs2a | prostaglandin-endoperoxide synthase 2a | 246227 | 2:20712496-20719864 | 16.71 | 32.62 | 0.97 |
| ENSDARG00000034503 | per2 | period homolog 2 (Drosophila) | 140633 | 2:48423771-48489514 | 3.90 | 1.17 | -1.74 |
| ENSDARG00000031683 | fos | v-fos FBJ murine | 394198 | 20:46803307- | 27.49 | 78.34 | 1.51 |

| | | | | | | | |
|---|---|---|---|---|---|---|---|
| | | osteosarcoma viral oncogene homolog | | 46805437 | | | |
| ENSDARG00000091131 | cry2b | cryptochrome 2b | 83780 | 22:745664-789091 | 7.28 | 4.01 | -0.86 |
| ENSDARG00000088371 | junbl | jun B proto-oncogene, like | 336038 | 3:8434975-8436624 | 21.69 | 64.19 | 1.57 |
| ENSDARG00000076221 | zgc:198419 | zgc:198419 | 100006523 | 3:32235717-32257330 | 16.60 | 38.99 | 1.23 |
| ENSDARG00000078342 | zgc:194125 | zgc:194125 | 100170833 | 3:32262322-32263438 | 12.20 | 29.38 | 1.27 |
| ENSDARG00000079938 | zgc:173594 | zgc:173594 | 100126128 | 3:32276513-32278057 | 19.80 | 44.07 | 1.15 |
| ENSDARG00000025428 | socs3a | suppressor of cytokine signaling 3a | 335409 | 3:58237024-58239849 | 6.86 | 13.86 | 1.01 |
| ENSDARG00000045768 | cry1a | cryptochrome 1a | 100003956 | 4:11077566-11091060 | 10.38 | 4.16 | -1.32 |
| ENSDARG00000028396 | fkbp5 | FK506 binding protein 5 | 368924 | 6:41026921-41046917 | 39.22 | 17.45 | -1.17 |
| ENSDARG00000042816 | mmp9 | matrix metalloproteinase 9 | 406397 | 8:25134454-25148890 | 6.19 | 13.62 | 1.14 |
| ENSDARG00000036572 | dusp2 | dual specificity phosphatase 2 | 445057 | 8:42272845-42276824 | 3.77 | 9.03 | 1.26 |
| ENSDARG00000041339 | zgc:92380 | zgc:92380 | 445086 | 9:48849050-48881933 | 40.15 | 50.74 | 0.34 |
| | SRP_euk_arch | | | 11:11559268-11559563 | 0.00 | 31.37 | 1.7976 9e+308 |
| | IER2 | | | 11:31914385-31914898 | 15.56 | 38.34 | 1.30 |
| | tef | | | 12:20241114-20249459 | 24.55 | 18.20 | -0.43 |

| | | | | | | | |
|---|---|---|---|---|---|---|---|
| | 7SK | | | 13:697629-697951 | 3.47 | 119.07 | 5.10 |
| | DKEY-111B14.2 | | | 16:16405421-16405989 | 5.16 | 60.15 | 3.54 |
| | JDP2 (2 of 2) | | | 20:46823546-46897470 | 9.97 | 20.79 | 1.06 |
| | 5_8S_rRNA | | | 20:55787532-55787686 | 64.54 | 2156.84 | 5.06 |
| | BX296557.1 | | | 20:55789783-55789875 | 7915.68 | 74376.90 | 3.23 |
| | DUPD1 (2 of 12) | | | 20:7245361-7255198 | 9.99 | 25.78 | 1.37 |
| | CT027638.1 | | | 20:55449381-55449469 | 2833.08 | 19977.70 | 2.82 |
| | CT956064.6 | | | 20:55775928-55776020 | 7915.68 | 74351.50 | 3.23 |
| | 5_8S_rRNA | | | 20:55778117-55778271 | 64.54 | 2156.84 | 5.06 |
| | SRP_euk_arch | | | 3:30399857-30400153 | 7.61 | 361.17 | 5.57 |
| | CT583728.5 | | | 4:43985365-43985784 | 10.29 | 113.35 | 3.46 |
| | 5_8S_rRNA | | | 4:43986292-43986446 | 64.54 | 2156.84 | 5.06 |
| | CU278559.3 | | | 4:44016453-44016872 | 10.29 | 113.35 | 3.46 |
| | 5_8S_rRNA | | | 4:44017380-44017534 | 64.54 | 2156.84 | 5.06 |
| | BX548011.3 | | | 4:49787860-49789795 | 46.53 | 388.23 | 3.06 |

| | | | | | | | |
|---|---|---|---|---|---|---|---|
| | 5_8S_rRNA | | | 4:43907850-43908004 | 64.54 | 2156.84 | 5.06 |
| | CT583728.20 | | | 4:43908512-43908931 | 10.29 | 113.35 | 3.46 |
| | 5_8S_rRNA | | | 4:43923410-43923564 | 64.54 | 2156.84 | 5.06 |
| | CT583728.8 | | | 4:43924072-43924491 | 10.29 | 113.35 | 3.46 |
| | 5_8S_rRNA | | | 4:43939606-43939760 | 64.54 | 2156.84 | 5.06 |
| | CT583728.12 | | | 4:43940269-43940688 | 10.29 | 113.35 | 3.46 |
| | 5_8S_rRNA | | | 4:49791968-49792122 | 64.75 | 2087.46 | 5.01 |
| | BX548011.5 | | | 4:49792629-49793048 | 10.29 | 113.35 | 3.46 |
| | AL935186.4 | | | 4:61296842-61296934 | 5144.75 | 56698.20 | 3.46 |
| | 5_8S_rRNA | | | 4:61299023-61299179 | 124.66 | 4769.95 | 5.26 |
| | PLA2G4C (4 of 5) | | | 5:2043308-2072826 | 3.73 | 1.88 | -0.99 |
| | BX537263.5 | | | 5:1187766-1187854 | 2833.08 | 19977.70 | 2.82 |
| | BX537263.8 | | | 5:1189499-1189591 | 7915.68 | 74351.50 | 3.23 |
| | 5_8S_rRNA | | | 5:1191688-1191842 | 64.54 | 2156.84 | 5.06 |
| | BX537263.6 | | | 5:1199413-1199501 | 2833.08 | 19977.70 | 2.82 |

| | | | | | | | |
|---|---|---|---|---|---|---|---|
| | BX537263.7 | | | 5:1201146-1201238 | 7915.68 | 74351.50 | 3.23 |
| | 5_8S_rRNA | | | 5:1203335-1203489 | 64.54 | 2156.84 | 5.06 |
| | 5_8S_rRNA | | | 5:4381835-4381989 | 64.54 | 2156.84 | 5.06 |
| | CU651569.4 | | | 5:4382497-4382916 | 10.29 | 113.35 | 3.46 |
| | C5H8orf4 (1 of 2) | | | 5:29511197-29512206 | 20.69 | 38.89 | 0.91 |
| | LONRF1 | | | 8:14160749-14304260 | 11.42 | 4.86 | -1.23 |
| | CABZ01045618.2 | | | Zv9_NA889:14423-14511 | 2833.08 | 19977.70 | 2.82 |

(b)CON vs MEEE-AuNPs

| Ensembl Gene ID | ZF Gene Symbol | ZF Description | ZF Gene ID | Locus | CON_ RPKM | MEEE_ RPKM | log2 (FC) |
|---|---|---|---|---|---|---|---|
| ENSDARG00000093494 | si:ch211-217k17.9 | si:ch211-217k17.9 | 798921 | 1:52892867-52895323 | 36.13 | 19.40 | -0.90 |
| ENSDARG00000015495 | klf3 | Kruppel-like factor 3 (basic) | 117603 | 1:17336040-17356958 | 24.46 | 13.65 | -0.84 |
| ENSDARG00000018308 | ets2 | v-ets erythroblastosis virus E26 oncogene homolog 2 (avian) | 326672 | 10:143057-261920 | 22.81 | 8.06 | -1.50 |
| ENSDARG00000005785 | elovl7b | ELOVL family member 7, elongation of long chain fatty acids (yeast) b | 327274 | 10:46572429-46574201 | 43.55 | 14.07 | -1.63 |
| ENSDARG00000019274 | rasd1 | RAS, dexamethasone- | 393504 | 12:1576091- | 22.52 | 13.20 | -0.77 |

| | | | | | | | |
|---|---|---|---|---|---|---|---|
| | | induced 1 | | 1577692 | | | |
| ENSDARG00000021372 | tob1b | transducer of ERBB2, 1b | 406245 | 12:1044227-1047498 | 68.85 | 39.63 | -0.80 |
| ENSDARG00000038639 | elovl6l | ELOVL family member 6, elongation of long chain fatty acids like | 1E+08 | 13:21806732-21812343 | 14.67 | 8.74 | -0.75 |
| ENSDARG00000012789 | plek2 | pleckstrin 2 | 567753 | 13:33347085-33358213 | 1.66 | 0.29 | -2.54 |
| ENSDARG00000077726 | ccrn4la | CCR4 carbon catabolite repression 4-like a (S. cerevisiae) | 572044 | 14:48963051-48975762 | 16.61 | 5.97 | -1.48 |
| ENSDARG00000062788 | irg1l | immunoresponsive gene 1, like | 562007 | 14:11625680-11629239 | 14.21 | 6.78 | -1.07 |
| ENSDARG00000015355 | fosl1 | FOS-like antigen 1 | 564241 | 14:31611182-31617315 | 8.61 | 0.41 | -4.39 |
| ENSDARG00000031929 | stard10 | START domain containing 10 | 100001416 | 14:34245372-34253070 | 11.62 | 5.50 | -1.08 |
| ENSDARG00000019949 | hsp47 | heat shock protein 47 | 30449 | 15:28732297-28736597 | 22.22 | 31.44 | 0.50 |
| ENSDARG00000055854 | nr4a3 | nuclear receptor subfamily 4, group A, member 3 | 548604 | 16:29573621-29597577 | 13.15 | 4.29 | -1.62 |
| ENSDARG00000039943 | fam46ba | family with sequence similarity 46, member Ba | 777768 | 16:36464081-36473792 | 22.86 | 13.55 | -0.75 |
| ENSDARG00000006598 | sgk2b | serum/glucocorticoid regulated kinase 2b | 559050 | 16:28781209-28787898 | 15.68 | 8.35 | -0.91 |
| ENSDARG00000028804 | ankrd9 | ankyrin repeat domain 9 | 492328 | 17:29335654-29336840 | 35.78 | 13.80 | -1.37 |
| ENSDARG00000040623 | fosl2 | fos-like antigen 2 | 558921 | 17:41427845-41443739 | 10.74 | 4.07 | -1.40 |
| ENSDARG00000007377 | odc1 | ornithine decarboxylase 1 | 114426 | 17:52270217- | 90.79 | 56.42 | -0.69 |

| | | | | | | | |
|---|---|---|---|---|---|---|---|
| | | | | 52283861 | | | |
| ENSDARG00000055751 | fosb | FBJ murine osteosarcoma viral oncogene homolog B | 492346 | 18:35109605-35119433 | 5.19 | 0.88 | -2.57 |
| ENSDARG00000061635 | myo5aa | myosin VAa | 562188 | 18:37337380-37479503 | 13.75 | 9.93 | -0.47 |
| ENSDARG00000035909 | mfsd2ab | major facilitator superfamily domain containing 2ab | 445176 | 19:32113242-32129452 | 39.03 | 22.26 | -0.81 |
| ENSDARG00000067848 | itgb1bp3 | integrin beta 1 binding protein 3 | 447879 | 2:56106355-56216886 | 59.94 | 37.74 | -0.67 |
| ENSDARG00000002412 | elovl1a | elongation of very long chain fatty acids (FEN1/Elo2, SUR4/Elo3, yeast)-like 1a | 449816 | 2:19237375-19299800 | 19.26 | 10.78 | -0.84 |
| ENSDARG00000031426 | csrnp1a | cysteine-serine-rich nuclear protein 1a | 560270 | 2:24060403-24073222 | 11.09 | 5.10 | -1.12 |
| ENSDARG00000078327 | si:ch73-212j7.1 | si:ch73-212j7.1 | 1E+08 | 20:3145229-3163516 | 3.84 | 1.92 | -1.00 |
| ENSDARG00000014947 | igfbp1a | insulin-like growth factor binding protein 1a | 317638 | 20:7029527-7033442 | 19.11 | 5.36 | -1.83 |
| ENSDARG00000007823 | atf3 | activating transcription factor 3 | 393939 | 20:37819240-37825345 | 7.83 | 2.75 | -1.51 |
| ENSDARG00000010276 | ptgs2b | prostaglandin-endoperoxide synthase 2b | 559020 | 20:34147105-34152005 | 7.12 | 2.22 | -1.68 |
| ENSDARG00000031683 | fos | v-fos FBJ murine osteosarcoma viral oncogene homolog | 394198 | 20:46803307-46805437 | 27.31 | 14.53 | -0.91 |
| ENSDARG00000091669 | si:dkey-17e16.17 | si:dkey-17e16.17 | | 21:25068445-25075182 | 23.50 | 7.83 | -1.58 |
| ENSDARG00000009544 | cldnb | claudin b | 81581 | 21:25145794-25146897 | 109.95 | 69.55 | -0.66 |
| ENSDARG00000077540 | f2rl1.2 | coagulation factor II | 1E+08 | 21:7193751- | 4.85 | 1.97 | -1.30 |

| | | | | | | | |
|---|---|---|---|---|---|---|---|
| | | (thrombin) receptor-like 1.2 | | 7201593 | | | |
| ENSDARG00000017843 | srsf1b | serine/arginine-rich splicing factor 1b | 393565 | 21:38403757-38412580 | 37.05 | 46.72 | 0.33 |
| ENSDARG00000020298 | btg2 | B-cell translocation gene 2 | 30079 | 22:745664-789091 | 99.50 | 57.81 | -0.78 |
| ENSDARG00000070907 | lcor | ligand dependent nuclear receptor corepressor | 558560 | 22:37648548-37682613 | 8.34 | 2.72 | -1.62 |
| ENSDARG00000025522 | sgk1 | serum/glucocorticoid regulated kinase 1 | 324140 | 23:31878817-31931888 | 60.67 | 33.44 | -0.86 |
| ENSDARG00000000796 | nr4a1 | nuclear receptor subfamily 4, group A, member 1 | 431720 | 23:32389911-32396444 | 41.18 | 20.82 | -0.98 |
| ENSDARG00000087303 | cebpd | CCAAT/enhancer binding protein (C/EBP), delta | 140817 | 24:37059294-37061674 | 36.89 | 16.94 | -1.12 |
| ENSDARG00000038429 | csrnp1b | cysteine-serine-rich nuclear protein 1b | 322795 | 24:20257035-20268667 | 42.85 | 27.83 | -0.62 |
| ENSDARG00000017665 | snrk1 | SNF related kinase 1 | 393806 | 25:13930212-13960215 | 7.05 | 4.20 | -0.75 |
| ENSDARG00000035719 | arl5c | ADP-ribosylation factor-like 5C | 393819 | 3:15754356-15762038 | 10.60 | 5.19 | -1.03 |
| ENSDARG00000007344 | tcap | titin-cap (telethonin) | 556258 | 3:21453654-21455521 | 7.49 | 1.44 | -2.37 |
| ENSDARG00000019420 | etnk1 | ethanolamine kinase 1 | 565971 | 4:15954037-15975107 | 35.54 | 23.94 | -0.57 |
| ENSDARG00000042909 | lifra | leukemia inhibitory factor receptor alpha | 541493 | 5:7820161-7886515 | 5.38 | 3.46 | -0.64 |
| ENSDARG00000068194 | klf9 | Kruppel-like factor 9 | 565869 | 5:27719778-27722714 | 14.03 | 5.26 | -1.42 |
| ENSDARG00000019360 | sec23b | Sec23 homolog B (S. cerevisiae) | 327268 | 6:6695928-6712811 | 73.11 | 34.45 | -1.09 |
| ENSDARG00000028396 | fkbp5 | FK506 binding protein 5 | 368924 | 6:41026921- | 38.96 | 14.90 | -1.39 |

| | | | | | | | |
|---|---|---|---|---|---|---|---|
| | | | | 41046917 | | | |
| ENSDARG00000060316 | cish | cytokine inducible SH2-containing protein | 767678 | 6:41434717-41437613 | 20.79 | 14.21 | -0.55 |
| ENSDARG00000009505 | slmo2 | slowmo homolog 2 (Drosophila) | 378855 | 6:59776158-59786039 | 78.14 | 37.66 | -1.05 |
| ENSDARG00000078619 | pnp5a | purine nucleoside phosphorylase 5a | 791647 | 7:7457930-7473128 | 75.50 | 41.11 | -0.88 |
| ENSDARG00000088589 | si:dkey-165a24.2 | si:dkey-165a24.2 | 1E+08 | 7:23842565-23844302 | 36.80 | 18.55 | -0.99 |
| ENSDARG00000087440 | si:dkey-165a24.4 | si:dkey-165a24.4 | 557748 | 7:23847650-23851383 | 17.16 | 6.31 | -1.44 |
| ENSDARG00000042816 | mmp9 | matrix metalloproteinase 9 | 406397 | 8:25134454-25148890 | 6.15 | 2.22 | -1.47 |
| ENSDARG00000010572 | slc25a25a | solute carrier family 25 (mitochondrial carrier; phosphate carrier), member 25a | 406541 | 8:2781135-2791394 | 27.26 | 14.70 | -0.89 |
| ENSDARG00000042725 | cebpb | CCAAT/enhancer binding protein (C/EBP), beta | 140814 | 8:29301376-29302892 | 39.82 | 17.78 | -1.16 |
| ENSDARG00000010437 | fam46c | family with sequence similarity 46, member C | 327154 | 9:21814157-21819950 | 24.87 | 16.54 | -0.59 |
| ENSDARG00000034961 | bzw1b | basic leucine zipper and W2 domains 1b | 406812 | 9:50227-57751 | 92.60 | 54.11 | -0.78 |
| ENSDARG00000041566 | adamts1 | ADAM metallopeptidase with thrombospondin type 1 motif, 1 | 565145 | Zv9_NA908:84739-93567 | 17.92 | 5.38 | -1.74 |
| | wu:fc34e06 | | | 1:41067044-41078571 | 13.56 | 6.16 | -1.14 |
| | MUC3A | | | 1:41080394-41120369 | 2.50 | 0.93 | -1.42 |

| | | | | | | | |
|---|---|---|---|---|---|---|---|
| | si:ch73-60g14.3,si:ch73-60g14.4 | | | 10:24825218-24847532 | 7.81 | 1.42 | -2.46 |
| | DHRS13 (2 of 5) | | | 10:38118057-38126716 | 92.14 | 28.11 | -1.71 |
| | FILIP1L (2 of 2) | | | 11:46291043-46293686 | 13.59 | 7.65 | -0.83 |
| | CABZ01048956.1 | | | 12:46994361-47010486 | 11.39 | 5.73 | -0.99 |
| | MCU | | | 13:4376328-4525409 | 10.51 | 6.60 | -0.67 |
| | wu:fj08f03 | | | 14:11649672-11655264 | 8.08 | 4.35 | -0.89 |
| | TUFT1 (1 of 2) | | | 16:24543993-24565999 | 7.51 | 3.32 | -1.18 |
| | BX005256.1 | | | 16:27061038-27068162 | 7.56 | 1.67 | -2.18 |
| | THBS1 (2 of 2) | | | 17:507055-521798 | 22.65 | 12.00 | -0.92 |
| | CABZ01064941.1 | | | 17:288686-297735 | 18.49 | 8.58 | -1.11 |
| | CU638738.1 | | | 17:50755159-50764033 | 5.07 | 2.11 | -1.26 |
| | CREM (1 of 2) | | | 2:43256632-43297713 | 13.03 | 4.75 | -1.45 |
| | CT956064.3 | | | 20:55774137-55775909 | 175.66 | 422.88 | 1.27 |
| | zgc:158463 | | | 20:55786254-55787467 | 258.70 | 665.68 | 1.36 |
| | BX296557.6 | | | 20:55789894- | 170.55 | 376.58 | 1.14 |

| | | | | | | | |
|---|---|---|---|---|---|---|---|
| | | | | 55791666 | | | |
| | ZNF462 | | | 21:537752-568922 | 12.31 | 6.62 | -0.89 |
| | KLF4 | | | 21:611997-627555 | 12.07 | 3.17 | -1.93 |
| | WWC1 | | | 21:35787421-35920071 | 4.34 | 2.00 | -1.12 |
| | CHST6 | | | 25:35925934-35939027 | 8.76 | 3.98 | -1.14 |
| | BX548011.3 | | | 4:49787860-49789795 | 46.22 | 112.76 | 1.29 |
| | AL935186.6 | | | 4:61294795-61296820 | 106.81 | 223.45 | 1.06 |
| | OSGIN1 | | | 6:50645617-50655992 | 10.02 | 20.06 | 1.00 |
| | VGF | | | 7:27352318-27354247 | 7.23 | 3.30 | -1.13 |
| | CU019646.2 | | | 7:21397518-21398924 | 7.41 | 1.90 | -1.97 |
| | BSN (2 of 3) | | | 8:55800920-55824614 | 4.60 | 3.25 | -0.50 |
| | SIK1 | | | 9:9169114-9178227 | 50.97 | 17.37 | -1.55 |

# CHAPTER 7 - CONCLUSIONS

Utilizing the rapid development and molecular and genetic tractability of the embryonic zebrafish model, we investigated the effects of different surface functionalization of lead sulfide nanoparticles (PbS-NPs) on developmental toxicity. The ligand groups were insufficiently coating the core material, which impacted the rate of decomposition. The decomposing PbS-NPs were releasing lead ions causing the differential biological responses.

To further investigate the impact of nanoparticle functionalization on developmental toxicity, we used nanoparticles with a benign gold core to assess the role of different ligand functional groups on biological responses. Using gold nanoparticles (AuNPs) functionalized with three ligands, we determined that each induced a differential biological response. Using inductively coupled-mass spectroscopy, we confirmed that the individual phenotypic responses were not caused by differing mass concentrations of gold in the zebrafish tissues. By conducting a global genome analysis, we identified that each gold nanoparticle perturbed different pathways. These results demonstrated that surface functional groups drive both biological and molecular response. Exposing the embryos to the same three AuNPs during early development and raising them in nanoparticle free medium until adulthood revealed that the functional groups impacted survivorship and behavior in both larvae and adults. Nanoparticle surface functionalities can

influence the decomposition rate, which leads to changes in gene expression profiles, behavior and survivorship in adult fish.

While investigating the physiochemical properties causing adverse responses, we found that the standard zebrafish medium caused agglomeration of nanoparticles, which could result in changed responses, therefore confounding the interpretation of the biological responses. The appropriate assay medium must allow the NPs to remain monodispersed. We varied the ionic strength of the assay medium, and found that low ions in the media favored dispersion. Next, we studied the impact of external ions on embryonic zebrafish development and discovered that the zebrafish can tolerate low to no ions in the media. This bodes well for the field of nanotechnology, since it is possible (and necessary) to adjust the exposure media conditions to optimize NP dispersion prior to assessment

Once the monodispersion problem was solved, we pursued the route by which AuNPs influence biological responses. We discovered that exposure to AuNPs functionalization with 3-mercaptoproponic acid caused an abnormal touch response. When tested alone, the functional group did not induce any adverse effects. Combining the use of a neuromuscular stimulus and immunohistochemistry we discovered that the exposed larvae could not sense the touch in the caudal fin due to underdeveloped axonal innervation. Further investigation using deep RNA sequencing (RNA-seq) and pathway analysis *in silico* suggested that perturbation of neurophysiological processes was a

major target of the 3-mercaptoproponic acid-functionalized AuNP. Our current hypothesis is that the highly elevated transcript, EGR1 (early growth response 1), leads to reduced levels of glutamate, thereby affecting the level of GABA, which leads to nerve underdevelopment and the lack of a touch response.

In summary, this thesis has established the embryonic zebrafish model as a powerful platform to conduct nanotoxicity assessments to identify nanostructure-response relationships and determine how nanomaterial characteristics influence bioactivity. The application of RNA-seq in conjunction with molecular techniques, allowed the development of a hypothesis that misexpression of a transcript, early growth response 1, plays a role in the reduced axonoal projections and abnormal touch response. By leveraging the molecular advantages of the zebrafish model and conducting numerous assays in a rapid manner, we quickly move toward developing safer nanoparticles. The data collected from these studies helps identify structure-activity relationships, and begin to establish nano-design principles.

# APPENDICES

# Appendix A. Evaluation of embryotoxicity using the zebrafish model

Lisa Truong, Stacey L. Harper and Robert L. Tanguay

Department of Environmental and Molecular Toxicology, Oregon State University

## Abstract

The embryonic zebrafish model offers the power of whole-animal investigations (e.g. intact organism, functional homeostatic feedback mechanisms and intercellular signaling) with the convenience of cell culture (e.g. cost- and time-efficient, minimal infrastructure, small quantities of nanomaterial solutions required). The model system overcomes many of the current limitations in rapid to high-throughput screening of drugs/compounds and casts a broad net to rapidly evaluate integrate system effects. Additionally, it is an ideal platform to follow up with targeted studies aimed at the mechanisms of toxic action. Exposures are carried out in 96-well plates so minimal solution volumes are required for the assessments. Numerous morphological, developmental and behavioral endpoints can be evaluated non-invasively due to the transparent nature of the embryos.

## Introduction

Numerous biological models can be employed for toxicity evaluations. In vitro techniques, such as cell culture systems, are often preferred because of they are both cost- and time-efficient. While these studies are useful, direct translation to whole organisms and human health is often difficult to infer. *In vivo* studies can provide improved prediction of biological response in intact systems but often require extensive facilities and infrastructure (Harper et al. 2008). Zebrafish (Danio rerio) offer a number of practical advantages as a model organism that overcome these limitations, making these vertebrates highly amenable for toxicologically relevant research. Zebrafish can be employed as a powerful *in vivo* model system to assess biological interactions and are an outstanding platform to detail the mechanisms by which substances elicit specific biological responses. A remarkable similarity in cellular structure, signaling processes, anatomy and physiology exist among zebrafish and other high-order vertebrates, particularly early in development (Blechinger et al. 2002, Rasooly et al. 2003, Rubinstein 2003, Spitsbergen and Kent 2003, Levin et al. 2004). Current estimates indicate that over 90% of the human open reading frames are homologous to genes in fish (Aparicio et al. 2002). Thus, investigations using this model system can reveal subtle interactions that are likely to be conserved across species.

Features of the zebrafish's biology are favorable for adapting this model system to high-throughput assays. Female zebrafish are able to produce hundreds of eggs weekly, so large sample sizes are easily achieved, allowing

for statistically powerful dose-response studies. This abundant supply of embryos also makes it possible to simultaneously assess the toxicity of a large number of substances in a short period. The vertebrate's rapid developmental progression compared to other mammals makes it an ideal model for high-throughput screening (Kimmel et al. 1995). For example, neuronal plate formation occurs at 10 hours post fertilization (hpf), followed by organogenesis at 24 hpf, which compared to a rat occurs at 9.5 days and 5-6 days respectively. The first heartbeat occurs at 30 hpf for the zebrafish and 10.2 days for rats (Westerfield 1995).

Zebrafish embryos can be individually exposed in wells of a multi-well plate so the required volume needed for the model is small; thus, only limited amounts of materials are needed to assess an entire suite of biological interactions and responses. Early developmental life stages are often uniquely sensitive to environmental insult, due in part to the enormous changes in cellular differentiation, proliferation and migration required to form multiple cell types, tissues and organs (Henken et al. 2003, Rubinstein 2003, Spitsbergen and Kent 2003, Levin, et al. 2004)). Since development is highly coordinated requiring specific cell-to-cell communications, if exposure to a substance during that critical period perturbed these interactions, development would be expected to be disrupted. Embryos are waterborne–exposed to a chemical using a continuous method in which 24 embryos are exposed per concentration in individual wells of a multi-well plate from 8 to 120 hpf.

Exposure until 120 hpf is the ideal duration for a developmental toxicity testing; primarily due to the vertebrate model's ability to obtain its nutrients from its yolk sac until five days, which will not introduce new confounding factors. Perturbed development can manifest as morphological malformations, behavioral abnormalities or death of the embryos. Zebrafish embryos develop externally and are optically transparent so it is possible to resolve individual cells *in vivo* throughout the duration of an exposure using simple microscopic techniques and numerous effects can be assessed non-invasively over the course of development.

## Materials

### Zebrafish Husbandry

1. Fish water: 0.3 g/L Instant Ocean salts (Aquatic Ecosystems, Apopka, FL) in reverse osmosis (RO) water.
2. Incubator set at 28 ± 0.1 °C.

### Dechorination

1. Compound stereo microscope for viewing embryos.
2. 90 mm glass petri dish.
3. 50 mg/mL pronase (Sigma-Aldrich, cat # 81750) in RO water. Measure 50 mg of pronase into a 1.5 mL microcentrifuge tube and fill it with 1 mL of RO water. Aliquot 50 μl into 1.5 mL microcentrifuge tube and place them into a freezer box, then

immediately place into the box into the freezer. This will make 20 1.5mL microcentrifuge tubes that can be stored for up to 4 months. Aliquots can be thawed just prior to use.

4. Timer.

**Exposure**

1. Multi-well plates.
2. 8 or 12 multichannel pipette.
3. 50 mL reagent reservoir.
4. Wide-bore Pasteur pipette.

**Assessment**

1. Anesthesia: 4mg/mL of 3-aminobenzoate ethyl ester methanesulfonate salt (tricaine, Sigma-Aldrich, cat # A-5040) in RO water, pH adjusted to 7.0 with Tris-HCl, pH 9.0.
2. Methyl cellulose: 10 mg/mL of methyl cellulose (Sigma-Aldrich, cat # 274429, *see* **Note 1**).

## Methods

### Zebrafish Husbandry

1. Rear adult zebrafish Danio rerio in standard laboratory conditions of 28□C with a pH of 7 ± 0.2 on a 14 h light/10 h dark photoperiod (Akimenko et al. 1995).

2. House zebrafish in 2.0-liter polycarbonate tanks with recirculating water system. Keep adult zebrafish in groups to allow for large quantities of embryos to be collected. Group spawning also helps to increase genetic diversity.

3. Feed the fish twice daily with either crushed TetraMin® Tropical Flake or live Artemia from INVE (Salt Lake City, UT).

4. Spawning: place male and female zebrafish into spawning baskets in polycarbonate tanks the afternoon before the embryos are needed. Zebrafish will typically spawn when the lights come on after the 10 h dark period.

5. The following morning, newly fertilized eggs are collected, rinsed several times in system water and placed into fresh fish water in a 150 mm plastic petri dish.

6. Remove embryos that are unfertilized or necrotic prior to placing the petri dish into the incubator to keep warm until the embryos reach six hours post fertilization (hpf) (**Figure A-1**) (Kimmel, et al. 1995).

7. Remove embryos that are not the same stage as the majority prior to experimental use (see **Note 2**).

**Dechorination**

1. To avoid barrier effects potentially posed by the chorion, all embryos should be dechorionated at six hours post fertilization (hpf) using a modified version of Westerfields (2000) (Akimenko, et al. 1995) protocol for pronase enzyme degradation.
2. Place six hpf embryos into a 60 mm glass petri dish with 25 mL fish water (see Note 3). Up to 1200 embryos can be processed in a single dish using this method.
3. Add 50 µl of 50 mg/mL pronase to the center of the dish and continuously swirl gently to mix the solution.
4. Set a timer for seven minutes, and continuously swirl the embryos while occasionally observing the petri dish under the microscope to check for embryos without chorions, chorion pieces in the solution and ‘deflated’ chorions.
5. When seven minutes have passed, or when the above are observed, remove the pronase solution by diluting the solution with fresh fish water, slowly decanting over the edge of the petri dish continuously for one minute, then repeat this procedure for a total of 10 minutes (see Note 4).

6. After the rinse, allow the embryos to recover in the petri dish in an incubator (or a room at 28°C) until eight hpf (see **Note 5**).

## Exposure

### *Waterborne exposure*

1. Chemicals should be dissolved in fish water if possible (see Note 6). In the case that this is not possible, the solvent of choice for exposure utilizing the embryonic zebrafish is dimethyl sulfoxide (DMSO) (see **Note 7**).
2. Pour each test solution into a 50 mL reagent reservoir, which will fit a multichannel pipette.
3. For each exposure concentration tested, use a multichannel pipette to fill 24 individual wells in a multi-well plate with 100 µl of chemical solution. Seven concentrations and one control group can be tested using two 96-well plates.
4. At eight hpf, transfer viable, appropriately developing embryos into individual wells of a multi-well plate using a wide-bore glass pipette (see Note 8).
5. Incubate at 28□C until 24 hpf, then perform assessments.

***Microinjection exposure***

1. If direct delivery of a chemical is necessary to ensure accurate dose delivery, embryos should be microinjected at eight hpf (see **Note 9**).
2. Align eight hpf embryos in troughs embedded in a 1% agarose plate filled with fish water as described by The Zebrafish Book (Akimenko, et al. 1995, Westerfield 1995).
3. Inject each embryo with 2.3 nL of the desired chemical concentration or the appropriate vehicle control directly into the yolk.
4. Place each embryo into individual wells of a 96-well plate, each filled with 100 µl of fish water. When directly delivering a chemical into the yolk sac, any concentration above 0.1% DMSO caused developmental defects not attributed to the chemical. If a chemical requires a solvent, two sets of serial dilutions should be made. The first serial dilution should be 100 times higher than the final concentration desired made with 100% DMSO. (see **Note 10**) For the second set of serial dilutions, from the 100% DMSO serial dilution, make a 1:10 dilution from the first serial dilution. Make sure to have an appropriate control for each chemical, which includes the correct percentage of solvent used in each solution.
5. Incubate at 28ºC until first assessments at 24 hpf.

**Assessment**

1. At 24 hpf, embryos are assessed for viability, developmental progression and spontaneous movements (earliest behavior in zebrafish). Developmental progression is considered perturbed if zebrafish are more than 12 hours delayed compared to control animals. Spontaneous movements are assessed over a 2 minute period and is considered perturbed if there is a lack of embryonic contractions and/or movement.
2. At 120 hpf, larval morphology (body axis, eye, snout, jaw, otic vesicle, notochord, heart, brain, somite, fin, yolk sac, trunk, circulation, pigment, swim bladder; **Figure A-2)** is evaluated and recorded and behavioral endpoints (motility, tactile response) are thoroughly evaluated *in vivo*. Test for behavioral endpoints and then anesthetize animals for thorough morphological analysis. At the end of the assessments, zebrafish are euthanized with tricaine.
3. Evaluations are completed in a binary notation (present or not present) (see **Note 11**). Control and chemical-exposed groups are statistically compared using Fisher's Exact test at $p<0.05$ (Sigma Stat, SPSS Inc., Chicago, IL) for each endpoint evaluated (see Note 12).

## Notes

1. Methyl cellulose is unique in that it ‘melts’ when cold and solidifies when hot. It dissolves best in cold water; however, it is best to disperse the powder form in warm water and then continue to mix while chilling. An alternate to the methyl cellulose is Protoslo® (Carolina Biological Supply Company, Burlington, NC).
2. Eggs can sometimes be laid and fertilized at different times in a group spawns, therefore always remove embryos that are developing more rapidly or significantly slower prior to using them for an experiment. As an alternate, male and female pairs can be set up in several divided tanks, and the dividers can be removed at the same time. The resulting stage matched embryos can then be pooled, prior to random embryo selection.
3. Do not bleach embryos is their chorions are to be removed by pronase digestion. Bleaching modifies the chorion and pronase treatment is completely ineffective. In addition, when dechorinating embryos it is essential to use glass petri dishes. Dechorinated embryos will stick to the bottom of plastic dishes and will be severely damaged during the procedure.
4. The newly dechorionated embryos are very delicate. Water should be administered with a gentle flow and not directly onto the embryos. Some of the embryos will not be out of their chorion even

once the ten minute rinsing period is done. More will emerge during the recovery period.

5. Once an embryo is dechorinated, do not bleach the embryos.
6. Chemicals or drugs that are thought to be inactive until metabolized to an active form, may be pre-exposed to induce and active conformation prior to waterborne exposures.
7. The Sinnhuber Aquatic Research Laboratory at Oregon State University has demonstrated that an embryo elicited no developmental deformities at 1% DMSO when waterborne-exposed (Usenko et al. 2007, Harper, et al. 2008, Usenko et al. 2008).
8. Be sure to allow the embryo to fall to the bottom of the wide-bore Pasteur pipette prior to touching the solution in the wells. If an embryo disintegrates when it reaches the solution, make sure to replace the solution and place a new embryo in the well.
9. All methods discussed are continuous waterborne exposure, but if no analytical method is available to determine biological uptake, an alternative is to directly deliver the chemical into the animal through microinjection. Because embryos are transparent, tissue dose and distribution can also be determined using fluorescently labeled materials and laser scanning confocal microscopy.
10. Make sure to vortex each microcentrifuge tube prior the next dilution to ensure it is a homogenous solution.

11. If more than 2 animals in the control group die, then the experiment is not valid and will need to be repeated. Test chemicals may have specific targets in humans, but this target may not be completely conserved-structurally in other vertebrate models. The structural differences between vertebrates and humans can result in either false negatives or false positives. For example, if a drug is designed to target a human specific structure that is not well-conserved in zebrafish, upon exposure, the drug would not influence the zebrafish target. The effects observed when this occurs are considered false negatives. Vice versa, a false positive can also occur when effects observed due to a drug impacting a specific target expressed only in zebrafish, but this target is not structurally conserved in humans. Another consideration is that chemical toxicity may be dependent on metabolic activity. False negatives and false positives may also occur if the metabolic activity in the zebrafish embryo is distinct from human metabolic activity. It is possible to use exogenous mammalian metabolic activation system to reduce false positive and false negatives (Busquet et al. 2008).

## References

Amacher SL 2001. Zebrafish Embryo as a Developmental System, John Wiley & Sons, Ltd.

Aparicio S, Chapman J, Stupka E, Putnam N, Chia J-m, Dehal P, Christoffels A, Rash S, Hoon S, Smit A, et al. 2002. Whole-Genome Shotgun Assembly and Analysis of the Genome of Fugu rubripes. Science 297: 1301-1310.

Barbazuk WB, Korf I, Kadavi C, Heyen J, Tate S, Wun E, Bedell JA, McPherson JD, Johnson SL. 2000. The syntenic relationship of the zebrafish and human genomes. Genome Res 10: 1351-8.

Bosi S, Feruglio L, Da Ros T, Spalluto G, Gregoretti B, Terdoslavich M, Decorti G, Passamonti S, Moro S, Prato M. 2004. Hemolytic effects of water-soluble fullerene derivatives. J Med Chem 47: 6711-6715.

Brand M, Granato M, Nusslein-Volhard C (2002). Keeping and raising zebrafish. In Zebrafish: A Practical Approach. C. D. Nusslein-Volhard, R. Oxford, Oxford University Press: 7-37.

Crispino L. 1983. Modification of responses from specific sensory systems in midbrain by cerebellar stimulation: experiments on a teleost fish. Journal of Neurophysiology 49: 3-15.

Forrest DR. 2001. Molecular Nanotechnology. IEEE: 11-20.

Furgeson D, Fako V. 2009. Zebrafish as a correlative and predictive model for assessing biomaterial nanotoxicity. Advanced Drug Delivery Reviews 61: 478-486.

Gao X, Yin S, Tang M, Chen J, Yang Z, Zhang W, Chen L, Yang B, Li Z, Zha Y, et al. 2011. Effects of Developmental Exposure to TiO(2) Nanoparticles on Synaptic Plasticity in Hippocampal Dentate Gyrus Area: an *In vivo* Study in Anesthetized Rats. Biol Trace Elem Res.

Gerlai R, Lee V, Blaser R. 2006. Effects of acute and chronic ethanol exposure on the behavior of adult zebrafish (Danio rerio). Pharmacology Biochemistry and Behavior 85: 752-761.

Görge G, Nagel R. 1990. Toxicity of lindane, atrazine, and deltamethrin to early life stages of zebrafish (Brachydanio rerio). Ecotoxicology and Environmental Safety 20: 246-255.

Harper SL, Carriere JL, Miller JM, Hutchison JE, Maddux BLS, Tanguay RL. 2011. Systematic Evaluation of Nanomaterial Toxicity: Utility of Standardized Materials and Rapid Assays. ACS Nano 5: 4688-7697.

Harper SL, Dahl JL, Maddux BLS, Tanguay RL, Hutchison JE. 2008. Proactively designing nanomaterials to enhance performance and minimize hazard. International Journal of Nanotechnology 5: 124-142.

Isakovic A, Markovic Z, Todorovic-Markovic B, Nikolic N, Vranjes-Djuric S, Mirkovic M, Dramicanin M, Harhaji L, Raicevic N, Nikolic Z, et al. 2006. Distinct cytotoxic mechanisms of pristine versus hydroxylated fullerene. Toxicological Sciences 91: 173-183.

Jones RE, Petrell RJ, Pauly D. 1999. Using modified length-weight relationships to assess the condition of fish. Aquacultural Engineering 20: 261-276.

Kimmel CB, Ballard WW, Kimmel SR, Ullmann B, Schilling TF. 1995. Stages of embryonic development of the zebrafish. Dev Dyn 203: 253-310.

Lecoanet HF, Bottero JY, Wiesner MR. 2004. Laboratory assessment of the mobility of nanomaterials in porous media. Environmental Science & Technology 38: 5164-5169.

Lecoanet HF, Wiesner MR. 2004. Velocity effects on fullerene and oxide nanoparticle deposition in porous media. Environmental Science & Technology 38: 4377-4382.

MacPhail RC, Brooks J, Hunter DL, Padnos B, Irons TD, Padilla S. 2009. Locomotion in larval zebrafish: Influence of time of day, lighting and ethanol. Neurotoxicology 30: 52-8.

Nakamura E, Isobe H. 2003. Functionalized fullerenes in water. The first 10 years of their chemistry, biology, and nanoscience. Accounts of Chemical Research 36: 807-815.

Okamoto Y. 2001. Ab initio investigation of hydrogenation of C-60. Journal of Physical Chemistry A 105: 7634-7637.

Oszlanczi G, Papp A, Szabo A, Nagymajtenyi L, Sapi A, Konya Z, Paulik E, Vezer T. 2011. Nervous system effects in rats on subacute exposure by lead-containing nanoparticles via the airways. Inhal Toxicol 23: 173-81.

Powers CM, Badireddy AR, Ryde IT, Seidler FJ, Slotkin TA. 2010. Silver Nanoparticles Compromise Neurodevelopment in PC12 Cells: Critical Contributions of Silver Ion, Particle Size, Coating and Composition. Environ Health Perspect.

Rubinstein AL. 2003. Zebrafish: from disease modeling to drug discovery. Curr Opin Drug Discov Devel 6: 218-23.

Sayes CM, Gobin AM, Ausman KD, Mendez J, West JL, Colvin VL. 2005. Nano-C60 cytotoxicity is due to lipid peroxidation. Biomaterials 26: 7587-95.

Scholars WWICf, PEW (2011). Project on Emerging Nanotechnologies, Woodrow Wilson International Center for Scholars. 2011.

Siccardi AJ, Garris HW, Jones WT, Moseley DB, D'Abramo LR, Watts SA. 2009. Growth and Survival of Zebrafish (Danio rerio) Fed Different Commercial and Laboratory Diets. Zebrafish 6: 275-280.

Sun O, Wang Q, Jena P, Kawazoe Y. 2005. Clustering of Ti on a C-60 surface and its effect on hydrogen storage. Journal of the American Chemical Society 127: 14582-14583.

Teodoro JS, Simões AM, Duarte FV, Rolo AP, Murdoch RC, Hussain SM, Palmeira CM. 2011. Assessment of the toxicity of silver nanoparticles in vitro: A mitochondrial perspective. Toxicology in Vitro 25: 664-670.

Truong L, Harper SL, Tanguay R 2011. Evaluation of embryotoxicity using the zebrafish model, Humana Press.

Truong L, Tilton SC, Zaikova T, Richman E, Waters KM, Hutchison JE, Tanguay RL. Submitted. Surface Functionalities of Gold Nanoparticles (AuNPs) Impact Gene Expression in the Developing Zebrafish. Small.

Warner MG, Hutchison JE. 2003. Linear assemblies of nanoparticles electrostatically organized on DNA scaffolds. Nature Materials 2: 272-277.

Woehrle GH, Brown LO, Hutchison JE. 2005. Thiol-functionalized, 1.5-nm gold nanoparticles through ligand exchange reactions: Scope and mechanism of ligand exchange. Journal of the American Chemical Society 127: 2172-2183.

Woehrle GH, Warner MG, Hutchison JE. 2004. Molecular-level control of feature separation in one-dimensional nanostructure assemblies formed by biomolecular nanolithography. Langmuir 20: 5982-5988.

Xu Z, Gu W, Huang J, Sui H, Zhou Z, Yang Y, Yan Z, Li Y. 2005. In vitro and *in vivo* evaluation of actively targetable nanoparticles for paclitaxel delivery. Int J Pharm 288: 361-8.

Zhu Z-J, Carboni R, Quercio MJ, Yan B, Miranda OR, Anderton DL, Arcaro KF, Rotello VM, Vachet RW. 2010. Surface Properties Dictate Uptake, Distribution, Excretion, and Toxicity of Nanoparticles in Fish. Small 6: 2261-2265.

## Acknowledgements

The authors would like to thank the Sinnhuber Aquatic Research Laboratory and the Environmental Health Sciences Center at Oregon State University where much of the protocols were developed. This work was supported by EPA STAR grant RD-833320 and NIEHS grants ES03850 and ES07060.

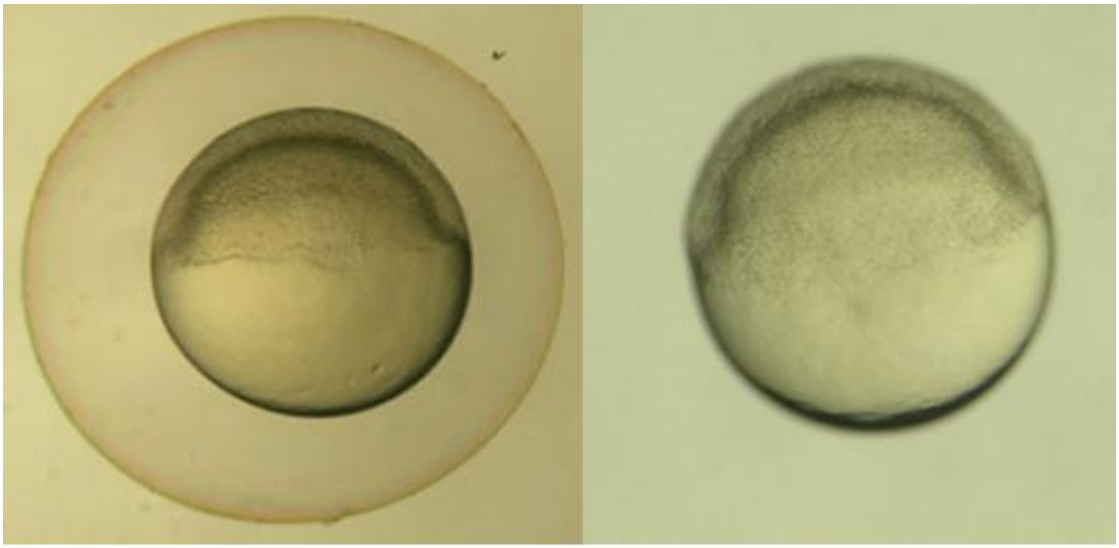

**Figure A- 1. Six hours post fertilization embryos.**
**a)** Six hpf embryo with its chorion. **b)** Six hpf embryo after using pronase to enzymatically remove its chorion.


1. **120 hr mortality** – dies between 24 and 120 hours post fertilization (hpf)
2. **24 hr mortality** – dies before 24 hpf
3. **24 hr sp. Mov** – no spontaneous movement at 24 hpf
4. **24 hr dev prog** - delayed development
5. **24 hr notochord** – notochord malformation (wavy notochord)
6. **axis** – curved or bent axis in either direction
7. **brain** - brain malformations or necrosis
8. **caudal fin** –malformed or missing
9. **circulation** – no circulation or blood flow
10. **eye** – eyes malformed, missing or smaller/larger than normal
11. **heart** – heart malformation, pericardial edema (fluid around the heart)
12. **jaw** – malformed
13. **otic** – malformed or missing
14. **pectoral fin** – malformed or missing
15. **pigmentation** – lack of pigmentation, overpigmentation
16. **snout** – shortened or malformed
17. **somite** – malformed or disorganized, missing somites
18. **swim bladder inflate** – failure of swim bladder to inflate
19. **touch response** – not responsive to touch at 120 hpf
20. **trunk** – short trunk, malformed or missing
21. **YSE** – yolk sac edema, swelling around the yolk sac





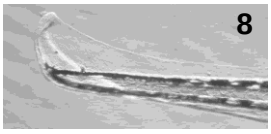


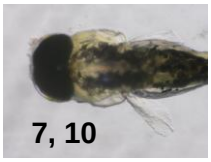


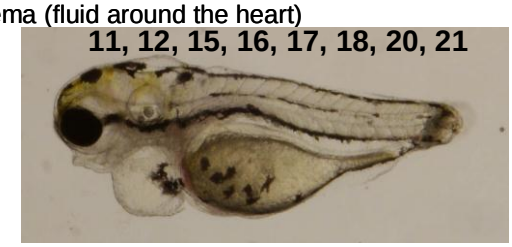


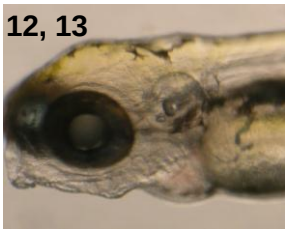


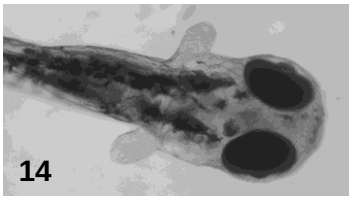


**Figure A- 2. Visual assessment of zebrafish morphology.**
Images are given as examples of typical chemical-induced malformations observed in the zebrafish.

# Appendix B. Automated zebrafish chorion removal and single embryo placement: optimizing throughput of zebrafish developmental toxicity screen

David Mandrell, Lisa Truong, Caleb Jephson, Mushfiqur R. Sarker, Aaron Moore, Christopher Lang, Michael T. Simonich and Robert L. Tanguay*

Department of Environmental & Molecular Toxicology, Oregon State University, Corvallis, OR

This was published in Journal of Laboratory Automation.

## Abstract

The potential of the developing zebrafish model for toxicology and drug discovery is limited by inefficient approaches to manipulating and chemically exposing zebrafish embryos; namely manual placement of embryos into 96 or 384 well plates, and exposure of embryos while still in the chorion, a barrier of poorly characterized permeability enclosing the developing embryo. We report the automated dechorionation of 1600 embryos at once at 4 hours post fertilization (hpf), and placement of the dechorionated embryos into 96 well plates for exposure by 6hpf. The process removed ≥95% of the embryos from their chorions with 2% embryo mortality by 24 hpf and 2% of the embryos malformed at 120 hpf. The robotic embryo placement allocated 6-hpf embryos to 94.7 ± 4.2% of the wells in multiple 96-well trials. The rate of embryo mortality was 2.8% (43 of 1536) from robotic handling, the rate of missed wells was 1.2% (18 of 1536) and the frequency of multipicks was <0.1%. Embryo malformations observed at 24-hpf occurred nearly twice as frequently from robotic handling (16 of 864; 1.9%) as from manual pipetting (9 of 864; 1%). There was no statistical difference between the success of performing the embryo placement robotically or manually.

## Introduction

Toxicology is undergoing a paradigm shift recognized by the U.S. Environmental Protection Agency (EPA), the National Toxicology Program (NTP) and the National Research Council (NRC) (Schmidt EHP 2009). This is nowhere more evident than the Tox21 agenda [1,2] and its European counterpart, the REACH initiative [3], which will fundamentally rely on high throughput screening methods made possible by enormous advances in robotics, digital imaging, computational and informational tools to assess a staggering backlog of over 60,000 chemicals now in production, for most of which little if any toxicology data exists. While the Tox21 vision emphasizes complete transition to in vitro screening for toxicity prediction, for the foreseeable future rapid in vitro methods will not eliminate animal toxicity testing, but serve to prioritize chemicals for further screening in animals. However, a bottleneck of time and money stands in the way of evaluating even a small fraction of the in vitro prioritized chemicals with conventional rodent models of human risk. A solution to the bottleneck is much faster, predictive animal models that are amenable to automation platforms. Zebrafish has emerged as the choice for such a model. No other vertebrate is better suited to high throughput chemical screening [4].

Zebrafish development is the most sensitive life stage to chemical exposure. The bulk of the model's utility, and hence the bulk of zebrafish toxicology work, is centered on development. Because zebrafish embryos

remain transparent throughout much of organogenesis, adverse effects of chemical exposure on development of the brain, notochord, heart, jaw, body segmentation, and body size can be continuously assessed in the living animal under low magnification. An important developmental feature is that zebrafish embryos that are malformed, missing organs, or displaying organ dysfunction, usually survive well beyond the point at which those organs normally start to function. This feature is in stark contrast to rodents where heart and other organ malformations, missing or dysfunctional organs, typically cause a generalized in utero lethality. In a large scale (>1000 animal) rodent screen, such endpoints would be missed with anything less than Herculean efforts at detection [4].

As the only vertebrate model meeting the rapid, predictive toxicology needs of the 21st century, zebrafish are increasingly used by public and private sector interests to conduct discovery screens of chemical libraries containing ≥1000 compounds (reviewed in [5] and [6]; see also [7-11]). These same studies also highlight near exclusive reliance on inefficient approaches to manipulating and chemically exposing zebrafish embryos; namely manual placement of embryos into 96 or 384 well plates, and exposure of embryos while still in the chorion, an acellular barrier of poorly characterized permeability enclosing the developing embryo.

Manual placement of embryos to microtiter wells is not a cost-effective use of laboratory personnel and, while barely feasible for screens of a few

thousand compounds, is completely impractical for the scale needed to address the rapidly growing backlog of conventional and nanomaterial chemistries already in use. When working with dechorionated embryos, manual placement by humans requires considerably more refined handling technique than embryos in the chorion. High precision, repetitive motions necessitate many breaks for lab technicians, and the mundane nature of the task equates to frequent personnel turnover and inefficiencies associated with continual retraining.

No chemically comprehensive assessment of chorion permeability has been reported, but the chorion is widely suspected to influence chemical uptake, and several reports confirm that it is an uptake barrier for metal nanomaterials [12,13]. Reported attempts at zebrafish chorion removal prior to 24-hpf on a large (>100 embryo) scale have been plagued by generally low survival [14], and exposure in the chorion continues to be a common practice in large screens. Such screens have yielded much information and potentially invaluable therapeutic discovery (reviewed in [6]), but it is tempting to speculate how much information has been missed because of permeability limitations of the chorion. A second, important limitation of not removing the chorion prior to exposure is that compounds that specifically inhibit the hatching process lead to secondary phenotypic responses. For example, the widely used insecticide cartap inhibits hatching resulting in secondary effects on the embryo such as wavy notochord, axis malformation, and somite defects[15]. These effects are

due to the lack of hatching, rather than a primary response to exposure to the chemical. The chorion can significantly confound the early life stage zebrafish toxicity assay by leading to false positives. When we consider the obvious potential for false negatives due to the aforementioned barrier effect, chorion removal is critical to improve the predictivity of the assay.

Herein we report rapid and cost-effective automated removal of the chorion from 2000 embryos at once at the 4-hpf stage, and placement of the dechorionated embryos into 96 well plates for exposure at 6hpf. Two approaches were key to developing these platforms: 1) the use of pronase degradation of the chorion combined with automated agitation and washing of the embryos, and 2) the application of machine vision-guided robotics to rapidly select and place the de-chorionated embryos into plate wells. A single station is used in our laboratory to plate >1000 dechorionated embryos per day, requiring approximately 4 hours and with a survival rate better than 95% by 120 hpf.

## Materials and Methods

### Zebrafish

Embryonic zebrafish were obtained from a Tropical 5D strain of zebrafish (Danio rerio) reared in the Sinnhuber Aquatic Research Laboratory (SARL) at Oregon State University. Adults were kept at standard laboratory conditions of 28°C on a 14-h light/10-h dark photoperiod in fish water (FW) consisting of reverse osmosis water supplemented with a commercially

available salt (Instant Ocean®) to create a salinity of 600 microsiemens. Sodium bicarbonate was added as needed to adjust the pH to 7.4. Zebrafish were group–spawned, and embryos were collected and staged as described by Kimmel[16].

**Automated Chorion Removal**

To establish an inexpensive and highly reproducible method of removing chorions from about 1600 embryos at a time at 4 hours post fertilization (hpf), a Belly Dancer shaker (ATR, Inc., Laurel, MD) was modified to accommodate a custom-machined, anodized aluminum shaker plate that holds 4 glass petri dish bottoms (100 mm x 15mm, VWR) and attached water delivery tubing, stainless steel nozzles and a drain port (**Figure 1**). The internal workings of the Belly Dancer were modified with a small pump and a parametric motion controller (Revolution Robotics, Inc., Corvallis, OR). The front panel was modified with an LED display and push button control. The on-board pump supplied rinse water from an external heated (28$^{o}$C) carboy via the tubing and nozzles to each glass dish at the appropriate time. The movement of the shaker was controlled by the same system to deliver pulsed agitation or gentle swirling, precisely when needed, to dislodge partially hydrolyzed chorions. The only manually performed steps were the addition of a pronase aliquot to commence digestion and pressing of the start button. No other steps were necessary to operate the device. The pronase digestion of

the chorion was performed at 4-hpf. Approximately 2000 zebrafish Tropical 5D strain embryos were received from the Sinnhuber Aquatic Research Laboratory's mass spawning facility in a 135 mm plastic dish and quickly cleaned by removing all dead, unfertilized or obviously abnormal embryos with an aspirator; a 5 – 10 minute process for a trained technician. Approximately 400 - 500 embryos were placed in each of the 4 glass dishes in 25 ml of FW with 50 µl of 50 mg/ml pronase (Fluka #81748) for 6.5 min while the dechorionator platform constantly agitated. The pronase was then flushed away by gently overflowing the dish with the pumped in FW for 10 minutes with 45 second agitation cycles separated by 15 seconds while still. The total volume of fish water consumed was about 1L. After the pronase and rinse phases, the embryos were incubated for 20 minutes at 28$^{o}$C, agitated once more to dislodge any remaining chorions and rinsed again to remove the dislodged chorions. The dechorionation was evaluated (**Table 1**) by gently removing approximately 100 embryos with a flame polished Pasteur pipette after the final rinse and examination under a dissecting microscope for pronase or mechanical damage. No further cleanup of the dechorionated batches was performed prior to allocation to 96-well plates.

**Automated allocation of dechorionated embryos to 96-well plates.**

After the rest period, dechorionated embryos at approximately 5 - 6-hpf were transferred to individual wells of a 96-well BD Falcon, tissue culture

polystyrene plate by a custom robotic pick and place system (**Figure 2**; video of the robotic system in operation can be viewed at http://tanguaylab.com/Automation.html). We noted that the use of non-tissue culture treated polystyrene plates caused rapid disintegration of 100% of embryos once removed from the chorion. The system consisted of a 4-axis Selective Compliant Assembly Robot Arm (SCARA) (Denso Inc., Long Beach, CA) with a custom end-effector designed to replicate a handheld, wide bore, flame polished Pasteur pipette (**Figure 2**). A 100 mm glass petri dish with approximately 400 embryos was loaded into a well lit area below a rigidly mounted machine vision camera (Allied Vision Inc., Stadtroda, Germany). Custom software was utilized to determine the precise coordinates of a suitable embryo which were then passed to the robot control unit. Under the lighting conditions used, normal embryos appeared semitransparent while dead embryos appeared bright white, a parameter easily distinguished by the machine vision. The robot was programmed to first draw 100 µl of embryo medium into the flame-polished pipette from a filling station at the beginning of each cycle, drive the pipette to coordinates several centimeters above the machine vision-selected embryo, and place the pipette tip 20 µm above the embryo coordinates. The embryo was gently aspirated along with an additional approximately 20 µl of embryo medium into the pipette via the onboard syringe pump, and the robot returned the pipette tip to the coordinates of the liquid surface of the next empty well of the plate. The wells had been prefilled with

50 µl of embryo medium. A quick, gentle touch of the liquid surface was all that was required to cause the embryo to be released to the well by capillary action. Positive dispensing pressure was not needed as the embryo had settled to the bottom of the liquid column while the robot pivoted between the source plate and 96-well plate. We noted that an additional 2 - 3 µl of embryo medium was transferred to the well by capillary release of the embryo. The cycle was completed with an aspirate and total dispense step at a wash station and a subsequent 100 µl recharge at the filling station. The cycle was then repeated 95 times. Due to the affinity of dechorionated 6-hpf embryos for each other, the source petri dish had to be given a brief, 1 second swirl once during the loading of a plate to re-disperse the embryos, improving machine vision selection.

### Statistical analysis

Performance of the robotic embryo placement was evaluated over 16 trials in parallel with manual embryo loading of 96-well plates. The frequencies of successful well allocations between each method were compared by one way ANOVA where $P < 0.05$ was the threshold for no significant difference between the two methods.

## Results

### Automated chorion removal at 4 hours post fertilization

The performance of 6 trials of enzymatic chorion removal from approximately 1600 zebrafish embryos at once was assessed from random samples of about 100 embryos from each trial and summarized in Table 1. In each trial at least 95% of the 4-hpf embryos were successfully removed from the chorion where success was defined as alive at 24-hpf with no malformations evident by 120-hpf. The automated chorion removal resulted in only about 2% embryo mortality by 24-hpf and only 2% of the embryos were malformed at 120-hpf. Figure 3 depicts the type of mortal damage that 1 – 2% of the embryos were observed to have immediately following the automated dechorionation process. Early damage that may have lead to 2% of the embryos being malformed at 120-hpf was not visibly detected.

**Automated placement of dechorionated embryos into 96-well plates**

We evaluated the success of robotic 96-well loading of embryos dechorionated at 4-hpf that were 5 – 6-hpf at the time of plate loading. The standard for comparison was our routine method of manual placement of dechorionated embryos using a handheld Pasteur pipette. Sixteen 96-well plate comparisons were performed in parallel and the results were summarized in Table 2. The manual loading data were derived from several of the personnel in our laboratory who are equally adept at the technique. The robotic system successfully allocated embryos to 94.7 ± 4.2% of the wells and manual loading successfully allocated embryos to 94.9 ± 3.6% of the well.

There was no statistical difference between the success of the two methods (ANOVA $F = 0.53$; $P < 0.01$ that a significant difference existed). The criterion for success was that each well received only 1 embryo and that the embryo was alive and not visibly damaged or malformed at 24-hpf. We note that 2.8% (43 of 1536) of the unsuccessful wells were from mortality directly as a result of robotic handling. Mortality from manual loading accounted for 4% (62 of 1536) of the unsuccessful wells. The robotic system missed 1.2% (18 of 1536) of the wells, but only one miss occurred from manual loading. The frequency of multipicks (2 embryos allocated to a single well) was similar for the robotic and manual loading (3 and 2 embryos, respectively out of 1536). Embryo malformations observed 18 hours after plate loading (24-hpf) occurred nearly twice as frequently from robotic handling (16 of 864; 1.9%) as they did from manual pipetting (9 of 864; 1%). No bias toward dead or malformed embryos occurring in certain wells was ever observed.

## Discussion

We have introduced automated platforms for high throughput chorion removal at 4-hpf and 96-well plate allocation at 6-hpf that consistently yielded 95% healthy embryos. Together, these automation platforms provide: 1) a rapid and inexpensive circumventing of the potential for false negative and false positive results imposed by the chorion on high throughput applications of the developmental zebrafish model and 2) a much less labor-intensive and

more reliable means of carefully allocating dechorionated embryos to 96-well plates at a rate amenable to high throughput screening.

This is the first report of an en masse chorion removal method for zebrafish embryos prior to 24 hpf, with a reproducibly high survival rate. While chorion removal at 24-hpf from 50-100 zebrafish embryos at once has been reported, initiating embryo exposure so late in development is likely to be of limited utility for large scale screens. Such screens lack *a priori* knowledge of compound activity and must therefore maximize opportunities for chemical 'hits' by chemically exposing during the widest practical window of development. A recent report sought to quantify the success of pronase-supported dechorionation at 6-hpf, as described by Westerfield [17], for replicates of 50 embryos [14]. That study concluded that the use of pronase was generally damaging to 6-hpf embryos and demonstrated a normal development rate of only 75% and a mortality rate of nearly 40% [14]. Our demonstration of pronase-supported, automated chorion removal, at 4-hpf, from 1600 embryos at once, consistently yielded ≥95% survival and normal development to 120-hpf indicating that a pronase-supported approach can be both practical and scalable to meet the embryo demands of high throughput screening.

To our knowledge this is also the first report of a reproducible method for robot- automated allocation of embryos to microtiter plates. A recent report described an image-based fluidic approach to rapid allocation of embryos to

96-well plates [18]. Evidence of that system's performance was largely limited to the handling of embryos still in the chorion with only cursory performance data from dechorionated embryos. We have demonstrated the highly reproducible use of a small, industrial robotic arm approach to retrieve single dechorionated embryos at 6 – 7-hpf from an unsorted dish and allocate them to a 96-well plate with a better than 95% survival rate. It would also be straightforward and, in some instances, desirable to allocate more than one embryo per well, such as for monitoring subtle locomotor activity where a higher signal to noise ratio is achieved with multiple embryos[7]. For gross malformation endpoints, one embryo per well minimizes the potential effects of dose titration from uptake by multiple animals in the same 100 µl volume. Another practical extension of the automation would be for sorting transient transgenic reporter animals fluorescing at the embryonic stage and fluorescent tagged morpholino injected embryos in high throughput gene knockdown assays.

We did not include the time to complete plate loading for any of the robotic trials shown in Table 2, focusing instead on the ability of the modified SCARA robot to handle embryos gently with high survival and low malformation rates. Figure 4 summarizes the entire process with approximate times for completion. We note that while several variables affected the time required for the robotic system to complete a 96-well plate, by far the most important variable was density and dispersal of embryos in the source dish. Having more than 300 embryos in the source dish, or failing to keep the

embryos well dispersed with periodic swirling, noticeably slowed the rate at which the machine vision camera and software could select a sufficiently isolated embryo to map and direct the robot to retrieve. Once the source dish was depleted to less than 300 embryos and the dispersal was kept at a maximum, the system consistently loaded one 96-well plate every 15 minutes. For comparison, laboratory personnel that perform the task on a daily basis consistently loaded one 96-well plate every 6 -10 minutes. However, three experienced loaders in our laboratory could only load a total of 18 - 20 plates before fatigue resulted in a successful loading rate of < 95% when the plates were observed at 24-hpf. The robotic system, facing no such limitation, offers an obvious advantage when throughput demands require ≥200 plates per week. Moreover, having developed the software for a single system, the cost of scaling the system to multiple SCARA robotic loading stations will be limited to hardware only.

The automation platforms herein obviate persistent concerns about the chorion and its potential to limit the effects of chemical exposures, and they relieve a serious bottleneck to high throughput use of the developing zebrafish by automating embryo allocations to assay plates. We believe that these advances, coupled with advances in automated imaging and phenotype analysis, will quickly enable researchers to expand the scale and scope of toxicology and discovery research.

## References


1. Hartung, T. Lessons learned from alternative methods and their validation for a new toxicology in the 21st century. J Toxicol Environ Health B Crit Rev 2010, 13 (2-4), 277-290.
2. Schmidt, C. W. TOX 21: new dimensions of toxicity testing. Environ Health Perspect 2009, 117 (8), A348-353.
3. Lilienblum, W., Dekant, W., Foth, H., Gebel, T., Hengstler, J. G., Kahl, R., Kramer, P. J., Schweinfurth, H., Wollin, K. M. Alternative methods to safety studies in experimental animals: role in the risk assessment of chemicals under the new European Chemicals Legislation (REACH). Arch Toxicol 2008, 82 (4), 211-236.
4. Zon, L. I., Peterson, R. T. *In vivo* drug discovery in the zebrafish. Nat Rev Drug Discov 2005, 4 (1), 35-44.
5. Sukardi, H., Chng, H. T., Chan, E. C., Gong, Z., Lam, S. H. Zebrafish for drug toxicity screening: bridging the in vitro cell-based models and *in vivo* mammalian models. Expert Opin Drug Metab Toxicol 2011, 7 (5), 579-589.
6. Zon, L. I., Peterson, R. The new age of chemical screening in zebrafish. zebrafish 2010, 7 (1), 1.
7. Kokel, D., Bryan, J., Laggner, C., White, R., Cheung, C. Y., Mateus, R., Healey, D., Kim, S., Werdich, A. A., Haggarty, S. J. and others. Rapid behavior-based identification of neuroactive small molecules in the zebrafish. Nat Chem Biol 2010, 6 (3), 231-237.
8. Paik, E. J., de Jong, J. L., Pugach, E., Opara, P., Zon, L. I. A chemical genetic screen in zebrafish for pathways interacting with cdx4 in primitive hematopoiesis. zebrafish 2010, 7 (1), 61-68.
9. Rihel, J., Prober, D. A., Arvanites, A., Lam, K., Zimmerman, S., Jang, S., Haggarty, S. J., Kokel, D., Rubin, L. L., Peterson, R. T. and others. Zebrafish behavioral profiling links drugs to biological targets and rest/wake regulation. Science 2010, 327 (5963), 348-351.
10. Wang, C., Tao, W., Wang, Y., Bikow, J., Lu, B., Keating, A., Verma, S., Parker, T. G., Han, R., Wen, X. Y. Rosuvastatin, identified from a zebrafish chemical genetic screen for antiangiogenic compounds, suppresses the growth of prostate cancer. Eur Urol 2010, 58 (3), 418-426.
11. Yen, J., Donerly, S., Levin, E. D., Linney, E. A. Differential acetylcholinesterase inhibition of chlorpyrifos, diazinon and parathion in larval zebrafish. Neurotoxicol Teratol 2011.

12. Johnson, A., Carew, E., Sloman, K. A. The effects of copper on the morphological and functional development of zebrafish embryos. Aquat Toxicol 2007, 84 (4), 431-438.

13. Bar-Ilan, O., Louis, K. M., Yang, S. P., Pedersen, J. A., Hamers, R. J., Peterson, R. E., Heideman, W. Titanium dioxide nanoparticles produce phototoxicity in the developing zebrafish. Nanotoxicology 2011, Epub ahead of print.

14. Henn, K., Braunbeck, T. Dechorionation as a tool to improve the fish embryo toxicity test (FET) with the zebrafish (Danio rerio). Comp Biochem Physiol C Toxicol Pharmacol 2011, 153 (1), 91-98.

15. Zhou, S., Dong, Q., Li, S., Guo, J., Wang, X., Zhu, G. Developmental toxicity of cartap on zebrafish embryos. Aquat Toxicol 2009, 95 (4), 339-346.

16. Kimmel, C. B., Ballard, W. W., Kimmel, S. R., Ullmann, B., Schilling, T. F. Stages of embryonic development of the zebrafish. Developmental Dynamics 1995, 203 (3), 253-310.

17. Westerfield, M., The Zebrafish Book. A Guide for the Laboratory Use of Zebrafish (Danio rerio), Editoin Edition, University of Oregon Press, Eugene, Oregon, 2007.

18. Graf, S. F., Hotzel, S., Liebel, U., Stemmer, A., Knapp, H. F. Image-based fluidic sorting system for automated Zebrafish egg sorting into multiwell plates. J Lab Autom 2011, 16 (2), 105-111.

## Acknowledgments

The authors wish to express their gratitude to Greg Gonnerman, Lindsey Chalker, Carrie Barton, Cari Buchner and Chapell Miller of the Tanguay Laboratory for providing a steady supply of high quality zebrafish eggs and for their insights on how to improve the automation. We thank Dr. Siba Das for Photoshop help with the figures. The presented work was funded in part by NIH grants RC4 ES019764, P42 ES016465 and P30 ES000210.


**Figure B- 1. A modified shaker platform-based instrument for the automation of chorion removal from zebrafish embryos at 4 hours post fertilization.**

**A)** A frontal view of the modified Bellydancer shaker. The custom machined and anodized aluminum plate is at top and holds 4 x 100 mm glass dishes. The control panel consists solely of a start and a stop button, and a small LCD status display. **B)** A closer view of the shaker platform during a rinse phase of chorion removal. Embryos are visible in the plates. The rinse water is pumped via the onboard pump from an off board heated source and delivered via the hose and nozzle assembly to gently overflow the plates and not suspend the embryos. The rinse water is channeled to a drain port at the rear of the platform. Agitation and pump control are via the custom onboard microcomputer.

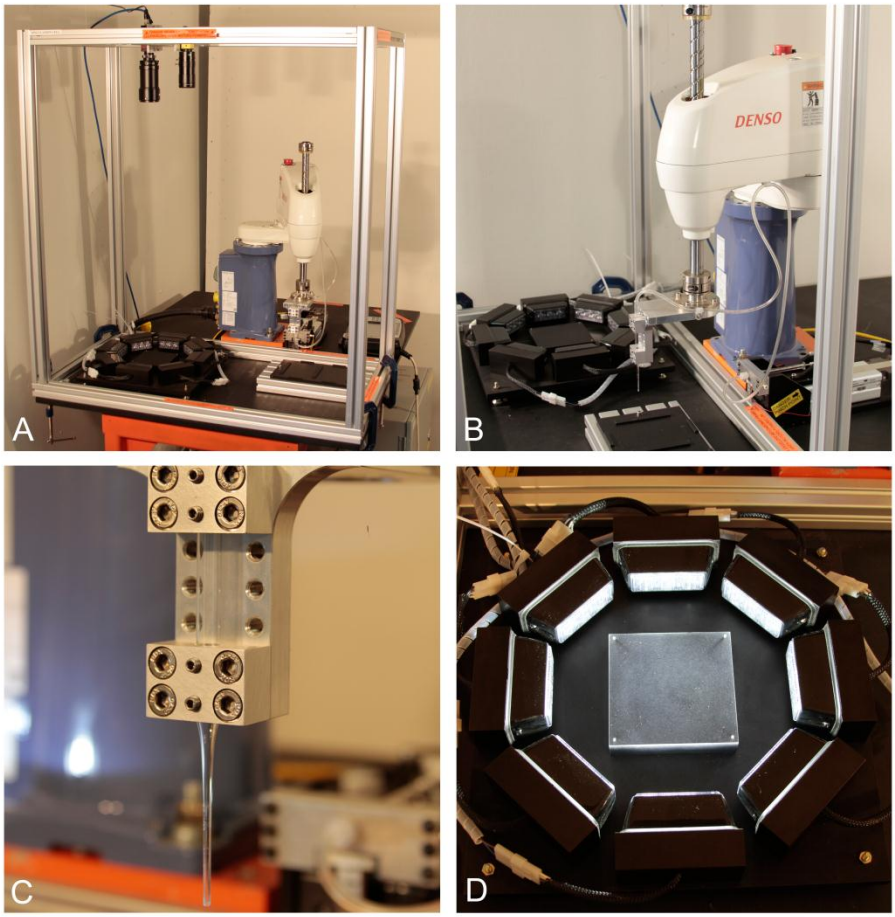


**Figure B- 2. A custom robotic station for the automated transfer of dechorionated zebrafish embryos from the dish in which chorion removal occurred to a 96-well plate.**

**A** and **B)** show a front and side view of the work station. An extruded aluminum strut assembly rigidly supports the overhead camera. The station is supported from below by a steel tooling plate welded to a rigid steel table. The 4-axis Denso SCARA robot is bolted to the tooling plate as it generates strong inertial forces during its movement. The syringe pump supplying the pipetting force is visible next to the base of the robot. Also visible are the lighted arena beneath the camera and the holder for the destination plate, and a second plate for pipette rinsing and preloading with water. **C)** The custom end effecter gently cradles a single, wide bore, flame polished Pasteur pipette connected to the syringe pump line. **D)** The lighted arena consists of an aluminum square with precisely located pins in the corners that serve as visible references for the machine vision software. The circular array of LED units provides the optimal amount of contrast needed for the machine vision to clearly see the embryos. The units are commercially available, high intensity LED assemblies. When operating, the station is protected by a light curtain that, if interrupted, stops the robot's motion in less than 50 milliseconds.

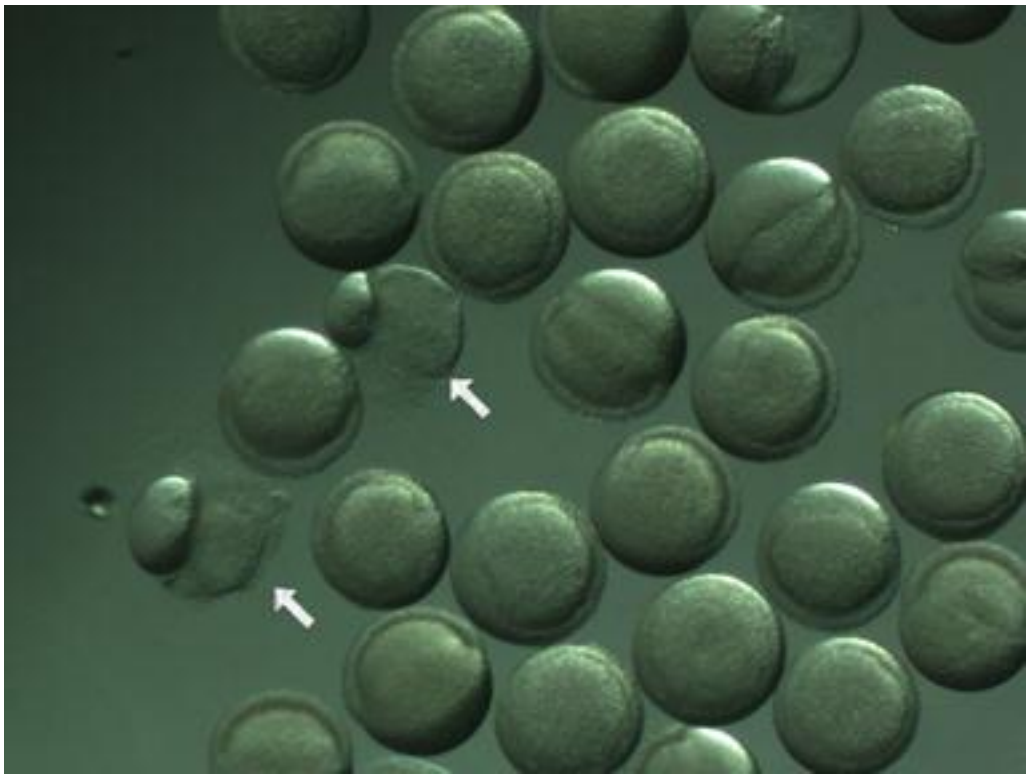

**Figure B- 3. Mortal damage typically observed in 1 – 2% of 5-hpf zebrafish embryos immediately after the automated dechorionation process.**

The damaged embryos are indicated by arrows, all other embryos in the field are normal. Whether the low frequency damage is due to the effects of pronase digestion or motion is unknown.

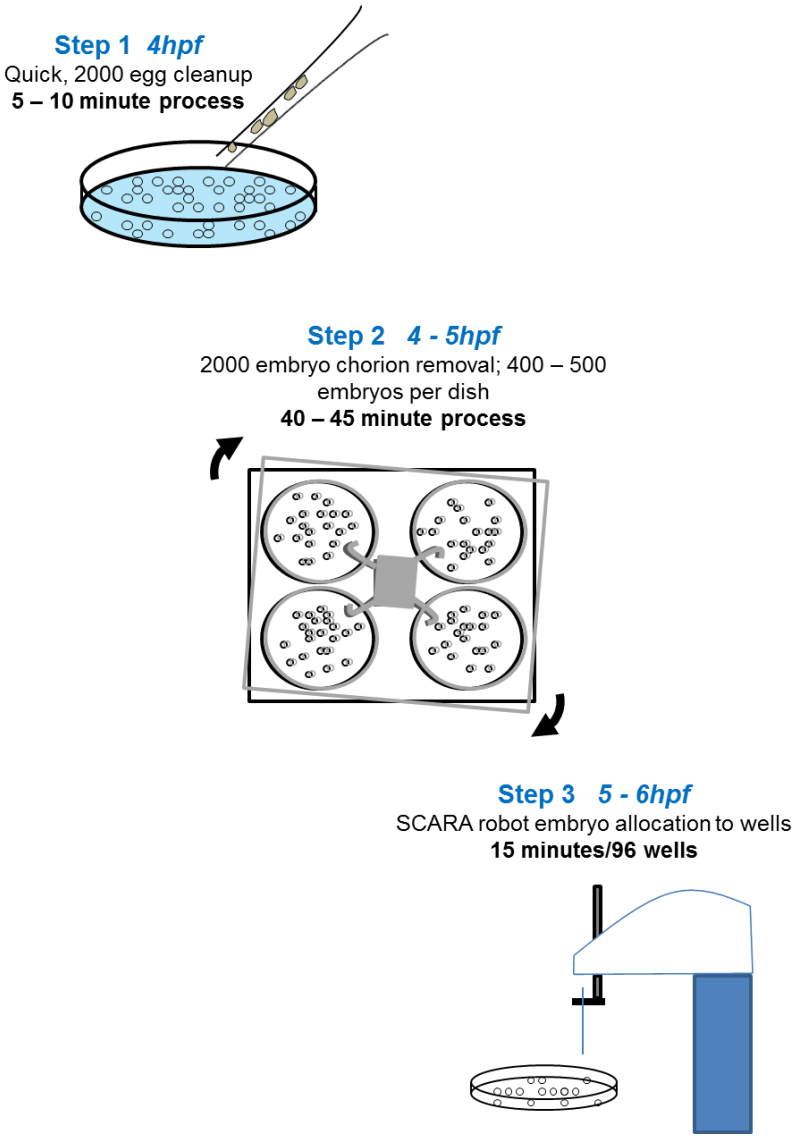


**Figure B- 4. Process summary and timeline for automated chorion removal and embryo allocation to plate wells.**
**Step 1**, beginning at 4 hours post fertilization (hpf) consists of removal of dead or obviously abnormal embryos from the mass of 2000 embryos in a 135 mm Petri dish. It requires 5 – 10 minutes to complete the cleanup using a Pasteur pipette connected to a vacuum aspirator. **Step 2**, beginning immediately after 1, requires the approximate division of the mass of embryos among 4; 100mm glass Petri dishes, the addition of a pronase aliquot to each and pressing the start button. The automated, gentle shaking, rinsing and rest period requires 40 – 45 minutes. **Step 3**, beginning immediately after the post-dechorionation rest period and rinse to remove any remaining traces of chorion, simply requires the movement of the plate of 400 embryos to the SCARA robot station and pressing the start button. A single embryo is delivered to each of the 96 wells in 15 minutes.

**Table B- 1. Results of automated chorion removal at 4-hpf, observed at 24- and 120-hpf.**

| | | Results | | | | |
|---|---|---|---|---|---|---|
| **Trial date** | **[a]Embryos sampled from ≈ 1600** | **Normal** | **Dead at 24-hpf** | **Malformed at 24-hpf** | **[b]Dead at 120-hpf** | **[c]Malformed at 120-hpf** |
| 7/18/2011 | 86 | 83 | 3 | 0 | 0 | 1 |
| 7/25/2011 | 100 | 97 | 3 | 0 | 0 | 1 |
| 7/26/2011 | 100 | 98 | 1 | 1 | 1 | 2 |
| 7/27/2011 | 100 | 92 | 1 | 7 | 6 | 2 |
| 7/28/2011 | 97 | 95 | 2 | 0 | 1 | 2 |
| 7/29/2011 | 99 | 95 | 0 | 4 | 3 | 1 |
| **Total** | 582 | 560 | 10 | 12 | 11 | 9 |
| **Percent** | 100.0 | 96.2 | 1.7 | 2.1 | 1.9 | 1.5 |

[a]The dechorionator holds 4 x 100 mm dishes; approximately 400 embryos each from which roughly 100 were removed at once by Pasteur pipette after the process for evaluation.

[b] Additional larval mortality at 120-hpf. Excludes mortality observed at 24-hpf

[c] Additional larval malformation at 120-hpf. Excludes malformation observed at 24-hpf.

**Table B- 2. Robotic pick & place performance on 6-hpf dechorionated zebrafish embryos compared to manual plate loading.**

| | | Overall P&P performance | | Specific P&P failures | | | |
|---|---|---|---|---|---|---|---|
| Trial date | Wells | [a]Wells allocated successfully | [b]Wells unsuccessful | [c]P&P mortality | [d]Missed wells | [e]Multi-picks | [f]Mal-formed |
| 8/1/2011 | 96 | 86 (89.6%) | 10 (10.4%) | 2 | 5 | 0 | 3 |
| 8/2/2011 | 96 | 90 (93.8%) | 6 (6.3%) | 4 | 0 | 0 | 2 |
| 8/2/2011 | 96 | 93 (96.9%) | 3 (3.1%) | 2 | 0 | 0 | 1 |
| 8/2/2011 | 96 | 95 (99.0%) | 1 (1.0%) | 0 | 0 | 0 | 1 |
| 8/4/2011 | 96 | 85 (88.5%) | 11 (11.5%) | 9 | 0 | 0 | 2 |
| 8/4/2011 | 96 | 91 (94.8%) | 5 (5.2%) | 2 | 1 | 0 | 2 |
| 8/5/2011 | 96 | 88 (91.7%) | 8 (8.3%) | 6 | 0 | 0 | 2 |
| 8/8/2011 | 96 | 87 (90.6%) | 9 (9.4%) | 6 | 0 | 1 | 2 |
| 8/9/2011 | 96 | 89 (92.7%) | 7 (7.3%) | 4 | 2 | 0 | 1 |
| 9/6/2011 | 96 | 95 (99.0%) | 1 (1.0%) | 0 | 1 | 0 | _ |
| 9/6/2011 | 96 | 91 (94.8%) | 5 (5.2%) | 0 | 5 | 1 | _ |
| 9/6/2011 | 96 | 96 (100%) | 0 | 0 | 0 | 0 | _ |
| 9/7/2011 | 96 | 84 (87.5%) | 12 (12.5%) | 8 | 1 | 3 | _ |
| 9/7/2011 | 96 | 95 (99.0%) | 1 (1.0%) | 0 | 1 | 0 | _ |
| 9/7/2011 | 96 | 95 (99.0%) | 1 (1.0%) | 0 | 1 | 0 | _ |
| 9/7/2011 | 96 | 95 (99.0%) | 1 (1.0%) | 0 | 1 | 0 | _ |
| | * | **Ave = 94.7 ± 4.2%** | | **2.8%** | **1.2%** | **0.3%** | **1.9%** |
| | | **N = 16 trials** | | | | | |

| | | Overall manual performance | | Specific manual failures | | | |
|---|---|---|---|---|---|---|---|
| Trial date | Wells | Wells allocated successfully | Wells unsuccessful | Manual load mortality | Missed wells | Multi-picks | Malformed |
| 8/1/2011‡ | 96 | 87 (90.6%) | 9 (9.4%) | 6 | 1 | 1 | 1 |
| 8/2/2011‡ | 96 | 89 (92.7%) | 7 (7.3%) | 7 | 0 | 0 | 0 |
| 8/2/2011‡ | 96 | 87 (90.6%) | 9 (9.4%) | 8 | 0 | 0 | 1 |
| 8/2/2011‡ | 96 | 91 (94.8%) | 5 (5.2%) | 1 | 0 | 1 | 3 |
| 8/4/2011‡ | 96 | 86 (89.6%) | 10 (10.4%) | 10 | 0 | 0 | 0 |
| 8/4/2011 | 96 | 91 (94.8%) | 5 (5.2%) | 5 | 0 | 0 | 0 |
| 8/5/2011 | 96 | 91 (94.8%) | 5 (5.2%) | 3 | 0 | 0 | 2 |
| 8/8/2011 | 96 | 88 (91.7%) | 8 (8.3%) | 6 | 0 | 0 | 2 |
| 8/9/2011 | 96 | 96 (100%) | 0 | 0 | 0 | 0 | 0 |
| 9/6/2011 | 96 | 96 (100%) | 0 | 0 | 0 | 0 | _ |
| 9/6/2011 | 96 | 96 (100%) | 0 | 0 | 0 | 0 | _ |
| 9/6/2011 | 96 | 89 (92.7%) | 7 (7.3%) | 7 | 0 | 0 | _ |
| 9/7/2011 | 96 | 89 (92.7%) | 7 (7.3%) | 7 | 0 | 0 | _ |
| 9/7/2011 | 96 | 96 (100%) | 0 | 0 | 0 | 0 | _ |
| 9/7/2011 | 96 | 94 (97.9%) | 2 (2.1%) | 1 | 0 | 1 | _ |
| 9/7/2011 | 96 | 95 (99.0%) | 1 (1.0%) | 1 | 0 | 0 | _ |
| | | **Ave = 94.9 ± 3.6%** | | **4.0%** | _ | **0.2%** | **1.0%** |
| | | **N = 16 trials** | | | | | |

*Robotic performance was not different from the overall success of manual loading (F = 0.53; P < 0.01)

[a]Well allocation is placement of one dechorionated 6-hpf embryo.

[b]An unsuccessful well allocation (errors [c-e]) was determined immediately after the trial and at 24-hpf for [f].

[c]Embryo dead, usually partly or completely disintegrated, immediately after trial

[d]Embryo or disintegrated residue absent from well immediately after trial.

[e]More than one embryo allocated to the same well

[f]Malformations observed at 24-hpf; not recorded 9/6-9/7

‡Lower apparent performance success of earlier trials reflects the performance of earlier software versions.